

THE GEOCHEMISTRY AND PETROGENESIS OF THE
Ni-Cu-PGE SHAKESPEARE DEPOSIT, ONTARIO,
CANADA

Ian R. Dasti

Department of Geology
Lakehead University
Thunder Bay, Ontario

A thesis submitted to the Faculty of Graduate Studies in partial
fulfillment of the requirements for the degree of Master of Science

© Ian Dasti, 2014

Abstract

The Shakespeare intrusion, which hosts the Shakespeare Ni-Cu-PGE sulfide deposit, is part of the 2.2 Ga Nipissing Gabbro magmatic event, a large mafic-ultramafic suite located in the southern Superior and Southern Province. The Shakespeare intrusion intrudes the 2.2-2.45 Ga Huronian Supergroup and is located in the northern part of the Southern Province, only a few km from the Archean – Proterozoic unconformity which separates the Superior Province from the Southern Province and is adjacent to the ~ 2450 Ma East Bull Lake and Agnew Lake intrusions.

The Shakespeare deposit is the largest Ni-Cu-PGE deposit in the Nipissing Large Igneous Province (LIP). Field mapping and drilling have provided a detailed stratigraphic understanding of the deposit and provide the framework for geochemical models of sulfide segregation related to assimilation. The U-enriched rocks that interacted with the intrusion during ascent through the crust provide an excellent opportunity to gauge the role of assimilation during the formation of the Shakespeare deposit while providing further evidence that crustal sulfur is necessary in order to generate economic concentrations of magmatic sulfides.

A detailed study of three drill holes representing poor, average, and above average intercepts of Ni-Cu-PGE sulfides was performed in order to establish the mechanism by which an immiscible sulfide liquid was produced and also to establish the contamination history of the Shakespeare deposit. Various geochemical techniques were employed, including SEM-EDS, ICP-MS, ICP-AES, total sulfur, sulfur isotope, and XRF analysis. During the course of the SEM-EDS study primary magmatic textures within hollingworthite-irarsite-platarsite were observed,

suggesting limited remobilization during metamorphism. Rheniite, cerium-rich allanite, and various tellurides and selenides were also observed.

$\delta^{34}\text{S}$ analysis yielded values between between 0.01‰ and 2.38‰, averaging 1.14‰. These values are indicative of an unfractionated sulfur source, suggesting that the source of sulfur in the Shakespeare deposit was either derived from the mantle or an unfractionated crustal source, such as the quartz pebble conglomerates of the Matinenda Formation. Sulfur : selenium ratios yielded values between 1245 to 3271, averaging 1810. The average value is significantly lower than accepted mantle values (2850-4000) and may point to an assimilated rich in selenium.

Spider diagrams of mantle normalized data from the Shakespeare intrusion indicate that all of the rocks of the Shakespeare intrusion display a geochemical profile which is characteristic of magmas that have undergone significant degrees of crustal contamination. Negative Nb and Ti anomalies, enrichment in HFSE relative to MREE, and enrichment in LREE relative to HREE indicate that ascending Shakespeare magmas assimilated significant quantities of upper crustal material.

The results of the study show that the Shakespeare intrusion is highly enriched in U, Th, and LREE, relative to other Nipissing intrusions. The most likely explanation for the enrichment is that the Shakespeare intrusion interacted with the pyritic quartz pebble conglomerates of the Matinenda Formation, possibly near the past producing Agnew Lake uranium mine. Geochemical and textural evidence suggests that magma mixing was the dominant mechanism responsible for the precipitation of an immiscible sulfide liquid. R factor calculations and sulfide metal concentrations suggest a second immiscible sulfide liquid precipitated from later

mixing with the PGE- and base metal-poor biotite quartz diorite magmas which ponded in the roof zone of the intrusion.

The results of this study have major implications for Ni-Cu-PGE exploration in the Nipissing LIP and indicate that any economically significant concentrations of magmatic sulfides will be found in gabbroic rocks which have assimilated significant amounts of U- and Th-rich crustal material from the Matinenda Formation, resulting in discernable differences in the U-contents of potential host intrusions versus intrusions that are not likely to host a Ni-Cu-PGE deposit.

Acknowledgements

The publication of this study is the result of years of hard work by many industry professionals and academics, without which I would not have had the opportunity to complete this project. First, I would like to thank Dr. Stephen Kissin for supervising this project and for his patience and the department for their support. My sincere thanks go to Anne Hammond and Kristi Tavener for making my thin sections and helping with the preparation of samples. I am indebted to Dr. Richard Sutcliffe, who has been an excellent mentor since I began my master's degree and is entirely responsible for the initial opportunity to study the Shakespeare deposit. I would also like to thank Mr. Harold Tracanelli, who patiently and thoroughly supervised (and participated in) my initial field work.

Without the generous financial support of Wellgreen Platinum and Accurassay Laboratories the scope and success of this study would have been significantly diminished – I will never forget their generosity and cannot thank them enough. I would also like to thank Margaret Hatton, for her assistance in the field, and Sara Mackie, for emotional support. Finally, I would like to thank my family and friends for their continued support through my journey through academia.

Table of Contents

Abstract	ii
Acknowledgements	v
List of Figures	viii
List of Tables	xi
Chapter 1: Introduction	Page 1
1.1 - Geological Setting	Page 3
1.2 – Geology of the Nipissing Gabbros	Page 4
1.3 – Geology of the Shakespeare Intrusion	Page 6
Chapter 2: Purpose	Page 11
Chapter 3: Methodology	Page 13
3.1 – Field work and sampling	Page 13
3.2 – Thin section analysis	Page 14
3.3 – Geochemical analysis	Page 15
Chapter 4: Results	Page 17
4.1 – Thin section analysis	Page 17
4.2 - Results of the SEM-EDS study	Page 39
4.3 – Geochemical analysis	Page 50
Chapter 5: Discussion	Page 71
5.1 – Contamination of Shakespeare magmas	Page 71
5.2 – Genesis of biotite quartz diorite	Page 76
5.3 – Autolithic and xenolithic fragments	Page 78
5.4 – The sulfur source for Ni-Cu-PGE sulfides	Page 79
5.5 – Precipitation of immiscible sulfide liquid	Page 85
5.6 – Sulfide metal content and R factor	Page 93
Chapter 6: Conclusions	Page 103
6.1 – Contamination of Shakespeare magmas	Page 103
6.2 – Genesis of biotite quartz diorite	Page 104
6.3 – Autolithic and xenolithic fragments	Page 104
6.4 – The sulfur source for Ni-Cu-PGE sulfides	Page 105

6.5 – Precipitation of immiscible sulfide liquid	Page 106
6.6 – Sulfide metal content and R factor	Page 108
6.7 – Summary of revised model	Page 110
Works Cited	Page 113
Appendix 1: Quantitative results of the SEM-EDS study	A1A, A1B
Appendix 2: Core logs from U-03-118, -119, and -122	A2A, A2B, A2C
Appendix 3: Laboratory results from ICP-MS analysis	A3
Appendix 4: Laboratory results from ICP-AES analysis	A4
Appendix 5: Laboratory results from FA/AAS analysis	A5
Appendix 6: Laboratory results from LECO analysis	A6
Appendix 7: Laboratory results from XRF analysis	A7

List of Figures

Figure 1: Area and location map of the Shakespeare deposit	Page 2
Figure 2: Idealized cross section of the Shakespeare deposit	Page 8
Figure 3: Schematic diagram of drill hole core logs	Page 18
Figure 4: Satellite image of the Shakespeare deposit and drill hole locations	Page 19
Figure 5: Long section of the Shakespeare deposit and drill hole locations	Page 20
Figure 6: Representative microphotograph of quartz diorite	Page 21
Figure 7: Photographs of various rock fragments in drill core	Page 23
Figure 8: Ilmenite-rutile-chalcopyrite grain in biotite quartz diorite	Page 24
Figure 9: Representative microphotograph of rock fragments within quartz gabbro	Page 25
Figure 10: Euhedral gersdorffite grain near pentlandite	Page 27
Figure 11: Representative microphotograph of well preserved plagioclase within melagabbro	Page 28
Figure 12: Ilmenite-rutile-chalcopyrite grain juxtaposed on fresh sulfide	Page 30
Figure 13: Medium-grained euhedral gersdorffite grain	Page 32
Figure 14: SEM-EDS image of ilmenite with pyrrhotite and pentlandite	Page 34
Figure 15: Ilmenite-rutile-chalcopyrite grain juxtaposed on fresh sulfide	Page 35
Figure 16: Sulfide being replaced by rutile	Page 36

Figure 17: SEM-EDS image of partially agglomerated pentlandite flames	Page 37
Figure 18: Pentlandite flames as fine lamellae	Page 38
Figure 19: SEM-EDS image of native copper within an ilmenite core	Page 40
Figure 20: SEM-EDS image of fracture fillings within a gersdorffite grain	Page 42
Figure 21: SEM-EDS image of extreme fracture fillings within a gersdorffite grain	Page 43
Figure 22: Backscatter electron images of PGE rich MCGA in solid solution with gersdorffite-cobaltite	Page 44
Figure 23: Backscatter electron image of argentopentlandite	Page 46
Figure 24: Backscatter electron image of partially meramict allanite	Page 47
Figure 25: Mantle normalized spider diagram for drill hole U-03-118	Page 52
Figure 26: Mantle normalized spider diagram for hole U-03-119	Page 53
Figure 27: Mantle normalized spider diagram for hole U-03-122	Page 54
Figure 28: Sulfur vs. depth, hole U-03-119	Page 55
Figure 29: Sulfur vs. depth, hole U-03-122	Page 56
Figure 30: Sulfide nickel concentration vs. depth, drill hole U-03-119	Page 57
Figure 31: Sulfide nickel concentration vs. depth, drill hole U-03-122	Page 58
Figure 32: Sulfide copper concentration vs. depth, drill hole U-03-119	Page 59

Figure 33: Sulfide PGE + Au concentration vs. depth, hole U-03-119	Page 60
Figure 34: MgO vs. depth, drill hole U-03-118	Page 62
Figure 35: Fe ₂ O ₃ vs. depth, drill hole U-03-118	Page 63
Figure 36: SiO ₂ vs. depth, drill hole U-03-118	Page 64
Figure 37: MgO vs. depth, drill hole U-03-119	Page 65
Figure 38: Fe ₂ O ₃ vs. depth, drill hole U-03-119	Page 66
Figure 39: SiO ₂ vs. depth, drill hole U-03-119	Page 67
Figure 40: MgO vs. depth, drill hole U-03-122	Page 68
Figure 41: Fe ₂ O ₃ vs. depth, drill hole U-03-122	Page 69
Figure 42: SiO ₂ vs. depth, drill hole U-03-122	Page 70
Figure 43: Mantle normalized La/Sm vs Nb/Th	Page 73
Figure 44: Sulfide nickel concentration vs. R factor, drill hole U-03-119	Page 97
Figure 45: Sulfide copper concentration vs. R factor, drill hole U-03-119	Page 98
Figure 46: Sulfide platinum concentration vs. R factor, drill hole U-03-119	Page 99
Figure 47: Sulfide palladium concentration vs. R factor, drill hole U-03-119	Page 100

List of Tables

Table 1: Results of the sulfur isotope analysis

Page 51

Chapter 1: Introduction

The Shakespeare deposit is hosted within the 2217 Ma Shakespeare intrusion, approximately 70 km west of Sudbury, Ontario (Figure 1) (Sproule et al., 2007). The Shakespeare deposit, which is presently owned by Wellgreen Platinum, was previously operated by URSA Major Minerals. Ursa Major Minerals began bulk sampling in 2007-2008 and commercial production commenced in 2010. The mine has been on care and maintenance since 2012. The deposit has probable reserves of 11.8 Mt grading 0.33% Ni, 0.35% Cu, and 0.87 g/t PGM + Au. Another 5.44 Mt of reserves exist as Indicated and Inferred, with similar grades to the probable reserve category (www.wellgreenplatinum.com).

Sproule et al. (2007) summarized previous work, which shows the Nipissing Gabbro Suite of rocks is host to multiple types of magmatic and hydrothermally modified mineralization including; the Co-Ag veins (Cobalt), disseminated Cu-Ni-Cr-(PGE) pipes (Casson Lake), internal disseminated Ni-Cu-PGE sulfides (Kelly, Davis-Kelly), internal massive-disseminated Ni-Cu-Co-PGE sulfides (Louise, Waters), and massive-disseminated basal Ni-Cu-PGE sulfides (Janes, and hydrothermally mobilized at Rathbun). They noted that the Shakespeare intrusion represented a different style of mineralization than had been observed elsewhere in the Nipissing Gabbro suite.

The Shakespeare intrusion is part of the 2.2 Ga Nipissing Gabbro magmatic event, a large mafic-ultramafic suite located in the southern Superior and Southern Province. It intrudes the 2.2-2.45 Ga Huronian Supergroup and is located in the northern part of the Southern Province, only a few km from the Archean – Proterozoic unconformity which separates the Superior Province from the Southern Province and is adjacent to the ~ 2450 Ma East Bull Lake and Agnew Lake intrusions.

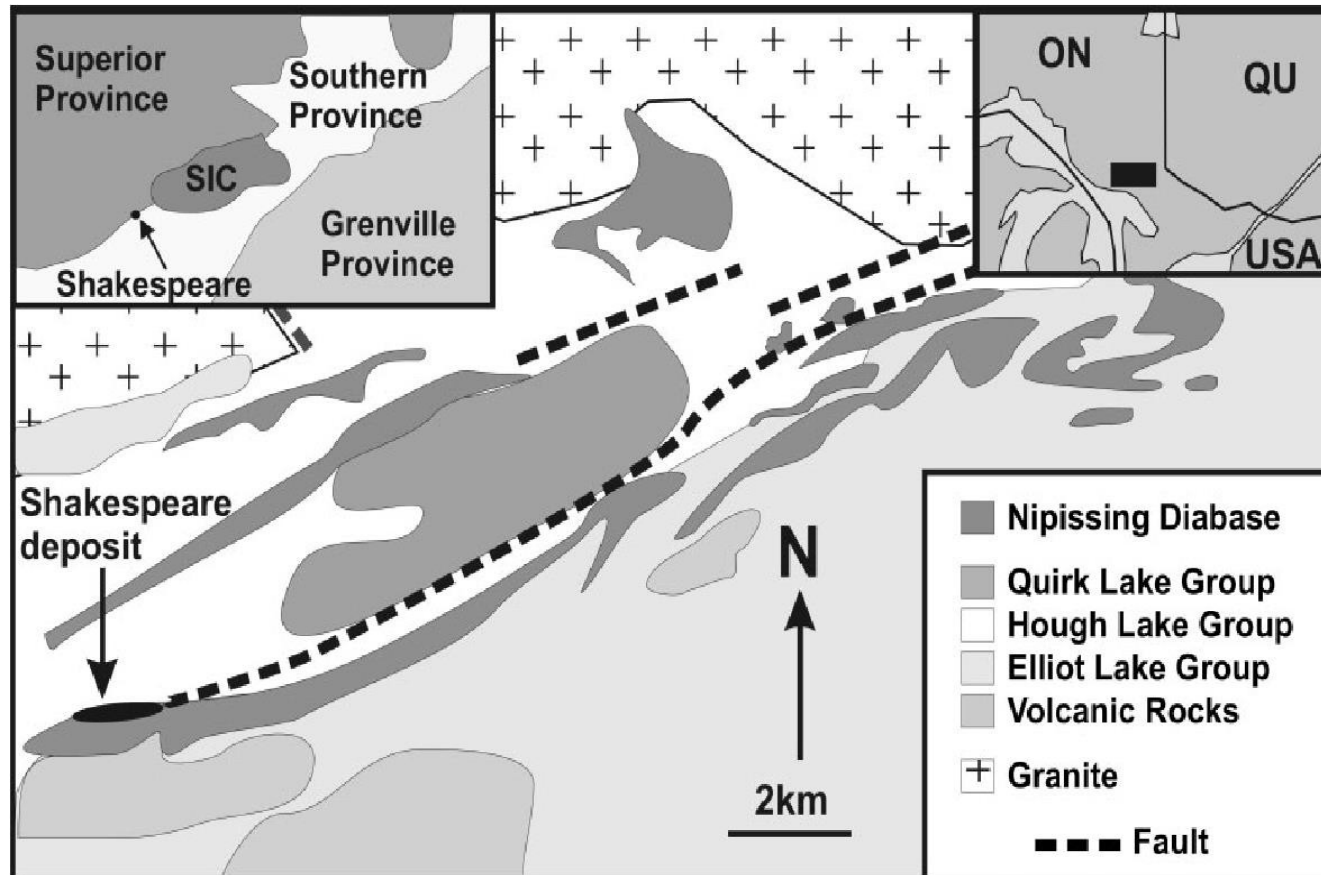


Figure 2: Geology of the Shakespeare deposit and surrounding area, reprinted from Sproule et al. (2007). ON: Ontario; QU: Quebec; SIC: Sudbury Igneous Complex

1.1 - Geological setting

As summarized by James et al. (2002), the majority of Nipissing Gabbro rocks were intruded into Archean basement rocks and the recently deposited sedimentary rocks of the Huronian Supergroup in a major magmatic event between 2210 and 2217 Ma, resulting in the development of the Nipissing Gabbro Large Igneous Province (LIP). At the time of emplacement, sedimentary strata were locally semi-lithified, still contained significant water, and frequently interacted with the intruding Nipissing magmas (Shaw et al., 1999).

As summarized by Sproule et al. (2007), the Southern Province has experienced an extensive tectonic and magmatic history from ~ 2450 – 1000 Ma, which began as a result of plume-related rifting, which lead to the development of the sedimentary and volcanic rocks of the 2.45-2.2 Ga Huronian Supergroup. Subsequently, it was intruded by the 2.4-2.5 Ga East Bull Lake suite as well as the 2.4-2.5 Ga Matachewan and Hearst Dyke swarms. Later, emplacement of the 2.2 Ga Nipissing Gabbro suite intrusions in the Huronian Supergroup and Archean basement occurred.

Noble and Lightfoot (1992) showed that the emplacement of intrusions of the Nipissing Gabbro suite was concurrent with the 2206-2223 Ma Blezardian Orogeny. Buchan et al. (1998) suggested that the Nipissing Gabbro suite was fed by the 2.2 Ga Senneterre Dykes, whose source was a mantle plume centered southeast of Ungava Bay. Lightfoot et al. (1987) suggested that the Nipissing Gabbros represented the eroded remnants of a continental flood basalt province.

The entire area in which the Nipissing Gabbro suite is hosted was deformed during the 1900-1850 Ma Penokean Orogeny, resulting in varying regional metamorphic grade across the

length of the Nipissing Gabbro suite (Sproule et al., 2007). In the Cobalt Plate area, the rocks are relatively undeformed and metamorphism is confined to sub-greenschist facies (Card and Pattison, 1973). However, Nipissing Gabbros between Sudbury, Ontario, and Blind River, Ontario, have undergone higher deformation and metamorphism ranging between greenschist and amphibolite facies.

1.2 - Geology of the Nipissing Gabbros

The Nipissing Gabbros of Ontario were emplaced at 2.22 Ga within the 2.4 Ga Huronian Supergroup and are localized along the Archean-Proterozoic unconformity (Lightfoot and Naldrett, 1996). They are composed of dominantly tholeiitic to calc-alkaline intrusions. The intrusions have a range of compositions and consist of some combination of chilled diabase to quartz diabase, gabbronorite, gabbro, varitextured gabbro, pegmatitic gabbro, quartz diorite, granodiorite, granophyre, and aplitic granitoids. The intrusions extend from Sault Ste. Marie, Ontario east through the Sudbury, Ontario region to the Cobalt, Ontario and Gowganda, Ontario regions.

Lightfoot and Naldrett (1996) conducted a thorough investigation into the petrology and geochemistry of the Nipissing Gabbro, described the geochemistry and textures of Ni-Cu-PGE mineralization contained therein, and provided a concise summary of the genesis of the Nipissing Large Igneous Province. They found that mineralization associated with magmatic processes in the Nipissing was largely in the form of disseminated Cu-Ni-PGE sulfides within the intrusion or as massive pods beneath the intrusions. They observed that the silicate hosts of the sulfides tended to be poorly differentiated to undifferentiated, with some evidence for

cyclical trends in composition (after Conrod, 1989). They also observed that the “intrusions which are heavily contaminated in their roof zones... appear to be relatively unmineralized, and the low Cu/Yb and Cu/Zr of the most contaminated granophyric rocks is attributed to large amounts of assimilation of sediment with very low Cu/Yb and Cu/Zr rather than the fractionation of an immiscible sulfide liquid”. The intrusions that tend to be mineralized are the least differentiated, have a basinal shape, and are composed of gabbros that have a higher modal proportion of hypersthene and as a result an elevated MgO and low incompatible element concentrations. They suggested that either the disseminated sulfides are related to late emplacement of magmas or that sulfide immiscibility was achieved by differentiation after initial crystallization of significant amounts of hypersthene. No olivine cumulates are present, but high Mg pyroxene cumulates exist, approaching 14 % MgO.

Lightfoot and Naldrett (1996) reported no obvious difference in magma type between unmineralized and mineralized Nipissing Gabbros. Undifferentiated quartz diabase, quartz gabbro, and chill zones have a narrow range in incompatible element ratios such as La/Sm and Th/Y as well as similar abundance levels. They suggest many of the intrusions were derived from the same source and that they did not differentially mix with or become contaminated by crustal reservoirs enroute to the surface. The Nipissing intrusions were emplaced with roughly the same degree of differentiation throughout the Nipissing event.

Cu/Zr ratios of gabbros with sulfur concentrations below detection limits are not significantly different when compared to mineralized intrusions suggesting very little differential depletion of intrusions in copper by the segregation of immiscible sulfide (Lightfoot and Naldrett, 1996). Fresh olivine from unmineralized intrusions show elevated nickel contents in olivines with Fo₆₀₋₇₀ suggesting the magma had not equilibrated with sulfide.

Lightfoot and Naldrett (1996) point out that mineralized Nipissing Gabbro intrusions with significant quantities of disseminated sulfide are located southwest of Sudbury in the Nairn, Lorne, Denison, Waters, Hyman, and Drury townships and east of Sudbury (Wanapetei) as well as to the northeast of Sudbury in the Kelly and Janes townships. Sulfides are fine disseminations of magmatic pyrrhotite (50-75%) with lesser chalcopyrite and pentlandite. Some sulfides exhibit blebby magmatic textures with pyrrhotite rich upper segments and chalcopyrite rich lower segments.

According to Lightfoot and Naldrett (1996) the Wanapetei intrusion has a small occurrence of copper rich massive sulfides, which carries 1-15% Cu, 2.5-6.3ppm Pt, 17-53 ppm Pd, and 1-6ppm Au. However, the disseminated sulfides tend to be focused in the interior of the sills with coarse gabbroites and hypersthene-rich gabbros. Disseminated sulfides from an intrusion in Janes Township carry 200–1100 ppb Pt and 50-4000 ppb Pd.

Lightfoot and Naldrett (1996) stated that the presence of magmatic sulfides towards the centre of sills suggests either that magmas were initially injected free of sulfide and that subsequent magmas were injected as sulphur saturated magmas or that the differentiating liquid became sulphur saturated only after it had time to fractionate and/or mix with a new pulse of more primitive liquid.

1.3 - Geology of the Shakespeare Intrusion

The Shakespeare intrusion intrudes the Hough Lake Group metasediments of the 2.45-2.2 Ga Huronian Supergroup and that the intrusion is hosted in the quartzites of the Mississagi Formation, which are medium-grained and massive to graded (Sproule et al., 2007 and

references therein). The intrusion dips north at a 40-80° and has experienced a greenschist to amphibolite facies regional metamorphism. The intrusion was dated at 2217 Ma by Sutcliffe et al. (2002) using the U-Pb single zircon TIMS method.

Sproule et al. (2007) separated the Shakespeare into two parts: The first, called the Lower Group, is composed of unmineralized pyroxenite and gabbro. The second, called the Upper Group, is composed of mineralized melagabbro, quartz gabbro, and biotite quartz gabbro (or diorite). They noted that the Upper Group is variably chilled against the Lower Group, suggesting the Lower Group was partially crystalized upon injection of the Upper Group magma. They also observed that mineralized melagabbro dykes cut into the unmineralized Lower Group and speculated that they could either be feeders to the Upper Group or small apophyses cutting the Lower Group (Figure 2). In samples that Sproule et al. (2007) observed, pyroxenes in all units were completely altered to chlorite, plagioclase was moderately to strongly altered to fine-grained micas, and trace biotite (< 2 %) was associated with sulfides in the mineralized melagabbros.

Sutcliffe (2002) described thin sections of the Shakespeare deposit lithologies from the first drill holes to intercept Ni-Cu-PGE bearing sulfides along the eastern extension of the deposit. He found that the rock known as biotite quartz diorite contains 25% Quartz, 20% plagioclase (which are strongly replaced to sericite and epidote), 15% chlorite, 15% biotite, 20% epidote/clinozoisite, 5% sericite as an alteration product of feldspars with epidote, and

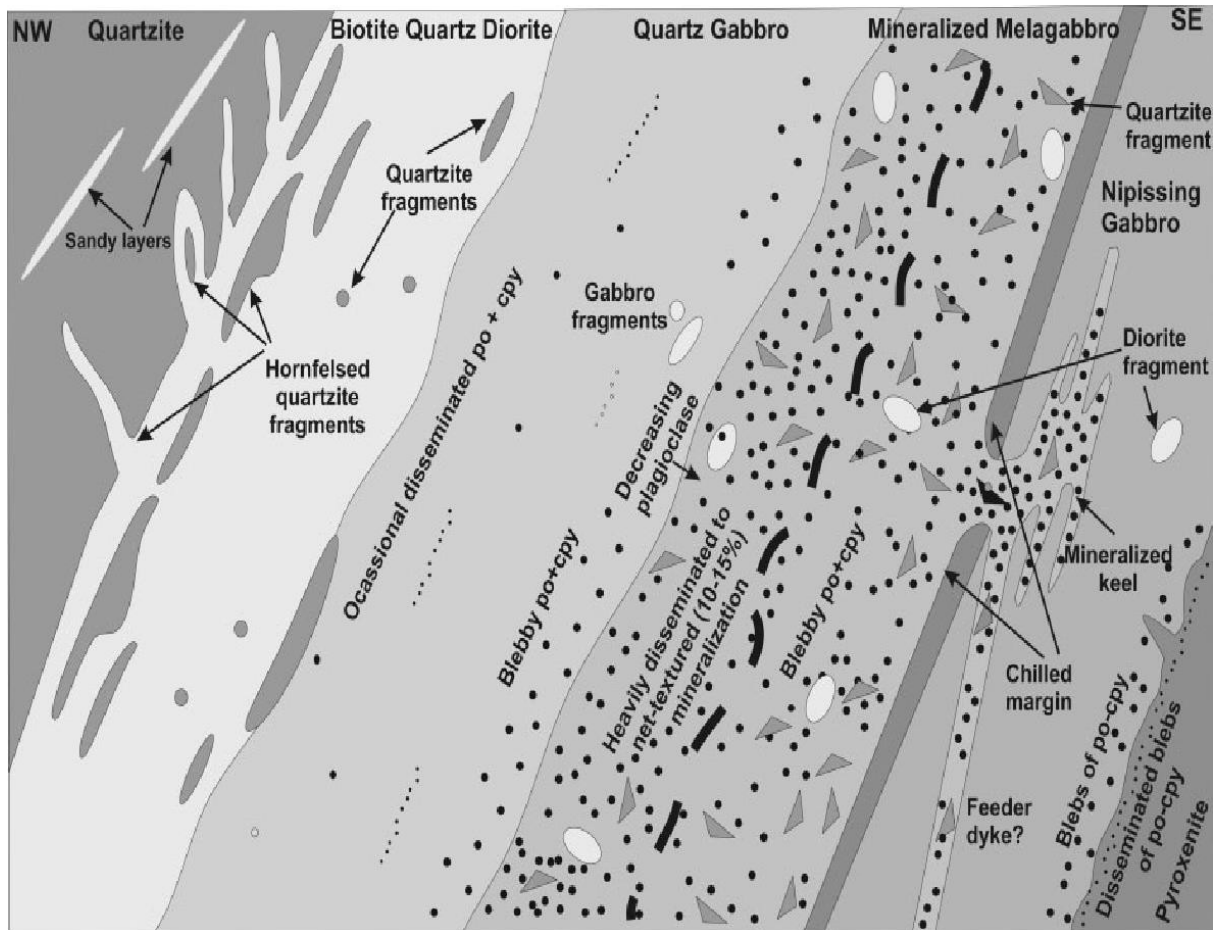


Figure 2: Illustrated cross section of the Shakespeare intrusion. cpy: chalcopyrite; po: pyrrhotite; pn: pentlandite. Reprinted from Sproule et al. (2007)

trace amounts of titanite. The rock was termed a tonalite at first based on field characteristics and then was changed to a biotite quartz diorite as a result of some similarities between the whole rock geochemistry of the Shakespeare biotite quartz diorite and the diorites of the Sudbury offset dykes.

Sutcliffe (2002) described the quartz gabbro as 40% plagioclase (moderately to strongly replaced), 3% quartz, 35% clinopyroxene, 15% amphibole, 5% epidote/clinozoisite (overgrowing plagioclase), trace opaques, and trace titanite. He also noted the presence of an altered quartz gabbro containing 25% plagioclase (strongly replaced), 5% quartz, 55% amphibole, 15% epidote/clinozoisite, trace opaques, and trace titanite.

The melagabbro was described as either : a “Melanocratic Biotite Amphibole Gabbro” containing 5% plagioclase(moderate replacement to epidote/clinozoisite), 50% amphibole, 10% quartz, 10% biotite, 10% chlorite, 5% epidote/clinozoisite, 8 % sulfide, trace titanite, trace oxide, trace phlogopite?, trace carbonate, and trace talc? (replacing a relict pyroxene grain) or as a “Biotite Amphibole Clinopyroxenite (Metapyroxenite)” containing 25% clinopyroxene (variably rimmed or replaced to green pleochroic amphibole), 20% chlorite, 15% opaques, 15% biotite, 15% amphibole, 5% quartz, 3% unknown (scapolite?, clinozoisite?), trace titanite, and trace carbonate in matrix (Sutcliffe, 2002).

Sproule et al. (2007) noted that the biotite quartz diorite, quartz gabbro, and parts of the melagabbro contained abundant blue quartz eyes, xenoliths of quartzite, and diorite fragments which were possibly autolithic. They also report the presence of minor, coarse disseminated to patchy net-textured zones of pyrrhotite, chalcopyrite, pentlandite, and

gersdorffite in the upper portion of the melagabbro and small blebs of pyrrhotite and chalcopyrite in the lower sections of the melagabbro and at the base of the quartz gabbro within the Upper Group. They also noted the presence of pyrite in trace amounts elsewhere in the intrusion.

Sproule et al. (2007) conducted an SEM study of several samples containing abundant concentrations of sulfide minerals and 738 – 1180 ppb Pt + Pd. They found abundant bismuth tellurides (tellurobismuthite or tsuomite) as well as much rarer Co-S-(As), Bi-Te-(S), and SbBiTeS(Fe) minerals.

The Shakespeare intrusion is similar to the typical Nipissing Gabbro because it shows “tholeiitic affinities, LREE-depletion, enrichment in HILE [highly incompatible lithophile elements], and is typical of magmas which have experienced crustal contamination” (Sproule et al., 2007). However, the Shakespeare intrusion appears to be more contaminated than other parts of the Nipissing Gabbro based on geological features (quartz eyes and fragments of quartzite and diorite) and geochemical features (Th/Zr and La/Sm).

Sproule et al. (2007) suggested crustal contamination led to the separation of an immiscible sulfide liquid which concentrated Ni, Cu, and PGE. The immiscible sulfide liquid then accumulated at the base of the deposit via gravitational settling onto the top of a cumulate pile. They noted that metal tenors in sulfide appeared independent of total sulfide content, suggesting the system was extremely well homogenized. Sproule et al. (2007) suggested that based on variable fragment types and the presence of potential feeder dykes, the contamination event that led to the production of an immiscible sulfide occurred prior to final emplacement.

Chapter 2: Purpose

The model that Sproule et al. (2007) proposed whereby the sulfide minerals present in the Shakespeare Intrusion were formed as a result of crustal contamination appears to be a plausible hypothesis to explain the genesis of economic concentrations of sulfides. However, the proposed model remains vague on the precise mechanisms by which such a contamination event could lead to the precipitation of an immiscible sulfide liquid.

For instance, many workers have suggested and shown that the addition of crustal sulfur via assimilation into an intruding magma of mafic–ultramafic affinity is a highly effective means of creating an immiscible sulfide liquid, which then interacts with the melt in order to upgrade the sulfide metal concentration (Ni, Cu, Co, PGE) in the sulfide liquid. The genesis of many world class Ni-Cu-PGE deposits are largely attributed to this process, and Keays and Lightfoot (2009) argue that magmatic Ni-Cu-PGE deposits cannot form without the addition of crustal sulfur.

Others, however, suggest that the addition of silica via assimilation into an intruding magma of mafic affinity has the effect of lowering the solubility of sulfur in the magma which could lead to a precipitation of immiscible sulfide liquid. Significant assimilation of crustal materials can increase the silica concentration in a mafic magma to the point that it will preferentially crystallize pyroxene first and not olivine as the magma cools (Ripley and Li, 2013). In open system environments where multiple batches of highly contaminated magma can mix and sulfides can be effectively segregated, it may be possible to produce an immiscible sulfide liquid without the addition of significant crustal sulfur.

Sproule et al. (2007) proposed that the fragments observed in the melagabbro – rock fragment phase and quartz gabbro phases were evidence of contamination close to or inside the magma chamber. They observed fragments of several different compositions but did not suggest mechanisms which could account for the differences in composition. Sproule et al. (2007) suggest that the diorite fragments might be autolithic, but provide no mechanism by which an autolith could form.

Additionally, a partially erroneous observation that sulfides in the Shakespeare deposit tend to have remarkably uniform sulfide metal concentrations requires clarification and investigation. The sulfide metal concentrations within sulfides with certain textural features, and the associated stratigraphic depth of those textures, are remarkably similar. However, the difference in sulfide metal concentrations between sulfides with different textural features is substantial. The interconnected sulfides described by Sproule et al. (2007), which straddle the quartz gabbro / melagabbro-rock fragment phase boundary, have significantly lower sulfide metal concentrations than the disseminated sulfides which are found within the melagabbro-rock fragment phase.

The difference between the types of contamination which can lead to sulfur saturation in a mafic-ultramafic magma has a direct impact on the genetic constraints of other Shakespeare-like deposits in the Nipissing LIP. In addition, textural features in the sulfides and silicate fragments, the mineralogy of the deposit, and observed geochemical data require answers to the following questions. By what mechanism did the magmas at Shakespeare become saturated in sulfur? What is the source of sulfur? Do autoclasts exist at Shakespeare? If so, how did they form? How did the interconnected sulfides form on top of the disseminated sulfides? What evidence is present to suggest gravity settling of sulfides into a cumulate mush? Are there differences in the sulfide mineral species present depending on textures and stratigraphic height? If so, how do they progress? Based on mineralogy, what are the proper names for the rocks at Shakespeare?

As a result of questions arising out of the model which Sproule et al. (2007) proposed and new data which appears to oppose earlier observations, a careful re-examination of the Sproule et al. (2007) model is warranted in order to better understand the genesis of the Shakespeare deposit.

Chapter 3: Methodology

3.1 - Field Work and Sampling

Diamond drill hole U-03-118 was logged by Ian Dasti supervised by Harold Tracanelli (P.Geo) during April, 2011. Diamond drill holes U-03-119 and U-03-122 were logged by Ian Dasti and Harold Tracanelli (P.Geo) during April and May, 2011.

Field sampling took place during May and June of 2012. Diamond drill holes U-03-118, U-03-119, and U-03-122 were chosen for sampling at 1.5 meter intervals for unmineralized lithologies and at 1 meter intervals for mineralized lithologies. Samples which had been previously sampled for industry use were quarter split, while drill core which had not been previously sampled were half split using a core saw. Holes U-03-118, U-03-119, and U-03-122 were the drill holes sampled, as they characterized the mineralogy and grade of the deposit better than any of the other drill holes that were available. Within the roof zone, if a sample interval fell within a medium sized quartzite xenolith (sub-meter scale), the sample interval was moved to the quartz diorite immediately adjacent to the xenolith. For other larger xenoliths (larger than 1 m and less common), samples were taken at the regular sample interval in order to reasonably preserve the presence and geochemical impact of these rafts within the intrusion.

Additional samples were taken in parts of the intrusion that were representative of the units or textures described in other holes logged by Ian Dasti and Harold Tracanelli. Those samples were used in addition to the samples taken at regular intervals for transmitted and reflected light petrography as well as SEM-EDS analysis.

In total, 284 samples were collected for analysis, and 64 polished thin sections were made for petrographic analysis and SEM-EDS analysis.

3.2 - Thin Section Analysis

The polished thin sections were made at Lakehead University in the Department of Geology's rock preparation lab by Anne Hammond or Kristi Tavener. Transmitted light

microscopy and reflected light microscopy was conducted using an Olympus DP-70 microscope located in the Department of Geology.

Scanning electron microscopy – energy dispersive X-ray spectroscopy (SEM-EDS) analysis was conducted at the Lakehead University Instrumentation Laboratory (LUIL) using the Hitachi Su-70 Schottky Field Emission SEM fitted with an Oxford Aztec 80mm/124 eV energy dispersive X-ray spectrometer. All slides were coated with a thin film of carbon prior to analysis. The Oxford Instruments software program Aztec was used to construct line scans, element maps, electron images, and spectrum diagrams.

During the course of SEM-EDS analysis of several thin sections, a multi contrast approach whereby low, medium, and high contrast displays of the same images were employed. This enabled the visual recognition of higher contrast (metallic phases and phases with atoms of higher atomic number), medium contrast phases (such as certain sulfide minerals, including possible solid solutions within sulfides), and low contrast phases (such as common iron sulfides). The method also provided an effective means of distinguishing between phases which might otherwise have been unobservable as a result of “white out”, where multiple phases appear as a singular phase as a result of very minor contrast differences at low settings.

Thin sections from blebby, interconnected, and disseminated sulfides were analyzed in order to determine what mineral species were associated with sulfide minerals within the Shakespeare deposit. However, previous studies by Sproule et al. (2007) focused on samples with the highest overall grade of base metals and platinum group elements (PGE) instead of samples containing sulfides with the highest metal tenors. By focusing more on samples with higher metal tenors, the chances of observing minerals containing PGE increased substantially. Standards for quantitative analysis were selected from the available standards at the LUIL and are listed in appendix 1. Appropriate standards for certain elements were unavailable, and as a result the factory calibration was used.

Initially, the Michel-Levy method was attempted in order to determine the anorthite content of plagioclase in various Shakespeare lithologies. Those attempts were generally unsuccessful as a result of partial or complete replacement of plagioclase by albite. However,

samples taken from the melagabbro generally had lower degrees of plagioclase replacement and yielded definitive anorthite compositions.

3.3 - Geochemical Analysis and Powder X-Ray Diffraction Analysis

In total, 284 samples were sent to Accurassay Laboratories in Thunder Bay, Ontario for inductively coupled plasma optical emission spectrometry (ICP-OES), fire assay – atomic absorption spectroscopy (FA/AAS), and fused disk X-ray fluorescence spectroscopy (XRF). 206 of those samples were analyzed by Accurassay Laboratories for total sulfur and total carbon by LECO analysis. Samples analyzed by ICP-OES were prepared using a multi acid closed beaker digestion method. 49 samples were later reanalyzed by Activation Laboratories Ltd in Thunder Bay, Ontario, via inductively coupled plasma mass spectrometry (ICP-MS) and were prepared using a four acid digestion method (laboratory preparation code UT-4).

The samples sent to Accurassay Laboratories for were dried, crushed, and then pulverized, with the final product grainsize passing $x > 90\%$ at 200 mesh (74μ). For ICP-OES, the pulps were digested using a multi-acid, closed beaker approach consisting of hydrofluoric, nitric, perchloric, and hydrochloric acids. The ICP-OES analysis was performed on a Varian ICP725 atomic emission spectrometer. A multi-acid, closed beaker digestion method was chosen because a small amount of residuum was noted in some of the samples that URSA Major Minerals conducted via aqua regia.

For XRF analysis, samples were made into fused disks with lithium metaborate / lithium tetraborate flux using a M4 fusion machine and were then analyzed on a S8 Tiger XRF. Values obtained were then normalized to 100%. FA/AAS was performed on an AA240 FS atomic absorption spectrometer.

Ten sulfide samples were sent to Activation Laboratories Ltd in Ancaster, Ontario, for $\delta^{34}\text{S}$ analysis. The sulfide samples were prepared by gravity settling followed by magnetic separation. Activation Laboratories Ltd. then weighed into tin capsules with 4mg of tungstic oxide and loaded them into a Costech (Italy) elemental analyser for flash combustion at 1100°C . The resulting gas was carried with helium in order to separate the sulfur dioxide via gas

chromatography. The clean sulfur dioxide was then analysed by a VG 602 IRMS. Analytical precision (1σ) for pure FeS_2 has been reported as $\pm 0.3\%$. All results are reported relative to CDT.

Metal tenors were calculated by the method described by Kerr (2003). The metal values for nickel, copper, and cobalt were taken from the ICP-OES data and platinum, palladium, and gold were taken from FA-AAS data. Sulfur data was obtained via LECO analysis. Sulfur/selenium ratios were calculated by dividing sulfur (ppm) by selenium (ppm). Selenium data was obtained via ICP-MS analysis. All geochemical models, tables, and graphs were generated using either loGas or Microsoft Excel.

R factors were calculated using the spreadsheets provided and method described by Kerr and Leich (2005). The assumed initial concentrations were taken from Sproule et al. (2007) and are as follows: 12 ppb platinum, 15 ppb palladium, 200 ppm nickel, and 160 ppm copper. Partition coefficients used were the same as applied by Sproule et al. (2007) except for copper ($D=1200$). The partition coefficient for copper ($D=1200$) was chosen as an approximate median of reported values. The partition coefficients for nickel are less than for copper and modeling is not sensitive to absolute values (Naldrett, 2011)

Powder X-ray diffraction (XRD) analysis of several pulps was conducted at the LUIL using a Pananalytical Expert Pro Diffractometer using $\text{CuK}\alpha$ radiation, scanning from a 2θ of 6° to 96° using a Pixel detector (linear 2θ step measurements with 3° 2θ measurement window). Each individual analysis took approximately 20 minutes to complete. The results were interpreted with the Hi Score Plus software using a ICDD PDF2 2008 database to match peaks. Samples were taken from reject pulps from the geochemical analysis. The pulps were pressed into the cavity of a sample slide and then analysed. The analysis was conducted in conjunction with transmitted light microscopy and reflected light microscopy in order to determine the mineralogical composition of Shakespeare rocks.

Chapter 4: Results

Diamond drill hole logs are presented in Appendix 2, are illustrated in Figure 3, and locations are shown in Figures 4 and 5. In addition to drill holes logged in this study, over 100 other drill holes have been logged by URSA Major Minerals staff and sampled in order to clearly define the stratigraphy of the Shakespeare deposit (some are shown in Figure 5).

4.1 - Transmitted and Reflected Light Petrography

Results of the transmitted light and reflected light study are grouped according to lithologies documented in field logs. Visual identification criteria for distinction between lithologies in drill core and hand samples are also provided.

Quartz diorite – Defined in hand sample by the abundance of quartz and biotite, moderate to intense mineral lineation, and abundant quartzite xenoliths, and abundant blue quartz. Widths from 0 to 90 meters have been intersected but are most commonly over 50m thick. This unit is composed of 20-50% biotite (variably replaced by chlorite, up to 20% abundance), 20-40% quartz, 5-15% clinozoisite, and 5-15% strongly albitized plagioclase and trace (locally 1%) opaques (Figure 6). Biotite, chlorite, and clinozoisite are generally fine- to medium-grained. Most quartz is usually in the form of multiple grains of varying sizes (0.01mm to 0.5mm) clumping together resulting in blebby aggregates up to 2mm in size. Commonly, small quartz grains are found disseminated amongst biotite/chlorite and clinozoisite grains. Generally, as biotite concentration goes up, clinozoisite and albitized plagioclase increase and quartz decreases.

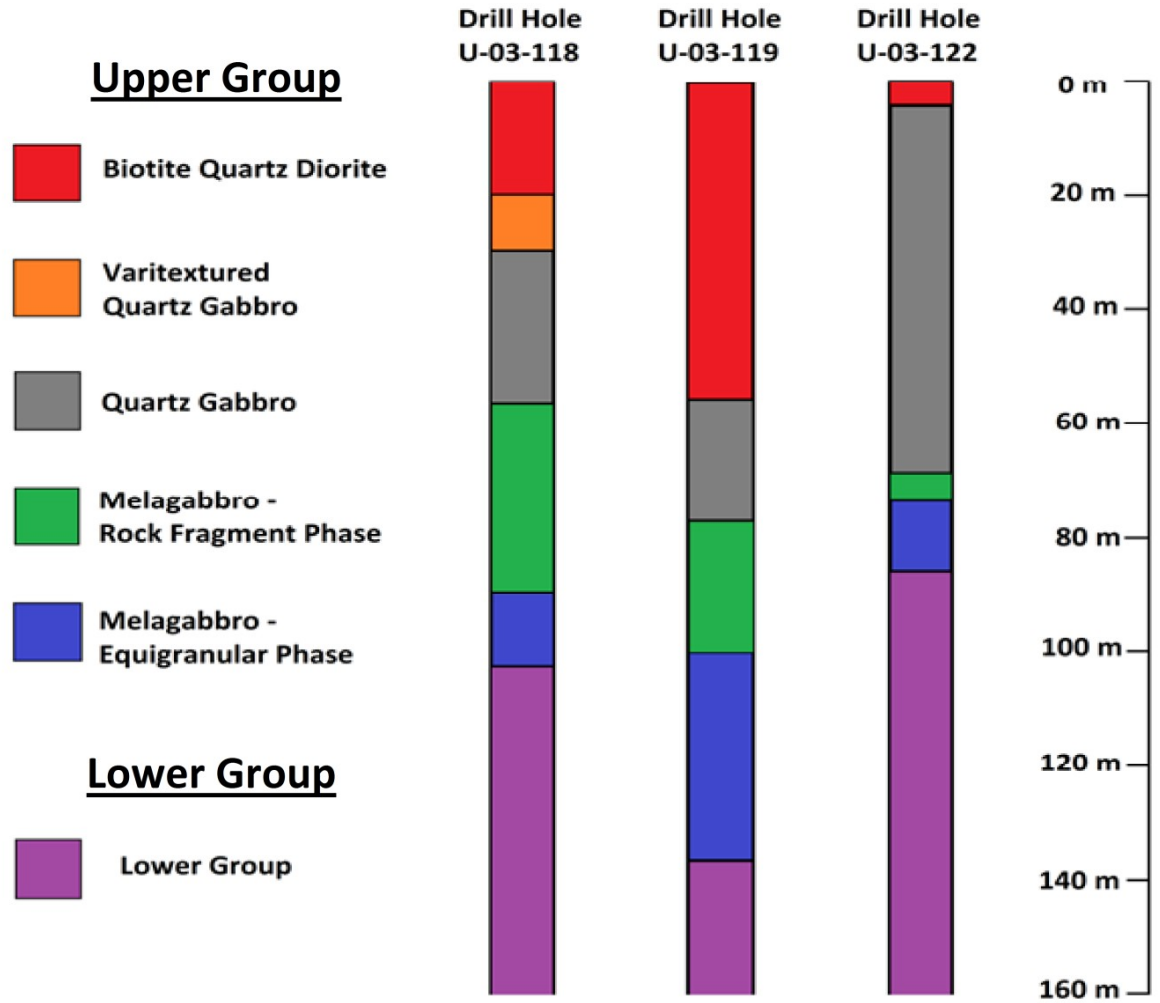


Figure 3: A schematic diagram of the diamond drill core logs for drill holes U-03-118, U-03-119, and U-03-122. 0m indicates the start of the Biotite Quartz Diorite lithology in the core logs.



Figure 4: A plan view satellite image of the Shakespeare deposit showing drill hole locations, the location of the west pit, and tailings pond. An approximation of the deposit, projected to surface, is also outlined. Drill holes were drilled at 14° azimuth. U-03-118 was drilled at a dip of 77.0° , U-03-119 was drilled at a dip of 65.9° , and U-03-122 was drilled at a dip of 75.0° . The respective intersections of the drill holes can also be found in Figures 3 and 5. Satellite image obtained using Google Earth (2012).

SHAKESPEARE Ni-Cu-PGE DEPOSIT

Long Section Looking North

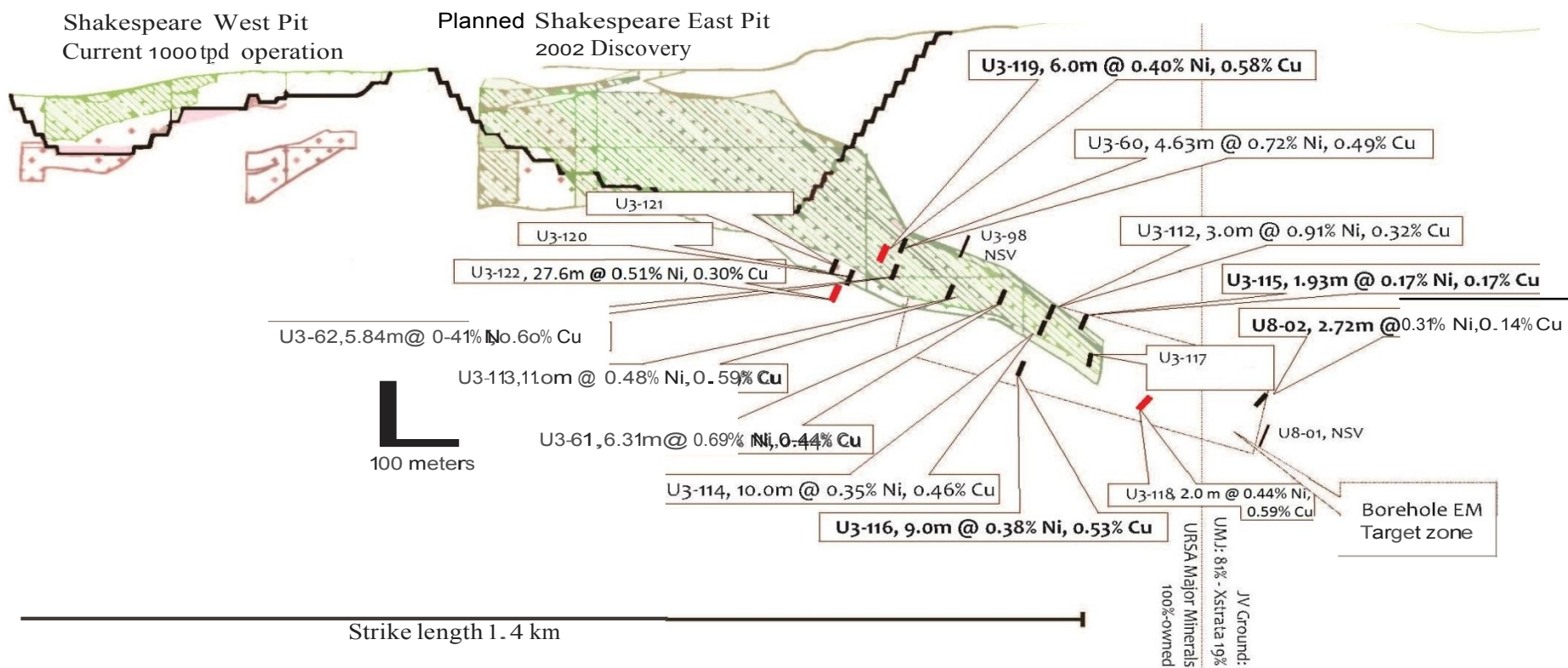


Figure 5: Shows an illustrated long section of the Shakespeare deposit, facing north. The various drill intercepts into the ore body, which dips north approximately 60°, are projected onto the section. Drill holes U-03-118, U-03-119, and U-03-122 are highlighted in red. Modified with permission from Wellgreen Platinum (2014).

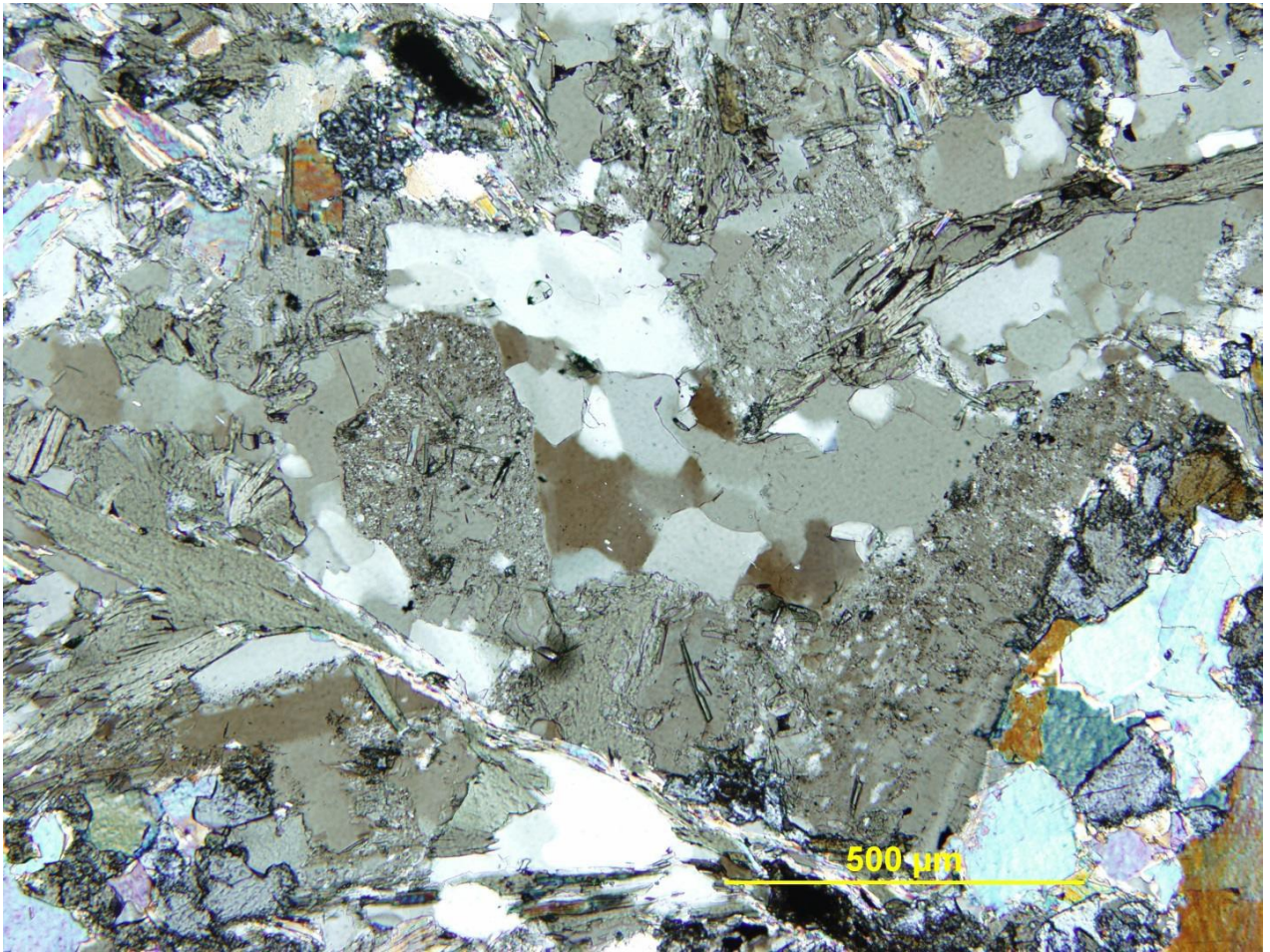


Figure 6: A microphotograph of biotite quartz diorite taken from sample 119-310.8 that shows heavily pitted plagioclase (and associated albite), actinolite (green), quartz, fine grained clinzoisite (high relief, blue color), and biotite. Microphotograph taken under plain polarized light and 10x magnification.

Opaques consist of 0.05-0.1mm grains of ilmenite with titanite rims or sulfide blebs. Ilmenite grains uncommonly contain lesser rutile and chalcopyrite (Figure 7). Sulfide blebs are of varying sizes, from as small as 0.01mm disseminations to 1.5mm blebs. The dominant mineral species is pyrrhotite, with lesser pyrite and very rare pentlandite. A number of observed sulfide grains have a very close spatial association with some ilmenite grains and occasionally appear to be replaced by oxides.

The contact between quartz diorite and quartz gabbro is usually gradational over 1 to 3 meters. In drill core, the change is marked by a decrease in quartz and biotite and an increase in amphibole, as well as a distinctive "salt and pepper" texture.

Quartz gabbro –In drill core, sulfides exist as coarse (occasionally over 1 cm) blebs, dominantly pyrrhotite / pentlandite with minor chalcopyrite. Generally this unit is fine- to medium-grained with coarser quartz grains (medium-grained) common. Coarse "diorite" rock fragments (Figure 7) are uncommon in this unit but tend to increase towards the melagabbro contact. Coarse quartzite xenoliths are common but decrease towards the melagabbro contact with less blue quartz eyes than in the quartz diorite unit. Widths from 5 to 65 meters have been intersected, but are more commonly between 10-20m thick.

Overall the silicate and oxide mineral phases present are 20-30% fine- to medium-grained biotite (chlorite replaces biotite, 5-10% total abundance), 10-15% fine clusters of acicular brown amphibole (actinolite), 15-20% fine- to medium-grained clinozoisite, 20-25% quartz, 15% variably albitized plagioclase, 5% fine- to medium-grained hornblende, 1-2% opaque minerals (Figures 8 and 9).

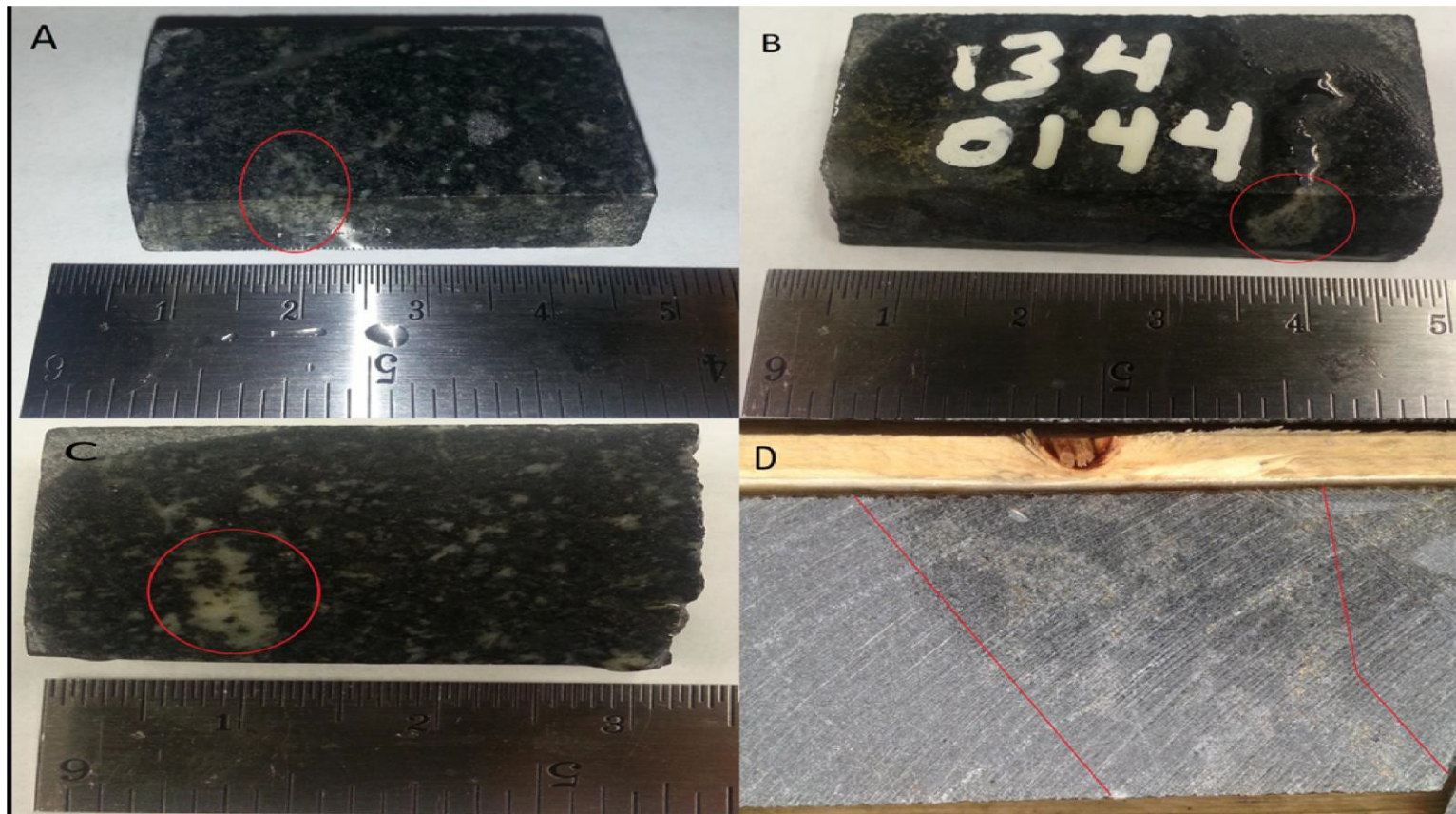


Figure 7: Photographs of various rock fragments as they appear in core samples. A) A small gabbroic rock fragment, circled in red. The sample was taken from U-03-119 at 302.5m depth. B) A rock fragment of possibly dioritic composition (circled in red). The sample was taken from U-03-118 at 533m depth. C) A rock fragment of gabbroic composition (circled in red). The sample was taken from U-03-118 at 530m depth. D) Rock fragments, between the red lines, containing chalcopyrite-pyrrhotite-pentlandite mineralization within an otherwise unmineralized section of melagabbro from U-03-118.

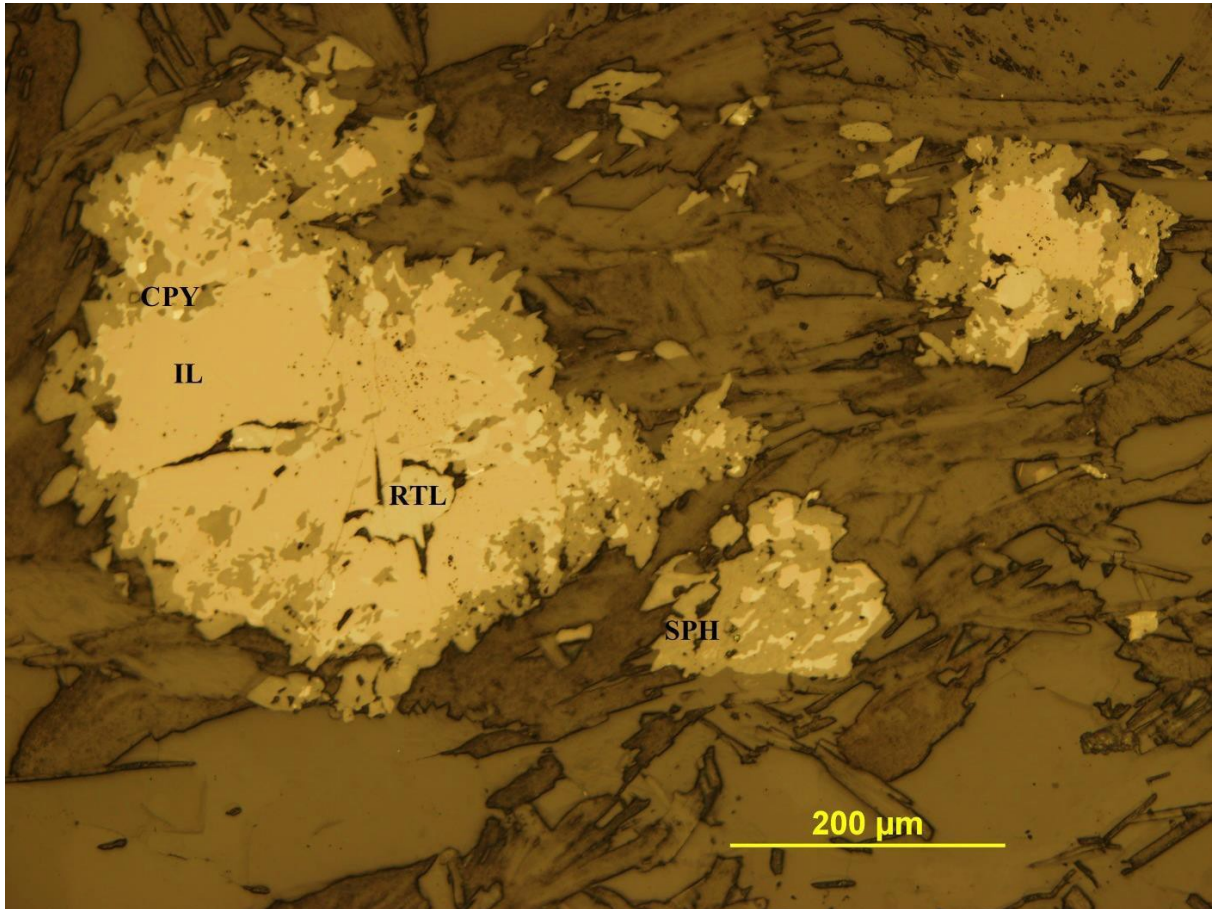


Figure 8: Photomicrograph taken from sample 119-310.8 of an ilmenite-rutile-chalcopyrite grain in the biotite quartz diorite unit, under reflected light and crossed polarized light at 20x magnification. IL: ilmenite; RTL: rutile; CPY: chalcopyrite; SPH: titanite

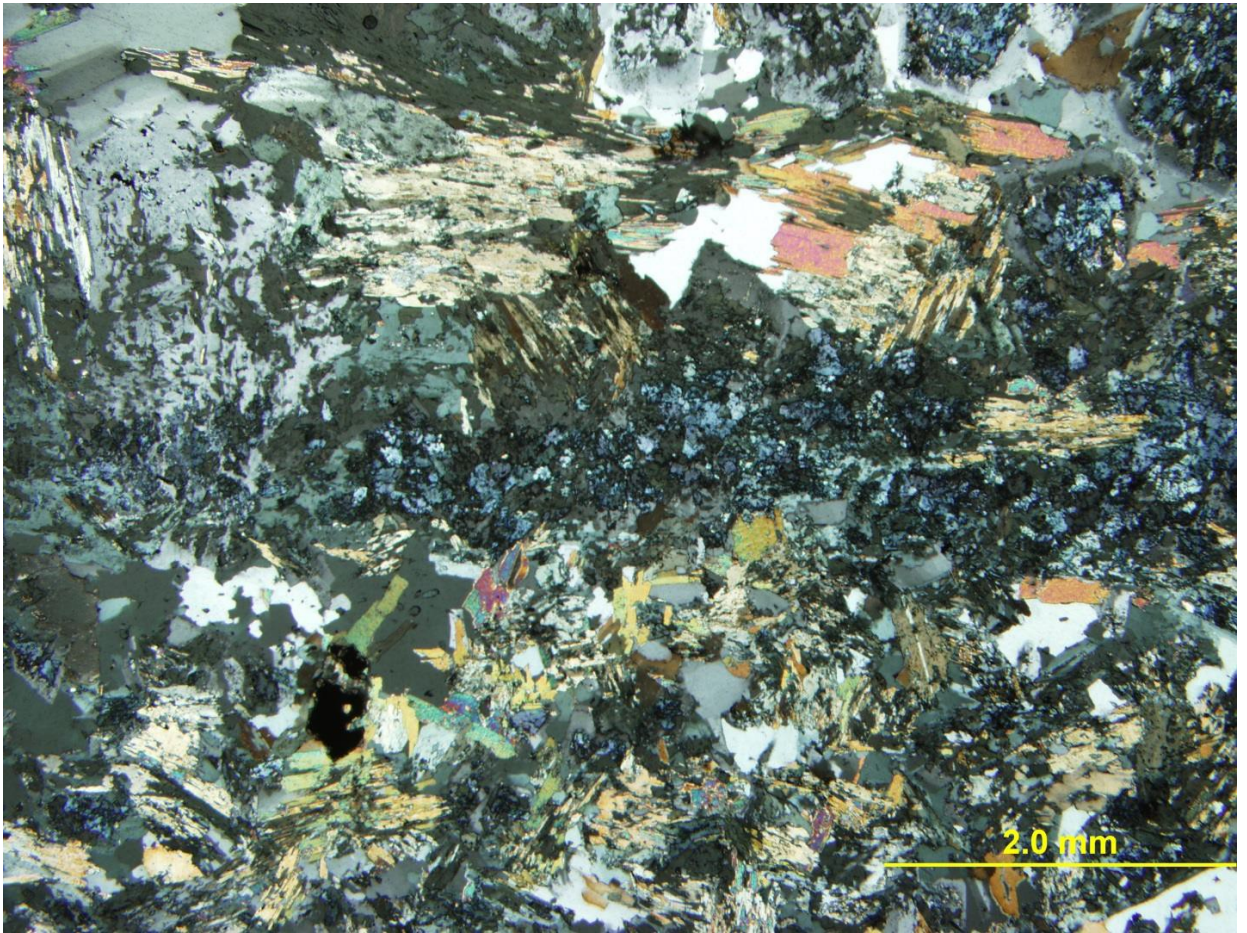


Figure 9: Photomicrograph taken from sample 119-340 of a rock fragment within the quartz gabbro lithology. The white rim which surrounds many rock fragments is fine clinozoisite, shown in this Photomicrograph as a band in the center of the image. The fragment contains coarser grains of the same minerals (in the same modal proportion) observed in the quartz gabbro lithology. Clinozoisite, actinolite, quartz, pitted plagioclase (with associated albite), and biotite are predominant minerals. Photomicrograph taken under crossed polarized light at 2.5x magnification

Plagioclase grains are commonly strongly albitized with lesser moderately albitized plagioclase. Unfortunately, attempts to determine the anorthite composition of the plagioclase via the Michel-Levy method were unsuccessful as a result of alteration. Quartz occurs mostly as coarser blebs as with the quartz diorite unit. The most common opaques are ilmenite with titanite rims, commonly with minor rutile and/or rare, 0.01mm sulfide grains.

Sulfides are present either as blebs and lesser disseminations (1-3% concentration) or as interconnected blebs to net textured sulfides near the contact between the quartz gabbro and melagabbro – rock fragment units. The sulfide minerals present in the blebs and lesser disseminations are dominantly pyrrhotite (90%) with lesser pentlandite (5-10%), and occasional chalcopyrite (0-5%). Fine to very fine grained, subhedral to anhedral cobaltite-gersdorffite grains were very rarely observed.

Net textured to interconnected blebby sulfides (15-25%, locally semi-massive 50%) are dominantly pyrrhotite (70-80%, uncommonly 50%), pentlandite (10-30%), and chalcopyrite (trace-10%, uncommonly 40%) and trace amounts of fine, euhedral to subhedral cobaltite-gersdorffite grains (Figure 10). Generally, there is a moderate to strong dissociation between pyrrhotite/pentlandite and chalcopyrite on a sub-meter scale. These sulfides commonly display a mild lineation fabric and uncommonly display a moderately to intensely lineated fabric.

Melagabbro (rock fragment phase) - Distinguished from the equigranular melagabbro unit (Figure 11) by the presence of visible rock fragments (Figure 7). It is distinguished from the quartz gabbro unit by the increase in amphibole and/or pyroxene, decrease in quartz, and loss of the “salt and pepper” texture in the quartz gabbro. Widths from 5-30m have been intersected but are most commonly 5-10m thick.

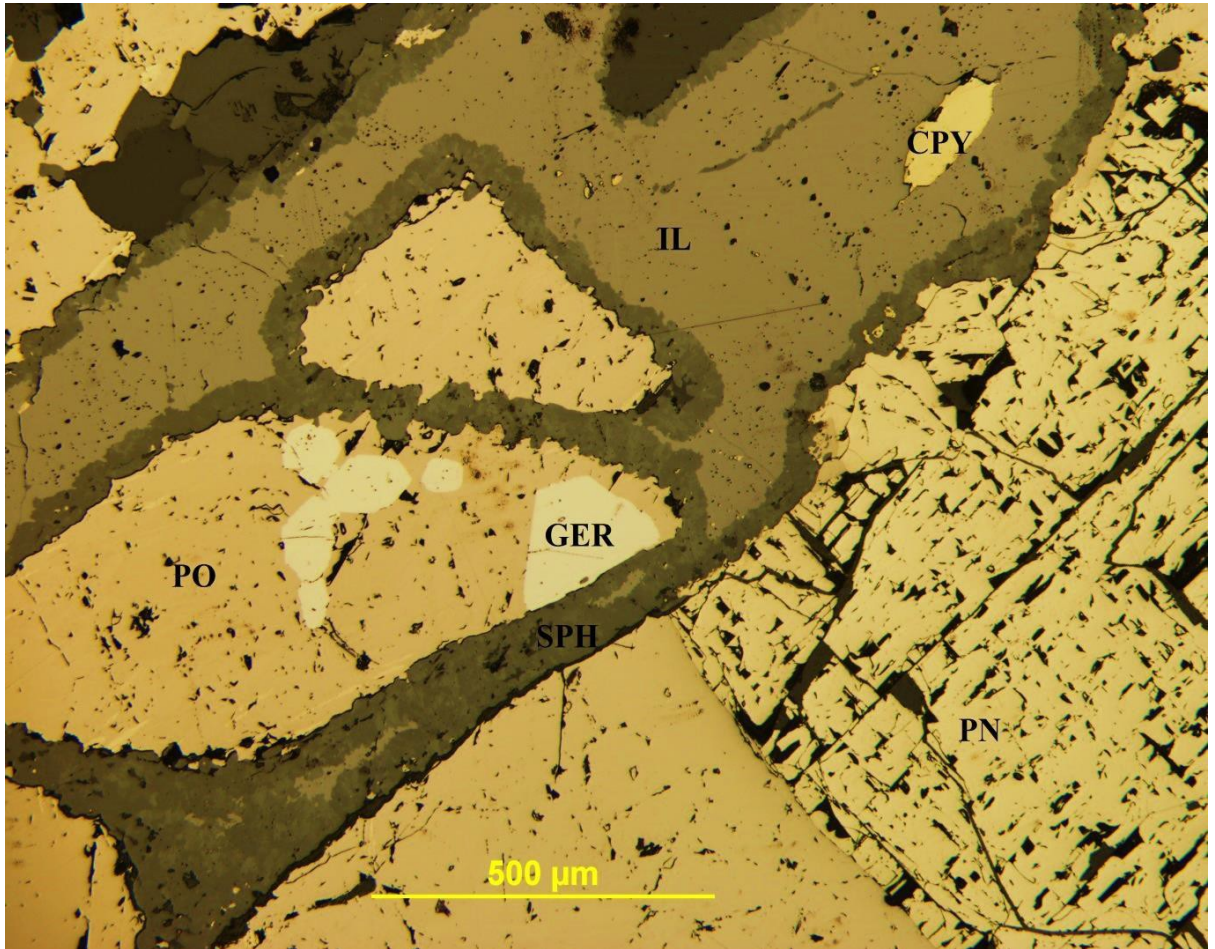


Figure 10: Reflected light photomicrograph of quartz gabbro sample 122-442.3 showing fine grained subhedral to euhedral gersdorffite-cobaltite within pyrrhotite and associated pentlandite under plain polarized light at 10x magnification. GER: gersdorffite-cobaltite; PO: pyrrhotite; PN: pentlandite; CPY: chalcopyrite; IL: ilmenite; SPH: titanite.

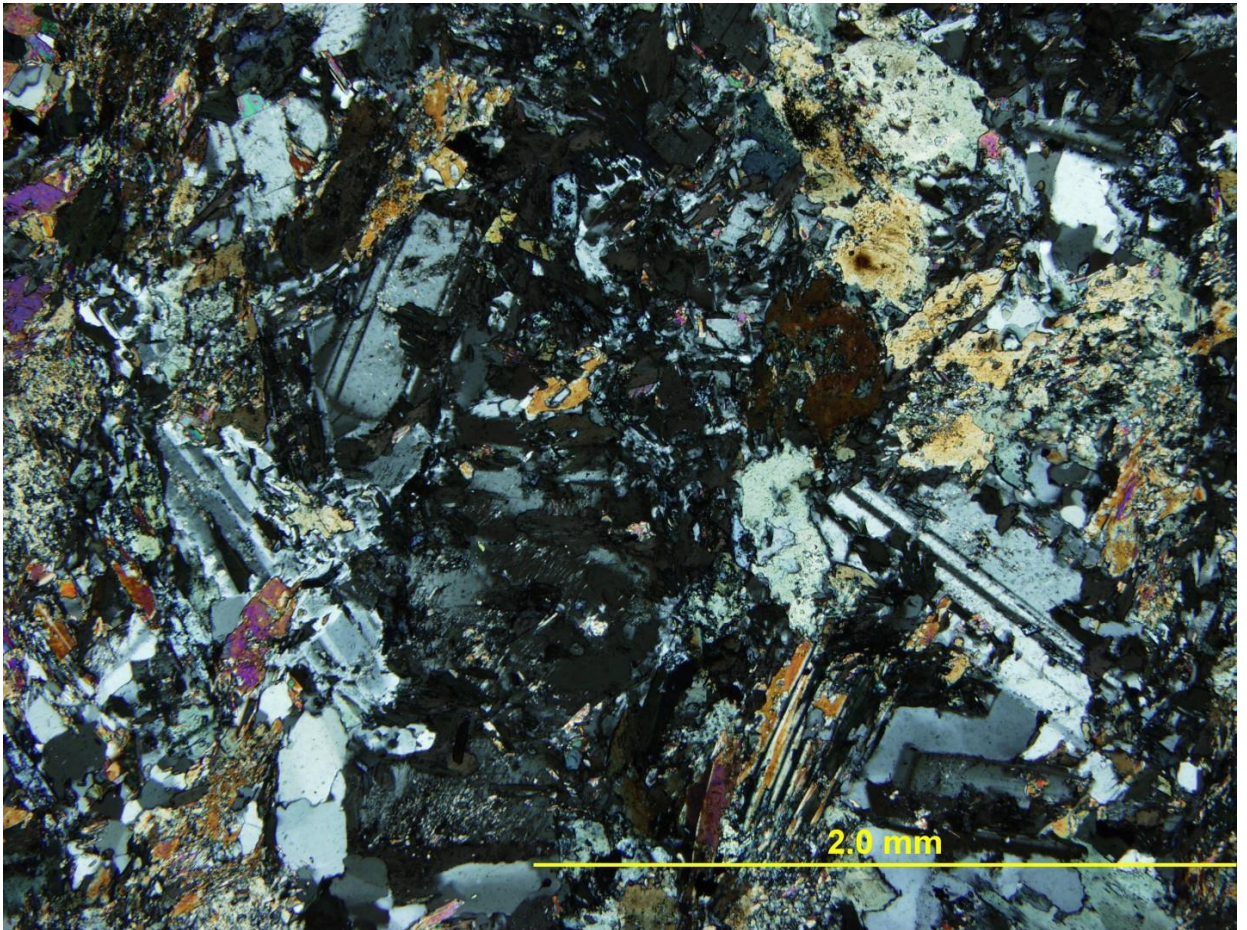


Figure 11: Photomicrograph taken from sample 119-376 (melagabbro – equigranular phase) displaying well preserved plagioclase, actinolite, and lesser quartz and biotite. Photomicrograph taken under crossed polarized light at 5x magnification.

The silicate and oxide content is highly variable, depending on the concentration and amount of rock fragments present and contains trace – 1% coarse rock fragments and up to 5% rock fragments of various sizes (Figure 11). This unit consists of 5-15% quartz, 15-25% clinozoisite, 5-10% biotite, 5-10% chlorite, 10-20% fine to medium grained hornblende, 20-30% actinolite replacing medium grained pyroxene (locally 5% less replaced to fresh clinopyroxene), 10-20% variably albitized plagioclase, and 0-5% titanite rimmed ilmenite, uncommonly with rutile +/- variable sulfide in the core (Figure 12).

Plagioclase grains vary from slightly fresh with minor albite to intensely pitted with abundant albite. Grains which still displayed good twins yielded compositions between An₄₈ and An₅₅. Relict simple twins in pyroxenes and amphiboles are common.

Rock fragments vary from 0.1mm (and possibly smaller) to over 1cm x 0.5cm (Figure 7). They have variable mineralogy and texture, but coarser grains are frequently rimmed with a 0.01-0.1mm fine grained clinozoisite-amphibole (actinolite?). Rock fragment types observed include:

- 1) Medium-grained materials containing clinozoisite, actinolite, hornblende, quartz, +/- biotite and chlorite – roughly equivalent to melagabbro
- 2) Fine-grained clinozoisite, fine-grained brown mineral, biotite – possibly representing a quartz gabbro or quartz diorite
- 3) Quartzite – large aggregates of quartz grains
- 4) Fine biotite, quartz, and actinolite – possibly representing a quartz gabbro or quartz diorite

Sulfides are present either as net textured to interconnected blebby pyrrhotite-pentlandite-chalcopyrite, as described in the quartz gabbro section, or as disseminated grains

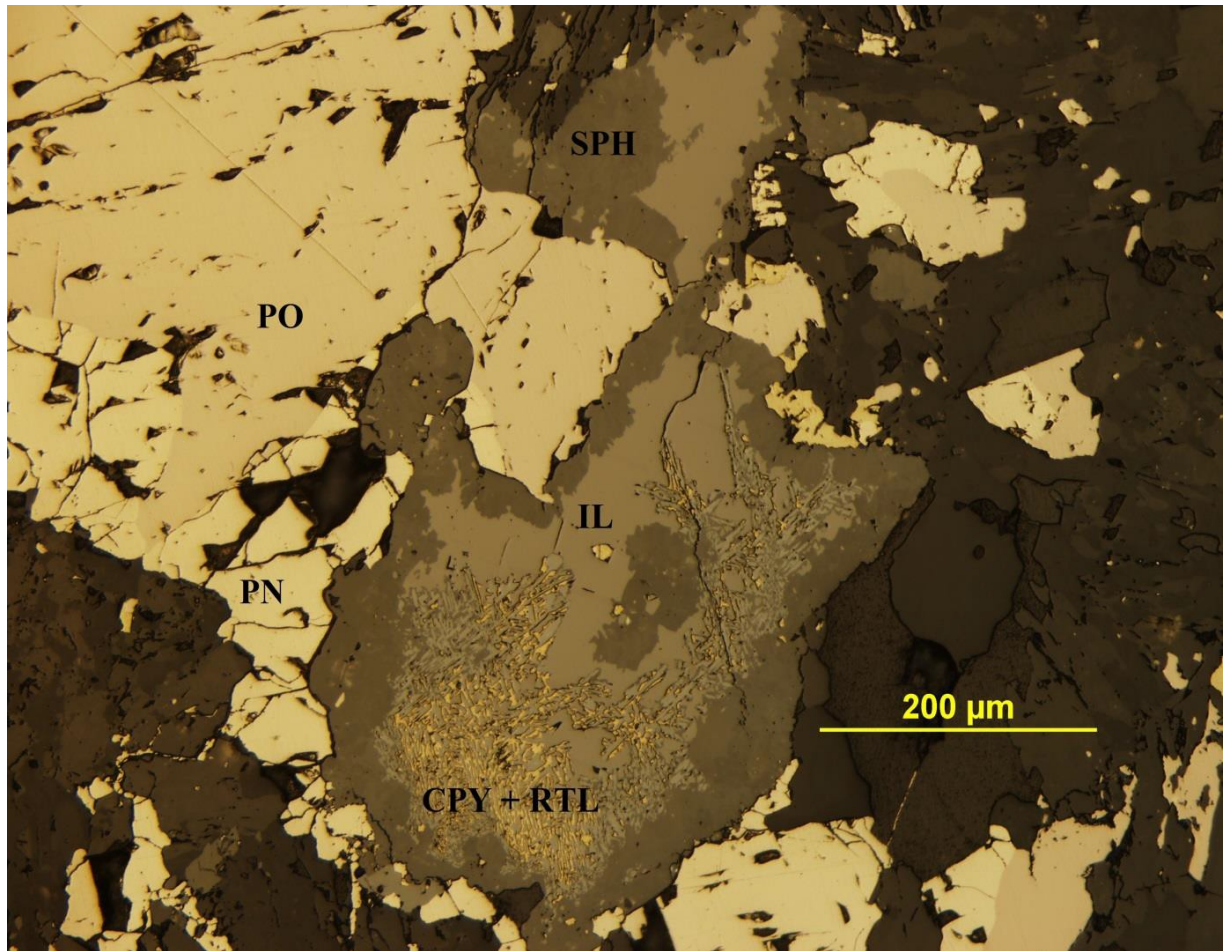


Figure 12: Photomicrograph taken from sample 119-356 of titanite rimmed ilmenite-rutile-chalcopyrite adjacent to unreplaced sulfide. The textures displayed by chalcopyrite and rutile suggest the replacement of sulfides with oxides. Chalcopyrite is common in the oxide cores whereas pyrrhotite and pentlandite are very rare. Photo taken under crossed polarized light at 20x magnification. IL: ilmenite; SPH: titanite; RTL: rutile; CPY: chalcopyrite; PO: pyrrhotite; PN: pentlandite.

to locally coarser blebs (aggregates of disseminated grains). Disseminated grains are composed of pyrrhotite (40-70%), pentlandite (15-35%), chalcopyrite (trace – 40%), and cobaltite-gersdorffite.

Cobaltite-gersdorffite exists as uncommon fine- to medium-sized grains, occasionally coarse, which are dominantly euhedral (sometimes subhedral) (Figure 13). A mild dissociation between chalcopyrite and pyrrhotite-pentlandite-cobaltite/gersdorffite exists; pyrrhotite-pentlandite-cobaltite/gersdorffite grains occasionally have only trace amounts of chalcopyrite. In other areas, chalcopyrite makes up approximately 40% of blebs while the pentlandite:pyrrhotite ratio remains constant.

Equigranular melagabbro – Medium-grained gabbro consisting of abundant green amphibole, pyroxene, plagioclase and lesser quartz (Figure 13). Hand samples have lesser variation in color, mineralogy, relative mineral abundances, and textures observed than in the melagabbro-rock fragment phase.

Overall, the silicate and oxide mineral phases present are 5-10% quartz as fine disseminated grains or as rarer medium-grained aggregates of fine grains, 15-20% fine-grained clinzoisite (uncommonly medium grained), 15-20% variably albitized plagioclase, 15% medium-grained hornblende, 35-45% actinolite replacing pyroxenes, trace-5% fine biotite, and 0-5% oxides dominantly as titanite rimmed ilmenite with uncommon rutile +/- sulfide within the cores of grains. Plagioclase is abundant as medium grains which usually moderately albitized and as fine grains which appear interstitial to coarser pyroxenes, hornblende, and plagioclase. Plagioclase grains that appeared unaltered yielded compositions between An_{47} and An_{55} .

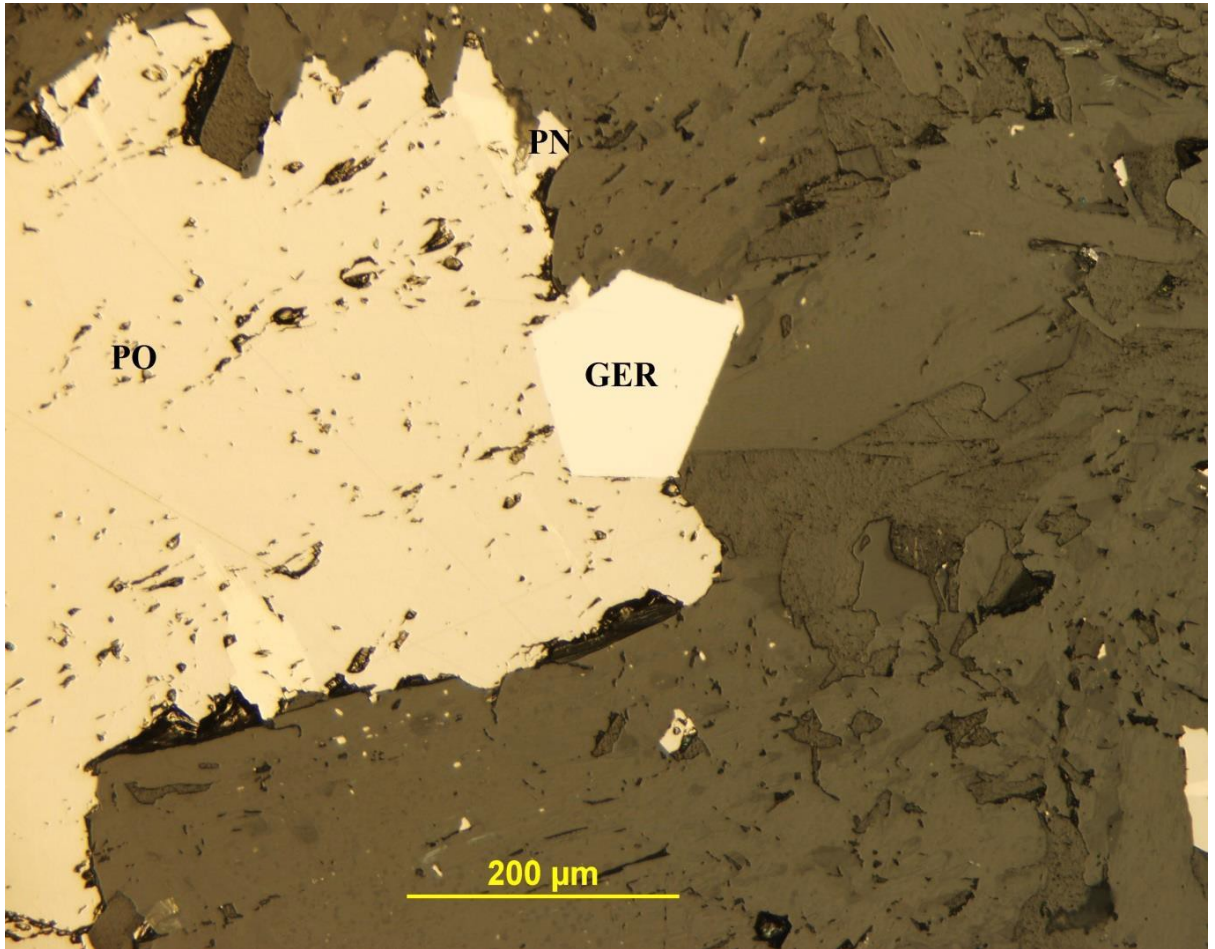


Figure 13: Photomicrograph of medium-grained euhedral gersdorffite-cobaltite and associated pyrrhotite-pentlandite, taken from drill hole U-03-118 (359.5m depth) and under plane polarized light at 20x magnification. GER: gersdorffite-cobaltite; PO: pyrrhotite; PN: pentlandite.

All ilmenite grains are rimmed by titanite, but the core of individual grains varies considerably in terms of texture and species present. Commonly, only ilmenite is found in the core. In other grains, blobby to wormy rutile intermingles with the ilmenite in the core of the grains. Occasionally, minor fine sulfide grains are found in the core with rutile and ilmenite (Figures 14 and 15) Uncommonly, significant sulfide (chalcopyrite) is found in the core of discrete grains and appears to be replaced by oxides (Figures 12 and 15), exhibiting interesting textures which appear as thin linear rutile / ilmenite crossing each other at sub-perpendicular angles. Interestingly, these grains appear juxtaposed immediately adjacent to fresh / non replaced sulfides.

Net textured to interconnected, blobby, and disseminated sulfides commonly have a spatial association with ilmenite grains (Figures 12 and 15). Occasionally the oxides appear to be surrounding and replacing some sulfides but not others (Figures 12 and 15).

Pentlandite commonly displays multiple textures, from discrete anhedral to locally subhedral grains within pyrrhotite (Figure 16), as fine- to medium-grained veinlets, as partially agglomerated grains near veins (Figure 17), and also commonly as grains which appear to be fine clusters of pentlandite flames that consist of lamellae and blebs at low to medium angles relative to the direction of elongation in the flame (Figure 18).

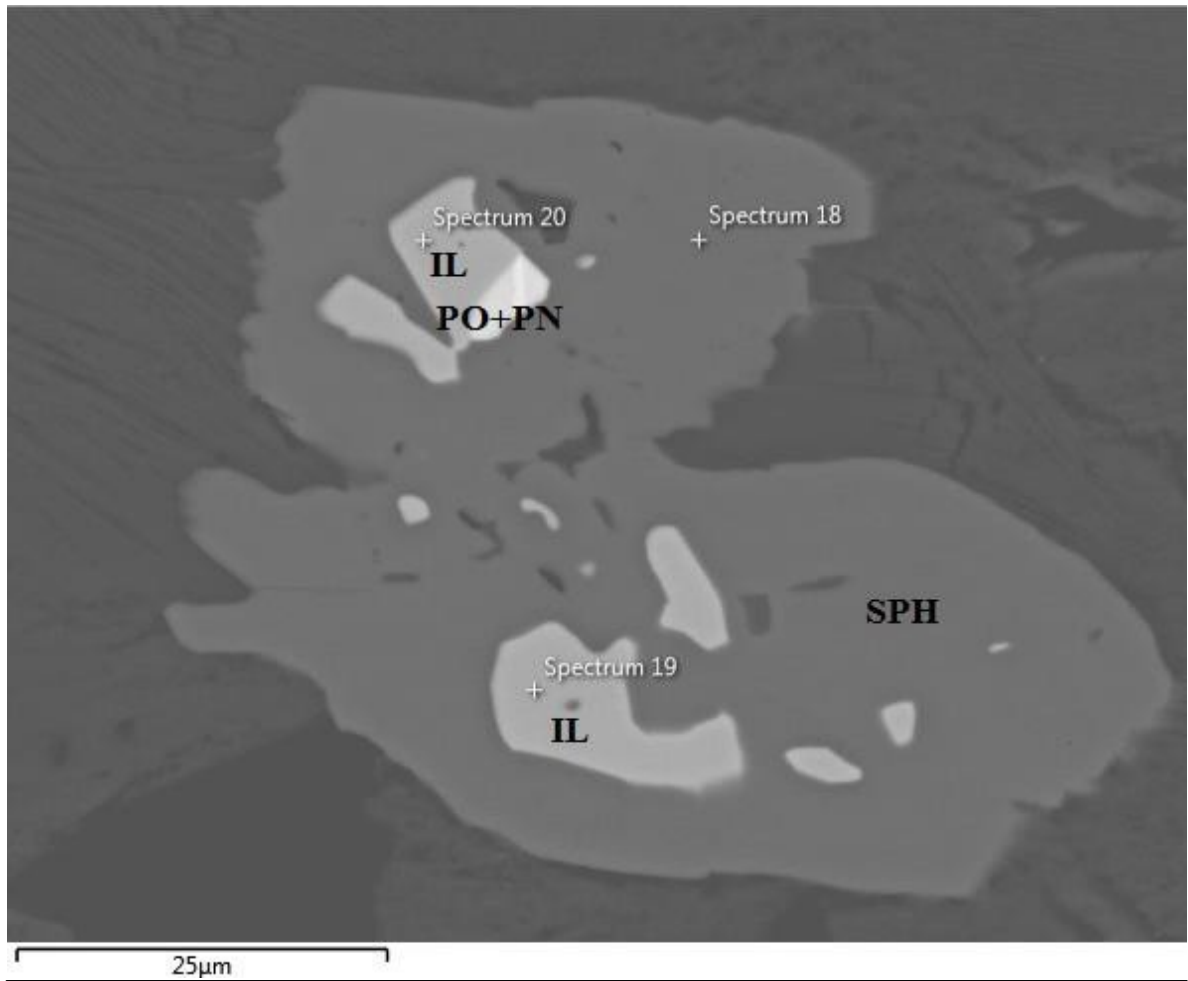


Figure 14: A backscatter electron image from the SEM-EDS study showing a very fine-grained oxide (ilmenite) with a small grain of pyrrhotite-pentlandite. The oxide is surrounded by titanite. IL: ilmenite; PO: pyrrhotite; PN: pentlandite; SPH: titanite.

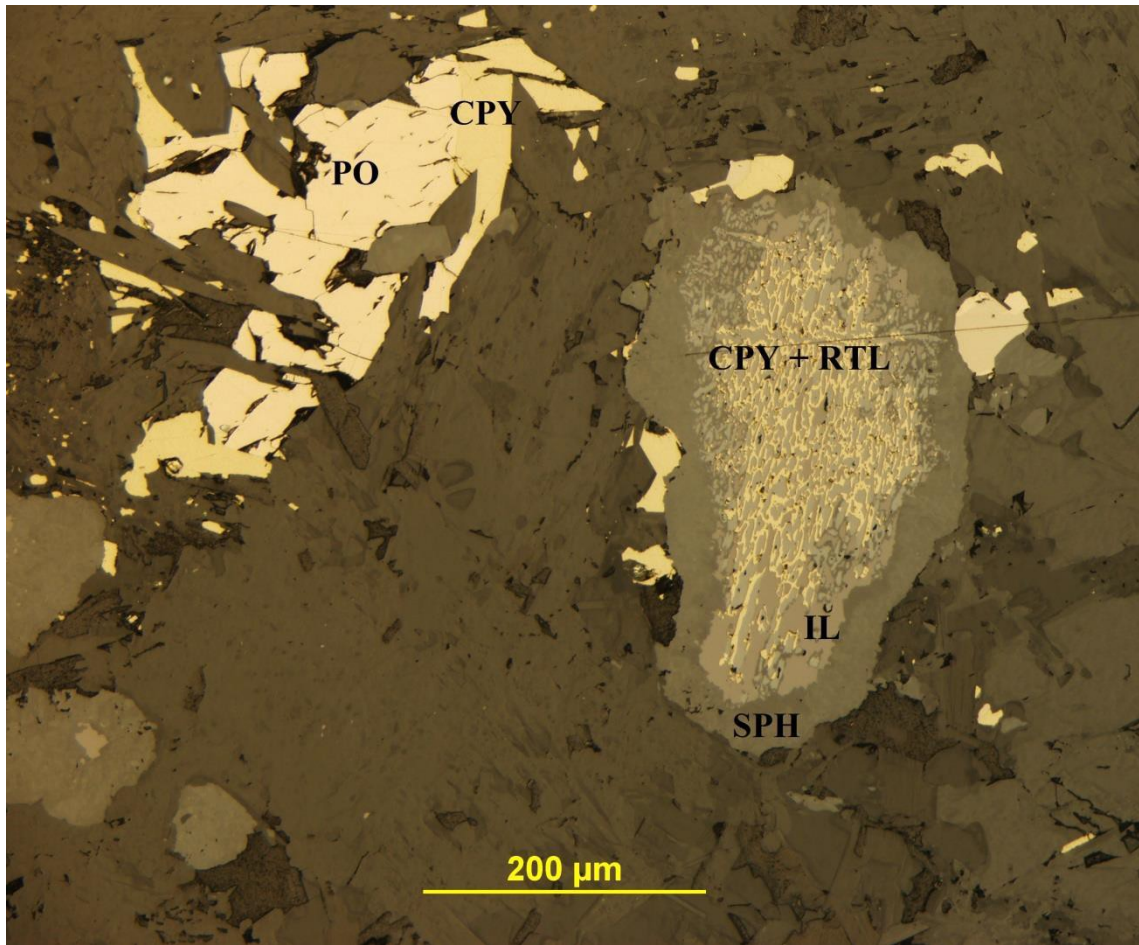


Figure 15: Photomicrograph of a rare sulfide grain near a chalcopyrite-rutile-ilmenite grain taken from U-03-118 (359.5m depth) . The chalcopyrite-rutile-ilmenite grain is surrounded by a titanite halo, interpreted to be from replacement during metamorphism. Photomicrograph taken under plain polarized light at 20x magnification. CPY: chalcopyrite; RTL: rutile; IL: ilmenite; PO: pyrrhotite.

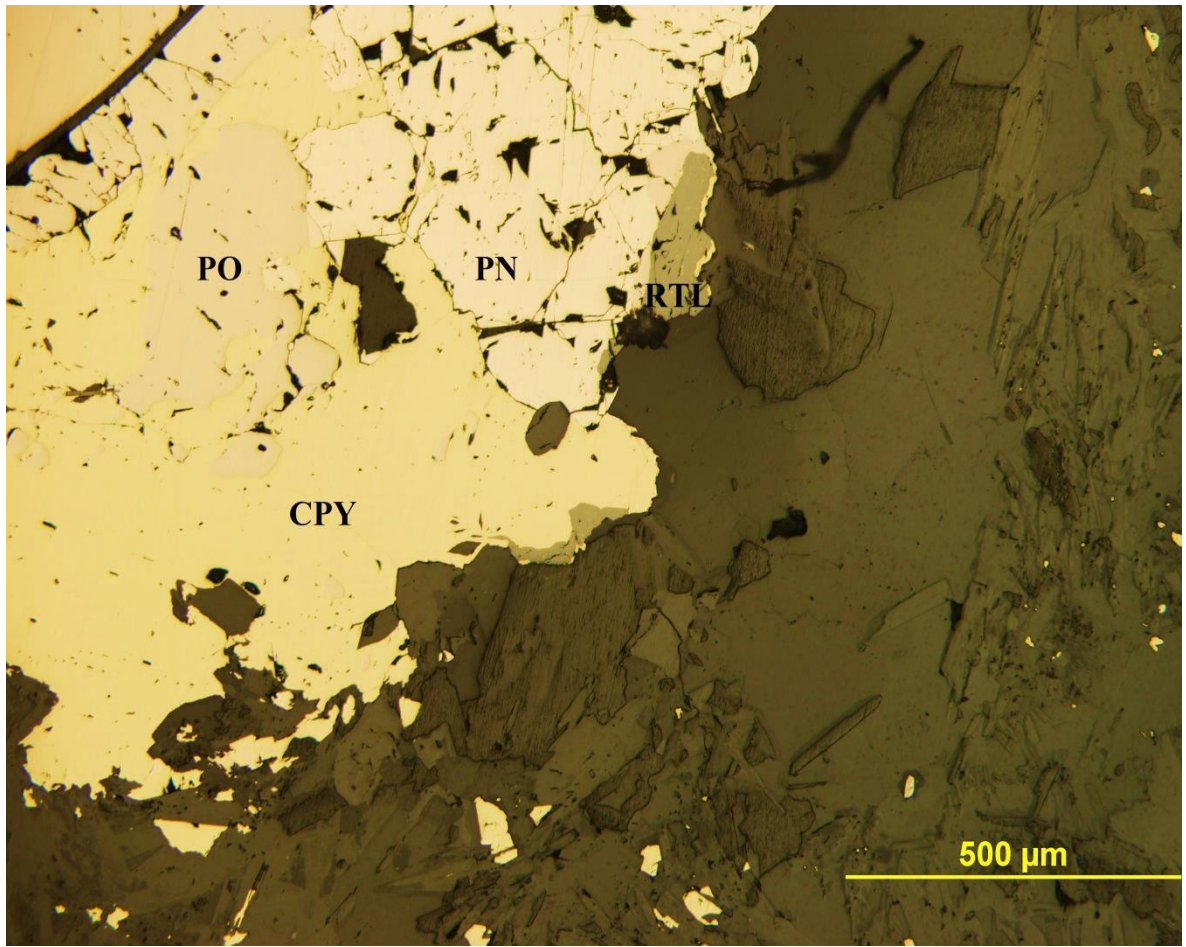


Figure 16: A Photomicrograph of rutile replacing the edge of a disseminated sulfide grain within the melagabbro - rock fragment unit of drill hole U-03-118 (535.2m depth). Photomicrograph was taken under plane polarized light at 10x magnification.

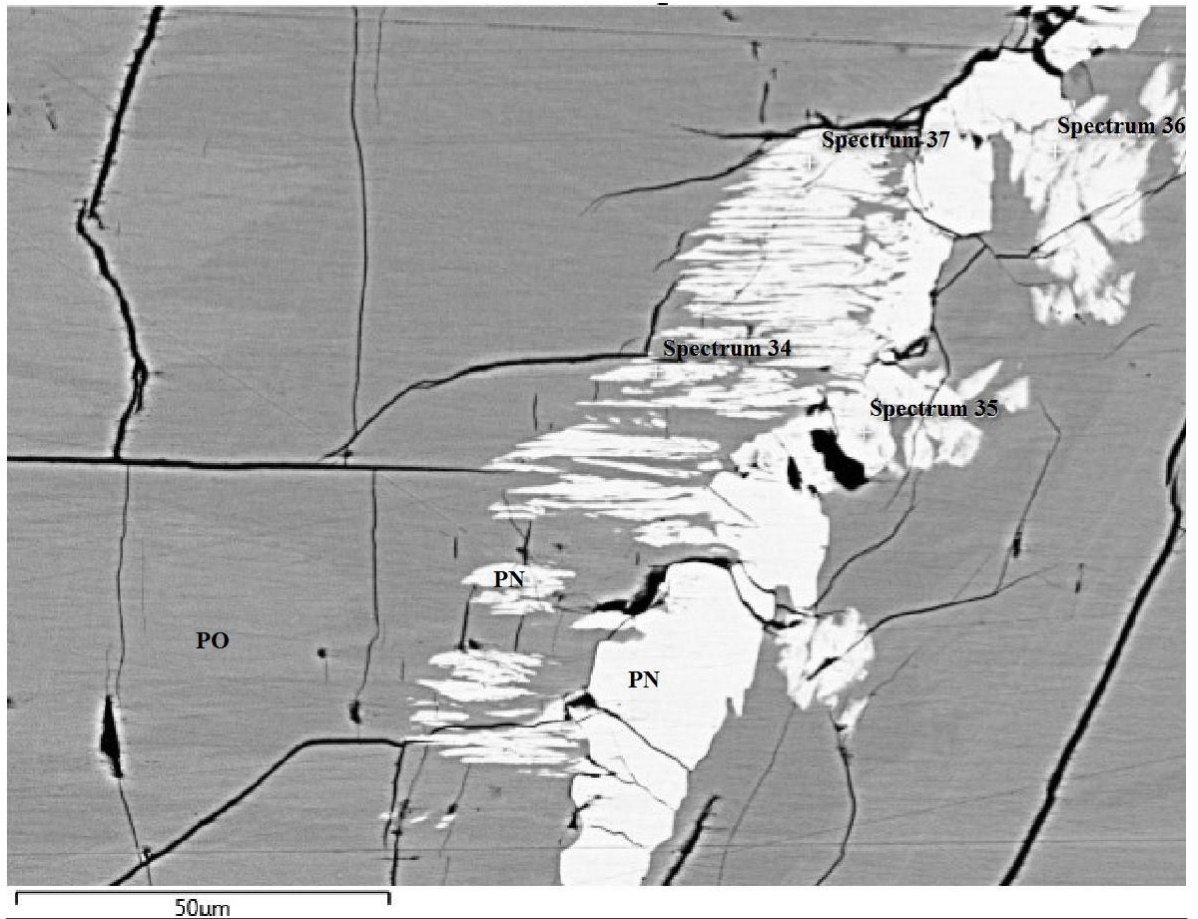


Figure 17: A backscatter electron image taken from the SEM-EDS study of sub-parallel partially agglomerated blades of pentlandite in a small vein of pentlandite, surrounded by pyrrhotite. The different grains of pentlandite are compositionally homogenous. PO: pyrrhotite; PN: pentlandite.

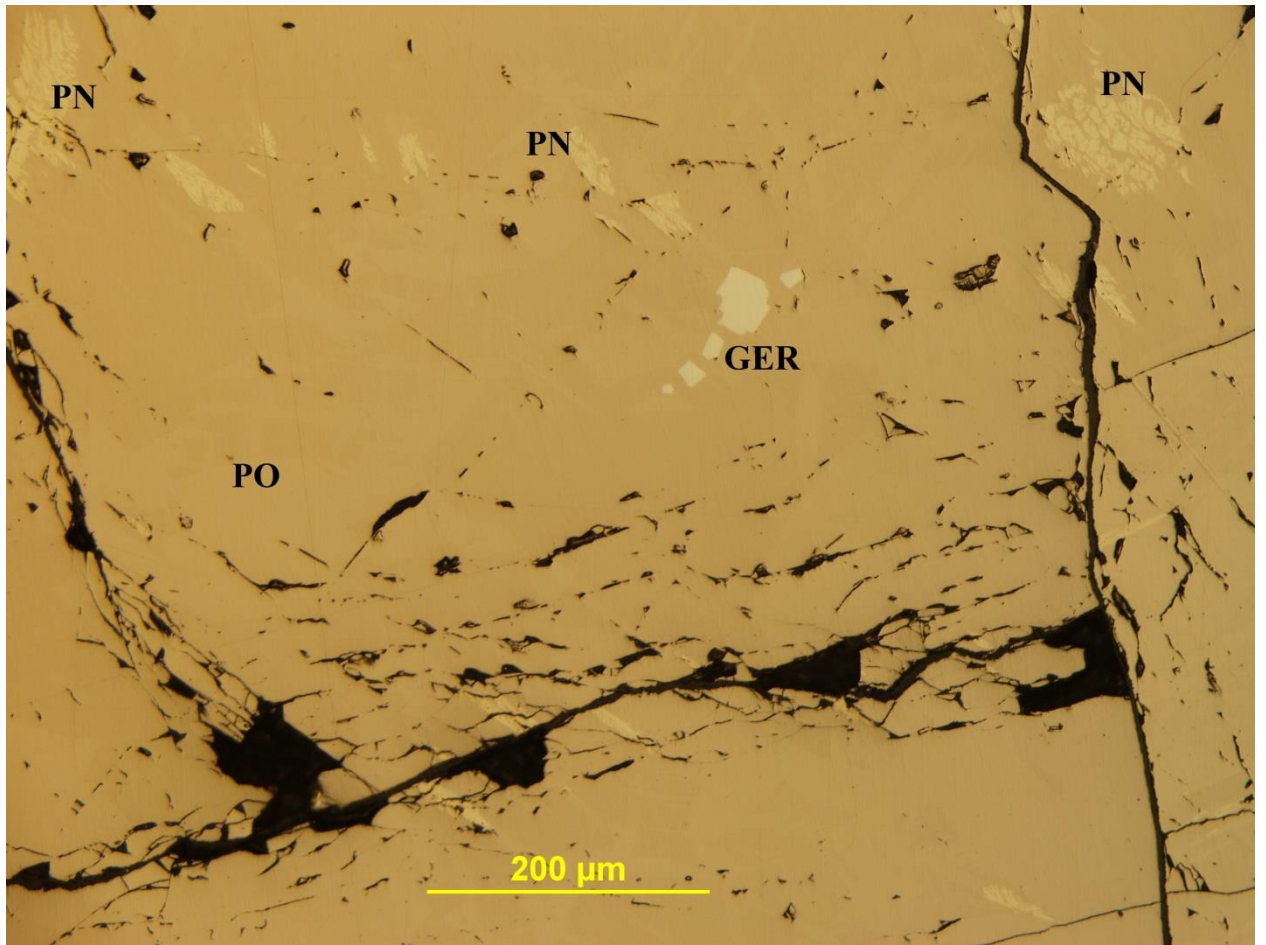


Figure 18: A photomicrograph of pentlandite flames and euhedral gersdorffite-cobaltite within pyrrhotite. The pentlandite flames are blebs and lamellae at medium to low angles relative to the direction of elongation of the flame. Note the complimentary orientation of the adjacent blades of pyrrhotite. Photo taken under plane polarized light at 20x magnification.

4.2 - Results of the Scanning Electron Microscopy - Energy Dispersive Spectroscopy Study

The results of the SEM analysis of polished thin sections reveal several identifiable species of tellurides, sulfarsenides, sulfselenides, native metals, and metal alloys. Several other species of tellurides and metal alloys are likely present. Results are provided as semi quantitative unless otherwise specified. Data obtained by quantitative analysis and semi quantitative analysis from the SEM-EDS study are presented in Appendix 1.

Oxide grains observed in reflected light contain Ilmenite and are always rimmed with titanite. They occasionally contain chalcopyrite, pyrrhotite, pentlandite, and / or rutile within ilmenite. Textural evidence gathered from the reflected light study (Figures 15 and 16) suggests rutile may be replacing sulfide through a reduction – oxidation reaction. During the course of the SEM-EDS study native copper (possibly with minor iron) was rarely observed within an otherwise pure ilmenite core (Figure 19).

Sulfide minerals and associated tellurides, sulfarsenides, sulfselenides, and metal alloys display a wide array of textural and sulfide species-dependent affinities. Disseminated sulfide textures that are encountered below the interconnected to semi massive sulfide in the idealized Shakespeare stratigraphy (Figure 1) are separated into three groups: those displaying an association with chalcopyrite, those displaying an affinity for pyrrhotite-pentlandite, and those not appearing to display any preference for sulfide mineral species present.

The most common mineral species present other than the major sulfide minerals (pyrrhotite-pentlandite-chalcopyrite) is a solid solution of cobaltite-gersdorffite-(arsenopyrite) and is most commonly observed in the disseminated sulfides located stratigraphically lower

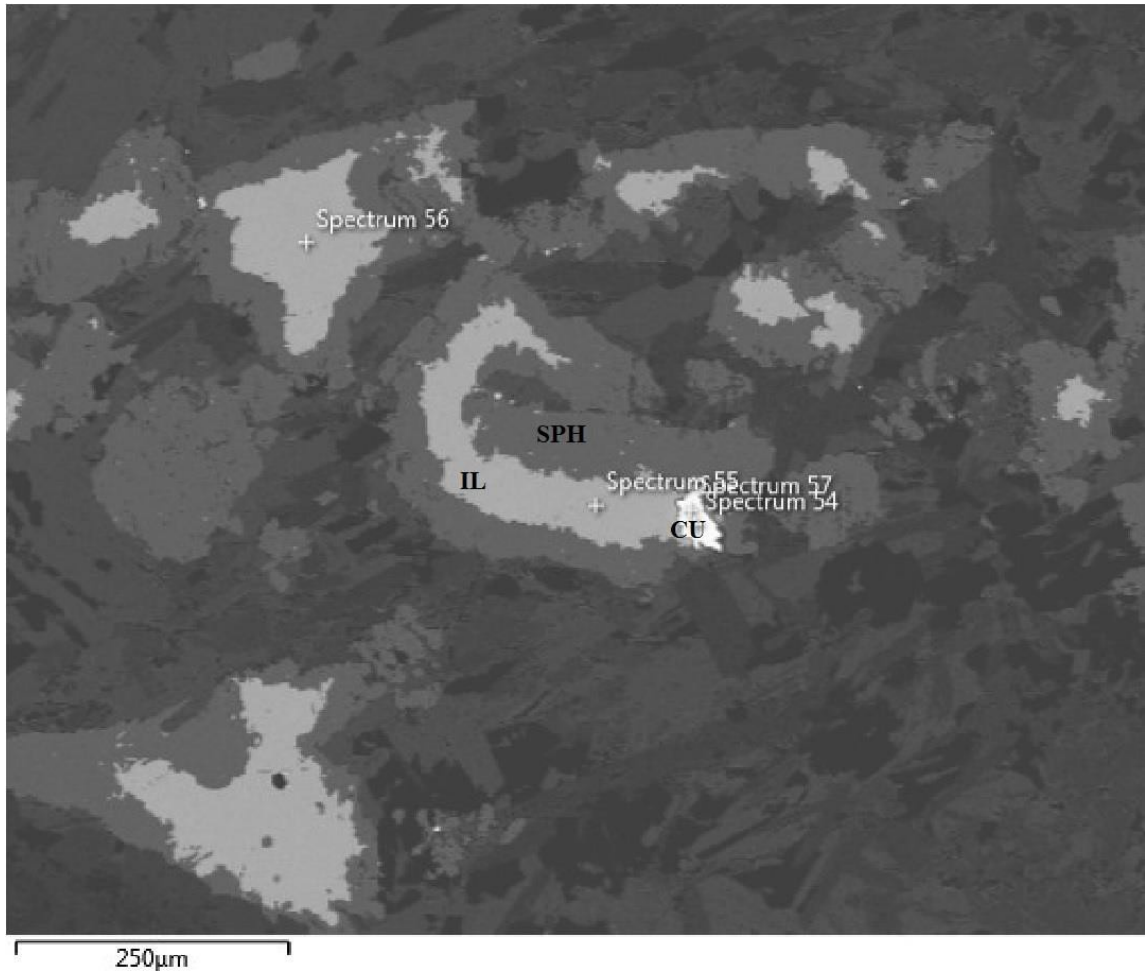


Figure 19: A backscatter electron image taken from a poorly mineralized portion of the melagabbro-rock fragment phase in drill hole U-03-118. The oxide cores are composed entirely of ilmenite, except in one instance where native copper was observed within the core of the ilmenite. All oxide cores are surrounded by titanite. CU: native copper; IL: ilmenite; SPH: titanite.

than the interconnected sulfides. Within the interconnected sulfides it is observed rarely and the grains are much smaller than the average grain encountered within the disseminated sulfide. It occurs as 10x10 μ m to 170x170 μ m euhedral to subhedral grains and is observed within, and associated with, larger pyrrhotite grains which contain abundant pentlandite.

The cobaltite-gersdorffite-(arsenopyrite) grains frequently display multiple microfractures with galena-clausthalite fillings (figure 20). Grains containing microfractures also frequently contain sub 3x3 μ m bismuth tellurides. The most euhedral grains also contain the least microfractures, tellurides, selenotelluride, and galena-clausthalite while the grains which appear the most anhedral (subhedral to moderately anhedral) contain the highest density of microfractures and galena-clausthalite (figures 20 and 21). Uncommonly, a mineral containing palladium and bismuth (possibly merenskyite) is observed in the disseminated sulfides. Rarely, fine grains containing palladium, bismuth, silver, and gold are observed within the disseminated sulfides. These grains likely represent the same palladium-bismuth mineral intergrown with very fine (sub micrometer) electrum (Ag-Au) grains.

Rarely, well zoned crystals of hollingworthite - irarsite - (platarsite) as a solid solution with the cobaltite-gersdorffite-(arsenopyrite) are observed (Figure 22). The PGE-cobaltite-gersdorffite-(arsenopyrite) (PCGA) crystals also frequently display textures indicative of partial resorption or dissolution (Figure 17). PCGA crystals are between 5x5 μ m and 10x5 μ m, are dominantly euhedral, and are mostly observed within coarser cobaltite-gersdorffite-(arsenopyrite) grains. Only once was a lone grain of PCGA observed, which was found in a pyrrhotite-pentlandite grain. Zonation within the PCGA is such that PGEs concentrate towards the centers. Rare bright cores produce the only detectable quantities of platinum and elevated

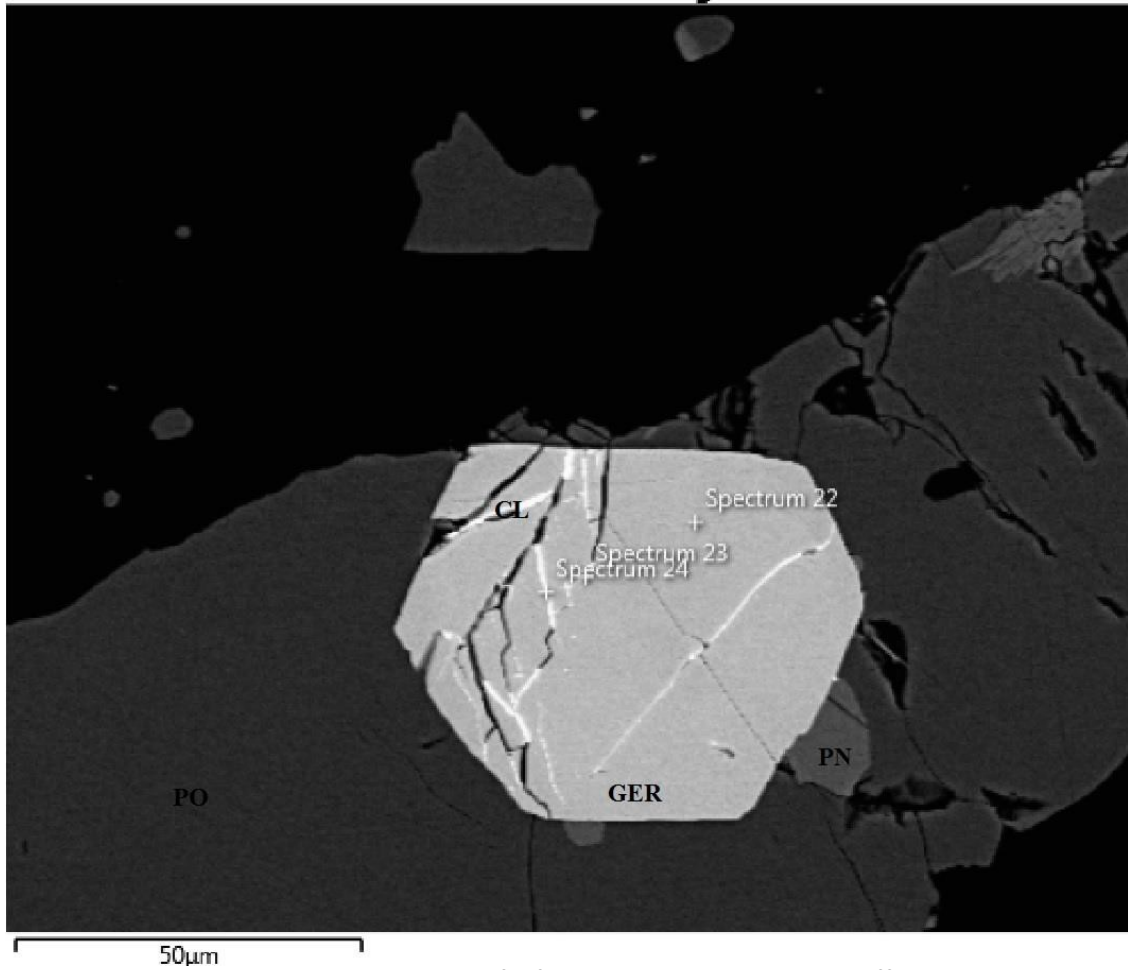


Figure 20: A backscatter electron image of a fractured, subhedral gersdorffite-cobaltite grain.

Fractures are filled with clauthalite-galena. CL: clauthalite-galena; GER: gersdorffite-cobaltite; PO: pyrrhotite; PN: pentlandite.

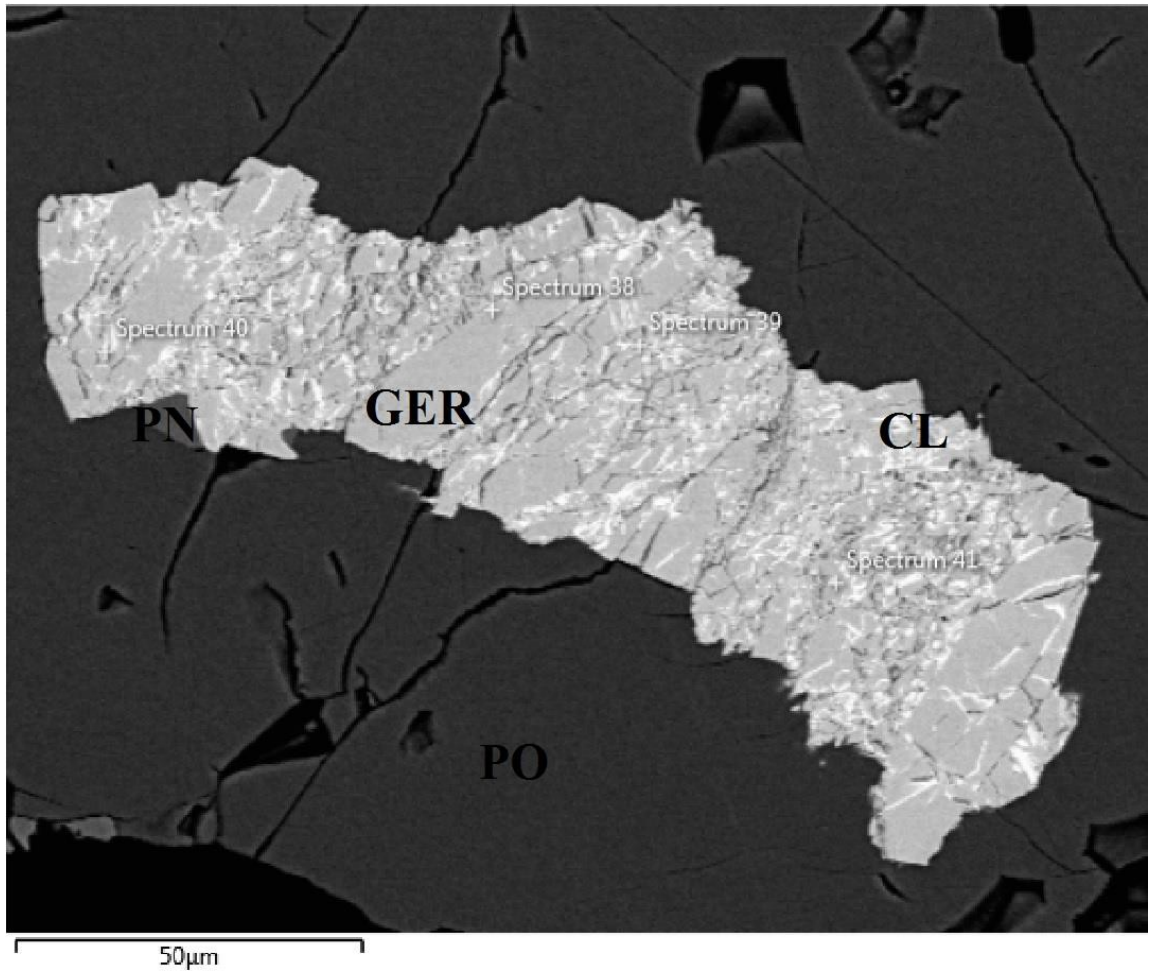


Figure 21: A backscatter electron image of an intensely fractured, subhedral to anhedral gersdorffite-cobaltite grain. Fractures are filled with clausthalite-galena. CL: clausthalite-galena; GER: gersdorffite-cobaltite; PO: pyrrhotite; PN: pentlandite.

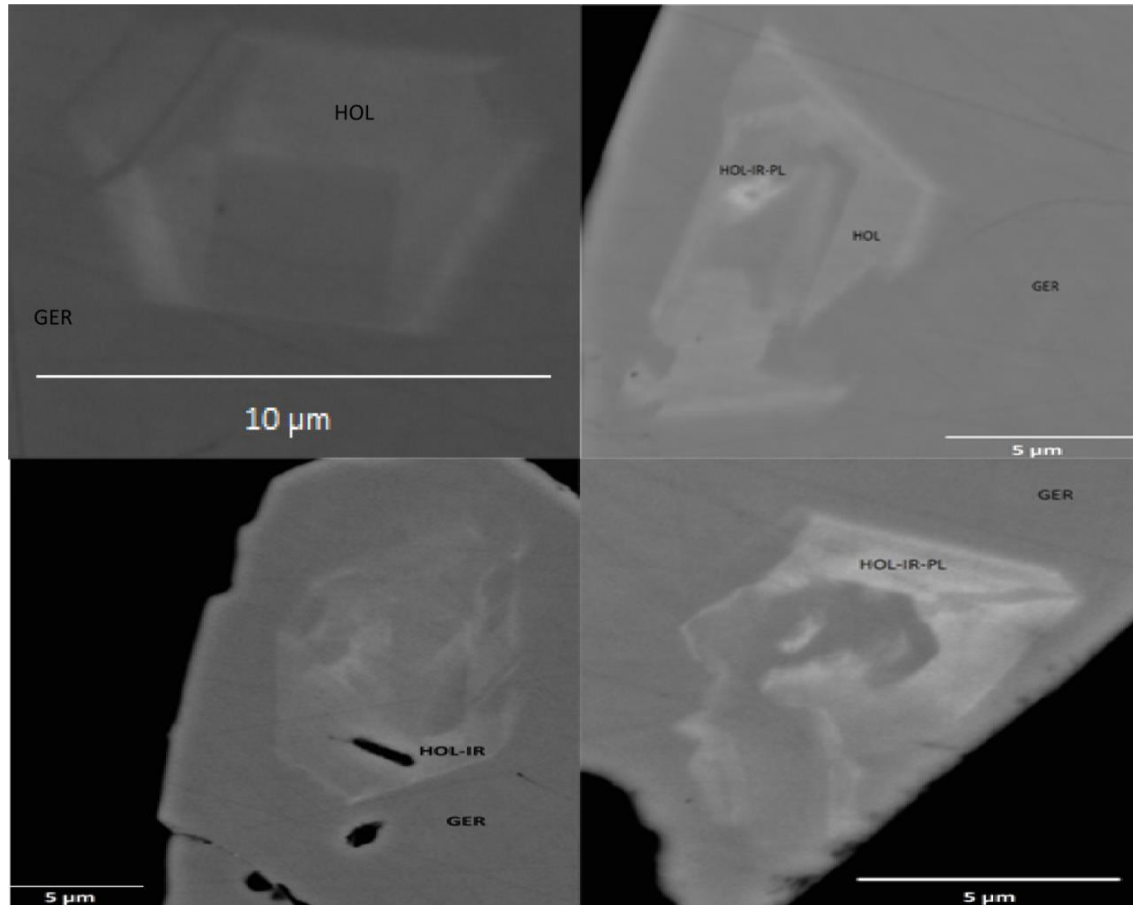


Figure 22: Backscatter images taken from the SEM-EDS study showing zoned solid solutions of PGE sulfarsenides within larger, PGE poor MCGS crystals. All images were taken from sample 1340148, taken from drill hole U-03-118 at a depth of 536m within the rock fragment bearing phase of the melagabbro lithology. Grains are dominantly euhedral, but where partially resorbed appear subhedral to anhedral (bottom right). Most crystals are well zoned. GER: Gersdorffite-Cobaltite; HOL: Hollingworthite; IR: Irarsite; PL: Platarsite.

quantities of rhodium and iridium (Figure 22). Generally, it appears that PGE replacement is cobalt >nickel>>iron based on the trends of increasing PGE with decreasing base metal (cobalt, nickel, and iron, respectively). These grains are only observed in the disseminated sulfides located stratigraphically lower than the interconnected sulfides.

The most common metallic phase present other than the sulfides and sulfarsenides was tsumoite (BiTe), which occurs as very fine ($1\text{x}1\mu\text{m}$ - $70\text{x}30\mu\text{m}$) bladed crystals which are commonly euhedral. Uncommonly, the crystals exist as fine ($1\text{x}1\mu\text{m}$ - $5\text{x}5\mu\text{m}$) aggregates of subhedral to locally rounded, anhedral grains. Tellurobismuthite (Bi_2Te_3) and pilsenite (Bi_3Te_4) are uncommonly to rarely observed as very fine ($1\text{x}1\mu\text{m}$ - $4\text{x}4\mu\text{m}$) grains within pyrrhotite, pentlandite, and chalcopyrite, as well as within various silicates. It does not appear that the bismuth telluride phases display a preference for a particular sulfide mineral species. In fact, they occur within and around various silicate phases (such as replaced pyroxenes) and various sulfide minerals (pyrrhotite, pentlandite, and chalcopyrite).

Phases associated with chalcopyrite mineralization include uncommon sphalerite with minor cadmium as fine ($1\text{x}1\mu\text{m}$ to $5\text{x}5\mu\text{m}$) euhedral to subhedral grains within and around interconnected and disseminated sulfides, argentopentlandite as fine ($3\text{x}3\mu\text{m}$ - $5\text{x}2\mu\text{m}$) euhedral grains surrounding chalcopyrite disseminations (Figure 23) , a silver telluride (probably hessite, Ag_2Te) as rare intergrowths within disseminated bismuth tellurides, surrounded by chalcopyrite.

Other observed minerals, which did not yield data meeting accuracy requirements for quantitative determination, include a tungsten mineral (possibly with iron and/or sulfur), a tin mineral (possibly with iron and/or sulfur) encountered near the tungsten mineral, and an iron



Figure 23: A backscatter electron image taken during the SEM-EDS study that shows euhehedral argentopentlandite and associated chalcopyrite grains. APN: argentopentlandite; CPY: chalcopyrite.

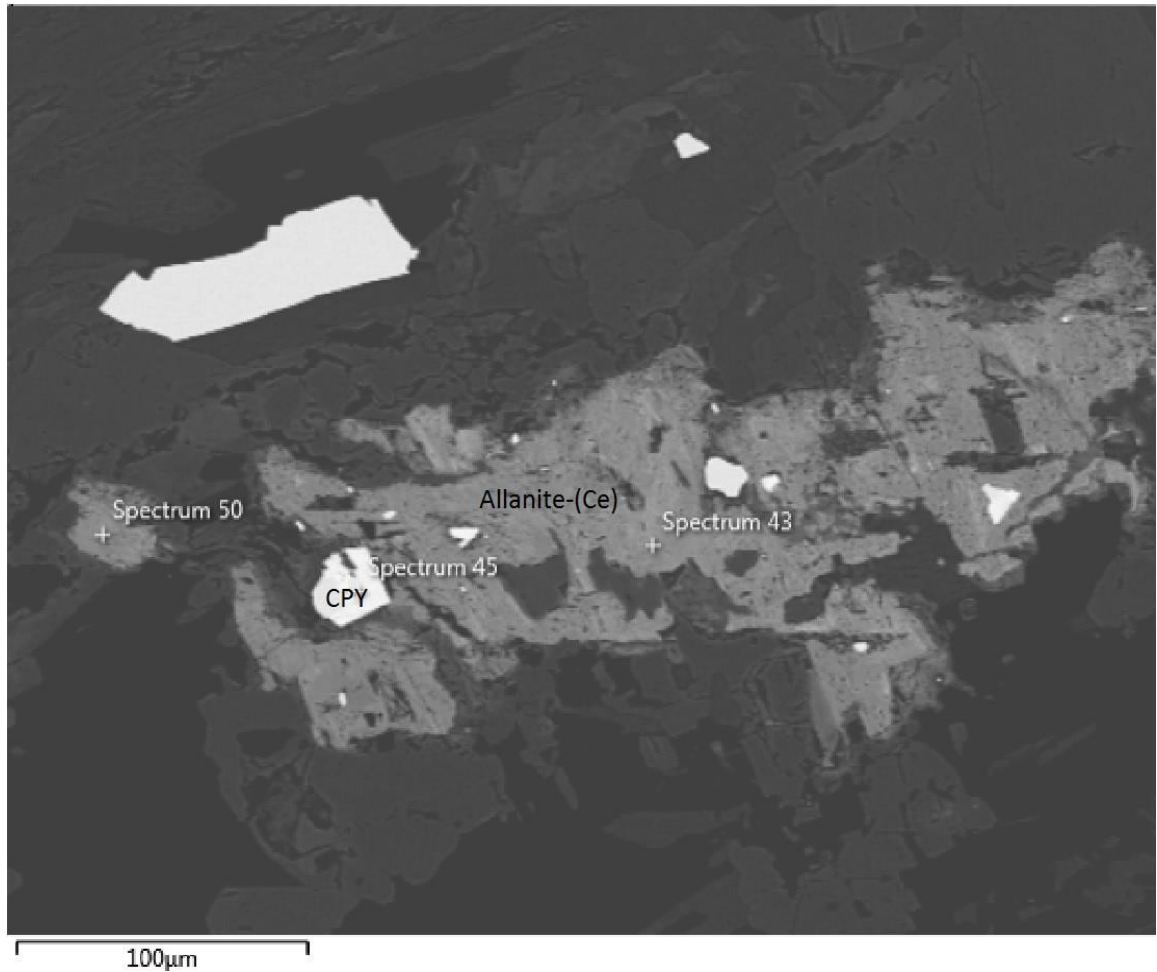


Figure 24: A backscatter electron image taken during the SEM-EDS study that shows a partially metamict grain of allanite-(Ce) surrounded by other silicates. The grain has multiple inclusions of fine chalcopyrite. Interestingly, the concentration of Nd is unusually high, such that the ratio of Ce:La:Nd approximates 8:4:3.

mineral (probably native iron) within ilmenite grains. The iron mineral was once observed as a discrete grain within a pyrrhotite-pentlandite grain and was located adjacent to the tungsten and tin minerals. Interestingly, the spectrum from pyrrhotite and pentlandite yielded reasonable results (96-97 total weight percent), while the spectrum focused on the iron mineral (probably native iron) grain yielded a sum of only 50 weight percent and contained no oxygen and almost no sulfur. Since the instrument was calibrated for iron within sulfide, it has been suggested that the counts per second was over detection limit for the instrument which resulted in a lower weight percent iron than what was actually present in the sample (Dr. Guosheng Wu, personal communication). A similar error occurred when data was collected on rare iron minerals within ilmenite grains, near the edge of sulfide inclusions. The tungsten and tin minerals were only observed within one interconnected - semi massive sulfide sample.

A rhenium sulfide (Rheniite) was encountered on multiple occasions within a sample of chalcopyrite- poor semi-massive sulfide. They exist as rare, very fine ($3\mu\text{m} \times 3\mu\text{m}$) grains within pyrrhotite-pentlandite and along the edges of microfractures.

Molybdenite was commonly observed in the interconnected sulfides as fine ($5\mu\text{m} \times 5\mu\text{m}$ - $25\mu\text{m} \times 8\mu\text{m}$) euhedral to subhedral grains along edges and as discrete grains within pyrrhotite-pentlandite. They commonly have abundant, very fine (micrometer to sub micrometer) bismuth tellurides within the core of the crystals and also adjacent to them.

On several occasions an elongate, pitted $350\mu\text{m} \times 100\mu\text{m}$ silicate mineral containing abundant (up to 1.2 atomic percent cerium, 0.6 atomic percent lanthanum, and 0.45 atomic percent neodymium), calcium, silicon, oxygen, aluminum, and iron (Figure 24) was observed in

the samples containing interconnected or disseminated sulfides. The mineral is likely allanite – (Ce) based on the chemical components present, the partially meramict texture, and the ratio of calcium + lanthanum + cerium : iron + aluminum : silica which approximates 2:3:3. The significant concentrations of Nd are highly unusual, as Nd enriched allanite is associated with extreme LREE enrichment relative to HREE (Hanson et al., 2011; Skoda et al., 2010). The results of the powder diffraction analysis show the progression in mineral assemblage from the Quartz Diorite unit through to the Equigranular Melagabbro unit. The mineral assemblage is as follows (in the order of highest statistical confidence as calculated by the Hi Score Plus software):

- 1) Quartz diorite – quartz, muscovite, clinocllore, clinozoisite, albite, biotite, chlorite (undifferentiated), serpentine.
- 2) Quartz gabbro – quartz, albite, biotite, serpentine, ferroactinolite, clinozoisite, magnesiohornblende
- 3) Quartz gabbro / melagabbro boundary (transitional) – quartz, albite, serpentine, phlogopite, magnesiohornblende, actinolite, clinozoisite, titanium rich biotite
- 4) Melagabbro (rock fragment phase) – quartz, biotite, clinozoisite, albite, magnesiohornblende, serpentine
- 5) Melagabbro (equigranular, mineralized) – quartz, serpentine, biotite, clinozoisite, albite, actinolite
- 6) Melagabbro (equigranular, unmineralized) – serpentine, quartz, muscovite, clinozoite, albite, actinolite, clinocllore
- 7) Nipissing gabbro - serpentine, actinolite, quartz, magnesiohornblende, clinozoisite

4.3 - Geochemical analysis

The results from sulfur isotope analysis are presented in Table 1. They yield $\delta^{34}\text{S}$ values between 0.01‰ and 2.38‰, averaging 1.14‰. Interestingly, the sample taken from the overlying Mississagi quartzite yielded a value of 0.37‰ which suggests either unfractionated sedimentary sulfur (in situ) or late sulfur contributions from the Shakespeare sulfides. The uniformly low values are indicative of an unfractionated sulfur source.

The results of the geochemical analysis via ICP-MS are presented in Appendix 3. The data for Cu, Ni, and Co that were obtained via ICP-AES analysis were reproduced in the ICP-MS analysis, within analytical error. Se values used for S/Se ratios were significantly above detection limits and provided greater accuracy and precision than the initial attempts via ICP-AES. Spider diagrams constructed from the ICP-MS data are presented in Figures 25, 26, and 27. They all exhibit elevated LREE vs HREE, enrichment in HFSE relative to MREE, pronounced negative Nb and Ti anomalies relative to elements of similar compatibility, and moderate negative Sr anomalies relative to elements of similar compatibility. Data from the geochemical analysis via ICP-AES are presented in Appendix 4. PGE and gold from the geochemical analysis via fire assay – atomic absorption spectroscopy (FA/AAS) are presented in Appendix 5. Assays reveal the strongest concentrations of Ni, Cu, and PGE are found in the interconnected sulfides of hole U-03-122. When taken in conjunction with the total carbon and total sulfur analysis (Appendix 6), a trend of relatively homogenous nickel concentrations based on 100% sulfide within the interconnected sulfides is observed, regardless of sulfide concentration (Figures 28, 29, 30, 31, 32, and 33). However, a trend of increasing sulfide metal concentration with decreasing sulfide concentration is observed for the stratigraphically lower disseminated sulfides.

Table 1: Laboratory results from the sulfur isotope analysis. Some samples contained less sulfide than was required for pure sulfide analysis and are presented in the center column. Other analyses were conducted with sulfide-only samples. All values are V-CDT. Data are presented in one of two columns depending on the type of sample submitted.

Sample ID	Rock type	$\delta^{34}\text{S}$ for rock sample with S	$\delta^{34}\text{S}$ for sulfide sample
122-437.7	Quartz Gabbro		1.38
119-360	Melagabbro - Rock Fragment Phase		1.00
122-464.7	Melagabbro - Equigranular		0.72
1340101	Quartzite		0.37
122-417	Quartz Gabbro		0.01
119-346	Melagabbro - Rock Fragment Phase		1.05
119-378	Melagabbro - Equigranular		0.50
119-324	Biotite Quartz Diorite (Lower contact)	1.83	
119-304.5	Biotite Quartz Diorite	2.38	
122-396.2	Quartz Gabbro	1.43	

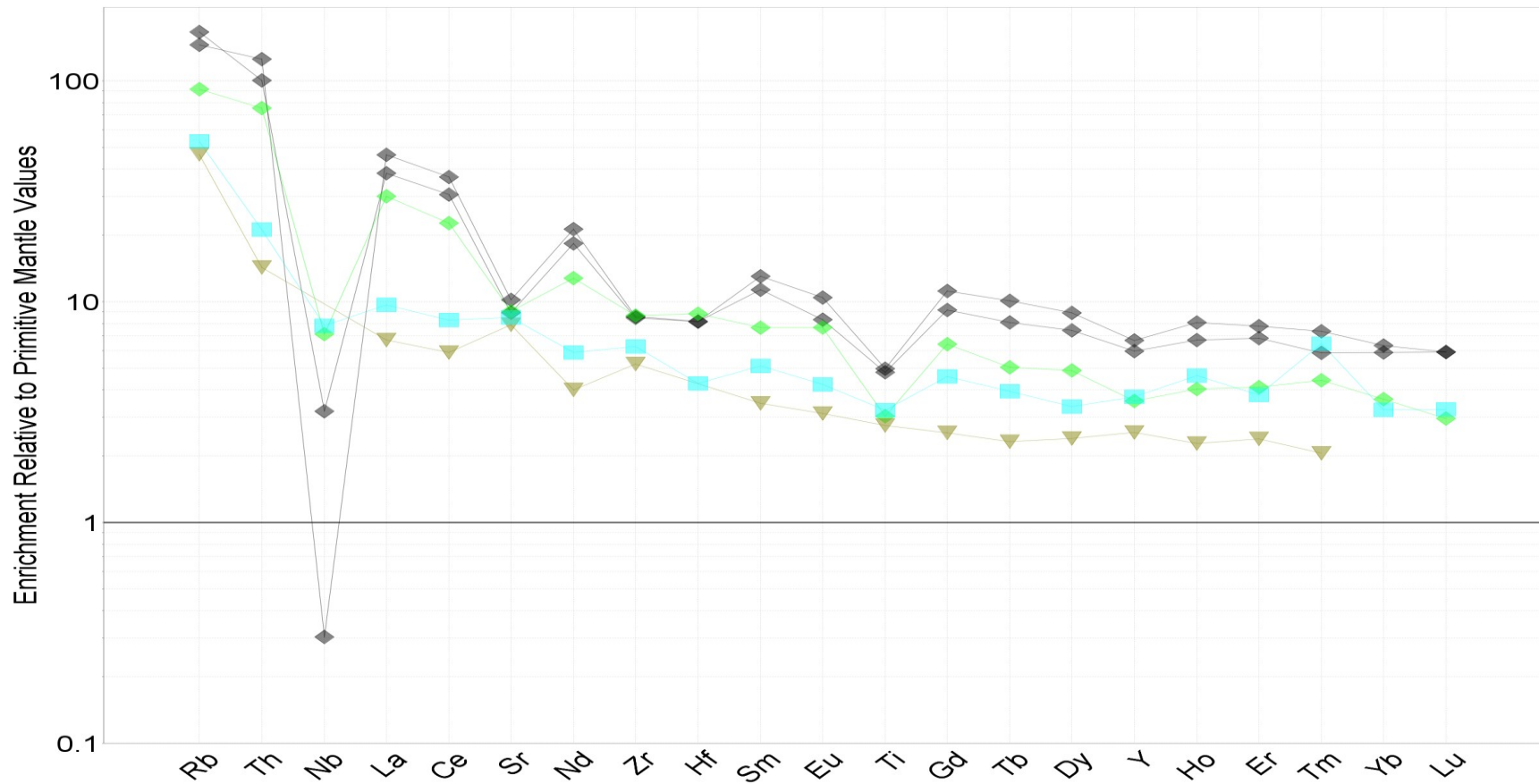


Figure 25: Primitive mantle normalized trace element spider diagram for diamond drill hole U-03-118. Green: Melagabbro – rock fragment phase; Grey/Black: Quartz Gabbro; Cyan: Nipissing Gabbro Average (Lightfoot and Naldrett, 1996); Yellow/Brown: Basswood Intrusion (Lightfoot and Naldrett, 1996). Primitive mantle values are from McDonough and Sun, 1995. Diamond points are from the upper group of the Shakespeare intrusion intercepted in drill hole U-03-118. Square points are Nipissing Gabbro Average points. Downwards pointing triangles are Basswood Intrusion points.

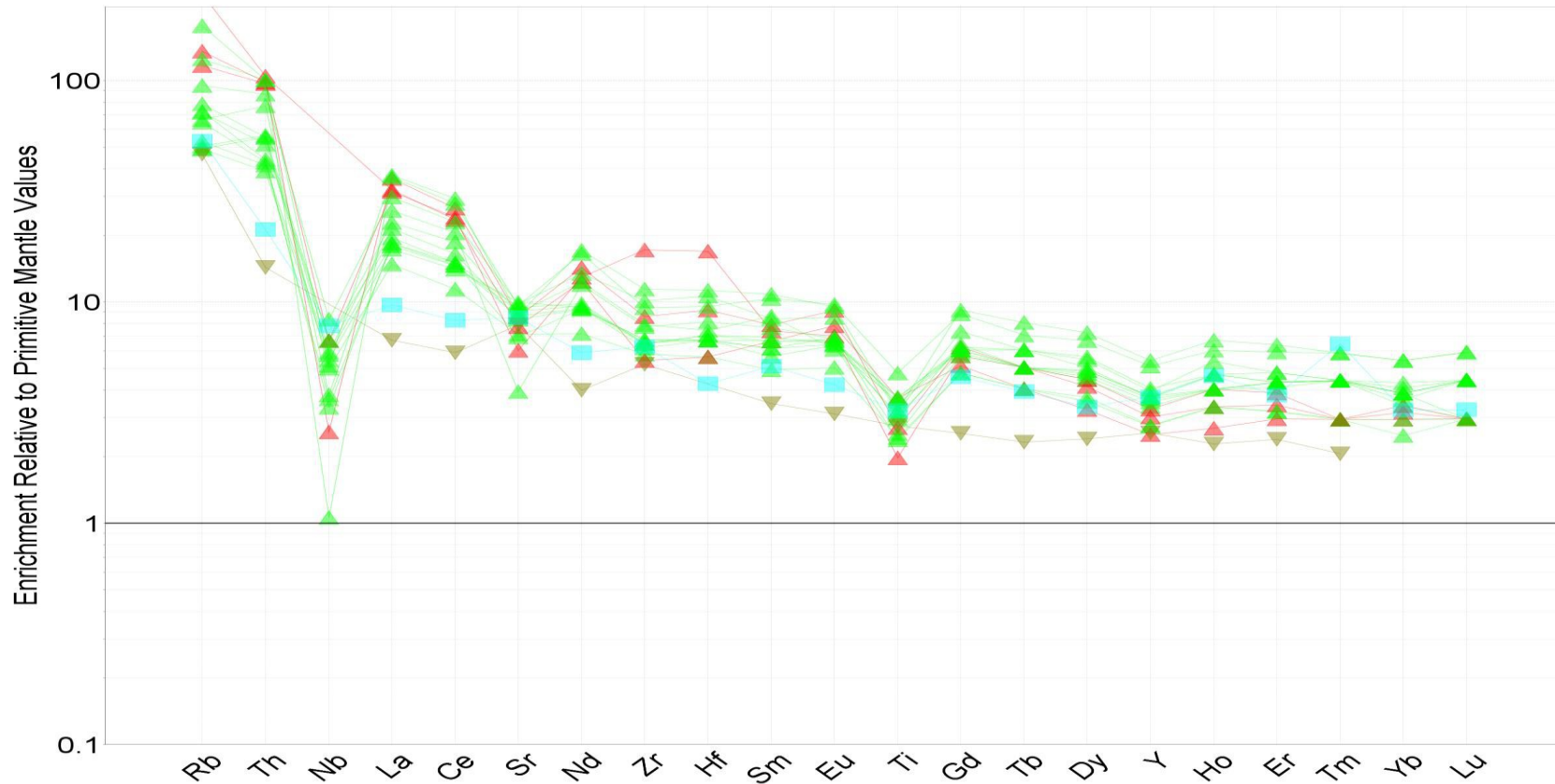


Figure 26: Primitive mantle normalized trace element spider diagram for diamond drill hole U-03-119. Green: Melagabbro – rock fragment phase; Red: Biotite Quartz Diorite; Cyan: Nipissing Gabbro Average (Lightfoot and Naldrett, 1996); Yellow/Brown: Basswood Intrusion (Lightfoot and Naldrett, 1996). Primitive mantle values are from McDonough and Sun, 1995. Upwards pointing triangles are points from the upper group of the Shakespeare intrusion intercepted in drill hole U-03-119. Square points are Nipissing Gabbro Average points. Downwards pointing triangles are Basswood Intrusion points.

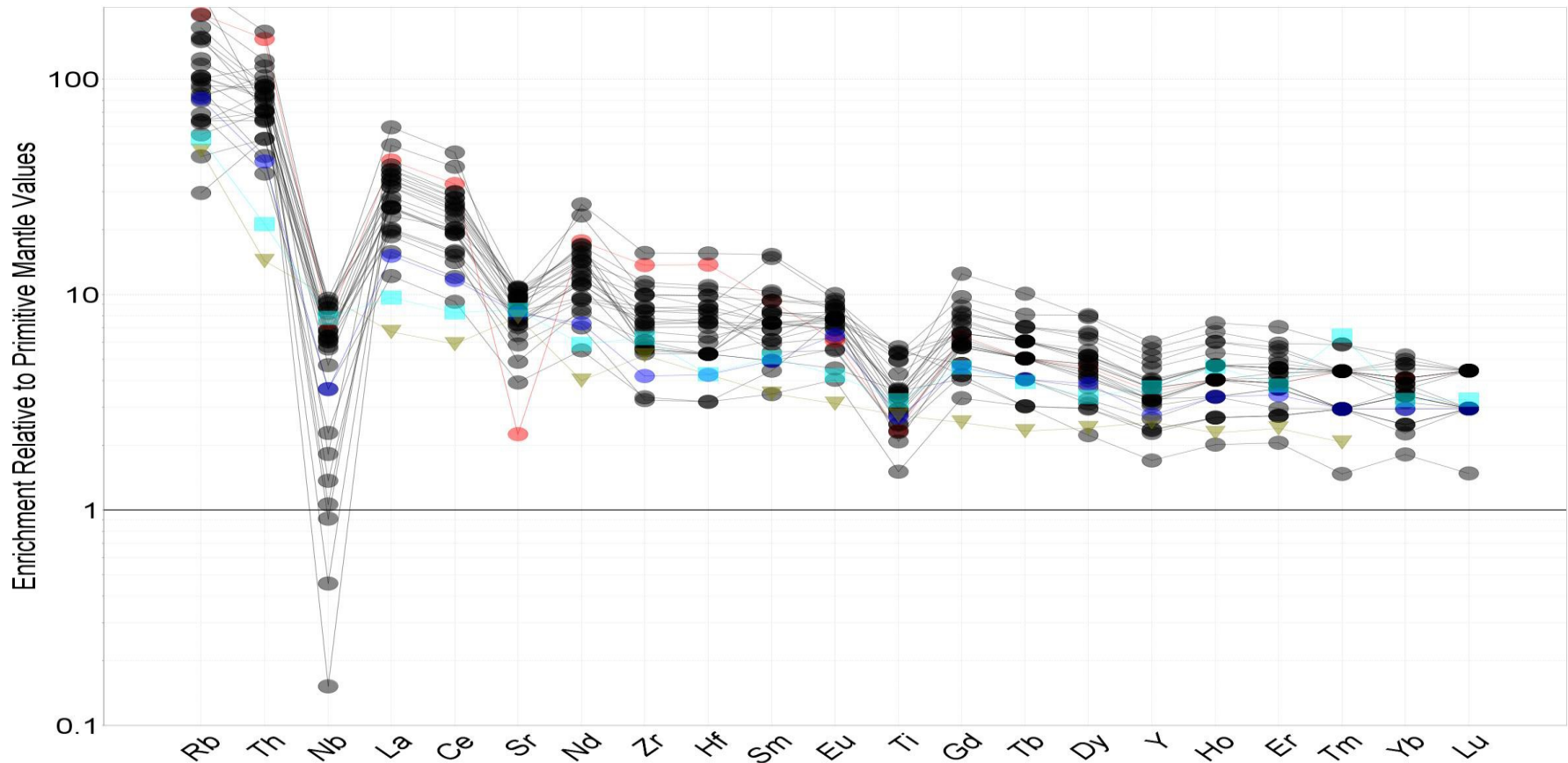


Figure 27: Primitive mantle normalized trace element spider diagram for diamond drill hole U-03-122. Red: Biotite Quartz Diorite; Grey/Black: Quartz Gabbro; Blue: Melagabbro – equigranular phase; Cyan: Nipissing Gabbro Average (Lightfoot and Naldrett, 1996); Yellow/Brown: Basswood Intrusion (Lightfoot and Naldrett, 1996). Primitive mantle values are from McDonough and Sun, 1995. Circle points are from the upper group of the Shakespeare intrusion intercepted in drill hole U-03-122. Square points are Nipissing Gabbro Average points. Downwards pointing triangles are Basswood Intrusion points.

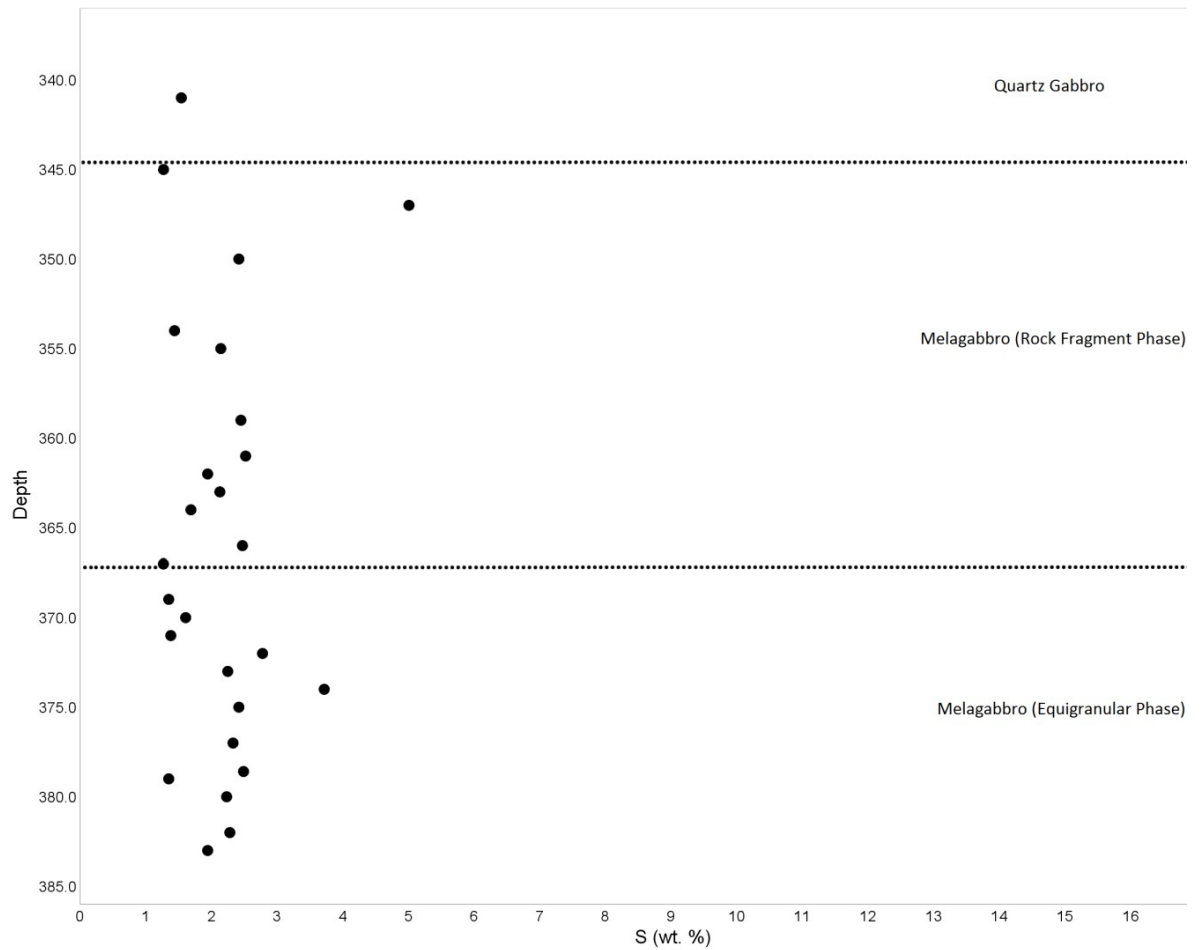


Figure 28: Sulfur obtained by LECO analysis versus depth for drill hole U-03-119. Depth is in meters, sulfur is in weight percent, and dotted lines mark unit boundaries. Since samples with sulfur concentrations less than one percent were omitted from the calculation of sulfide metal concentrations, they are also omitted from this graph to avoid confusion.

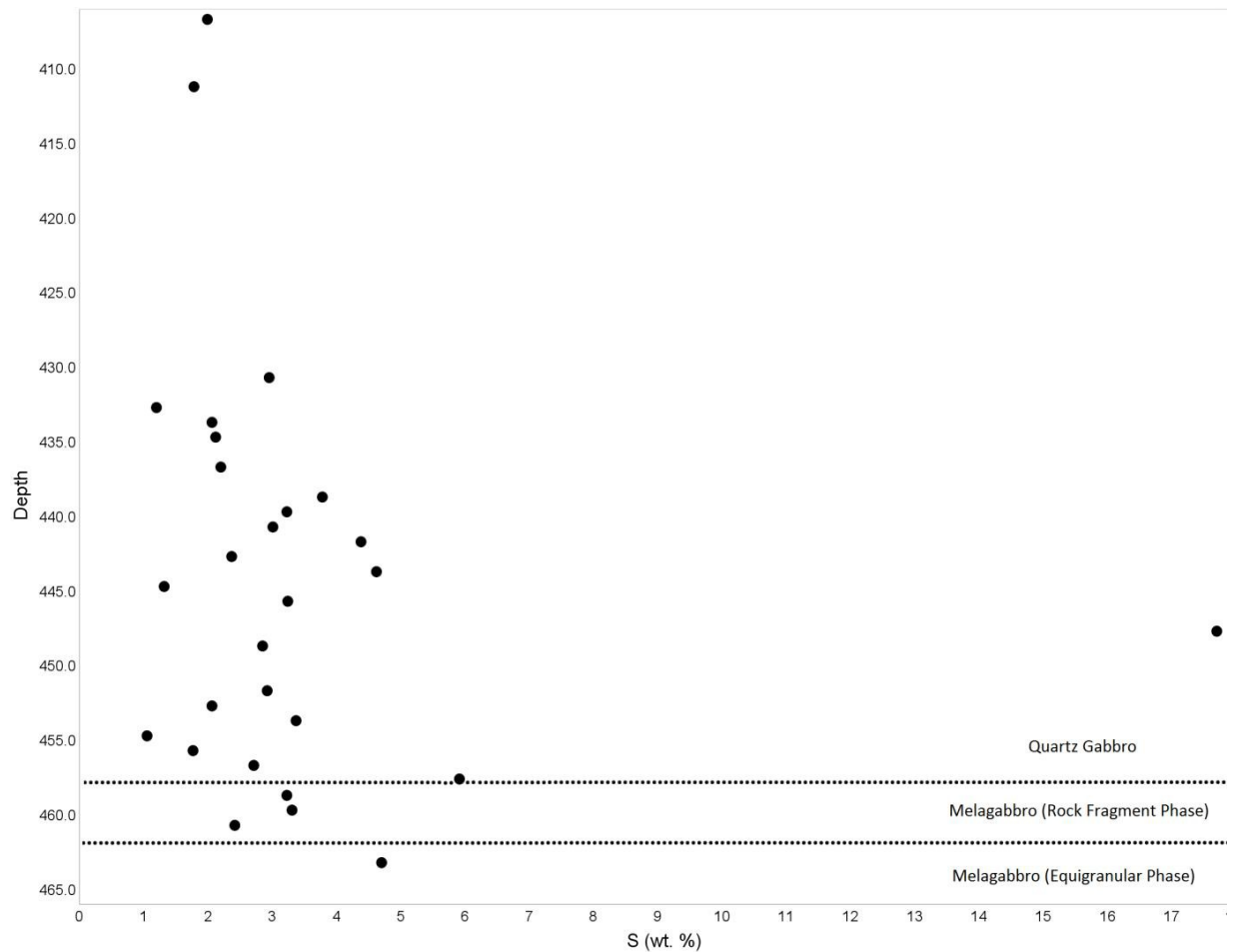


Figure 29: Sulfur obtained by LECO analysis versus depth for drill hole U-03-122. Depth is in meters, sulfur is in weight percent, and dotted lines mark unit boundaries. Since samples with sulfur concentrations less than one percent were omitted from the calculation of sulfide metal concentrations, they are also omitted from this graph to avoid confusion.

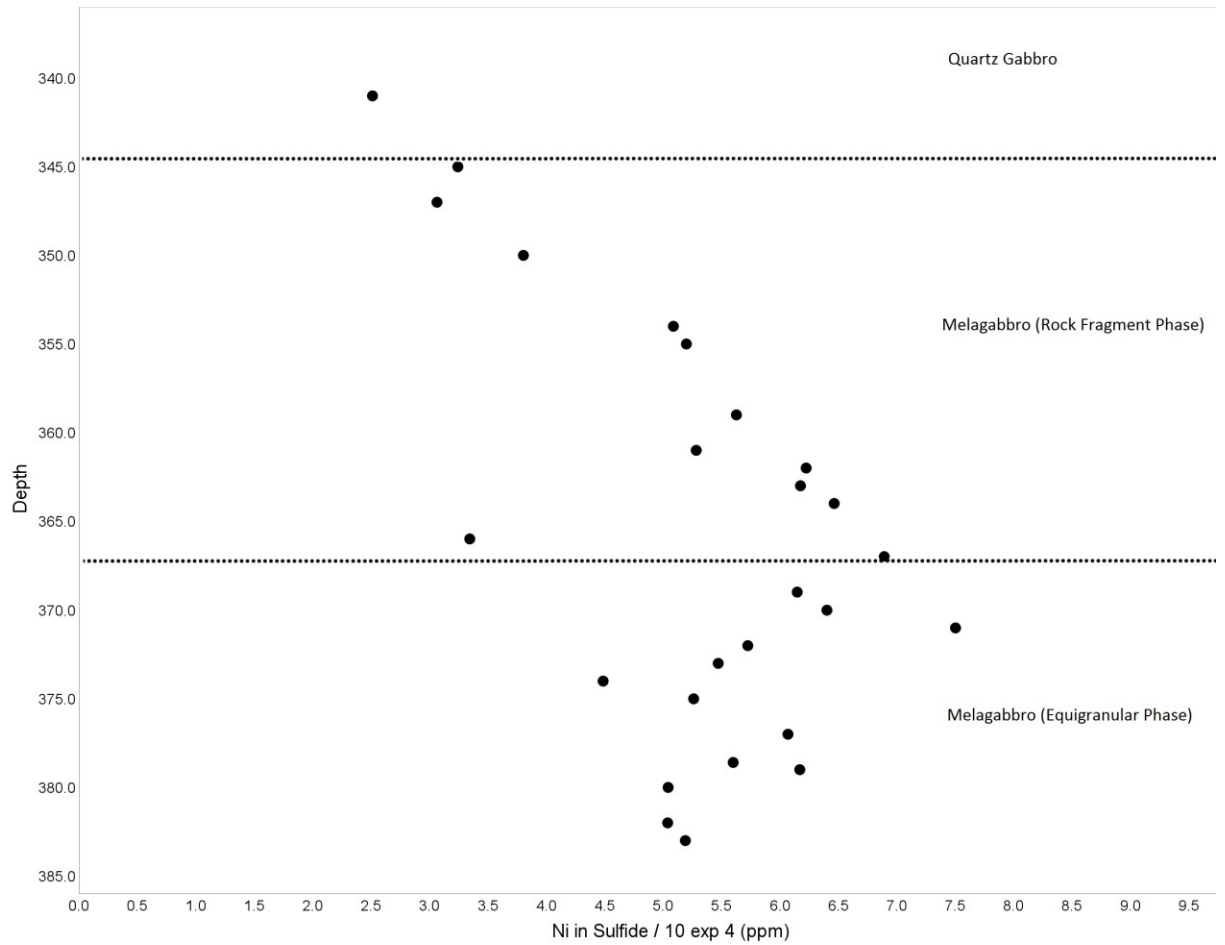


Figure 30: Sulfide nickel concentrations, based on 100% sulfide, versus depth for drill hole U-03-119. Depth is in meters, nickel is ppm divided by 10^4 , and dotted lines mark unit boundaries. Samples with sulfur concentrations lower than one percent are omitted as per the recommendations of Kerr (2003). Interconnected sulfides, i.e. those points near and above the quartz gabbro boundary, display significantly lower metal tenors than the disseminated sulfides, i.e. all other points.

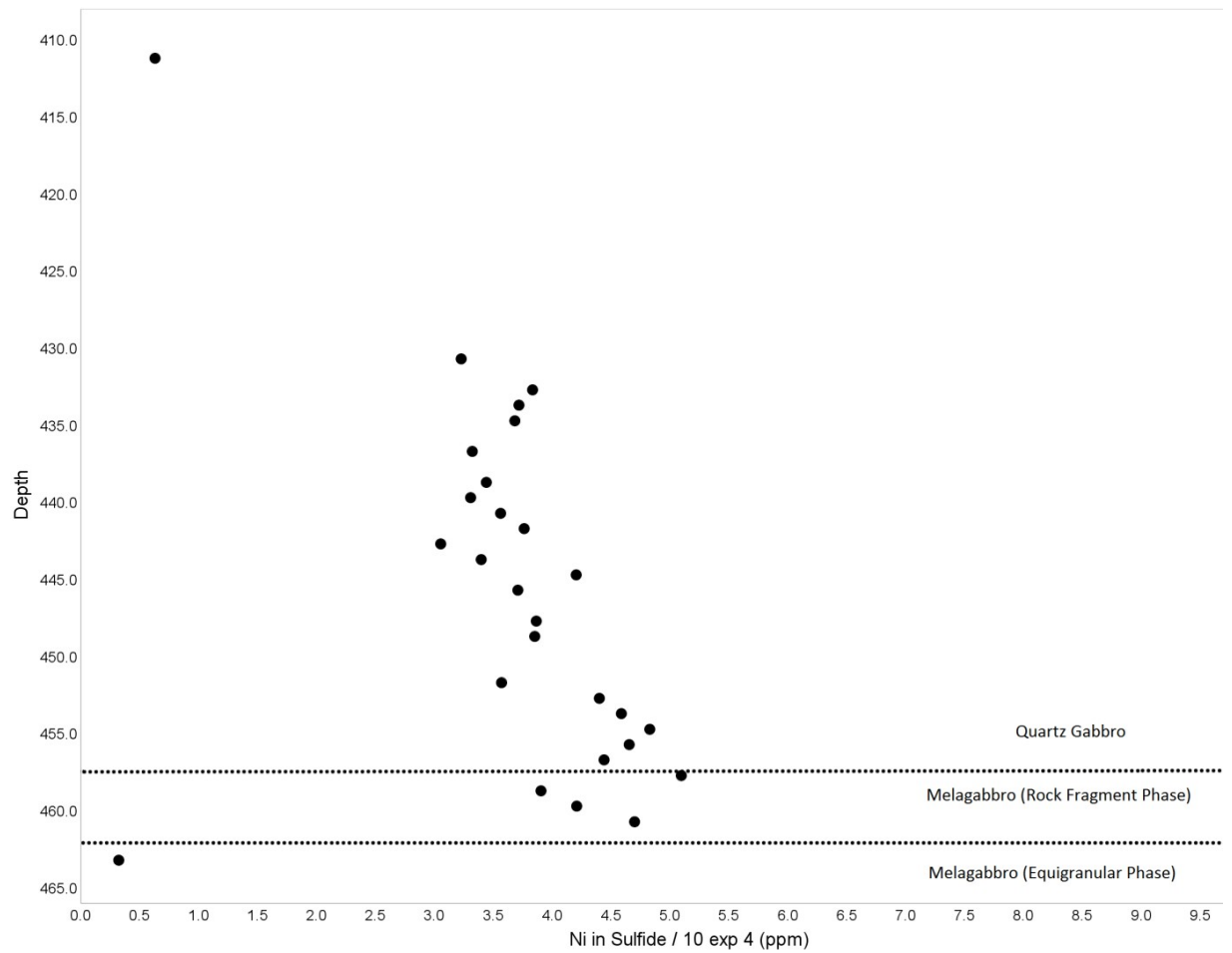


Figure 31: Sulfide nickel concentrations, based on 100% sulfide, versus depth for drill hole U-03-122. Depth is in meters, nickel is ppm divided by 10^4 , and dotted lines mark unit boundaries. Samples with sulfur concentrations lower than one percent are omitted as per the recommendations of Kerr (2003). Interconnected sulfides, i.e. those points near and above the quartz gabbro boundary, display significantly lower metal tenors than the disseminated sulfides, i.e. all other points.

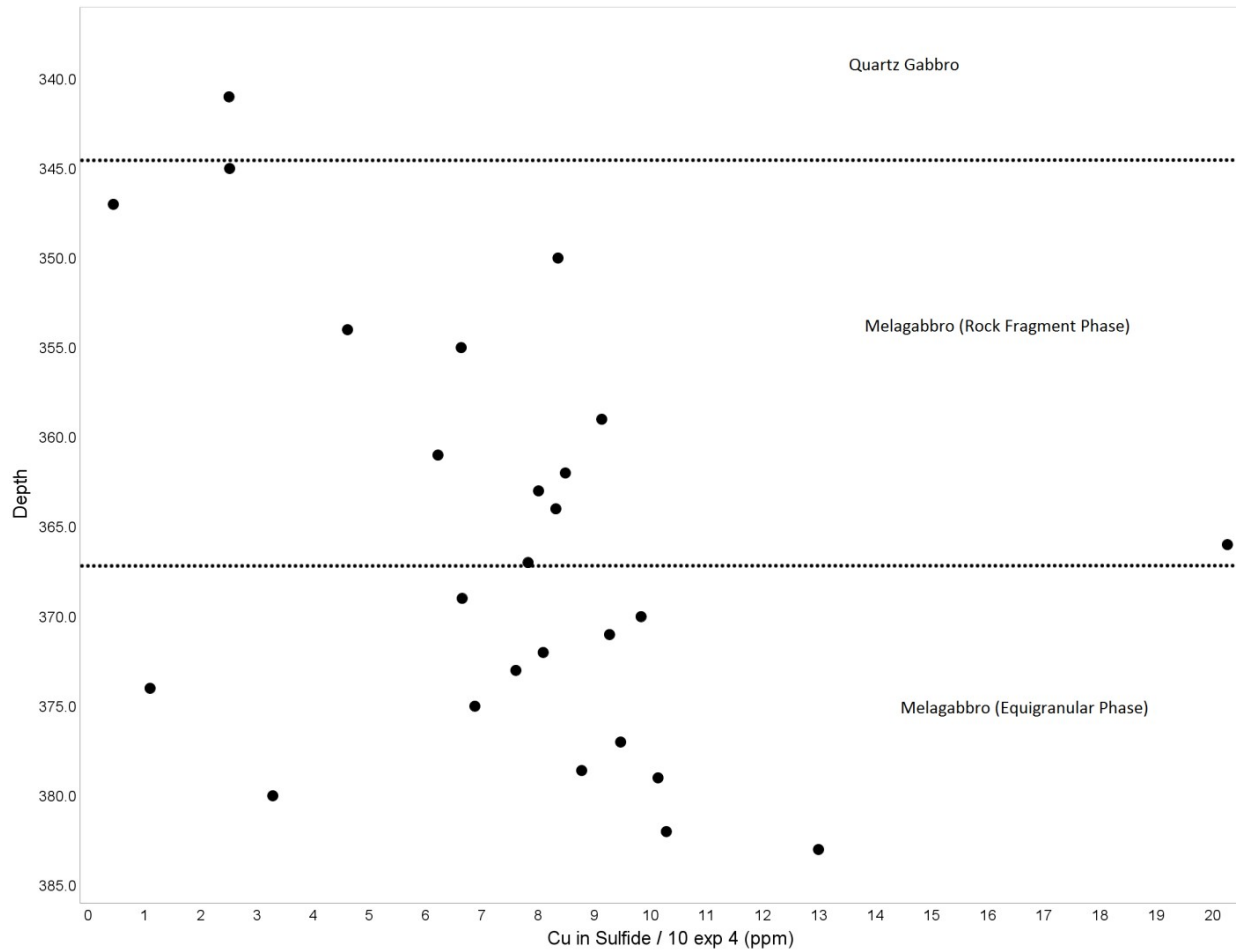


Figure 32: Sulfide copper concentrations, based on 100% sulfide, versus depth for drill hole U-03-119. Depth is in meters, copper is ppm divided by 10^4 , and dotted lines mark unit boundaries. Samples with sulfur concentrations lower than one percent are omitted as per the recommendations of Kerr (2003). Interconnected sulfides, i.e. those points near and above the quartz gabbro boundary, display significantly lower metal tenors than the disseminated sulfides, i.e. all other points.

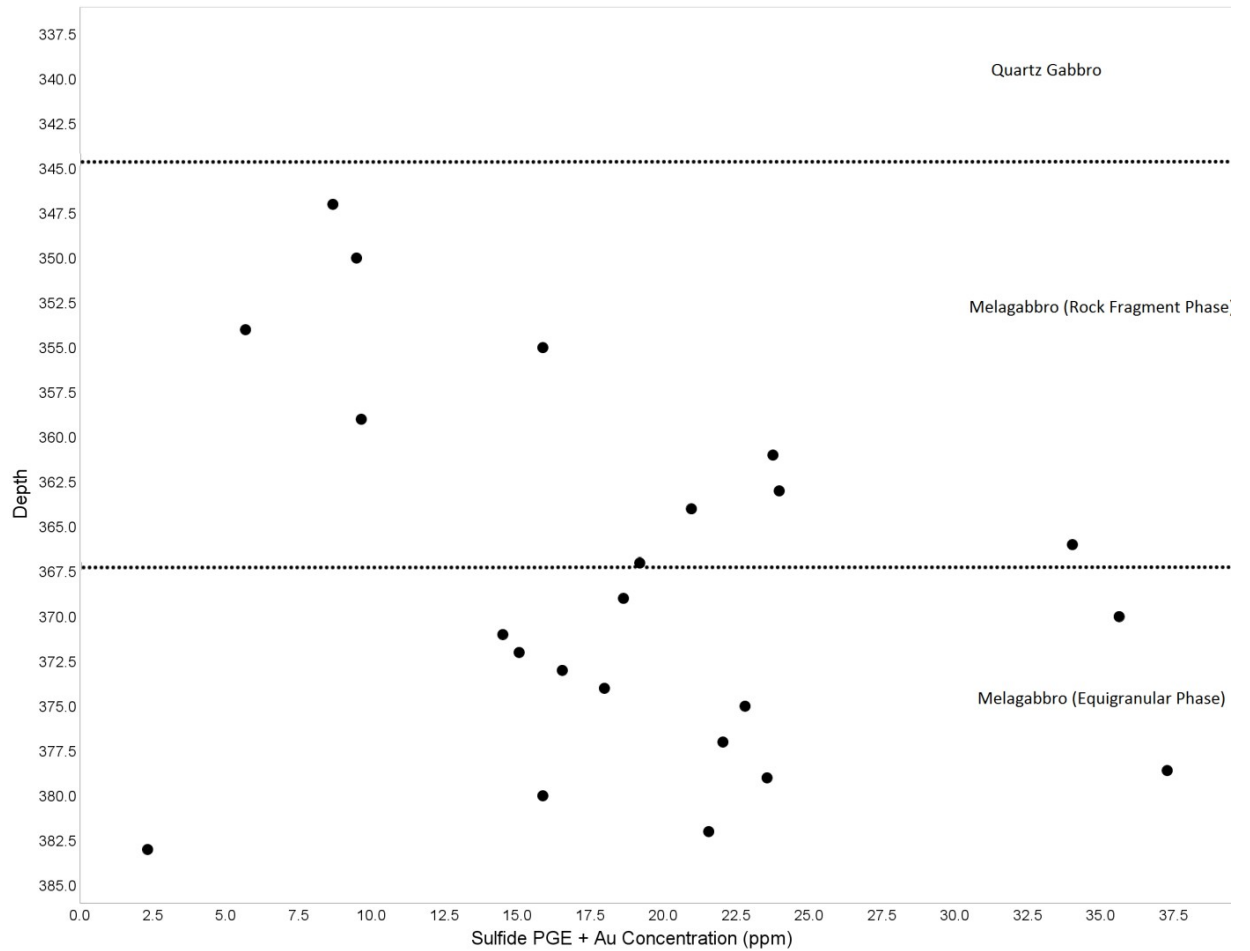
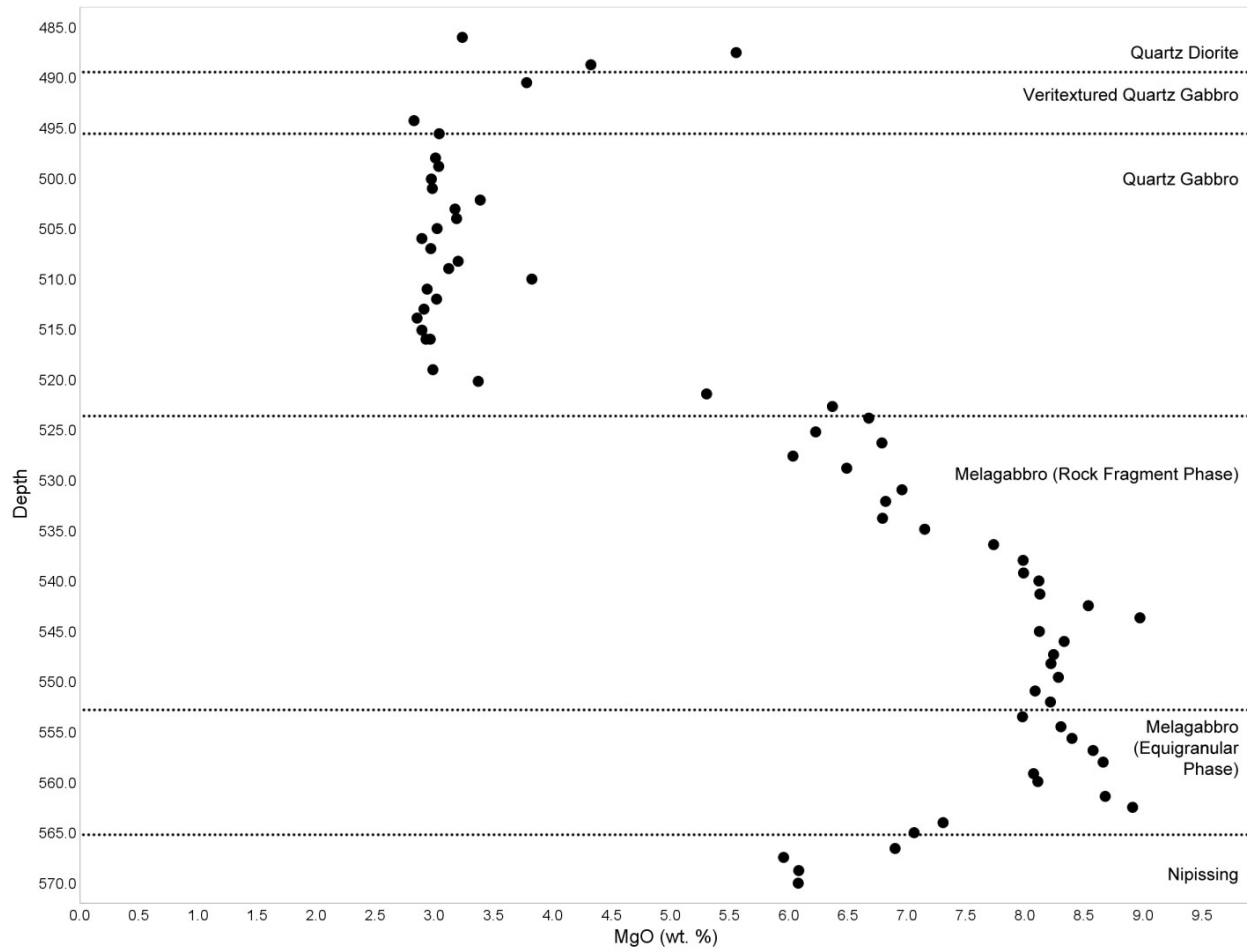


Figure 33: Sulfide platinum group elements + gold concentrations, based on 100% sulfide, versus depth for drill hole U-03-119. Depth is in meters, PGE + Au is ppm, and dotted lines mark unit boundaries. Samples with sulfur concentrations lower than one percent are omitted as per the recommendations of Kerr (2003). Samples with PGE lower than detection limits are also omitted. Interconnected sulfides, i.e. those points near and above the quartz gabbro boundary, display significantly lower metal tenors than the disseminated sulfides, i.e. all other points.

Data obtained from analysis via XRF are presented in Appendix 7. Graphs displaying SiO_2 , MgO , and Fe_2O_3 vs. depth were constructed for holes U-03-118 (Figures 34, 35, and 36), U-03-119 (Figures 37, 38, and 39), and U-03-122 (40, 41, and 42). U-03-122 appears to be the least differentiated based on SiO_2 and MgO , followed by U-03-119 and U-03-118. Fe_2O_3 is intended to be a general proxy to indicate the intensity and frequency of iron sulfides.

Further analysis of whole rock and isotopic data yields important insights into the character and genesis of the Shakespeare deposit and are further separated into interpretation of geochemical results as they apply to sulfide mineralogy and genesis, contamination of Shakespeare magmas, and the cause of differentiation within the Shakespeare deposit.



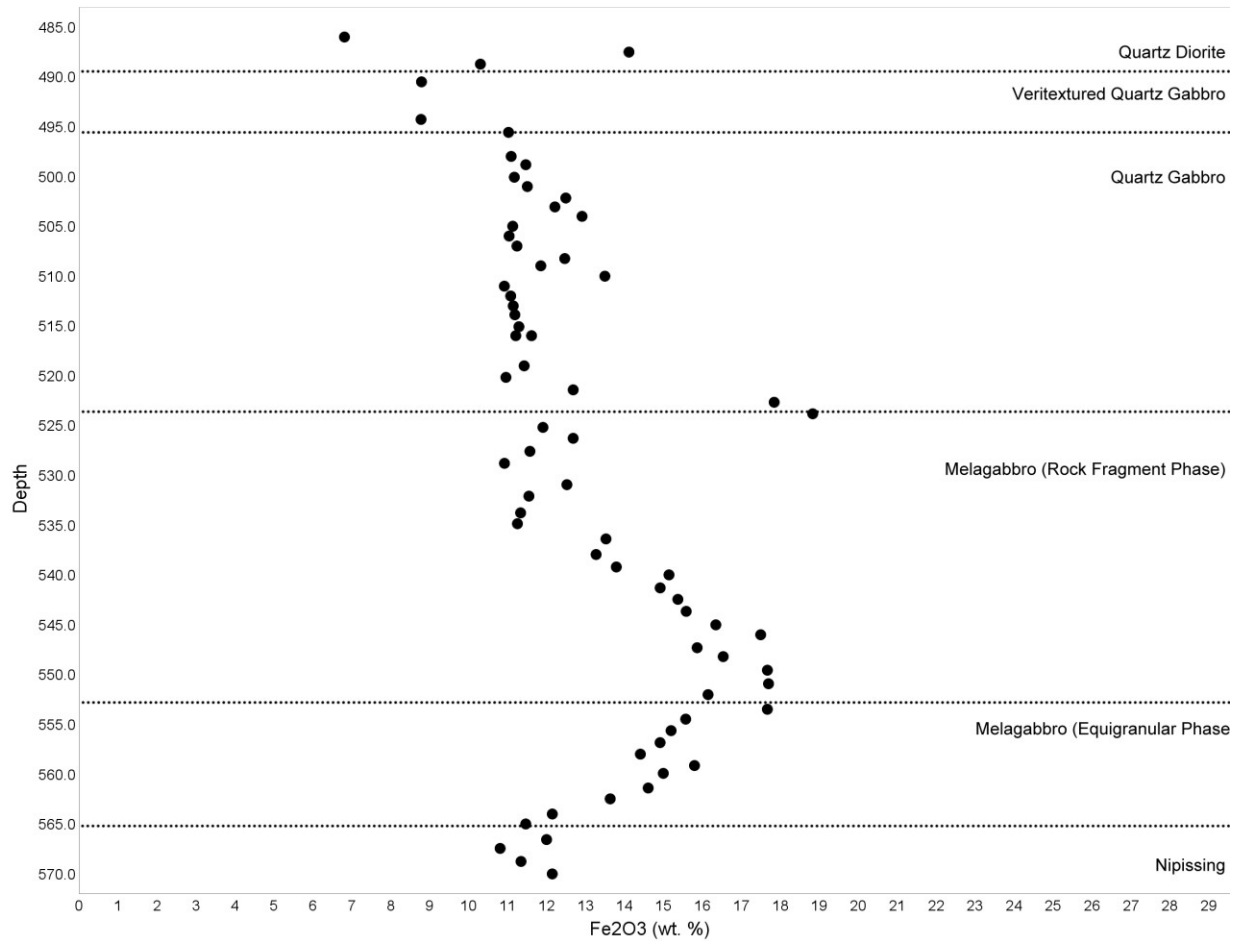


Figure 35: Fe₂O₃ versus depth for drill hole U-03-118. Fe₂O₃ data is from the XRF analysis and is displayed in weight percent. Depth is in meters and dotted lines mark unit boundaries. The increases in Fe₂O₃ concentration observed in the melagabbro and at the quartz gabbro / melagabbro boundary are the result of disseminated and interconnected Ni-Cu-PGE sulfides, respectively.

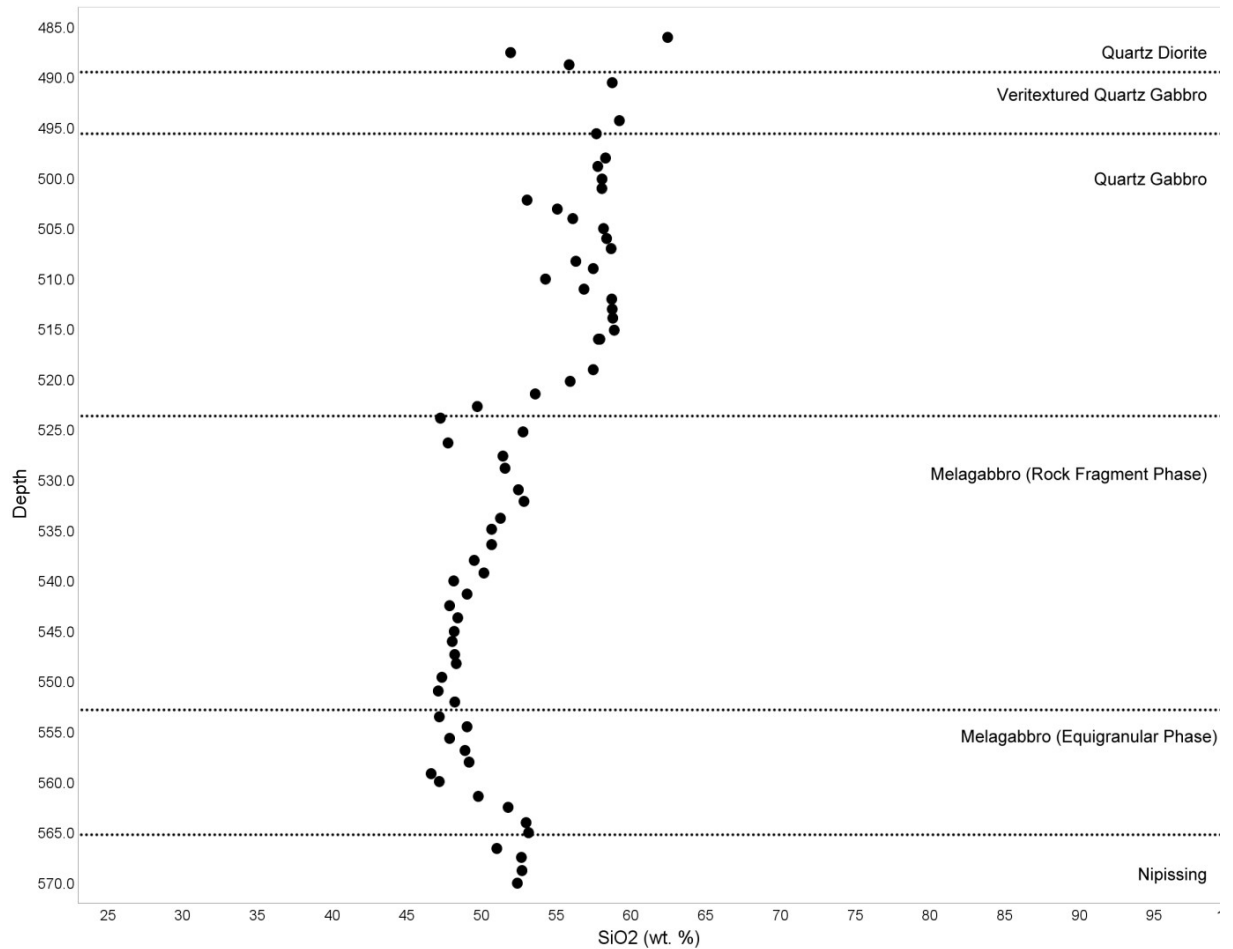


Figure 36: SiO₂ versus depth for drill hole U-03-118. SiO₂ data is from the XRF analysis and is displayed in weight percent. Depth is in meters and dotted lines mark unit boundaries. Note the prominent trough which begins developing at the quartz gabbro / melagabbro boundary and then tapers towards the contact with the lower group, labelled "Nipissing". The beginning of the trough at the quartz gabbro / melagabbro boundary is skewed as a result of abundant iron sulfides which depresses the composition relative to Fe₂O₃.

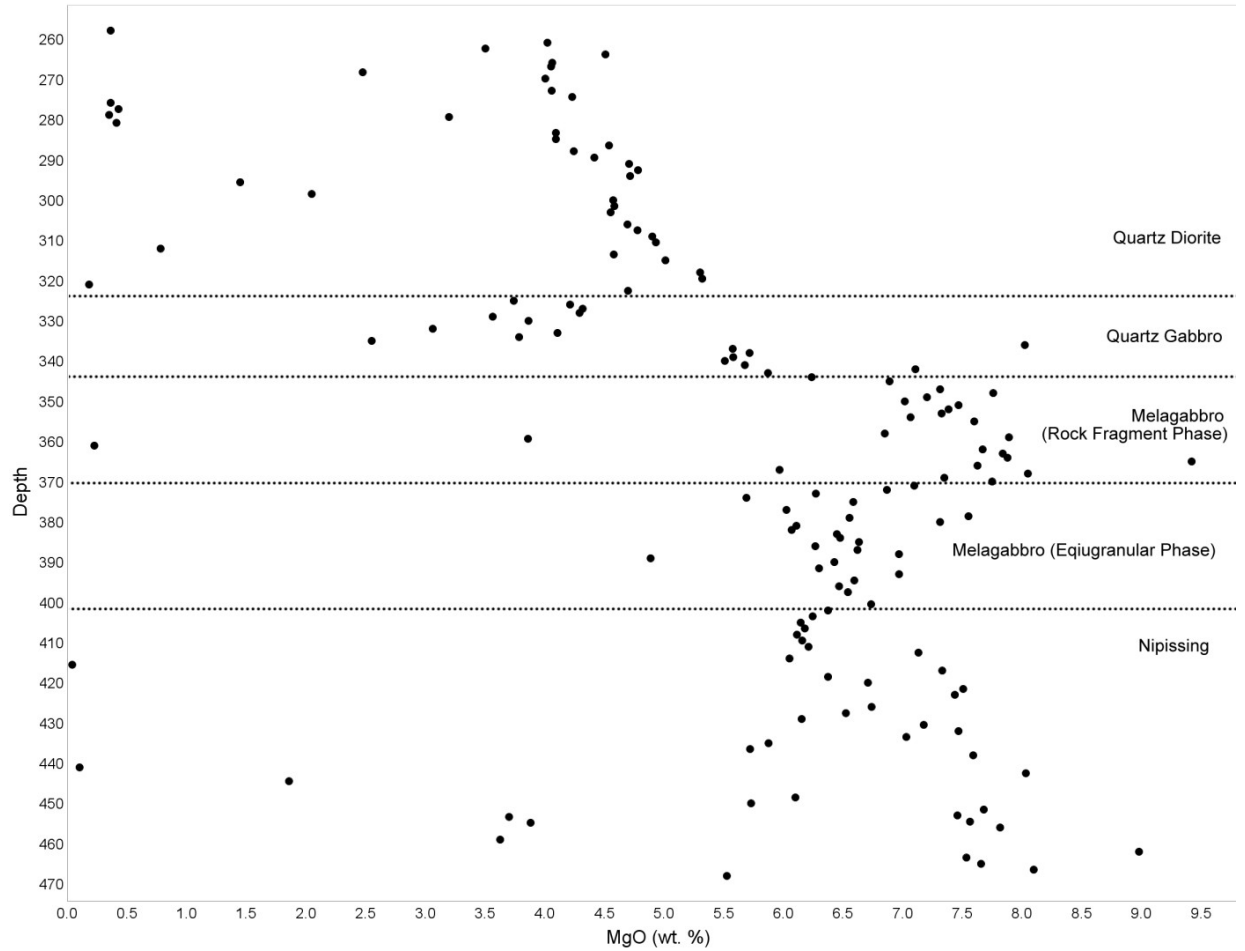


Figure 37: MgO versus depth for drill hole U-03-119. MgO data is from the XRF analysis and is displayed in weight percent. Depth is in meters and dotted lines mark unit boundaries. Note that the hump begins developing within the quartz gabbro unit and then tapers towards the contact with the lower group, labelled "Nipissing".

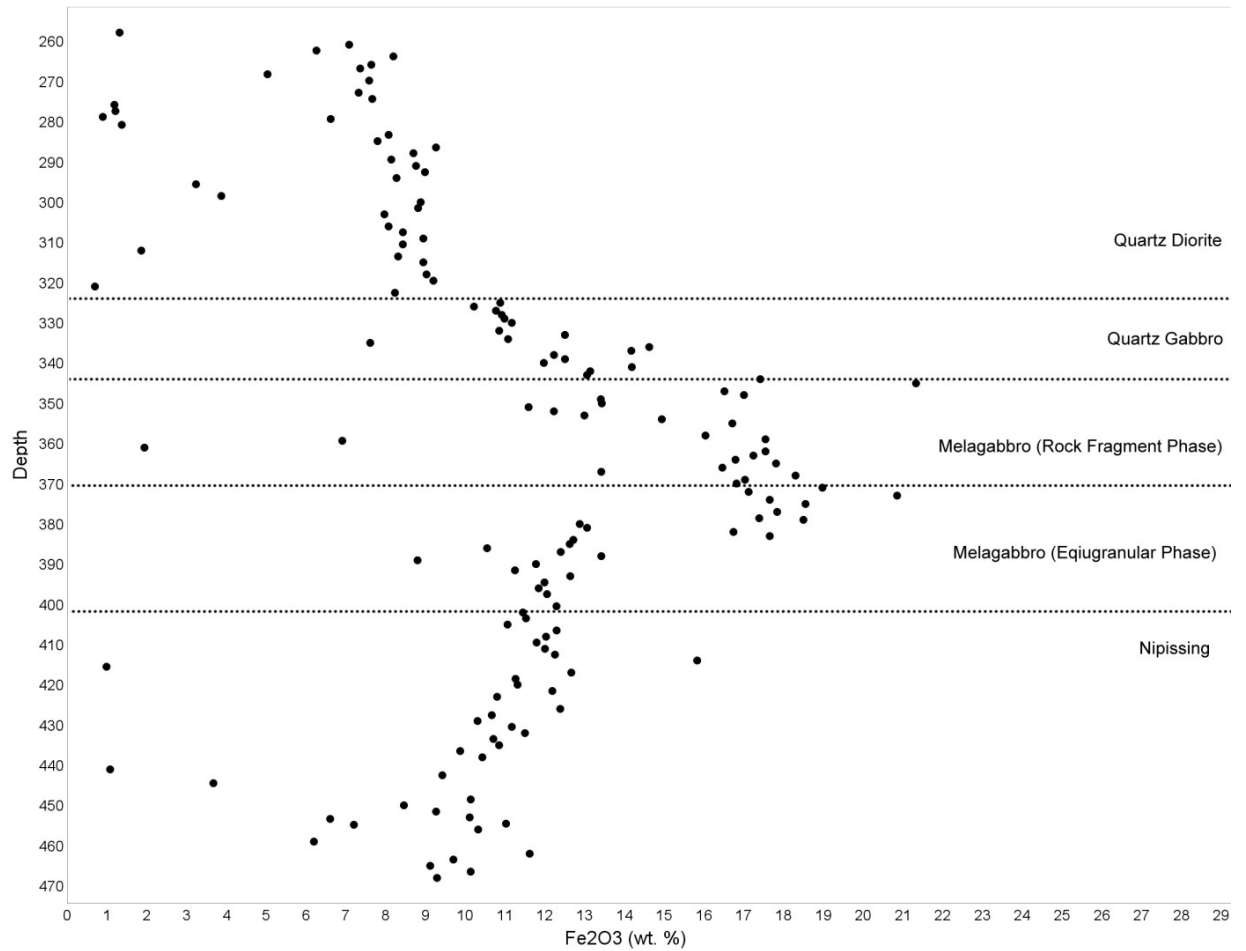


Figure 38: Fe₂O₃ versus depth for drill hole U-03-119. Fe₂O₃ data is from the XRF analysis and is displayed in weight percent. Depth is in meters and dotted lines mark unit boundaries. The increases in Fe₂O₃ concentration observed in the melagabbro and at the quartz gabbro / melagabbro boundary are the result of disseminated and interconnected Ni-Cu-PGE sulfides, respectively.

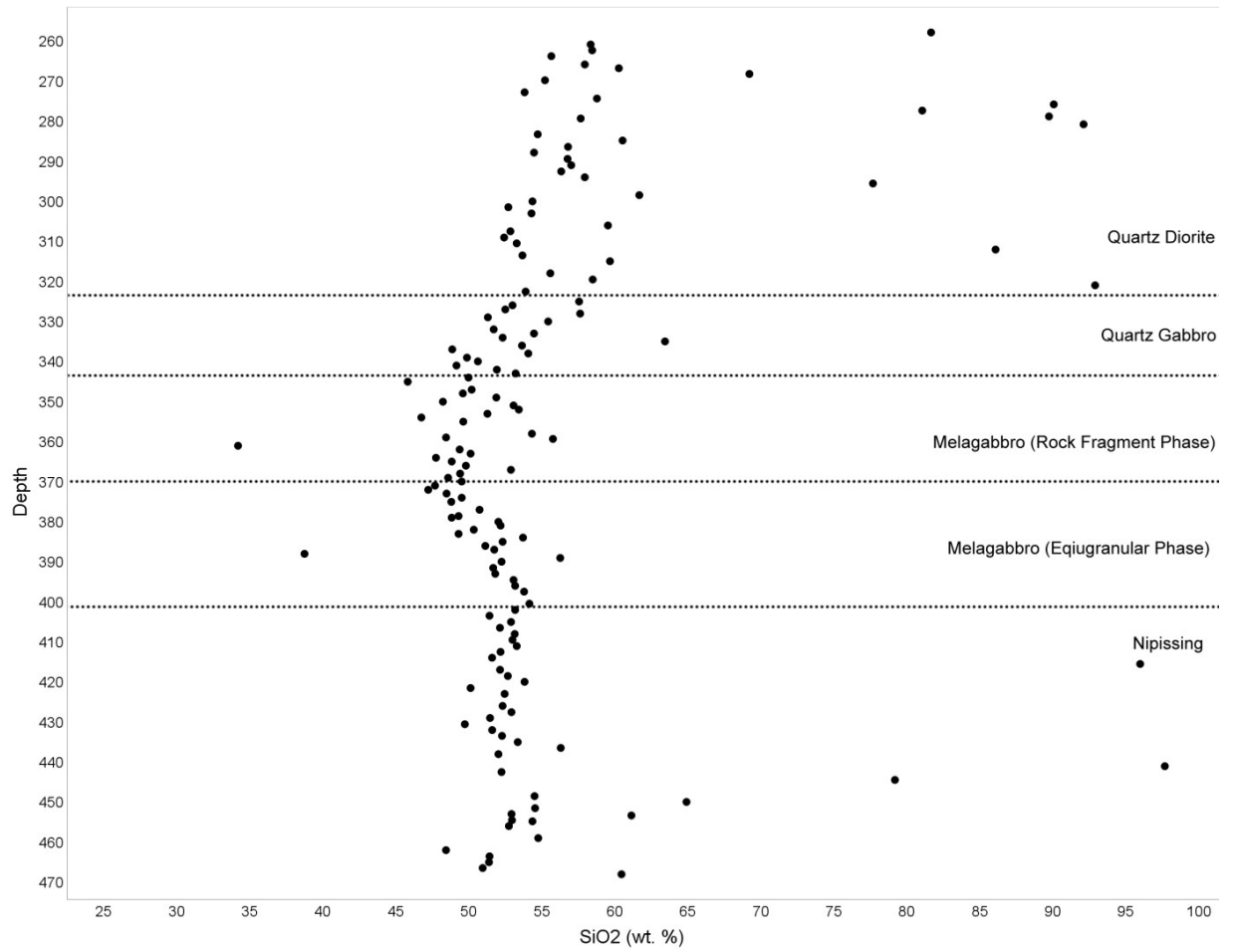


Figure 39: SiO₂ versus depth for drill hole U-03-119. SiO₂ data is from the XRF analysis and is displayed in weight percent. Depth is in meters and dotted lines mark unit boundaries. Note that the trough begins developing within the quartz gabbro unit and then tapers towards the contact with the lower group, labelled "Nipissing".

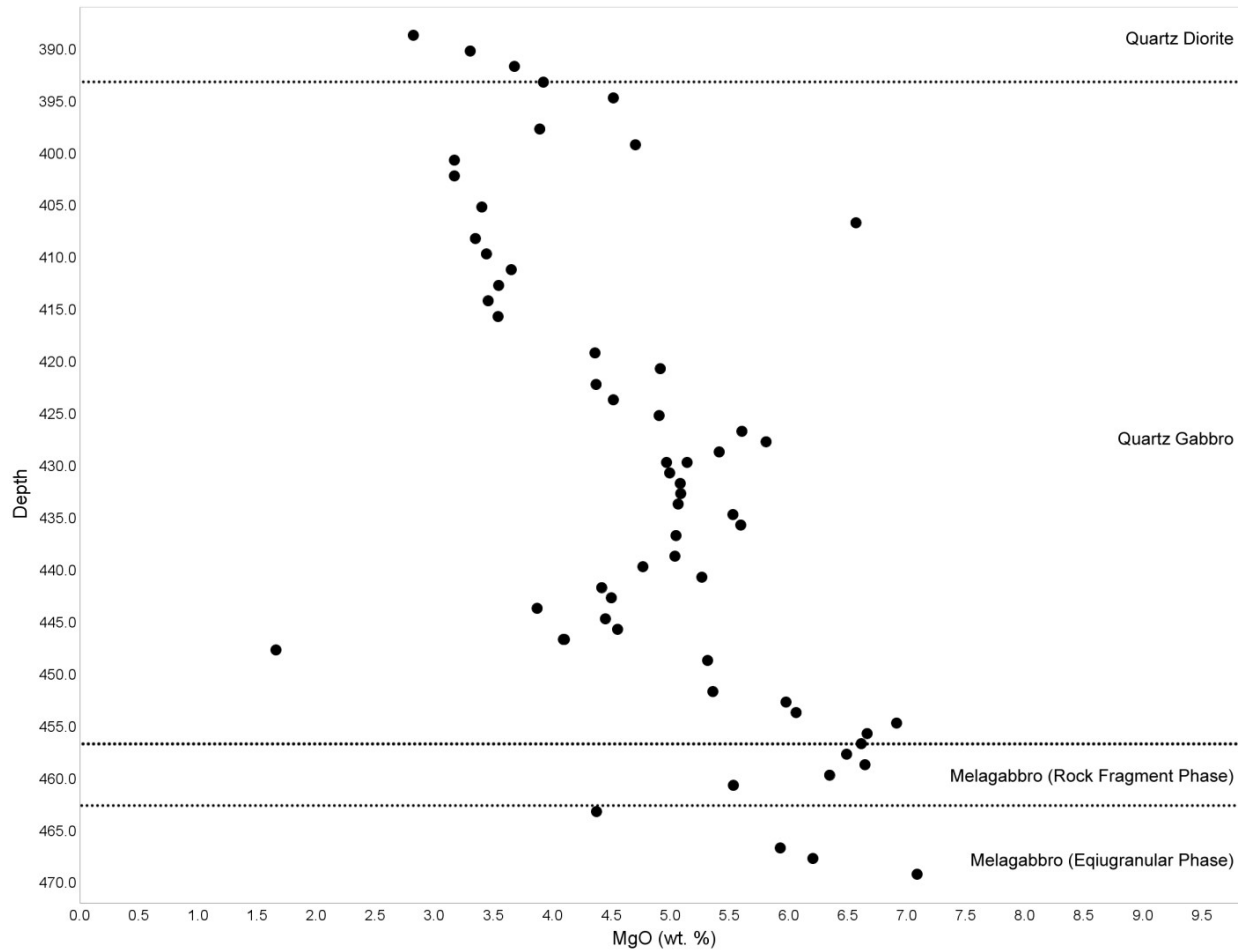


Figure 40: MgO versus depth for drill hole U-03-122. MgO data is from the XRF analysis and is displayed in weight percent. Depth is in meters and dotted lines mark unit boundaries. Note that the hump is entirely developed within the quartz gabbro unit and then increases in concentration until it reaches the quartz gabbro / melagabbro boundary. The hump in U-03-122 has a lower maximum concentration (5.5 percent MgO) compared to U-03-118 (8.5 percent MgO).

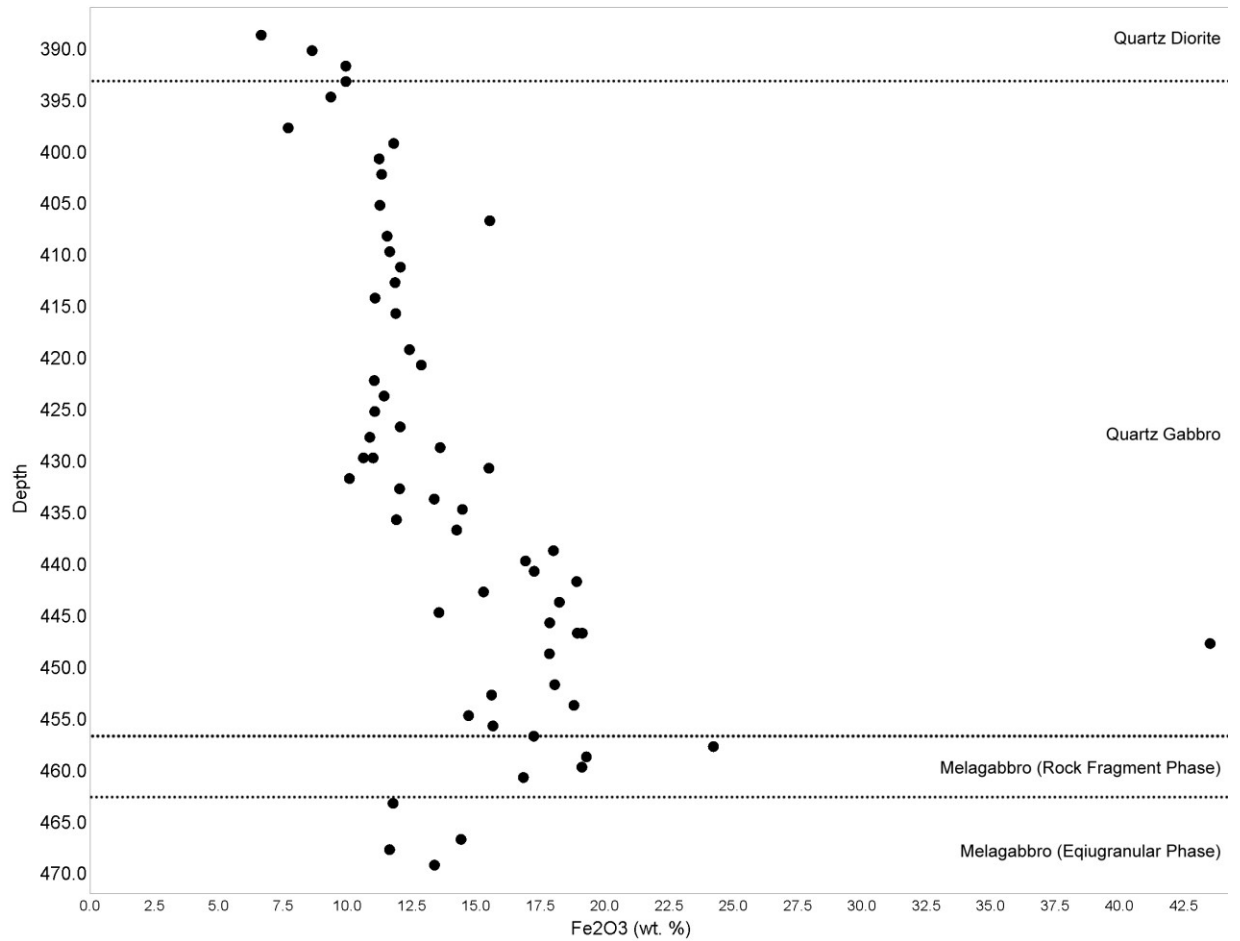


Figure 41: Fe₂O₃ versus depth for drill hole U-03-122. Fe₂O₃ data is from the XRF analysis and is displayed in weight percent. Depth is in meters and dotted lines mark unit boundaries. The increases in Fe₂O₃ concentration observed in the melagabbro and at the lower portions of the quartz gabbro unit are the result of disseminated and interconnected Ni-Cu-PGE sulfides, respectively.

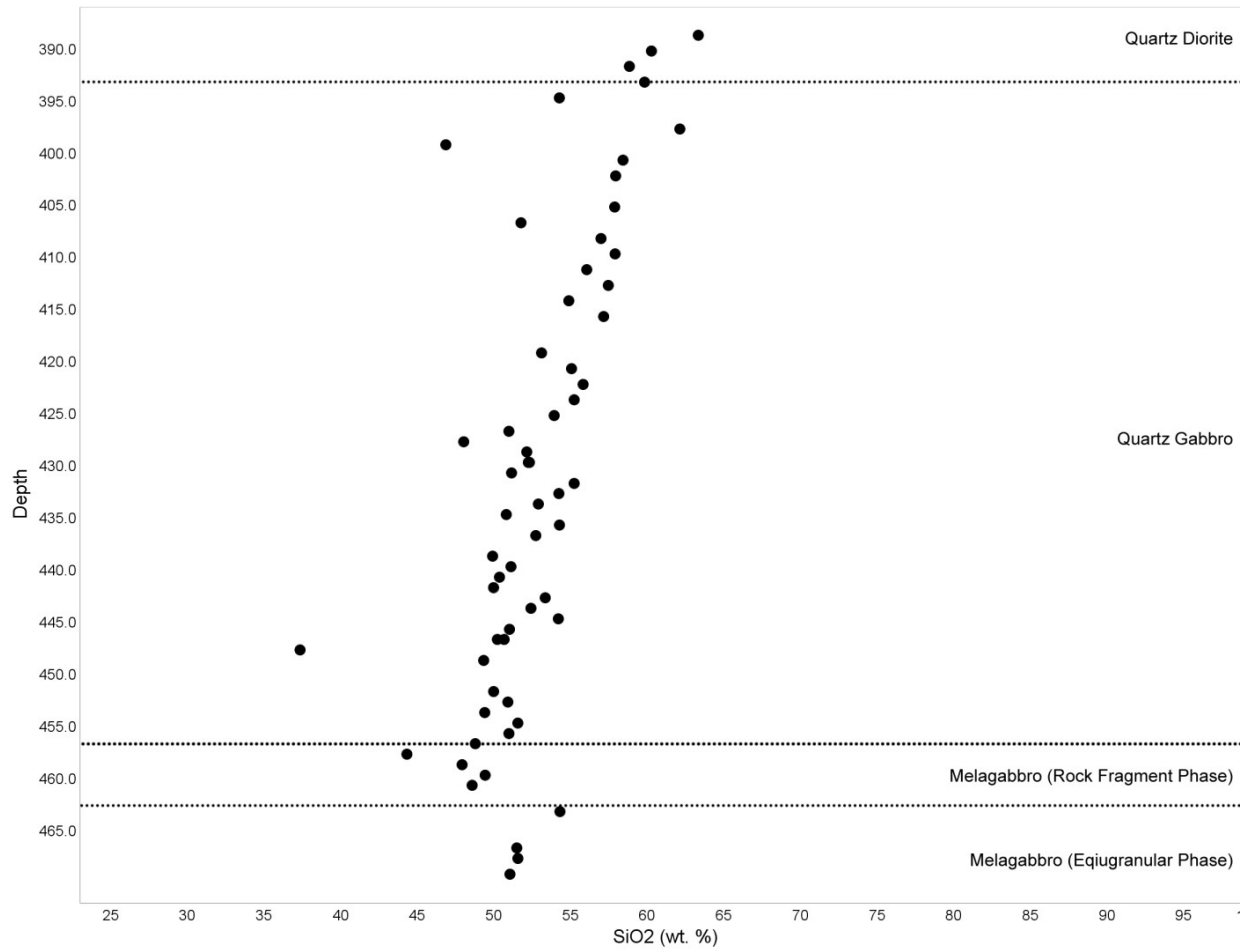


Figure 42: SiO₂ versus depth for drill hole U-03-122. SiO₂ data is from the XRF analysis and is displayed in weight percent. Depth is in meters and dotted lines mark unit boundaries. Note that no trough exists. Rather, a strikingly linear trend from the base of the quartz gabbro to the lower portions of the biotite quartz diorite unit is observed.

Chapter 5: Discussion

5.1 - Contamination of Shakespeare Magmas

Sproule et al. (2007) compared the contamination history of the Shakespeare intrusion with other Nipissing magmas, concluding that the Shakespeare intrusion displays characteristics of magmas that have interacted with upper continental crust. Those characteristics include enrichment in U, Th, Nb, and LREE relative to MREE and pronounced negative Nb and Ti anomalies, relative to similarly compatible elements. These features have been observed elsewhere in the Nipissing LIP and are considered to be a defining feature of the Nipissing Gabbros (Lightfoot and Naldrett, 1996). Sproule et al. (2007) suggested that the Shakespeare intrusion is more contaminated than other Nipissing Gabbros based on mantle normalized La/Sm, Nb/Th, and Th/Zr. Primitive mantle normalized trace element spider diagrams (Figures 25, 26, and 27) all exhibit elevated LREE vs HREE, enrichment in HFSE relative to MREE, pronounced negative Nb and Ti anomalies relative to elements of similar compatibility, and moderate negative Sr anomalies relative to elements of similar compatibility. They also show significant fluctuations in the severity of the Nb and Ti depletions, with poorly mineralized samples from the Quartz Gabbro lithology displaying the most pronounced depletion. The results of this study indicate that many of the statements made about the geochemical profile of the Shakespeare deposit by Sproule et al. (2007) are valid; i.e. the Shakespeare lithologies are highly contaminated as a result of the assimilation of upper crustal materials by ascending Shakespeare magmas.

Sproule et al. (2007) utilized only five data points from the Shakespeare intrusion and many dozens of points from other Nipissing gabbros for the construction of geochemical plots,

such as La/Sm versus Nb/Th. As a result, some geochemical characteristics of the Shakespeare intrusion were not adequately documented. The data presented in Figure 43 clearly show a variable but depressed Nb/Th ratio relative to the values reported by Sproule et al. (2007).

Further examination of the data reveals that Shakespeare samples have values which deviate from the Nipissing trend as follows (Appendix 4):

- 1) The average concentration of Nb is 3.05 ppm in Shakespeare samples (high of 5.7 ppm, low of <0.1 ppm). The average concentration in other Nipissing gabbro samples is 5.12 ppm. The average of 3.05 ppm represents a concentration of approximately 6 times mantle values (0.658 ppm). The average of 5.12 ppm in other Nipissing gabbro samples represents a concentration of eight times mantle values.
- 2) The average concentration of Th is 6.51 ppm in Shakespeare samples (high of 13.2 ppm, low of 2.1 ppm). The average concentration in other Nipissing gabbro samples is 1.69 ppm. The average of 6.51 ppm represents a concentration of approximately 82 times mantle values (0.079 ppm). The average of 1.69 ppm in other Nipissing gabbro samples represents a concentration of approximately 21 times mantle values.
- 3) The average concentration of U is 2.22 ppm in Shakespeare samples (high of 5.2 ppm, low of 0.9 ppm). The average concentration of U in other Nipissing gabbro samples is 0.52 ppm. The average of 2.22 ppm represents a concentration of 109 times mantle values. The average concentration of 0.52 ppm in other Nipissing gabbros represents a concentration of 26 times mantle values.

Thus, the average mantle normalized Nb/Th for Shakespeare samples is approximately 0.07, a ratio lower than that of the Proterozoic pelitic rock used by Sproule et al. (2007) to represent the contaminant. Obviously, this suggests that the contamination trend proposed by

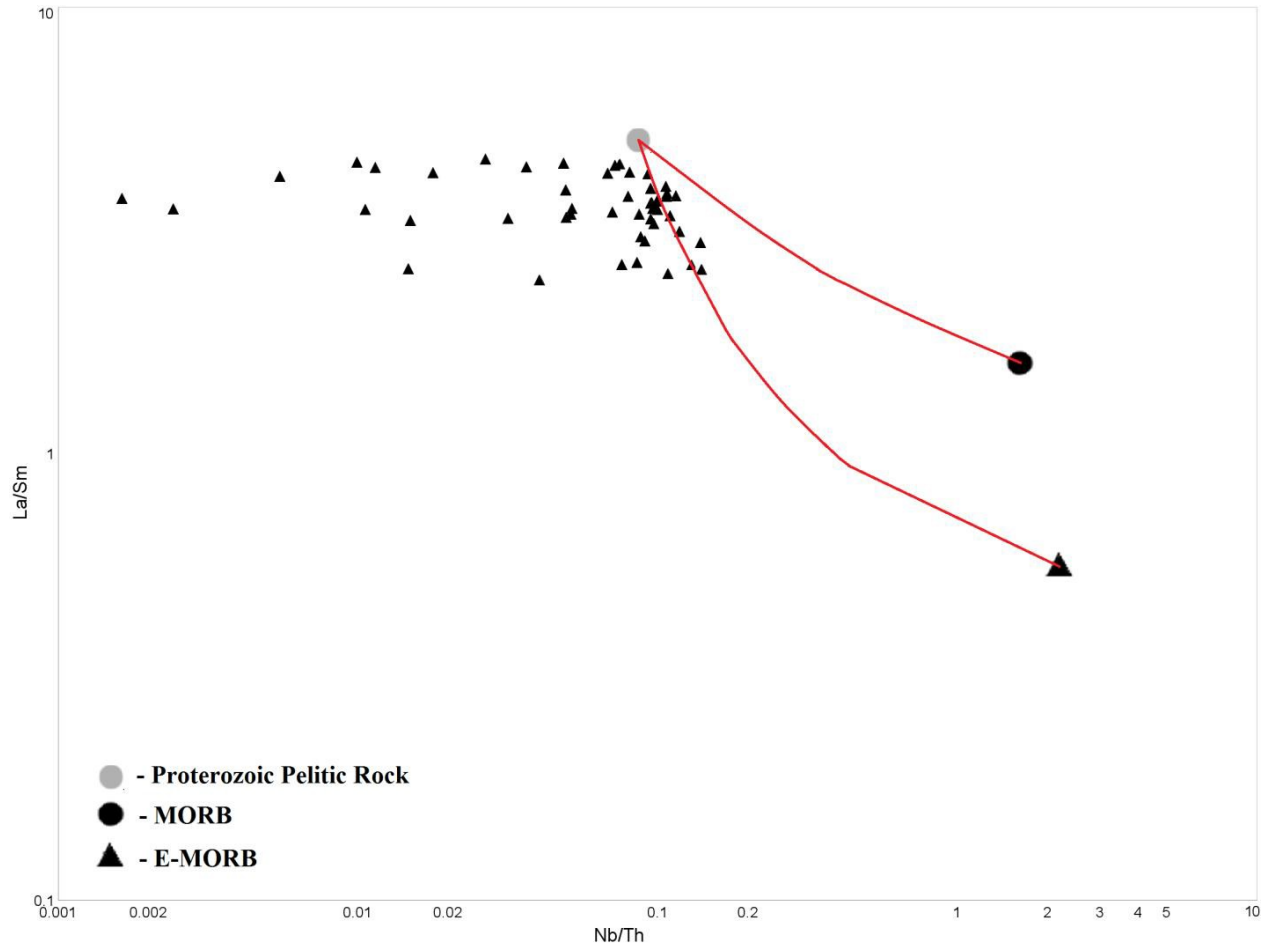


Figure 42: Mantle normalized La/Sm versus Nb/Th . Values are normalized to those presented by McDonough and Sun, 1995. Proterozoic Pelitic Rock, MORB, and E-MORB points are taken from Sproule et. al. (2007). The Proterozoic Pelitic Rock is the contaminant proposed by Sproule et al. (2007), which follows a mixing curve (red lines) between both MORB and E-MORB. Based on five data points from Shakespeare they suggested the primitive magmas were more contaminated than other Nipissing magmas. The data presented clearly show that an assimilant with the composition of the Proterozoic pelitic rock cannot explain the La/Sm or Nb/Th values observed.

Sproule et al. (2007) cannot be correct, as the decrease in the Nb/Th ratio is supposed to reflect increased contamination; an average magmatic ratio should never be lower than that of the contaminant. Additionally, samples with Th values elevated relative to the average of 6.51 ppm generally yield Nb/Th values lower than 0.07 (approaching 0.03): further implying the increase in thorium is generally the control on the depressed Nb/Th ratios. The intense enrichment of average Shakespeare samples in U, as well as Th, relative to other reported Nipissing gabbros (Figures 25, 26, and 27) suggests the presence of a different local contaminant. The highest previously reported value of 0.81 ppm U, i.e. the Obabika intrusion, Ontario, (Lightfoot and Naldrett, 1996) is less than the lowest reported value of 0.9 ppm U at Shakespeare. The significant (one and a half to three times) enrichment of LREE of Shakespeare samples relative to other Nipissing samples further suggests a distinct contaminant, unique to the Shakespeare intrusion. The concentration of Ce and La is particularly elevated amongst the LREE, with both exhibiting a three times concentration on average versus other Nipissing gabbro samples.

A reasonable candidate for a crustal contaminant that could explain Shakespeare's unique geochemistry is found in the Matinenda Formation of the Huronian Supergroup. This formation is variably present throughout the Huronian Supergroup and hosts the detrital uranium deposits located near Elliot Lake and Agnew Lake. The ore bodies, hosted by the quartz pebble conglomerate unit, are "elongate or tabular and vary greatly in size and are nearly all located in two troughs. The main uranium minerals are uraninite and brannerite which are associated with varying amounts of monazite, uranothorite, uranothorianite, coffinite, allanite, anatase, rutile, zircon, and titanite. Th: U ratios change from 1:4 to 4:1 depending on the proportion of thorium to uranium minerals. At Agnew Lake, for example,

uraniothorite and monazite predominate over uraninite and brannerite.”(Bowie, 1979). The matrix of the quartz pebble conglomerate also contains abundant pyrite (Long, 1987 with references therein). For reference, the past producing Agnew Lake uranium mine is less than 15 km from the western pit of the past-producing Shakespeare mine.

It is likely that the enrichment in Th, U, and LREE in Shakespeare rocks relative to other Nipissing Gabbros is a result of the intruding Shakespeare magmas interacting with (and assimilating) portions of the stratigraphically lower Matinenda Formation. More particularly, the magmas likely assimilated the detritus-rich quartz pebble conglomerate. The elevated Ce and La concentrations relative to other LREE are further explained by the presence of abundant detrital monazite ($[(\text{Ce},\text{La})\text{PO}_4]$) grains in the quartz pebble conglomerates associated with the past producing Agnew Lake uranium mine. This could provide an alternate explanation for the elevated La/Sm ratios observed for rocks in the Shakespeare intrusion other than higher degrees of crustal contamination. Sproule et al. (2007) acknowledged a different contamination history, when they suggested the Shakespeare intrusion was more contaminated; it is more likely that the degree of contamination (i.e. total percent assimilate) is similar, but that the assimilation of uraniferous quartz pebble conglomerates from the Matinenda formation imparted a robust geochemical signature as a result of that contamination. Thus, the difference in the contamination history based on geochemistry between the rocks that host the Shakespeare deposit and other rocks from the Nipissing gabbro suite is the contaminant and not necessarily the degree of contamination en route to the magma chamber. Unfortunately, a new contamination profile for the Shakespeare intrusion cannot be created as analysis of Th, Nb, La, and Sm from the past-producing Agnew Lake mine are not published.

5.2 - Genesis of the Biotite Quartz Diorite and Roof Zone

The biotite quartz diorite unit contains abundant xenoliths of varying size and shape (meter scale to microscopic scale) and textural evidence for significant anatexis / assimilation of overlying materials largely contributing to the siliceous nature of the biotite quartz gabbro is frequently observed. The melting and/or assimilation of the overlying quartzite mandate a higher thermal budget than required for a single pulse of gabbroic magma (Leshner and Sproule, personal communication). While a significant portion of the quartz in the biotite quartz diorite is likely unmelted / unassimilated microfragments of quartzite (very small clusters of quartz grains), the ratio of assimilated / unassimilated quartzite is difficult to determine. It is important to note that it is possible, if not probable, that the water contents in the proto-quartzite (pure quartz sandstone) were a few weight percent or more. Previous workers (Shaw et al., 1999) and field observations (Dr. Phillip Fralick, personal communication) indicate magmas from the Nipissing gabbro suite interacted with poorly lithified to non-lithified sedimentary material from the Huronian Supergroup.

The presence of very small fragments of quartzite within the roof zone (biotite quartz diorite unit) suggests a mechanical or chemical breakdown of coarser xenolithic materials. This breakdown could either be from melting, depending on amount of volatiles present, or assimilation between magma and quartzite. Assimilation is the preferred mechanism because the thermal energies necessary are much lower and the extremely high concentration of biotite in the unit suggests hydrated chemical interaction with the Mississagi quartzites. Additionally, the concentration of Th, U, and LREE more adequately reflect a contaminated Shakespeare magma that may have undergone partial crystallization and has interacted with

and assimilated the overlying Mississagi quartzite. The elevated Th, U, and LREE concentrations suggest contribution by Shakespeare magmas while the high SiO₂ concentrations are indicative of significant assimilation of the Mississagi quartzite.

Lightfoot and Naldrett (1989) suggest that the aplitic dikes of the Kerns intrusion were the result of a less dense magma that ponded at the roof of the intrusion and represented incomplete coupling of assimilation and fractional crystallization. They suggest that a double diffusive interface initially separated the magma but then eventually broke down under convective erosion. A similar phenomenon appears to have occurred within the Shakespeare intrusion, where Shakespeare magmas interacted with very large volumes of country rock to produce the biotite quartz diorite unit. The extreme variation in thickness of the biotite quartz diorite and quartz gabbro units are plausibly explained by the convective erosion described by Lightfoot and Naldrett (1989) and is supported by the presence of diorite fragments in the quartz gabbro and melagabbro-rock fragment units. Multiple pulses of magma might explain the more robust thicknesses of the unit relative to the example provided by Lightfoot and Naldrett (1989) as a result of a more intense thermal conduit.

Unfortunately, the nature of the silicate textures precluded an accurate investigation of the role of fractional crystallization in the upper group of the Shakespeare intrusion. While the melagabbro portion of the upper group contains a significantly higher proportion of phenocrysts, no definitive cumulates were observed.

5.3 - Discussion of Autolithic and Xenolithic Fragments

It is fair to note that the presence of autolithic fragments of diorite and xenolithic fragments of quartzite within the melagabbro could be the product of density currents in a magmatic chamber as proposed by Irvine et al. (1998). However, the presence of autolithic quartz gabbro and melagabbro fragments within the rock fragment phase of the melagabbro cannot be explained by density currents. The key factors in the generation of autolithic fragments are that some portion of the magma in the chamber (or pipe) becomes partially crystalline and is then dislodged via mechanical action, i.e. magmatic currents in the case of the Skaergaard (Irvine et al., 1998). The Shakespeare intrusion does not display any rhythmic or graded layering and the autolithic fragments encountered are centimeter scale or less. The random distribution and delicate nature of the fragments suggest pulse like mechanical action instead of prolonged and relatively consistent mechanical action. The autolithic fragments were formed in situ, or close to in situ, as Sproule et al. (2007) suggested, and the textural features of the autolithic fragments suggest a more pulse-like flow; multiple pulses of intermittent magma provide the most reasonable explanation for the observed textural features. The term intermittent is important, as it allows for the partial crystallization of earlier pulses, including a degree of earlier differentiation between the melagabbro and quartz gabbro. It also facilitates the formation of the biotite quartz diorite as it implies that later pulses could provide the necessary thermal budget to expand the volume of assimilated quartzite in the roof zone.

The rocks of the Shakespeare intrusion are quartz normative (Sproule et al., 2007). Importantly, Kennedy et al. (1993) found that the distribution coefficient (K_D) for Ni between melt and pyroxene or olivine is dependent on the composition of the melt. However, they

found that nickel partitions more strongly into olivine ($K_D = 3-9$) than into pyroxene ($K_D = 0.72-2$). The lower compatibility of Ni in the pyroxene crystal structure relative to olivine places fewer constraints on the degree of crystallization of the earlier pulses which may have taken place prior to later pulses of magma. As the intruding magma of the earliest pulses cooled, the crystallizing pyroxenes would likely not scavenge Ni from the melt.

MgO and SiO₂ profiles for the rocks that host the Shakespeare intrusion indicate moderate but variable degrees of crystallization occurred which led to the differentiation between the quartz gabbro and melagabbro units. The trend is most obvious in hole U-03-118 (Figures 34, 35, and 36) and to a lesser extent hole U-03-119 (Figures 37, 38, and 39) while hole U-03-122 displays a much weaker crystallization trend (Figures 40, 41, and 42). The distinctive silica trough observed in holes U-03-118 and U-03-119 in the center portion of the melagabbro unit and the subsequent increase in MgO is not observed in hole U-03-122. Instead, the expected MgO increase is observed in the middle of the quartz gabbro unit. The differences between the SiO₂ and MgO trends observed in U-03-118 and U-03-122 are most easily and reasonably explained as localized differences in the degree of mixing.

5.4 - Determining the sulfur source for magmatic sulfides in the Shakespeare deposit

For some time there has been strong evidence suggesting the precipitation of magmatic sulfides in concentrations and volumes high enough to be economic requires a crustal sulfur source (Leshner and Keays, 2002; Keays and Lightfoot, 2009). Mavrogenes and O'Neill (1999) showed that while there are several major controls on the solubility of sulfur in a silicate melt, the effect of pressure on an ascending magma is the dominant one. As magma ascends

through the crust, pressure drops significantly, greatly increasing the solubility of sulfur in the magma. Thus, even if the magma was close to sulfur saturation when a melt was extracted, sulfur generally needs to be assimilated into the rising magma in order to produce economically significant quantities of Ni-Cu-PGE bearing sulfides. In many cases, the sulfur-rich assimilant will carry an identifiable geochemical signature usually in the form of highly fractionated $\delta^{34}\text{S}$ values or high S/Se ratios. A magma which assimilates significant quantities of crustal sulfur will also take on the isotopic signature of the sulfur source (Ripley and Li, 2003). Keays and Lightfoot (2009), Lightfoot and Keays (2005), Lesher and Keays (2002), and many others have used this line of reasoning to suggest many of the world's large Ni-Cu deposits could not form without the addition of crustal sulfur from sulfur-rich country rocks as in the case of Norilsk (Keays and Lightfoot, 2009), Kabanga (Maier et al., 2010), and Voiseys Bay (Ripley et al., 2002). In those deposits, sulfide bearing rocks yield a large range of $\delta^{34}\text{S}$ values and generally show a source which was isotopically fractionated. Samples taken from the Shakespeare deposit for isotope analysis returned $\delta^{34}\text{S}$ values from 0.01 ‰ to 2.38 ‰, averaging 1.14 ‰ (Table 2) and demonstrate consistency regardless of sulfide concentration or host lithology. As a result, sulfur isotope data suggest the sulfur from which the magmatic sulfides originated was derived from a mantle source or from an unfractionated crustal source (Naldrett, 2011).

The only potential source of sulfur from the rocks belonging to the Huronian Supergroup might be from pyrite associated with the Matinenda Formation's quartz pebble conglomerate. This unit is observed near the Shakespeare intrusion and could have interacted with it during the ascension of Shakespeare magmas. Hattori et al. (1983a) found the average $\delta^{34}\text{S}$ of sampled Matinenda pyritic shales to be +0.2 ‰, with samples ranging from -1.5 to +1.2 ‰. Hattori et al. (1983b) note that "sulfides found in continental sedimentary rocks of ~2.2 to ~2.7

Ga in Canada and South Africa have $\delta^{34}\text{S}$ values close to the mantle value (0 ‰)". Furthermore, a pyrite sample taken during this study from a Mississagi quartzite adjacent to the Shakespeare intrusion yielded a $\delta^{34}\text{S}$ value of +0.37 ‰, which appears to confirm the statements made by Hattori et al. (1983a). Based on $\delta^{34}\text{S}$ values alone it is not possible to distinguish between sulfur derived from this sedimentary source and a mantle derived source.

It is apparent that the degree of isotopic fractionation in sulfur alone is a dangerous approach when determining the source of sulfur in magmatic deposits because some sulfides of clearly sedimentary origin do not possess isotopically fractionated sulfur, such as the sulfide-rich quartz pebble conglomerate of the Matinenda Formation (Hattori et al., 1983b). However, the use of S/Se ratios in conjunction with sulfur isotope analysis can yield more definitive results because the variables that control each method are different. Both methods of determining the source of sulfur in magmatic Ni-Cu-PGE are useful but they both also have their disadvantages. Interpretations based on a combination of methods (i.e. $\delta^{34}\text{S}$ and S/Se ratios) that suggest a sulfur source for the Ni-Cu-PGE can be taken as more conclusive evidence than either method alone.

Many researchers (Eckstrand et al., 1989; Eckstrand and Cogulu, 1986; Hinchey and Hattori, 2005; Maier et al., 2008; Ripley, 1990) employed the ratio of S/Se in order to discern the difference between crustal sulfur and mantle derived sulfur in magmatic Ni-Cu-PGE deposits. Ni-Cu-PGE deposits have S/Se ratios between 100 to 100 000 (Queffurus and Barnes, 2013) while the S/Se of the mantle is between 2850 and 4350 (Eckstrand and Hulbert, 1987). Other estimates for the S/Se of the mantle include a S/Se of 3333 (McDonough and Sun, 1995) and a S/Se of 3150 (Lorand et al., 2003). Many igneous rocks have a S/Se ratio similar to the proposed mantle values, such as the Merensky reef (Godel et al., 2007). S/Se ratios that are

significantly higher than mantle values are interpreted to have had a large contribution of crustal sulfur (Leshner and Burnham, 2001, Maier and Barnes, 2010). S/Se values lower than mantle values are interpreted to signify a sulfur loss, as is the case with Lac des Iles, Heazlewood River, or the Penikat intrusion (Queffurus and Barnes, 2013, Barnes et al., 2008, Hinchey and Hattori, 2005, Peck and Keays, 1990).

Recently it has been suggested that S/Se values lower than mantle values could represent a variety of other processes as summarized by Queffurus and Barnes (2013): 1) Preferential retention of Se during partial melting (Hattori et al., 2002); 2) Refertilization of mantle lithosphere by metal-rich sulfide melts (Lorand and Alard, 2010); 3) Changes in the silicate to sulfide liquid ratio, i.e. the R-factor (Thériault and Barnes, 1998); 4) Segregation of the sulfide liquid (Barnes et al., 2009); 5) Partial desulfurization caused by a sulfur under saturated fluid (Godel and Barnes, 2008).

The S/Se ratio for rocks of the Shakespeare intrusion range from 1245 to 3271. The values have an average of 1810, significantly lower than the mantle value range (2850-4350). These data suggest that the sulfur source could be mantle derived or could be derived from country rocks with very low S/Se. It is possible that the depressed S/Se ratio is the result of the assimilation of a crustal contaminant that is highly enriched in Se, such that significant assimilation of the contaminant has depressed the S/Se ratio. Additionally, S/Se ratios of basalts tend to be somewhat higher than those of mantle values as a result of Se retention in the source during partial melting (Hattori et al., 2002).

Without high quality Se analyses from the Matinenda Formation from or near the Agnew Lake Uranium mine, it is impossible to adequately evaluate the potential for Se

contributions to Shakespeare magmas from the quartz pebble conglomerates. The rocks that host the Shakespeare deposit display low to very low S/Se regardless of sulfide concentration or stratigraphic depth. This suggests that remobilization of Se in late magmatic fluids may explain local deviation from average values but does not explain the lower than mantle values observed throughout the intrusion. Unfortunately, the adjacent Pecors and Mississagi Formations have not been sampled.

While discussing the impact the composition of the country rocks will have on an intruding magma, Queffurus and Barnes (2013) pointed out that if the S/Se and the concentration of sulfur in the country rocks is low, then the S/Se ratio of the magma will not display large variations from the primitive mantle values and other mechanisms should be considered for sulfur saturation. Furthermore, they stated that the S/Se of contaminants can be close to or lower than mantle S/Se ratios which can complicate the interpretation of results. They suggested that several processes could be responsible for S/Se values such as:

- 1) elevated selenium values in Ni-Cu-PGE sulfides are the result of unusually high selenium levels in the sulfides of some country rocks (as is the case with nickel deposits in the Vammala Nickel Belt)
- 2) S/Se ratios are heavily influenced by the R factor, as deposits with the highest R factors and PGE contents also have the lowest S/Se ratios

It is unlikely that the R factor has had a severe concentrating effect at Shakespeare as the R factors calculated in this study (See Chapter 5.6) and by Sproule et al. (2007) are generally low. It is possible that rocks from the stratigraphically lower formations in the

Huronian Supergroup could have elevated Se levels, thus impacting the S/Se within the Shakespeare deposit.

The input of crustal sulfur would also support the suggestion of Sproule et al. (2007) that the Shakespeare magmas formed from a source that had previously experienced partial melting, as sulfur is highly mobile and would have progressively lower concentrations in the mantle source as melts were extracted (Hattori et al., 2002). Ghiorso et al. (2002) showed that no sulfide exists for extraction in a mantle source after approximately 17% partial melt extraction.

The interpretations made by Sproule et al (2007) were based on SiO₂ concentrations, Al₂O₃/TiO₂ ratios, and MgO concentrations taken from data sets that merge Shakespeare data and other Nipissing data (i.e the sum of data from other studies), even though they acknowledged a different contamination history for the Shakespeare magmas. Sproule et al. (2007) utilized very few from the Shakespeare deposit and frequently combined Shakespeare data with more robust (i.e., more data points) Nipissing Gabbro data, skewing the results to display trends that may be accurate when describing other Nipissing Gabbros but may not be accurate for the rocks which host the Shakespeare intrusion. Still, data from this study confirm the moderate to high Al₂O₃/TiO₂ and moderate MgO contents (7-8%). SiO₂ concentrations generally appear higher (50.02% average melagabbro) than those suggested by Sproule et al. (2007).

Significant variation in SiO₂ (44-54%), MgO (4.37-9.42%), Al₂O₃ (10.62-17.74%), and TiO₂ (0.50-2.85%) concentrations within the melagabbro unit of the Shakespeare intrusion may also suggest multiple pulses with evolving geochemical signatures. These pulses could contain

sulfur from mantle and crustal sulfur, with the earlier pulses containing more mantle sulfur, if they represented the first melts from a source.

5.5 - Precipitation of an Immiscible Sulfide liquid at Shakespeare

The addition of sulfur to the Shakespeare magmas as they ascended through the crust is a necessary process, but does not explain how sulfide saturation, and thus an immiscible sulfide liquid, was reached. Mavrogenes and O'Neill (1999) have shown that as basaltic magma ascends through the crust, sulfur becomes increasingly soluble in the magma as pressure drops. No other significant magmatic Ni-Cu-PGE mineralization is associated with the Nipissing gabbros in the area, even though significant volumes of Nipissing magmas have probably interacted with some amount of the Matinenda Formation (both near Agnew Lake and Elliot Lake). Thus, some other process that appears unique to the Shakespeare deposit is likely responsible for the precipitation of an immiscible sulfide liquid.

One important characteristic of the disseminated sulfide mineralization within the Shakespeare deposit is its spatial association with fragile autolithic fragments, first described by Sproule et al. (2007). They acknowledged that the mineralization was associated with the presence, but not concentration, of these fragments. The results of this study have shown that the fragments have mineralogical compositions that match the compositions of other units observed at Shakespeare. The results also confirm the delicate nature of the fragments. These fragments were not observed in the biotite quartz diorite unit and generally start to appear near the base of the quartz gabbro.

Another characteristic of the mineralization within the Shakespeare deposit is that the most intense mineralization (Appendix 1; Figures 5 and 31) is associated with a thinner than

average biotite quartz diorite unit (Figure 3), a thicker quartz gabbro unit (65 meters instead of the average 20 meters), and a thinner than average rock fragment melagabbro unit (5 meters instead of the average 20-25 meters). Conversely, lower than average mineralization (Appendix 1) is associated with average thicknesses in the biotite quartz diorite unit (Figure 3), a veritextured quartz gabbro unit (8 meters), an average to slightly above average thickness in the quartz gabbro unit (26 meters), and an average to above average thickness in the melagabbro - rock fragment unit (32 meters).

The autolithic fragments are likely the result of a new pulse of magma interacting and mixing with a partially crystallized earlier pulse. This theory is supported by the presence of fragments that appear to be fragments of melagabbro, as well as fragments of lesser quartzite, diorite, and quartz gabbro. The delicate appearance of the fragments suggests they did not travel far (Sproule et al., 2007) and further supports a mixing event. The wide variation in unit thickness in conjunction with autolithic fragments further suggests aggressive mixing of magmas from stratigraphically higher units (biotite quartz diorite and quartz gabbro) with lower units (intruding pulses of melagabbro-like magma). Uncommon 1-5 meter intersections of Ni-Cu-PGE sulfides (0.1-0.2% Ni and Cu) in the middle and upper portions of the quartz gabbro unit seem to support the notion of magma mixing within the Shakespeare deposit.

Another characteristic of the mineralization within the Shakespeare deposit is that only very rare, low grade sulfides occur in the equigranular portion of the melagabbro unit. This could suggest that the individual pulses (or early pulses) of magma were near sulfur saturation, but that sulfur saturation only occurred uncommonly in localized settings. It is unlikely that later pulses would reach sulfur saturation on their own without interacting with other materials. Li and Ripley (2005) have shown that mixing a basaltic magma with a felsic

contaminant can reduce the solubility of sulfur in magma significantly, such that sulfide saturation is reached and an immiscible sulfide liquid is precipitated. The work of Naldrett et al. (2011a) supports the conclusions of Li and Ripley (2005) by showing that the hybridization of mafic and more felsic magmas will cause the precipitation of sulfide liquid. Additionally, the cooling of an intruding magma decreases the solubility of sulfur and can be a contributing mechanism to the precipitation of an immiscible sulfide liquid (Naldrett, 2011). It is important to note that the findings of Li and Ripley (2005) require both magmas to be close to sulfur saturation at the time of mixing in order to precipitate an immiscible sulfide liquid. Given the silica saturated nature of the biotite quartz diorite, and quartz gabbro to a lesser extent, interaction between new pulses of magma and the cooler, more felsic biotite quartz diorite and/or quartz gabbro would cause the precipitation of an immiscible sulfide liquid. Additionally, some crystals caught up in the mixing may melt, further decreasing the temperature of the mixing magmas. The extent and severity of the mixing event would likely be a main control on the degree of sulfide mineralization; the more felsic materials mixed with fresh magma, the less sulfur would be retained. Thus, the more aggressive the mixing environment, the more sulfide would be produced.

There is strong evidence for multiple pulses of magma and the mixing of those pulses in the form of autolithic fragments (of stratigraphically higher and lower levels) and variable widths of units associated with fluctuating SiO₂ and siliceous fragments from the roof zone. There is also a correlation between the strength of sulfide concentration and the degree of mixing, such that the intersections with the least fractionated rocks have the best intercepts of economic sulfide mineralization (Appendix 5, Appendix 2; Figure 41). The most reasonable explanation for the observed trend is that magma mixing is the most reasonable mechanism by which an immiscible sulfide liquid could be produced at Shakespeare. In line with the findings

of Li and Ripley (2005), a more felsic magma, possibly one with a similar composition to the biotite quartz diorite and/or quartz gabbro, and a mafic magma, such as a fresh pulse of melagabbro-like magma, could have mixed to produce an immiscible sulfide liquid. Thus, the precipitation of an immiscible sulfide liquid as a result of a magma mixing event is a plausible explanation for the bulk of the disseminated ores in the Shakespeare deposit, but it does not explain the presence of interconnected sulfides at a stratigraphically higher level than the disseminated sulfides.

According to Sproule et al. (2007) the intruding Shakespeare magmas contained xenolithic fragments, had already become sulfur saturated, and were carrying an immiscible sulfide liquid in suspension prior to emplacement. Then the sulfide liquid settled on top of a cumulate pile, i.e. Nipissing gabbro, resulting in a low R factor. The low R factor, they argued, suggested that the sulfides had not travelled very far in suspension and that the intruding magmas did not convect vigorously. They also observed that sulfide metal contents were independent of sulfide concentration in the rock.

Several factors suggest the notion of a cumulate pile of crystal mush immediately below the equigranular melagabbro is incorrect. Firstly, the presence of a single chill margin at the base of the Shakespeare deposit (Dr. Richard Sutcliffe and Dr. Rebecca Sproule, personal communication), immediately overtop of a granophyric (field terminology) unit indicates that the lower Nipissing gabbros were partially crystalline when the Shakespeare magmas were emplaced. Elsewhere, the admix zone commonly exhibits textures and compositions intermediate between the equigranular melagabbro and the upper units of the underlying Nipissing gabbro suite (Dr. Richard Sutcliffe and Mr. Harold Tracaneli, personal communication). The granophyre (field terminology) unit commonly located at the top of the

underlying Nipissing gabbro suite suggests a later stage melt which is enriched in volatiles, likely the result of the last products of crystallization within the Nipissing gabbros. Cumulates are found in the basal sections of the Nipissing gabbro suite underneath the Shakespeare deposit, but the Shakespeare deposit is not immediately on top of them, i.e there are other non-cumulate units in between them.

Additionally, Sproule et al. (2007) did not speculate as to how potentially autolithic fragments were produced or why there would be an unmineralized melagabbro underneath the mineralized melagabbro if the sulfides had been carried in suspension in an intruding magma. Even more importantly, they suggested that gravity settling would produce a higher concentration of interconnected to locally semi-massive sulfides immediately above the disseminated portion of the deposit; if gravity settling were responsible for the textures and placement of sulfides, the semi-massive to interconnected sulfides should be underneath the disseminated sulfides. In addition, work by Chung and Mungall (2005) suggests that liquid sulfide droplets of any size will settle in a crystal-free zone, but that as crystals develop the sulfide droplets behave as if settling through a tube, i.e. wall effects. They found generally that single droplets of sulfide become stranded in a cumulate pile and are unable to migrate through the crystal mush. Thus, gravity settling does not appear capable of explaining the presence of the disseminated sulfides at Shakespeare.

Data presented in this study are inconsistent with a number of the characteristics of the Shakespeare deposit originally identified by Sproule et al. (2007). For instance, sulfide metal content varies considerably with sulfide concentration in disseminated ores but does not vary significantly with sulfide concentration with interconnected to semi-massive ores. These

differences were not oversights, as the first drill holes in the Shakespeare deposit contained larger than average interconnected sulfide zones. They were also the result of extremely limited sampling (very few drill holes existed), such that the true characteristics of the Shakespeare deposit have been partially overlooked.

Sproule et al. (2007) noted the dominant sulfide species as pyrrhotite, pentlandite, chalcopyrite, and gersdorffite and trace amounts of pyrite. During the SEM-EDS study, they observed common tsuomite (erroneously calling it tellurobismuthite), rare tellurobismuthite, a CoS(As) mineral, a BiTe(S) mineral, which they speculated may be Joesite, and a rare SbBiTeS(Fe) phase. They were unable to identify any platinum group minerals (PGMs), and no PGEs were detected during the course of their investigation. Sproule et al. (2007) examined samples with the highest Ni, Cu, and PGE values for whole rock assays, neglecting the higher sulfide metal concentrations of the disseminated sulfides.

For the purposes of this study, samples were collected and analyzed with the understanding that the textural and geochemical characteristics of the blebby, interconnected, and disseminated sulfides were different and that different textures may be the result of differing magmatic processes. The results of the SEM analysis of polished thin sections reveal several identifiable species of sulfides, tellurides, sulfarsenides, sulfselenides, native metals, and metal alloys. Several other species of tellurides and metal alloys are likely present and are provided as semi-quantitative results.

Barkov et al. (1999) studied zoning and substitutions of PGE in Co-Ni-Fe sulfarsenides from the Mount General 'Skaya layered intrusion, Russia. They performed a detailed microprobe analysis and found many rarer ore minerals such as members of the Cobaltite-Gersdorffite series (MCGS), argentopentlandite, hessite, altaite, sphalerite, Se-rich clausthalite-

galena, an Au-Ag alloy, molybdenite, pilsenite, and a Bi-Te-Se-S mineral. They also noted the presence of Ce-rich allanite and abundant zircon in close spatial association with some zoned sulfarsenides. They suggested this contrasting mineral assemblage represented localized enrichment in PGEs and incompatible lithophile elements but that other zoned sulfarsenides are not necessarily associated with that mineral assemblage. Aside from the PGEs found in the MCGS, merenskyite, palladian melonite, kotulskite, sperrylite, and minor michenerite, hollingworthite, and Bi-rich telluropalladinite were observed. Barkov et al. (1999) found the PGE-rich MCGS contained up to 12 atm. % PGE, mostly Pd and Rh. Other occurrences include Karik'yarv, Russia (Distler and Laputina, 1979), Pipe, Manitoba (7 wt. % Rh; Cabri, 1992), and Lukkulaivaara, Russian Karelia (9 wt. % Rh; Barkov et al., 1996), and rarely at Sudbury (Cabri, 1986), Stillwater (Volborth et al., 1986), Penikat (Halkoaho et al., 1990), and the Shetland ophiolite complex (Tarkian and Prichard, 1987). Barkov et al. (1999) argues that the zonation of PGE-rich MCGS is a primary textural feature and preserves a temperature dependent crystallization history, such that the temperature of crystallization decreases in order from highest to lowest in the Ir – (Pt)-rich sulfarsenides, Rh – (Pd)-rich sulfarsenides, and PGE poor sulfarsenides. They concluded that the source of As was either from the contamination of ascending magmas by pyritic shales or by an initial enrichment of As in the primary melt.

The PGE-bearing MCGS found within the Shakespeare deposit exhibit many similarities with those previously reported by Barkov et al. (1999). The zoned nature of the crystals such that Ir, Pt, and Rh are concentrated in the core, followed by Rh (with lesser or non-detectable Ir), followed by PGE-poor MCGS (none detected). However, some of the more complex observations regarding preferential substitution of Co by PGE were not observed, and no Pd was detected within the MCGS. While many PGE-rich MCGS crystals are euhedral and display

striking zonation, others appear washed out or faded. The faded crystals commonly have a close spatial association with bismuth tellurides and minor fracture fillings (rare galena-clausthalite) and appear texturally resorbed.

The abundance of galena-clausthalite fracture fillings within barren (no PGM) MCGS suggests that a later fluid interacted with primary magmatic sulfides and manipulated some of the original textures (Figures 20 and 21). However, the (local) presence of pristine PCGA within the MCGS suggests that secondary replacement/ alteration processes affecting sulfides in the Shakespeare deposit are not unilateral and that the textural characteristics of the sulfides reflect the original magmatic conditions which produced them.

Evidence for magmatic processes which occurred between pulses, such as a crystal-melt reaction after the earlier pulses, are apparent from the oxidization of sulfides (Figures 12, 14, 15, and 16). The replacement textures may locally appear to be either a sulfidation of oxides or an oxidation of sulfides. However, the presence of chalcopyrite that is surrounded by ilmenite within some of the ilmenite cores suggests the oxidation of sulfides is the more likely chemical reaction. Interestingly, sulfide blebs are commonly juxtaposed against the oxide cores containing sulfide (Figures 12 and 15). This could either imply the sulfidation of an oxide grain or the oxidation of a sulfide grain followed by the addition of sulfide droplets. The addition of sulfide droplets could occur in multiple ways, such as mixing of magmas or the precipitation of another immiscible sulfide liquid. However, native copper was observed rarely within the core of ilmenite grains with no sulfide present, possibly representing a later product in the oxidation process. The presence of native copper in the cores of some ilmenite grains suggests the oxidation of sulfide grains is a more reasonable explanation than the sulfidation of oxide grains, as native copper could not be a product from a sulfidation process. At present, it is

unknown what implication this has on the genesis of Shakespeare, as the relative timing is difficult to determine. Rutile is not observed in all ilmenite-sulfide grains and may represent an intermediate oxidation state between the sulfide and ilmenite. The replacement does not appear to be due to metamorphic processes as evidenced by the replacement textures being found in the core that is surrounded by a relatively thick sphene rim and the mineral species present .

5.6 - Sulfide Metal Content, R Factor Calculations, and a Second Immiscible Sulfide Liquid

Sulfide metal content, also referred to as sulfide metal tenor in some other works, is an analytical tool used to compare and classify magmatic deposits based on the metal contents in sulfides (Kerr, 2003 and references therein). Sulfide metal content removes the variations in metal content based on sulfide concentration by normalizing sulfide concentration to 100%, i.e. the calculation is based on 100% sulfide. Sulfide metal content frequently increases with decreasing sulfide content (Sproule et al., 1999). When sulfide metal contents for multiple metals, most notably nickel, copper, and platinum group elements, are compared, general information can be garnered about how sulfides might have interacted with an intruding magma and how much magma was involved in the genesis of an ore body (Kerr and Leich, 2005; Kerr, 2003; Lightfoot et al. 2001 a, b). The latter calculation is known as the R factor and is defined as the mass ratio of silicate melt to sulfide melt.

Campbell and Naldrett (1979) first introduced the concept of the R factor in a closed system. They showed that only very high R values could yield sulfide metal concentrations,

normalized to 100% sulfide, that approached D (distribution coefficient) times X_0 (initial concentration in the melt), such that R values were much greater than D . This early calculation did not take into account the effects that multiple pulses of magma would have on the concentration of metals in sulfides or the potential dissolution of sulfides back into the silicate melt. When applied to natural open systems, calculations yielded unreasonably large R factors which suggested other key variables may have been missed by oversimplifying dynamic systems (Kerr and Leich, 2005). Simple multistage upgrading has been proposed as a mechanism by which large total R values (R_{cum}) can be obtained by periodic replenishment in a magma chamber by smaller pulses (R_{inc}) (Naldrett et al., 1995; Naldrett and Lightfoot, 1999, Li and Naldrett, 1999, and Li et al., 2002). In these calculations N (number of melt batches) times R_{inc} yields R_{cum} . The theory rests on the idea that sulfide droplets are much denser than the surrounding silicate melt and that this difference in density will tend to separate the two liquids during transport in a conduit-like system. Kerr and Leich (2005) proposed the concept of complex multistage upgrading, which rests on the same theory as simple multistage upgrading, but takes into account how the metal concentration in sulfide (X_{sulf}) will be impacted as sulfides are dissolved into the silicate melt. Loss of sulfide (L) is a representation of dissolution on a percent basis. For instance, where $L=0.05$ there has been a 5% dissolution of sulfide back into the silicate melt. Metals with a high D will partition heavily into a sulfide liquid during the precipitation of an immiscible sulfide liquid and will refuse to partition back into the silicate melt during dissolution. As a result, the progressive precipitation and dissolution of sulfides has a concentrating effect for elements with a high distribution coefficient (Kerr and Leich, 2005).

R factors calculated using the method provided by Kerr and Leich (2005) yield low average R factors between 450 and 700, depending on the initial composition used (Table 3).

There is marginally better agreement between Ni, Cu, Pt, and Pd when R factors are calculated using a complex multistage calculation with low sulfide dissolution when compared against conventional closed system R factor calculation (Table 3; Figures 44, 45, 46, and 47). The differences between these methods are subtle as a result of the low R factors. However, higher R factors as a result of more interaction between immiscible sulfide liquid and fertile magma can only occur if the immiscible sulfide liquid ponds or is otherwise separated from melt which has had Ni, Cu, and PGE scavenged from it. Thus, it is possible the sulfides were carried in suspension with the melt they had already interacted with which would decrease the amount of fresh, fertile magma they interacted with. The homogenous, continuous nature of the disseminated ore zone within the Shakespeare deposit would seem to support this idea.

Further evidence disproving the concentration of disseminated sulfides through gravity settling is the difference in sulfide metal concentrations of the sulfides. If the interconnected sulfides and disseminated sulfides were produced from the same process they would exhibit similar sulfide metal concentrations and change in sulfide metal concentrations with increasing or decreasing sulfide concentration. However, the observed trend of increasing sulfide metal concentration with decreasing sulfide (Figures 26 and 28) within the disseminated sulfides is different than the observed trend of no increase in sulfide metal concentration with decreasing sulfide (Figures 27 and 29) within the interconnected sulfides. Also, sulfide metal concentrations of disseminated sulfides are two to three times higher than interconnected sulfides, even when both contain the same amount of sulfide. This characteristic suggests that either the disseminated sulfides have interacted with significantly more fertile magma, thus boosting their metal tenors, or that relatively barren iron sulfides were added to the interconnected sulfides.

A key parameter when discussing the enrichment of an immiscible sulfide liquid is the ability for an immiscible sulfide to separate itself from the melt which it has already scavenged Ni, Cu, and PGE from. For instance, if small disseminated blebs are carried a short distance from their origin without significant separation from the initial melt from which they precipitated, low R factors will be obtained from those grains. In other deposits such as Norilsk (Keays and Lightfoot, 2009), Kabanga (Maier et al., 2010), and Voiseys Bay (Ripley et al., 2002), high R factors and variations in R factor are expressed as differences in the volume of fertile magma that interacted with immiscible sulfides. If the disseminated sulfides had interacted with larger volumes of fertile magmas, the difference between Ni, Cu, and PGE in the metal tenors of the sulfides would provide supporting evidence through the R factor and high PGE:Ni ratios. This is not the case, as R factor calculations indicate low volumes of magma for both disseminated and interconnected sulfides (table 3). In turn, this suggests that the immiscible sulfide liquid was unable to separate itself from magmas in which it was suspended during transport, to the extent that its ability to scavenge more Ni, Cu, and PGE from fresh, fertile magma was inhibited.

There is no evidence for a fresh pulse of fertile magma interacting with only the interconnected sulfides and not the disseminated sulfides. Therefore, the higher sulfide metal tenors of the disseminated ores do not reflect the preferential upgrading of sulfides relative to the interconnected ores. Rather, it appears that the interconnected sulfides have a lower sulfide metal content as a result of the addition of a relatively Ni, Cu, and PGE poor sulfide liquid.

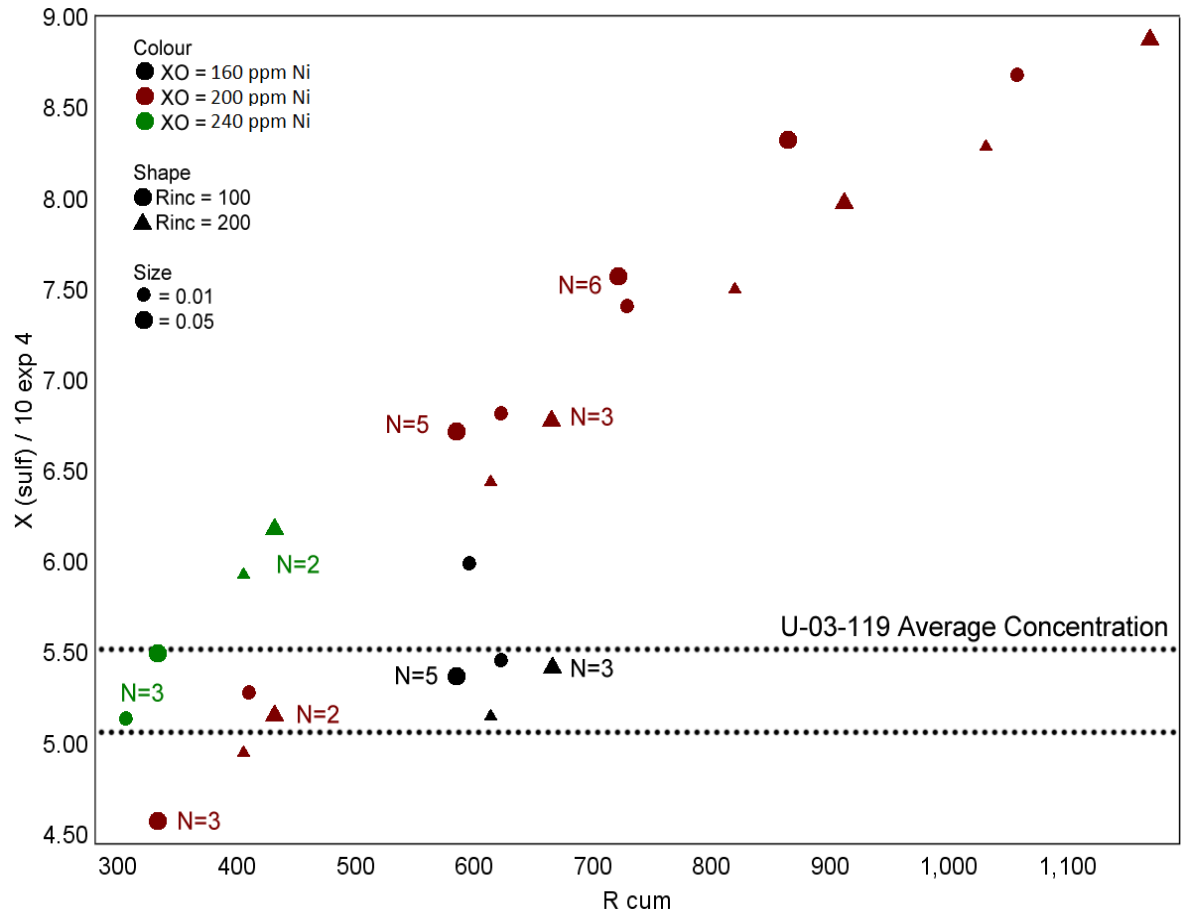


Figure 44: Sulfide nickel concentration versus cumulate R factor values for drill hole U-03-119. Sulfide nickel concentration is given in ppm / 10^4 . The shape of plotted points represents R_{inc} , color denotes the initial concentration of nickel in each pulse (X_0), and size is the amount of sulfide which redissolves into the melt after each pulse, expressed as a fraction of the sulfide liquid; i.e. 0.05 is 5% redissolution of sulfide liquid into the melt. N is the number of pulses required in order to reach the corresponding $R_{cum} / X(\text{sulf})$ point on the graph. The dotted black line represents the range of values for the disseminated sulfides of hole U-03-119. The presentation is not meant to assert the initial composition, amount of dissolution, or number of pulses. Rather, the presentation is meant to visually demonstrate how sensitive these calculations are to the initial concentration, extent of dissolution, and the size of each pulse. The total (cumulative) R factor for the sulfides of average composition is between 425 and 500, with an initial concentration of 200 ppm.

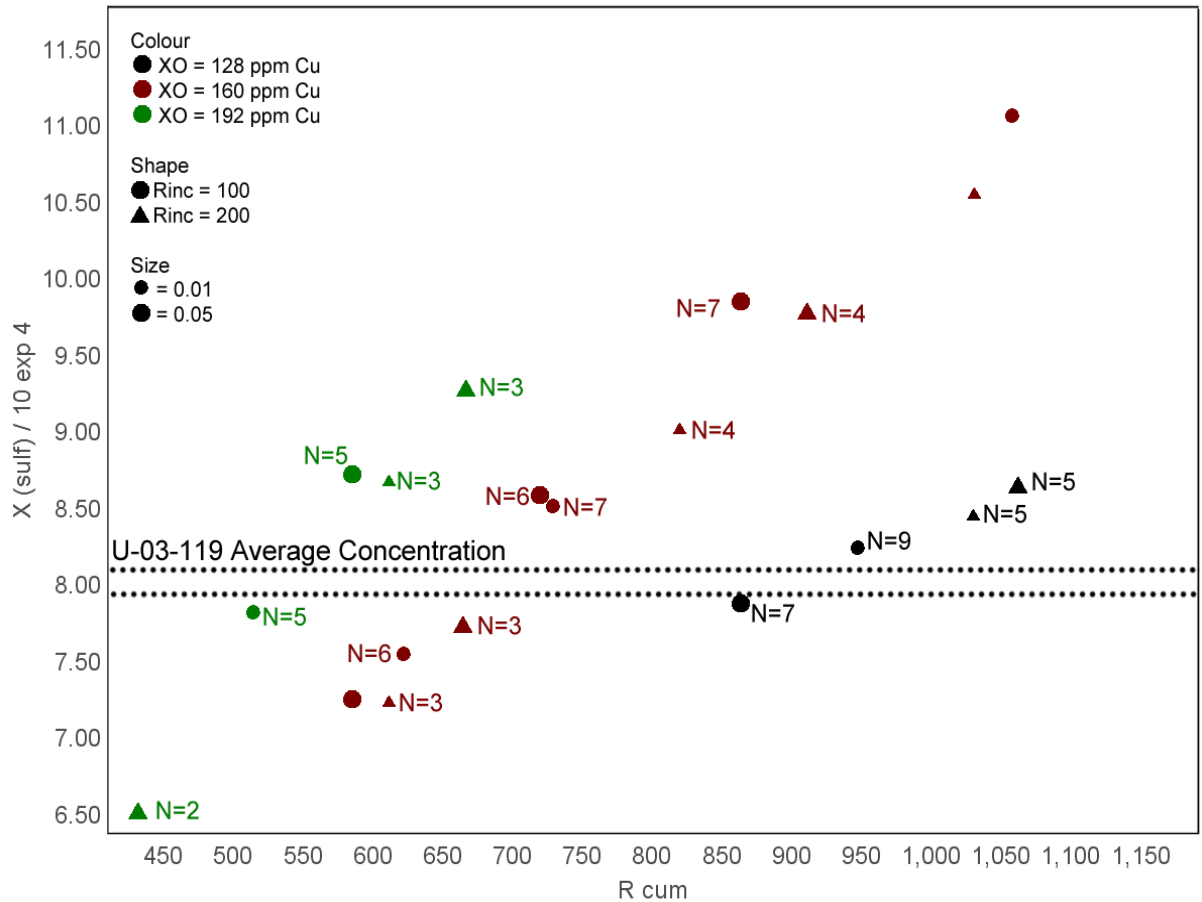


Figure 45: Sulfide copper concentration versus cumulate R factor values for drill hole 119. Sulfide copper concentration is given in $\text{ppm} / 10^4$. The shape of plotted points represents R_{inc} , color denotes the initial concentration of nickel in each pulse (X_0), and size is the amount of sulfide which redissolves into the melt after each pulse, expressed as a fraction of the sulfide liquid; i.e. 0.05 is 5% redissolution of sulfide liquid into the melt. N is the number of pulses required in order to reach the corresponding $R_{cum} / X(\text{sulf})$ point on the graph. The dotted black line represents the range of values for the disseminated sulfides of hole U-03-119. The presentation is not meant to assert the initial composition, amount of dissolution, or number of pulses. Rather, the presentation is meant to visually demonstrate how sensitive these calculations are to the initial concentration, extent of dissolution, and the size of each pulse. The total (cumulative) R factor for the sulfides of average composition is between 650 and 725, with an initial concentration of 160 ppm.

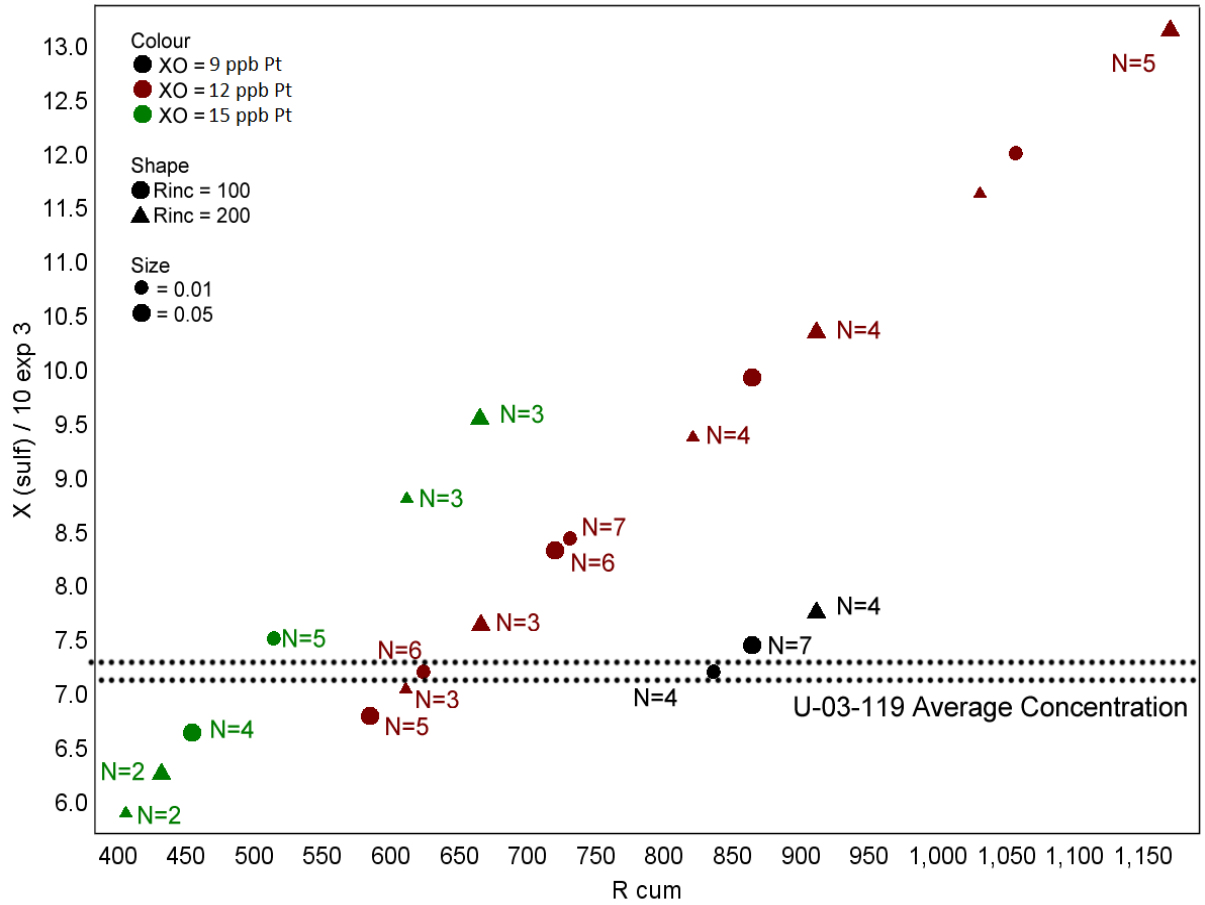


Figure 46: Sulfide platinum concentration versus cumulate R factor values for drill hole 119. Sulfide platinum concentration is given in $\text{ppb} / 10^3$. The shape of plotted points represents R_{inc} , color denotes the initial concentration of nickel in each pulse (X_0), and size is the amount of sulfide which redissolves into the melt after each pulse, expressed as a fraction of the sulfide liquid; i.e. 0.05 is 5% redissolution of sulfide liquid into the melt. N is the number of pulses required in order to reach the corresponding $R_{cum} / X(\text{sulf})$ point on the graph. The dotted black line represents the range of values for the disseminated sulfides of hole U-03-119. The presentation is not meant to assert the initial composition, amount of dissolution, or number of pulses. Rather, the presentation is meant to visually demonstrate how sensitive these calculations are to the initial concentration, extent of dissolution, and the size of each pulse. The total (cumulative) R factor for the sulfides of average composition is between 460 and 525, with an initial concentration of 15 ppb.

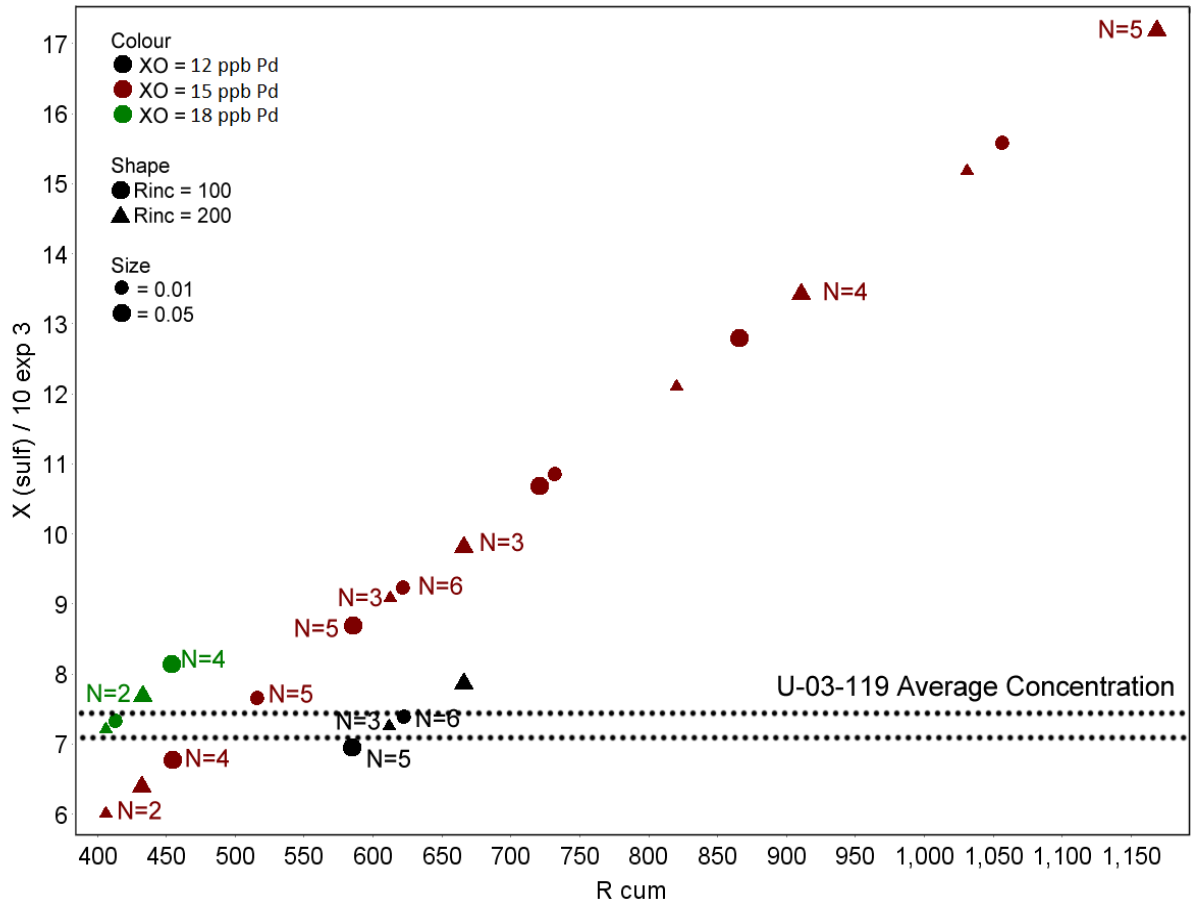


Figure 47: Sulfide palladium concentration versus cumulate R factor values for drill hole 119. Sulfide palladium concentration is given in $\text{ppb} / 10^3$. The shape of plotted points represents R_{inc} , color denotes the initial concentration of nickel in each pulse (X_0), and size is the amount of sulfide which redissolves into the melt after each pulse, expressed as a fraction of the sulfide liquid; i.e. 0.05 is 5% redissolution of sulfide liquid into the melt. N is the number of pulses required in order to reach the corresponding $R_{cum} / X(\text{sulf})$ point on the graph. The dotted black line represents the range of values for the disseminated sulfides of hole U-03-119. The presentation is not meant to assert the initial composition, amount of dissolution, or number of pulses. Rather, the presentation is meant to visually demonstrate how sensitive these calculations are to the initial concentration, extent of dissolution, and the size of each pulse. The total (cumulative) R factor for the sulfides of average composition is between 610 and 660, with an initial concentration of 9 ppb.

Nickel concentrations in sulfides display a consistent trend of increasing metal tenors with stratigraphic depth (Figures 30 and 31), such that metal tenors of blebby sulfides < interconnected sulfides << disseminated sulfides. Copper (Figure 32) and platinum group elements (Figure 33) follow a similar trend but with more scatter. Metal tenors of disseminated sulfides tend to be highly consistent, as do sulfide concentrations, with metal tenors increasing with decreasing sulfide, while metal tenors of interconnected sulfides tend to fluctuate with little indication of metal tenors increasing or decreasing with decreasing sulfide. This trend is best exemplified in Figures 29 and 31, where the nickel tenor of samples taken from drill hole 122, which has a large interconnected sulfide intercept, does not fluctuate significantly, but sulfur concentrations from samples collected fluctuates, from 1.2 to 17.7 weight percent. The sulfide nickel concentrations within interconnected sulfides vary between 30000ppm and 42000ppm (Figure 30).

In theory, further mixing of a melt carrying suspended immiscible sulfide liquid with a cooler, more felsic melt would cause the precipitation of more immiscible sulfide liquid. This is because the initial melt carrying the immiscible sulfide liquid would still contain some dissolved sulfur and has the potential to redissolve the sulfide liquid (Kerr and Leich, 2004), such that a continued depression in solubility, as a result of mixing with a highly siliceous melt, would result in a further precipitation of immiscible sulfide liquid. The later precipitation event(s) would yield sulfide droplets with significantly lower sulfide metal concentrations. Thus, the initial sulfide droplets, which would coalesce with the later droplets, would be diluted, reducing the total sulfide metal concentration. Those droplets could then settle due to gravitational forces, since there would be no crystal mush to inhibit them. The elevated silica concentration in and around the intersections displaying the strongest sulfide mineral concentrations (DDH U-O3-122, Appendix 2) seem to support this theory. Additionally, a

hybridized sulfide consisting of an earlier sulfide liquid, which preferentially scavenged all of the PGE, and a later sulfide liquid, which would have almost no PGE available to scavenge, would explain some of the decoupling from the theoretical R factor curve published by Sproule et al. (2007).

The textural profile of sulfides above the interconnected to locally semi-massive sulfides matches the expected trend of decreasing sulfides (blebby) with an increase in stratigraphic height, tapering over approximately 20 meters in most intersections. This also indicates that the lowermost portion of the interconnected sulfides represents a physical boundary through which the sulfides could not navigate, which generally coincides with the transition from quartz gabbro unit and the rock fragment phase of the melagabbro unit.

Chapter 6: Conclusion

6.1 - Contamination of Shakespeare Magmas

The Shakespeare intrusion, like other Nipissing intrusions, displays geochemical characteristics that suggest its magmas interacted with upper continental crust. However, the Shakespeare is also highly enriched in U, Th, and LREE relative to other Nipissing gabbros. These characteristics suggest that the contamination history of the Shakespeare magmas is different than other Nipissing intrusions. The Nb/Th ratio for rocks from the Shakespeare intrusion plot to the left of average pelitic compositions (Figure 41) and indicate a contaminant significantly enriched in Th relative to Nb. Thus, the Shakespeare intrusion is not necessarily more contaminated than any of the other Nipissing magmas, as Sproule et al. (2007) contend, but rather the Shakespeare magmas were contaminated, at least partially, by a different contaminant. The geochemical characteristics of the Shakespeare deposit also suggest that element ratios used in the conventional sense, are not as effective at showing the desired trends. However, they do provide valuable insight into the contamination history at Shakespeare.

The quartz pebble conglomerates of the Matinenda Formation, which host the detrital uranium deposits at Elliot Lake and Agnew Lake, are a likely candidate for assimilation into ascending Shakespeare magmas. The quartz pebble conglomerates contain ore grade U, associated Th, and have the potential to host economic concentrations of REE. The past producing Agnew Lake uranium mine is less than 15 km away from the Shakespeare deposit and is known to come in contact with Nipissing gabbros.

6.2 - Genesis of the Biotite Quartz Diorite and Roof Zone

The biotite quartz diorite roof zone contains abundant xenoliths of quartzite with sizes ranging from individual grains to meter scale rafts. The biotite quartz gabbro is a hybrid of assimilated quartzite, xenolithic fragments, and more mafic Shakespeare magmas which were probably of similar composition to the melagabbro unit. It is difficult to determine the ratio of assimilated quartzite to unassimilated quartzite in the unit, but textural and geochemical evidence suggests that very high degrees of assimilation have occurred.

Even though there appears have been significant quantities of water available during assimilation, significant heat energy is required in order to assimilate large quantities of country rock. In the case of Shakespeare it is impossible to imagine such high degrees of assimilation without multiple pulses of intruding magmas, thus providing the necessary thermal energies to assimilate large quantities of quartzite.

The biotite quartz diorite unit could represent a ponded magma which was less dense than the underlying magmas and was variably eroded via the convection of intruding magmas, similar to the model proposed by Lightfoot and Naldrett (1986). This would explain the wide range in the thickness of the biotite quartz diorite unit and the presence of diorite and/or quartzite fragments in the quartz gabbro and melagabbro units.

6.3 - Discussion of Autolithic and Xenolithic Fragments

The presence of autolithic fragments within the melagabbro – rock fragment unit is best explained by mixing two intermittent pulses of magma. One is partially crystallized, cooler, and more felsic from localized contamination; the other is still molten and hot. As a result, the mixed magmas contain suspended aggregates of crystals formed from the first

pulse, i.e. the melagabbro, and also mix with the upper portions, i.e. biotite quartz diorite, of the intrusion.

Differentiation as a result of crystallization is best exhibited by MgO vs. depth and SiO₂ vs. depth. SiO₂ also acts as a proxy for the amount of mixing which took place, as a significant reservoir of SiO₂ is found in the biotite quartz diorite unit. The intercepts which display the most mixing, i.e. U-03-122, also display unusual MgO profiles, i.e. the expected MgO trough commonly observed in the melagabbro is instead partially observed in the quartz gabbro.

6.4 - Determining the sulfur source for magmatic sulfides in the Shakespeare deposit

In order to precipitate an immiscible sulfide liquid in quantities great enough to host economic concentrations of Ni-Cu sulfides, crustal sulfur must be assimilated (Lesher and Keays, 2002; Keays and Lightfoot, 2009). This is dominantly because as the magma rises through the crust, the decrease in pressure increases the solubility of sulfur within the magma (Mavrogenes and O'Neill, 1999). Data from multiple samples for isotopic analysis yield $\delta^{34}\text{S}$ values which are only slightly positive on average and approximate a mantle composition of 0‰. The S/Se ratio for Shakespeare samples have a range between 1245 to 3271, which is lower than expected mantle values. Any potential sulfur source must be isotopically unfractionated, and in the case of a crustal source it must also contain abundant selenium in order to depress the S/Se ratio as sulfur is assimilated.

It is convenient that there is only one potential assimilant, the Matinenda Formation, with the geochemical characteristics necessary to explain the data obtained from the Shakespeare intrusion. These characteristics include the presence of abundant detrital sulfide

grains, average $\delta^{34}\text{S}$ values approximating mantle values, and enrichment in U, Th, and REE.

From these characteristics and the absence of any other candidate, it is very likely that the intruding magmas assimilated significant quantities of the quartz pebble conglomerates of the Matinenda Formation near the Agnew Lake uranium mine.

6.5 - Precipitation of an Immiscible Sulfide liquid at Shakespeare

The economic concentrations of magmatic Ni-Cu-PGE sulfides within the Shakespeare deposit are associated with autolithic fragments, but not the concentration of fragments, implying a mechanical association. As discussed earlier, the most reasonable explanation for the presence of the autolithic fragments is the mixing of intermittent pulses of magma. According to Li and Ripley (2005) and Naldrett et al. (2011a), an immiscible sulfide liquid can be produced by mixing two mafic magmas if both are nearly saturated in sulfur. Mineralogical evidence in the melagabbro-equigranular unit suggests earlier pulses were close to sulfur saturation at the time of emplacement and that locally an immiscible sulfide liquid was produced. As a result, the mixing of two pulses of magma that were both close to sulfur saturation reasonably explains how an immiscible sulfide liquid was produced in the Shakespeare deposit. Additionally, the least differentiated intercepts, i.e. the intercepts with the most mixing, also have the highest concentration of Ni-Cu-PGE mineralization.

The presence of PGE sulfarsenides within some gersdorffite-cobaltite implies that PGE's in the Shakespeare deposit partitioned heavily into the As-S system during crystallization. Their textural characteristics also suggest that little or no mobilization occurred during metamorphism and that later metamorphic events do not appear to have any control over extent or location of Ni-Cu-PGE mineralization within the Shakespeare deposit.

Additionally, the abundant nature of the gersdorffite-cobaltite grains suggests Shakespeare magmas assimilated significant quantities of arsenic prior to emplacement, possibly from the pyrite within the quartz pebble conglomerates of the Matinenda Formation.

Sproule et al. (2007) argue the distribution and concentration of Ni-Cu-PGE sulfides within the Shakespeare deposit are best explained by gravity settling on top of a cumulate pile. However, no cumulates exist except in the basal portions of the lower group and multiple non-cumulate units are between the disseminated ores of the melagabbro-rock fragment unit and the basal cumulate pyroxenites of the unmineralized lower group. The gravity settling model also fails to explain how interconnected to locally semi-massive sulfides could occur at a stratigraphically higher level than the disseminated sulfides which make up the bulk of the deposit.

Ilmenite grains frequently contain variable concentrations of sulfide, mostly chalcopyrite, and rutile. They are always rimmed with sphene which is a product of chemical reactions which took place during metamorphism. Rarely, native copper was observed in the ilmenite grains during the SEM-EDS study. The textural and mineralogical evidence suggests that some of the ilmenite grains are actually replaced (oxidized) sulfide grains. These grains are commonly juxtaposed against pristine looking sulfide grains. This suggests that some intermediary magmatic process, such as the mixing of intermittent pulses of magma, is responsible for the apparent oxidation of some sulfide grains.

6.6 - Sulfide Metal Content, R factor calculations, and a Second Immiscible

Sulfide Liquid

Sproule et al. (2007) utilized large volumes of data from intrusions that are genetically associated with the Shakespeare intrusion. However, their study had very few samples taken from the Shakespeare deposit itself. As a result of poor sample density and very few drill holes to sample from, Sproule et al. (2007) used element ratios, such as La/Sm vs Nb/Th, with assimilated compositions reflecting the average composition of Proterozoic rocks. While this approach is generally appropriate to determine the extent of contamination an intrusion has experienced, the approach becomes inappropriate if the probable assimilated has a drastically different geochemical profile. The rocks of the Matinenda Formation, which are enriched in U, Th, LREE, and are a probable assimilated for ascending Shakespeare magmas, are geochemically distinct from the average Proterozoic pelitic rock used by Sproule et al. (2007) to determine the degree of contamination and thus invalidate the degree of contamination proposed by Sproule et al. (2007) .

Sproule et al. (2007) also stated that there was no difference in the sulfide metal concentrations as the concentration of sulfide changed. While this statement is generally true for the interconnected to locally semi-massive sulfides which straddle the melagabbro / quartz gabbro boundary, the disseminated sulfides have a distinctly different characteristic with regards to their sulfide metal concentrations. The disseminated sulfides, which contain the bulk of the mineral resource within the Shakespeare deposit, display increasing sulfide metal concentrations with decreasing concentrations of sulfides. Furthermore, they have significantly higher sulfide metal concentrations than their counterparts within the interconnected sulfides, even within narrow differences in sulfide concentration. This suggests that either the

interconnected sulfides had an addition of relatively Ni-Cu-PGE poor iron sulfides or that the disseminated sulfides interacted with significantly more fertile magma.

There appears to be no textural or geochemical evidence to suggest that the disseminated sulfides interacted with a higher volume of fertile magmas than did the interconnected sulfides. However, numerous textural and geochemical observations suggest, directly or indirectly, that a second immiscible sulfide precipitation event occurred. First, the ordered appearance of interconnected sulfides at or near the quartz gabbro/melagabbro boundary followed by blebby sulfides immediately on top of them, which decrease rapidly in concentration, suggests gravity settling through a crystal free zone. Secondly, the high sulfide nickel concentrations which depart from the expected Ni sulfide concentrations vs. Pt and Pd sulfide concentrations (Sproule et al. 2007) suggest further extraction of nickel from the melt after all of the PGE had been scavenged. The deviation from the calculated R factor curve expressed by Sproule et al. (2007) is likely from the precipitation of a second immiscible sulfide liquid, probably when melagabbro-like magmas mixed with significant quantities of the biotite quartz diorite roof zone, but without any further interaction with fresh magmas. This would also explain the thinner biotite quartz diorite unit encountered in U-03-122 and the thicker than average interconnected mineralization. In this scenario, the Shakespeare intrusion essentially acts as a natural smelter. As silica is added and the temperature drops from assimilation, the solubility of sulfur in the melt decreases quickly which produces a second immiscible sulfide liquid. This liquid scavenges the remaining Ni and Cu, but no PGE remain. Presumably, disseminated sulfides are caught up in the melagabbro portion of the melt that is mixing with the silica rich roof zone, which then settles through the crystal free zone, coalescing with other immiscible sulfide droplets. The ratio of a Ni-Cu-PGE-rich immiscible sulfide liquid, carried in suspension by the melagabbro-like melt, to a Ni-Cu-PGE poor sulfide

from the resulting mixture of melts is fixed. This is because the reserve of the sulfur which enables the second precipitation event is the melagabbro portion of the melt. The proposed model explains the geochemical and textural differences between the interconnected and disseminated sulfide textures and also provides a reasonable explanation for the homogeneity of sulfide metal concentrations relative to sulfide concentration in the interconnected sulfide. Additionally, a second sulfide precipitation event also explains the presence of interconnected sulfides stratigraphically higher than disseminated sulfides.

6.7 - Summary of the revised Shakespeare model

In summary, the Shakespeare magmas have undergone several processes that distinguish it from other Nipissing intrusions. First, the ascending magmas, which were sulfur undersaturated, assimilated significant quantities of the uraniferous quartz pebble conglomerates of the Matinenda Formation. As a result of this assimilation, the Shakespeare magmas became enriched in U, Th, REE, and S.

The ascending magmas, now close to sulfur saturation, travelled through the conduit-like system which makes up the Shakespeare deposit. This includes the portion of the deposit which is open at depth and along strike. All of the drilling and evidence collected so far indicates that the Shakespeare intrusion probably continues at depth until it is truncated by a structure or until it intersects with a feeder-pipe.

The magmas then intruded in intermittent pulses, partially crystallizing and developing the biotite quartz diorite roof zone with each successive pulse. As fresh pulses arrived, they mixed with the previous pulses that were partially crystallized in the conduit, thus creating the autolithic fragments found in the quartz gabbro and melagabbro-rock fragment

units. The mixing event also triggered the first immiscible sulfide precipitation event. Then the portions of the melt that mixed, as a result of later convective erosion of roof zone materials, precipitated a second immiscible sulfide liquid. The mixing was more rigorous locally, hybridizing most of the melagabbro-like melt with the roof zone materials and causing a more intense secondary immiscible sulfide precipitation event. After the precipitation of a second immiscible sulfide liquid, the sulfide blebs coalesced and concentrated at the crystal-melt boundary, also known as the quartz gabbro/ melagabbro boundary. After complete crystallization of the Shakespeare intrusion, the Penokean orogeny subjected the Shakespeare deposit to greenschist facies metamorphism, causing low to moderate replacement of some magmatic silicate minerals but largely preserving the textures and composition of magmatic sulfides.

Thus, the results and analysis taken from this study on the Shakespeare deposit provide insight into the potential for the Nipissing LIP to host magmatic Ni-Cu-PGE deposits. The demonstrated necessity for an ascending magma to assimilate crustal sulfur in this and other studies provides strict controls on exploration for Ni-Cu-PGE deposits. When applied to the Nipissing LIP, this suggests that only magmas that have assimilated significant quantities of the Matinenda Formation should be considered as potential hosts to Ni-Cu-PGE deposits. Further, the revised model suggests that by exploring for Nipissing Gabbros that are heavily enriched in U, Th, and LREE, the unmineralized host rock for a Ni-Cu-PGE deposit could be recognized. Additionally, the rocks that host the Shakespeare deposit are an excellent example of differentiation within a magma chamber as a result of localized assimilation of an essentially pure silica source, i.e. Mississagi Quartzite. The identification of rare PGE bearing MCGS and a more detailed description of the lithologies that host the Shakespeare deposit add to the present understanding of the Shakespeare deposit. The replacement textures observed in

various ilmenite grains that suggest some sulfides were oxidized at an intermediary phase, possibly between the first and second precipitation events which produced immiscible sulfide liquids. In the future, a study focusing on the geochemical characteristics of the Matinenda Formation could be used to determine if the unusual S/Se ratio of Shakespeare rocks are the result of the assimilation of the Matinenda Formation by ascending Shakespeare magmas. Additional studies to determine how some sulfides within the Shakespeare deposit could be partially or entirely oxidized are warranted and may provide important insights into the genesis of magmatic Ni-Cu-PGE deposits in other mafic-ultramafic conduits.

References

- Barkov, A.Y., Thibault, Y., and Laajoki, K.V.O., 1999. Zoning and substitutions in Co-Ni-(Fe)-PGE sulfarsenides from the Mount General 'Skaya layered intrusion, arctic Russia; *Canadian Mineralogist* 37, pp. 127-142.
- Barkov, A.Y., Alapieti, T., Laajoki, K., and Peura, R., 1996. Osmian hollingworthite and rhodian cobaltite-gersdorffite from the Lukkulaivaara layered intrusion, Russian Karelia; *Mineralogical Magazine* 60, pp. 973-978.
- Barnes, S.-J., Prichard, H.M., Cox, R.A., Fisher, P.C., and Godel, B., 2008. The location of the chalcophile and siderophile elements in platinum-group element ore deposits (a textural microbeam and whole rock geochemical study): Implications for the formation of the deposits; *Chemical Geology* 248, pp. 295-317.
- Barnes, S.-J., Savard, D., Bedard, P., and Maier, W.D., 2009. Selenium and sulfur concentrations in the Bushveld Complex of South Africa and implications for formation of the platinum-group element deposits; *Mineralium Deposita* 44, pp. 647-663.
- Bowie, S.H.U., 1979. The Mode of Occurrence and Distribution of Uranium Deposits; *Philosophical Transactions of the Royal Society of London A*, pp. 291.
- Buchan, K.L., Mortensen, J.K., Card, K.D., and Percival, J.A., 1998. Paleomagnetism and U-Pb geochronology of diabase dyke swarms of Minto Block, Superior Province, Quebec, Canada; *Canadian Journal of Earth Sciences* 35, pp. 1054-1069
- Cabri, L.J., 1986. A third issue devoted to platinum deposits; Preface, *Economic Geology* 81, pp. 1045-1048.

Cabri, L.J., 1992. The distribution of trace precious metals in minerals and mineral products; Mineralogical Magazine 56, pp. 289-308.

Campbell, I.H. and Naldrett, A.J., 1979. The influence of silicate:sulfide ratios on the geochemistry of magmatic sulfides; Economic Geology 74, pp. 1503-1506.

Card, K.D. and Pattison, E.F., 1973. Nipissing Diabase of the Southern Province, Ontario; Geological Association of Canada, Special Paper 12, pp.7-30.

Chung, H.Y. and Mungall, J.E., 2009. Physical constraints on the migration of immiscible fluids through partially molten silicates, with special reference to magmatic sulfide ores; Earth and Planetary Science Letters 286, pp. 14-22.

Conrod, D.M. 1988. Petrology, geochemistry and PGE potential of Nipissing intrusions; Unpublished Master's dissertation, University of Toronto, Canada.

Distler, V.V. and Laputina, I.P., 1979. Sulfarsenides of nickel and cobalt containing platinoids; Doklady Akademii Nauk SSSR 248, pp. 718-721.

Eckstrand, O.R., Cogolu, E., 1986. Se/S evidence relating to genesis of sulphides in the Crystal Lake gabbro, Thunder Bay, Ontario; Geol. Assoc. Canadian - Mineralogical Association of Canada Abstract Programs 11, pp. 66.

Eckstrand, O.R., Hulbert, L.J., 1987. Selenium and the source of sulfur in magmatic nickel and platinum deposits; Geological Association of Canada - Mineralogical Association of Canada Abstract Programs 12, pp. 40.

Eckstrand, O.R., Grinenko, L.N., Krouse, H.R., Paktunc, A.D., Schwann., P.L., and Scoates, R.F., 1989. Preliminary data on sulphur isotopes and Se/S ratios, and the source of sulphur in

magmatic sulphides from the Fox River Sill, Molson Dykes and Thompson nickel deposits, northern Manitoba; In: Current Research, Part C. Geological Survey of Canada 89-1C, pp. 235-242.

Ghiorso, M.S., Hirschmann, M.M., Reiners, P.W., and Kress, V.C., III, 2002. The pMELTS: A revision of MELTS aimed at improving calculation of phase relations and major element partitioning involved in partial melting of the mantle at pressures up to 3Gpa; *Geochemistry, Geophysics, Geosystems* 33, pp. 1029.

Godel, B., and Barnes, S.-J., 2008. Platinum-group elements in sulfide minerals and the whole rocks of the J-M Reef (Stillwater Complex): implication for the formation of the reef. *Chemical Geology* 248, 272-294.

Godel, B., Barnes, S.-J., and Maier, W.D., 2007. Platinum-group elements in sulfide minerals, platinum-group minerals, and the whole rocks of the Merensky Reef (Bushveld Complex, South Africa): Implication for the formation of the Reef; *Journal of Petrology* 48, pp. 1569-1604.

Halkoaho, T.A.A., Alapieti, T.T., and Lahtinen, J.J., 1990. The Sompujarvi PGE Reef in the Penikat layered intrusion, northern Finland; *Mineralogy and Petrology* 42, pp. 39-55.

Hattori, K., Campbell, F.A., and Krouse, H.R., 1983(a). Sulphur isotope abundances in Archean clastic rocks: implications for the coeval atmosphere; *Nature* 302, pp. 323-326.

Hattori, K., Krouse, H.R., and Campbell, F.A., 1983(b). The start of sulfur oxidation in continental environments: about 2.2 billion years ago.; *Science* 221, pp. 549-551

Hattori, K.H., Arai, S., and Clarke, D.B., 2002. Selenium, tellurium, arsenic and antimony contents of primary mantle sulfides. *Canadian Mineralogist*, pp. 637-650

Hinchey, J.G. and Hattori, K.H., 2005. Magmatic mineralization and hydrothermal enrichment of the High Grade Zone at the Lac des Iles palladium mine, northern Ontario, Canada; *Mineralium Deposita* 40, pp. 13-23.

Irvine, T.N., Andersen, J.C.O., and Brooks, C.K., 1998. Included blocks (and blocks within blocks) in the Skaergaard intrusion: Geologic relations and the origins of rhythmic modally graded layers; *Geological Society of America Bulletin* 110, pp. 1398-1447.

James, R.S., Easton, R.M., Peck, D.C., and Hrominichuk, J.L., 2002. Platinum-group element mineralization in Paleoproterozoic basic intrusions in central and northeastern Ontario, Canada; (Ed. Cabri, L.J.) *The geology, geochemistry, mineralogy, and mineral beneficiation of platinum group elements*, 339-365, Canadian Institute of Mining and Metallurgy

Keays, R.R. and Lightfoot, P.C., 2009. Crustal sulfur is required to form magmatic Ni-Cu sulfide deposits: evidence from chalcophile element signatures of Siberian and Deccan Trap basalts; *Mineralium Deposita* 45, pp. 241-257.

Kennedy, A.K., Lofgren, G.E., and Wasserburg, G.J., 1993. An experimental study of trace element partitioning between olivine, orthopyroxene and melt in chondrules: equilibrium values and kinetic effects; *Earth Planetary Science Letters* 115, pp. 177-195.

Kerr, A., 2003. Guidelines for the calculation and use of sulphide metal contents in research and mineral exploration; *Current Research, Newfoundland Department of Mines and Energy, Geological Survey, Report 03-1*, pp. 223-229.

Kerr, A. and Leitch, A.M., 2005. Self-Destructive Sulfide Segregation Systems and the Formation of High-Grade Magmatic Ore Deposits; *Economic Geology* 100, pp. 311-332.

Leshner, C.M. and Burnham, O.M., 2001. Multicomponent elemental and isotopic mixing in Ni-Cu-(PGE) ores at Kambalda; Western Australia. *Canadian Mineralogist* 39, pp. 421-446.

Leshner, C.M. and Keays, R.R., 2002. Komatiite-associated Ni-Cu-(PGE) deposits: geology, mineralogy, geochemistry and genesis; In: Cabri, L. (ed) *The geology, geochemistry, mineralogy, and beneficiation of the platinum-group elements*. Canadian Institute for Mining, Metallurgy, and Petroleum 54, pp. 579-618.

Li, C. and Naldrett, A.J., 1999. Geology and petrology of the Voisey's Bay intrusion: Reaction of olivine with silicate and sulfide liquids; *Lithos* 47, pp. 1-31.

Li, C. and Ripley, E.M., 2005. Empirical equations to predict the sulfur content of mafic magmas at sulfide saturation and applications to magmatic sulfide deposits; *Mineralium Deposita* 40, pp. 218-230.

Li, C., Ripley, E.M., Maier, W.D., and Gomwe, T.E.S., 2002. Olivine and sulfur isotopic compositions of the Uitkomst Ni-Cu sulfide ore-bearing complex, South Africa: Evidence for sulfur contamination and multiple magma emplacements; *Chemical Geology* 188, pp. 149-159.

Lightfoot, P.C. and Keays, R.R., 2005. Siderophile and chalcophile metal variations in flood basalts from the Siberian trap, Noril'sk region: Implications for the origin of the Ni-Cu-PGE sulfide ores; *Economic Geology* 100, pp. 439-462.

Lightfoot, P.C., and Naldrett, A.J., 1989. Assimilation and crystallization in basic magma chambers: trace-element and isotopic variations in the Kerns sill, Nipissing diabase province, Ontario; *Canadian Journal of Earth Sciences* 26, pp. 737-754.

Lightfoot, P.C. and Naldrett, A.J., 1996. Petrology and Geochemistry of the Nipissing Gabbro: Exploration Strategies for Nickel, Copper, and Platinum Group Elements in a Large Igneous Province; Ontario Geological Survey, Study 58, pp. 81

Lightfoot, P.C., Conrod, D., Naldrett, A.J., and Evensen, N.M., 1987. Petrologic, Chemical, Isotopic, and Economic-Potential Studies of the Nipissing Diabase; Grant 230, p. 4-26 in Geoscience Research Grant Program, Summary of Research 1986-1987, edited by V.G Milne, Ontario Geological Survey, Miscellaneous Paper 136, pp. 241

Lightfoot, P.C., Keays, R.R., and Doherty, W., 2001(a). Chemical evolution and origin of nickel sulfide mineralization in the Sudbury Igneous Complex, Ontario, Canada; *Economic Geology* 96, pp. 1855-1873

Lightfoot, P.C., Bell, C.C., and Muggridge, M.G., 2001(b). Sulphide saturation history of the Voisey's Bay Intrusion, and formation of the nickel sulphide deposits; *Geological Association of Canada Abstracts* 26, pp. 87.

Long, D.G.F., 1987. Sedimentary framework of uranium deposits in the southern Cobalt Embayment, Ontario Canada; D. Pretorius (Ed.), *Uranium deposits in Proterozoic quartz-pebble conglomerates*. International Atomic Energy Agency, Technical Documents, pp. 155-188

Lorand, J.P. and Alard, O., 2010. Determination of selenium and tellurium concentrations in Pyrenean peridotites (Ariege, France): New insight into S/Se?Te systematics of the upper mantle sample; *Chemical Geology* 278, 120-130

Maier, W.D. and Barnes, S.-J., 2010. The Kabanga Ni sulfide deposits, Tanzania; II. Chalcophile and siderophile element geochemistry. *Mineralium Deposita* 45, pp. 443-460.

Maier, W.D., Barnes, S.-J., Chinyepi, G., Barton Jr, J.M., Eglington, B., and Setshedi, I., 2008. The composition of magmatic Ni-Cu-(PGE) sulfide deposits in the Tati and Selebi-Phikwe belts of eastern Botswana; *Mineralium Deposita* 43, pp. 37-60.

Maier, W.D., Barnes, S.-J., Sarkar, A., Ripley, E.M., Li, C., and Livesey, T., 2010. The Kabanga Ni sulfide deposit, Tanzania: I. Geology, petrography, silicate rock geochemistry, and sulfur and oxygen isotopes; *Mineralium Deposita* 45, pp. 419-441.

Mavrogenes, J.A. and O'Neill, H.StC., 1999. The relative effects of pressure, temperature and oxygen fugacity on the solubility of sulfide in mafic magmas; *Geochimica et Cosmochimica Acta* 63, pp. 1173-1180.

McDonough, W.F. and Sun, S.S., 1995. The composition of the earth; *Chemical Geology* 120, pp. 223–253.

Naldrett, A.J. and Lightfoot, P.C., 1999. Ni-Cu-PGE deposits of the Noril'sk region, Siberia: Their formation in conduits for flood-basalt volcanism; *Geological Association of Canada Short Course Notes* 13, pp. 195-249.

Naldrett, A.J., Wilson, A., Kinnaird, J.A., Yudovskaya, M., and Chunnnett, G., 2011. The origin of chromitites and related PGE mineralization in the Bushveld Complex: New mineralogical and petrological constraints; *Mineralium Deposita* 47, pp. 209-232.

Naldrett, A.J., Fedorenko, V.A., Lightfoot, P.C., Kunilov, V.E., Gorbachev, N.S., Doherty, W. and Johan, J., 1995. Ni-Cu-PGE deposits of the Noril'sk region Siberia: Their formation in conduits for flood basalt volcanism; *Transactions of the Institute of Mining and Metallurgy* 104, pp. B18-B36.

Naldrett, A.J., 2011. Fundamentals of Magmatic Sulfide Deposits; *Reviews in Economic Geology* 17, pp. 1-50.

Noble, S.R. and Lightfoot, P.C., 1992. U-Pb Baddeleyite ages for the Kerns and Triangle Mountain Intrusions, Nipissing Diabase, Ontario; *Canadian Journal of Earth Sciences*, 29, pp. 1124-1129

Peck, D.C and Keays, R.R., 1990. Insights into the behavior of precious metals in primitive, S-undersaturated magmas; evidence from the Heazlewood River Complex, Tasmania.; *Canadian Mineralogist* 28, pp. 553-577.

Queffurus, M. and Barnes, S.J., 2013. A review of the use of S/Se ratios - Processes affecting the sulfur to selenium ratio in magmatic nickel-copper and platinum-group element deposits; *Ore Geology Reviews*, in press.

Ripley, E.M. and Li, C., 2003. Sulfur isotope exchange and metal enrichment in the formation of magmatic Cu-Ni-(PGE) deposits; *Economic Geology* 98, pp. 635-641.

Ripley, E.M., Li, C., and Shin, D., 2002. Paragneiss assimilation in the genesis of magmatic Ni-Cu-Co sulfide mineralization at Voisey's Bay, Labrador: $\delta^{34}\text{S}$, $\delta^{13}\text{C}$ and S/Se evidence; *Economic Geology* 97, pp. 1307-1318

Ripley, E.M., 1990. Se/S ratios of the Virginia Formation and Cu-Ni mineralization in the Babbitt area, Duluth Complex, Minnesota. *Economic Geology* 85, 1935-1940

Shaw, C. S.J., Young, G.M., Fedo, C.M., 1999. *Canadian Journal of Earth Sciences* 39, pp. 1435-1448.

Sproule, R.A, Lambert, D. D., and Hoatson, D. M., 1999. Re-Os isotopic constraints on the genesis of the Sally Malay Ni-Cu-Co deposit, East Kimberley, Western Australia; *Lithos* 47, pp. 89–106.

Sproule, R.A., Sutcliffe, R., Tracanelli, H., and Lesher, C.M., 2007. Palaeoproterozoic Ni-Cu-PGE mineralization in the Shakespeare intrusion, Ontario, Canada: a new style of Nipissing gabbro-hosted mineralization; *Applied Earth Science (Transactions of the Institute of Mining and Metallurgy, Section B)* 116, pp. 188-200

Sutcliffe, R., 2002. Unpublished internal petrographic report for URSA Major Minerals Inc.

Sutcliffe, R., Tracanelli, H., and Davis, D.W., 2002. Shakespeare intrusion; Abstract volume for the 2002 Ontario Prospectors Association Meeting, Toronto, Canada, OPA.

Tarkian, M. and Prichard, H.M., 1987. Irarsite-hollingworthite solid-solution series and other associated Ru-, Os-, Ir- and Rh-bearing PGM's from the Shetland ophiolite complex. *Mineralium Deposita* 22, pp. 178-184.

Theriault, R.M. and Barnes, S.-J., 1998. Compositional variations in Cu-Ni-PGE sulfides of the Dunka Road deposit, Duluth Complex, Minnesota: the importance of combined assimilation and magmatic processes; *Canadian Mineralogist* 36, pp. 869-886.

Volborth, A., Tarkian, M., Stumpfl, E.F, and Housley, R.M., 1986. A survey of the Pd-Pt mineralization along the 35-km strike of the J-M reef, Stillwater complex, Montana, USA; *Canadian Mineralogist* 24, pp. 329-346.

Wellgreen Platinum (V.WG) website, accessed February 27, 2014

Appendix 1a: Quantitative results of the SEM-EDS study

Mineral ID	Spectrum ID	Abundance (wt. %)	Atomic Abundance
Argentopentlandite	Spectrum 29		
	S	31.77	47.39
	Fe	36.17	30.99
	Ni	19.45	15.84
	Ag	13.03	5.78
	Total	100.42	
Galena	Spectrum 11		
	S	33.73	
	Fe	7.66	
	Zn	59.45	
	Total	100.84	
Hollingworthite-irarsite within gersdorffite-cobaltite	Spectrum 5		
	S	17.9	32.26
	Fe	4.2	4.35
	Co	19.67	19.29
	Ni	7.89	7.76
	As	43.72	33.72
	Rh	2.97	1.67
	Ir	3.2	0.96
	Total	99.54	100
Hollingworthite-irarsite within gersdorffite-cobaltite	Spectrum 10		
	S	18.11	32.95
	Fe	4.05	4.23
	Co	19.55	19.35
	Ni	7.26	7.21
	As	43.01	33.49
	Rh	2.45	1.39
	Ir	4.56	1.38
	Total	99	100
Gersdorffite-cobaltite	Spectrum 22		
	S	18.67	32.16
	Fe	5.56	5.5
	Co	20.4	19.12
	Ni	10.02	9.43
	As	45.84	33.79
	Total	100.49	100

Mineral ID	Spectrum ID	Abundance (wt. %)	Atomic Abundance
Very small merenskyite grain in fracture within gersdorffite adjacent to molybdenite	Spectrum 14		
	S	16.23	37.41
	Fe	3.16	4.18
	Co	11.8	14.8
	Ni	5.09	6.41
	As	15.96	15.74
	Mo	18.38	14.16
	Pd	2.36	1.64
	Te	1.42	0.82
	Bi	13.66	4.83
	Total	88.05	100
Hollingworthite-irarsite- platarsite solid solution within gersdorffite-cobaltite	Spectrum 109		
	S	17.52	31.88
	Fe	4.47	4.67
	Co	17.46	17.29
	Ni	7.53	7.49
	As	43.28	33.71
	Rh	7.51	4.26
	Pt	0.89	0.27
	Ir	1.44	0.44
	Total	100.1	100
Hollingworthite-irarsite- platarsite solid solution within gersdorffite-cobaltite	Spectrum 101		
	S	17.95	32.71
	Fe	4.02	4.21
	Co	18.88	18.71
	Ni	5.85	5.82
	As	42.95	33.49
	Rh	7.59	4.31
	Pt	1.24	0.37
	Ir	1.23	0.37
	Total	99.72	100
Galena-clausthalite fracture filling near chalcopyrite grain	Spectrum 133		
	S	32.69	50.32
	Fe	29.6	26.15
	Cu	28.43	22.08
	Pb	6.08	1.45
	Total	96.8	100

Mineral ID	Spectrum ID	Abundance (wt. %)	Atomic Abundance
Very fine Rheniite grain within chalcopyrite	Spectrum 50		
	S	31.27	65.82
	Fe	11.83	14.3
	Cu	4.56	4.85
	Re	41.47	15.03
	Total	89.13	100
Silver telluride within chalcopyrite	Spectrum 30		
	S	24.45	44.6
	Fe	23.1	24.19
	Cu	22.75	20.94
	Ag	13.19	7.15
	Te	6.79	3.11
	Total	90.29	100
Tsuomite	Spectrum 79		
	Fe	0.97	2.9
	Te	37.03	48.39
	Bi	61.05	48.71
	Total	99.06	100
Native Copper with minor Fe and Ti, possibly from surrounding ilmenite	Spectrum 57		
	Ti	0.85	1.11
	Fe	2.14	2.39
	Cu	97.93	96.5
	Total	100.92	100
Allanite-(Ce)	Spectrum 50		
	O	35.12	60.75
	Al	10.93	11.21
	Si	15.05	14.83
	Ca	11.03	7.62
	Fe	6.99	3.47
	La	2.93	0.58
	Ce	5.58	1.1
	Nd	2.31	0.44
	Total	89.93	100
Unidentified fine W mineral surrounded by pyrrhotite	Spectrum 80		
	S	34.14	56.15
	Fe	39.69	37.47
	W	22.24	6.38
	Total	96.07	100

Appendix 1b: Origin and type of standards used in the SEM-EDS study. LUIL: Lakehead University Instrumentation Laboratory

Element	Standard	Factory setting or LUIL standard
Na	Na-Jadeite BM	LUIL
Mg	Periclase	LUIL
Al	Garnet RHM	LUIL
Si	Garnet RHM	LUIL
S	NiS, CuFeS ₂	LUIL
Ti	Ti	LUIL
Fe	FeCuS ₂	LUIL
Co	Co	LUIL
Ni	Ni	LUIL
Cu	FeCuS ₂	LUIL
Zn	Zn	Factory
As	InAs	Factory
Se	Bi ₂ Se ₃	LUIL
Mo	Mo	Factory
Rh	Rh	Factory
Pd	Pd	LUIL
Ag	Ag	LUIL
Sn	Sn	Factory
Te	Bi ₂ Te ₃	LUIL
La	LaB ₆	Factory
Ce	CeO ₂	Factory
Nd	Nd	Factory
W	W	Factory
Re	Re	LUIL
Os	Os	Factory
Ir	Ir	Factory
Pt	Pt	LUIL
Au	Au	Factory
Pb	PbTe	Factory
Bi	Bi ₂ Se ₃	LUIL

Appendix 2a: Core logs for diamond drill hole U-03-118

URSA Diamond Drill Hole Number: **U-03-118**

Azimuth of Diamond Drill Hole: **147 Degrees Az.**

Inclination of the Diamond Drill Hole: **-77.5 Degrees**

Diamond Drill Core Logging Carried Out By: **Ian Dasti**

Total Depth of Diamond Drill Hole: **624 Meters**

<u>From Meters</u>	<u>To Meters</u>	<u>Distance Meters</u>	<u>Lith Code</u>	<u>Discription Major Interval</u>	<u>Description Code</u>	<u>Description Minor Internal Interval</u>	<u>Measured Feature</u>	<u>Alignment TCA</u>	<u>From Meters</u>	<u>To Meters</u>	<u>Distance Meters</u>
0.00	3.00	3.00		Casing – Not Recovered							
3.00	333.00	330.00	1a	Quartzite							

<u>From</u> <u>Meters</u>	<u>To</u> <u>Meters</u>	<u>Distance</u> <u>Meters</u>	<u>Lith</u> <u>Code</u>	<u>Discription</u> <u>Major Interval</u>	<u>Description</u> <u>Code</u> <u>Minor Internal Interval</u>	<u>Measured</u> <u>Feature</u>	<u>Alignment</u> <u>TCA</u>	<u>From</u> <u>Meters</u>	<u>To</u> <u>Meters</u>	<u>Distance</u> <u>Meters</u>
				Quartzite, light white – grey blue, overall fine to medium grained with common rhythmic coarsening followed by fining of grainsize.. Commonly bedded in 900 to 1080 mm to over 3000mm intervals (commonly 2000 - 2500mm). Individual beds are marked by a fine grained, laminated siltstone that sometimes exhibits evidence of ductile deformation (stretching, lineation of minerals). The siltstone varies from 8-16mm to over 600mm, but is usually 50-100mm in thickness. Siltstone intervals increase in width down hole. Quartzite beds vary in purity, with occasional clean beds and more common beds with silt / mica impurities. Commonly dark, fine silt/mica bands cross bedding.		Joint / Limonite Alteration	3	36.48	36.48	0.00
						Joint / Limonite Alteration	66	36.60	36.60	0.00
						Joint / Limonite Alteration	15	36.90	36.90	0.00

<u>From</u> <u>Meters</u>	<u>To</u> <u>Meters</u>	<u>Distance</u> <u>Meters</u>	<u>Lith</u> <u>Code</u>	<u>Discription</u> <u>Major Interval</u>	<u>Description</u> <u>Minor Interval</u>	<u>Measured</u> <u>Feature</u>	<u>Alignment</u> <u>TCA</u>	<u>From</u> <u>Meters</u>	<u>To</u> <u>Meters</u>	<u>Distance</u> <u>Meters</u>
				Quartzite continued		Joint	24	40.25	40.25	0.00
						Fracture Filling – Mica, Pyrite, Marcassite	28	40.35	40.36	0.01
						Cross Bedding / joint	40	40.42	40.42	0.00
						Fracture Filling – Mica, Pyrite, Marcassite	70	40.62	40.62	0.00
						Cross Bedding / joint	47	55.35	55.35	0.00
						Joint	70	63.37	63.37	0.00
						Cross Bedding / joint	25	67.86	67.86	0.00
					Around 81.47 (for about 1000 mm either way) qtzite becomes quite clumpy / viscous looking (possibly due to differential erosion from drill)	S (or Z) folded Fracture Filling and sucrosic quartzite	78	81.47	81.47	0.00
					Beautiful, textbook quality trough cross lamination	Trough Cross Lamination	N/A	90.00	91.00	1.00

<u>From</u> <u>Meters</u>	<u>To</u> <u>Meters</u>	<u>Distance</u> <u>Meters</u>	<u>Lith</u> <u>Code</u>	<u>Discription</u> <u>Major Interval</u>	<u>Code</u>	<u>Description</u> <u>Minor Internal Interval</u>	<u>Measured</u> <u>Feature</u>	<u>Alignment</u> <u>TCA</u>	<u>From</u> <u>Meters</u>	<u>To</u> <u>Meters</u>	<u>Distance</u> <u>Meters</u>
				Quartzite continued		Quartz vein with some carbonate and large aggregates of Kspar. Sulfide bearing, with pyrite and marcassite. Limonite on fracture surface	Quartz Vein	44	113.55	113.65	0.10
							Quartz Vein	40	113.75	113.77	0.02
						Hematite alteration can invade core up to 30 mm. Altered area (corresponding to multiple joints) is approximately from 129.92 to 130.92	Joint / Hematite Alteration	53	130.92	130.92	0.00
							Joint / Broken zone	48	141.89	141.99	0.10
							Joint	7	143.11	143.11	0.00
							Joint / Broken zone	48	143.11	143.31	0.20
						Small (50 mm) zone of broken siltstone material followed by a 350mm quartzite breccia. Individual fragments over 40mm.	Annealed Fault/ minor Broken Zone	50	205.86	206.26	0.40
						Fe – carbonate fracture filli	Joint / Hematite Alteration	63	216.65	216.65	0.00

<u>From</u> <u>Meters</u>	<u>To</u> <u>Meters</u>	<u>Distance</u> <u>Meters</u>	<u>Lith</u> <u>Code</u>	<u>Discription</u> <u>Major Interval</u>	<u>Code</u>	<u>Description</u> <u>Minor Internal Interval</u>	<u>Measured</u> <u>Feature</u>	<u>Alignment</u> <u>TCA</u>	<u>From</u> <u>Meters</u>	<u>To</u> <u>Meters</u>	<u>Distance</u> <u>Meters</u>
				Quartzite continued		213-221 large interval of jointing with hematite clay on surface (and penetrating into core). Near center jointing (and thus hematite) increases.		38	216.81	216.81	0.00
								13	222.39	222.39	0.00
								28	222.40	222.40	0.00
						5mm qtz vein cutting core at low angle	Quartz Vein	10	225.00	225.00	0.00
							Joint	50	260.42	260.42	0.00
							Bedding	35	300.39	300.39	0.00
							Lineation / Fabric	35	300.39	300.52	0.13
						Contact is wavy and very sharp.	Contact	10	333.00	333.00	0.00
						100mm breccia zone (cream carbonate? Cement with angular lamprophyre fragments)	Breccia / Joint	20	333.21	333.21	0.00
							mineral lineation	20	333.40	333.40	0.00
							Contact is sharp and strait	49	341.67	341.67	0.00
							broken zone / joint	59	358.01	358.14	0.13

<u>From</u> <u>Meters</u>	<u>To</u> <u>Meters</u>	<u>Distance</u> <u>Meters</u>	<u>Lith</u> <u>Code</u>	<u>Discription</u> <u>Major Interval</u>	<u>Code</u>	<u>Description</u> <u>Minor Internal Interval</u>	<u>Measured</u> <u>Feature</u>	<u>Alignment</u> <u>TCA</u>	<u>From</u> <u>Meters</u>	<u>To</u> <u>Meters</u>	<u>Distance</u> <u>Meters</u>
333.00	334.36	1.36	7a	Lamprophyre – Fine grained, exhibiting mineral lineation (angle varies, obviously larger scale folding). Dark brown color, has Xenoliths? Of lighter colored aphanitic material (5mm to 25 mm)		Higher density of jointing and hematite staining. Hematite stains go through core up to 30mm.			358.01	359.67	1.66
							Mineral lineaton / joint / hematite alteration	60	359.00	359.00	0.00
							Fault Gouge	60	359.17	359.27	0.10
334.36	335.54	1.18	1a	Quartzite – fine to medium grained			Fault Gouge	62	359.66	359.67	0.01
335.54	341.67	6.13	7a	Lamprophyre – Fine grained, exhibiting mineral lineation (angle varies, obviously larger scale folding). Lighter brown/green – grey color, has Xenoliths? Of lighter colored aphanitic material (5mm to 25 mm)			Joint	51	370.38	370.38	0.00

<u>From</u> <u>Meters</u>	<u>To</u> <u>Meters</u>	<u>Distance</u> <u>Meters</u>	<u>Lith</u> <u>Code</u>	<u>Discription</u> <u>Major Interval</u>	<u>Description</u> <u>Code</u> <u>Minor Internal Interval</u>	<u>Measured</u> <u>Feature</u>	<u>Alignment</u> <u>TCA</u>	<u>From</u> <u>Meters</u>	<u>To</u> <u>Meters</u>	<u>Distance</u> <u>Meters</u>
341.67	467.74	126.07	1a	Quartzite, light white – grey blue, overall fine to medium grained with common rhythmic coarsening followed by fining of grainsize.. Commonly bedded in 900 to 1080 mm to over 3000mm intervals (commonly 2000 - 2500mm). Individual beds are marked by a fine grained, laminated siltstone that sometimes exhibits evidence of ductile deformation (stretching, lineation of minerals). The siltstone varies from 8-16mm to over 600mm, but is usually 50-100mm in thickness. Siltstone intervals increase in width down hole. Quartzite beds vary in purity, with occasional clean beds and		Microfolding Z's (or S) of fracture filling		370.80	371.2	0.40
						Joint	70	394.05	394.05	0.00
						Joint	76	397.08	397.08	0.00
						Joint / cross bedding	50	398.46	398.46	0.00

<u>From</u> <u>Meters</u>	<u>To</u> <u>Meters</u>	<u>Distance</u> <u>Meters</u>	<u>Lith</u> <u>Code</u>	<u>Discription</u> <u>Major Interval</u>	<u>Code</u>	<u>Description</u> <u>Minor Internal Interval</u>	<u>Measured</u> <u>Feature</u>	<u>Alignment</u> <u>TCA</u>	<u>From</u> <u>Meters</u>	<u>To</u> <u>Meters</u>	<u>Distance</u> <u>Meters</u>
				Quartzite continued			Wavy chalcopyrite and pyrite		420.92	420.96	0.04
						minor kspar in small vein beside joint	Joint	60	421.19	421.19	0.00
						First shot of Quartz Diorite material. Heavy assimilation of quartz (doesn't look exactly like quartz diorite, but similar)			424.52	424.75	0.23
							Quartz Vein with pyrite and minor chalcopyrite	14	424.5	424.52	0.02
						Mineral lineation within splash of qtz diorite	mineral lineation	51	431	431	0.00
							Pyrite following lineation	51	431.17	431.17	0.00
						Small (5mm) fault gouge Large Broken zone with no hematite alteration on fracture surfaces. Joints increase exponentially towards the fault gouge at 437.83 (12mm gouge)	Fault Gouge	50	424.75 435.84	424.76 438.25	0.01 2.41
							Fault Gouge	48	437.83	437.84	0.01
							Quartz Vein with pyrite	42	446.6	446.74	0.14
							Joint	40	458.13	458.13	0.00
							contact/ lineation	42	467.74	467.74	0.00

<u>From</u> <u>Meters</u>	<u>To</u> <u>Meters</u>	<u>Distance</u> <u>Meters</u>	<u>Lith</u> <u>Code</u>	<u>Discription</u> <u>Major Interval</u>	<u>Code</u>	<u>Description</u> <u>Minor Internal Interval</u>	<u>Measured</u> <u>Feature</u>	<u>Alignment</u> <u>TCA</u>	<u>From</u> <u>Meters</u>	<u>To</u> <u>Meters</u>	<u>Distance</u> <u>Meters</u>
				Quartzite Continued			mineral lineation	42	472.04	472.04	0.00
							mineral lineation	36	474.92	474.92	0.00
						small (5mm) quartz vein at low angle	Quartz Vein	12	477.18	477.19	0.01
						Quartz Diorite coarsens from fine (mm to sub mm grains) to medium grained (1-2mm)			478.00	480.00	2.00
							Joint / Mineral lineation	24	480.93	480.93	0.00
						Becomes more gabbroic – lesser quartz, more mafic minerals and plagioclase, but is still a Quartz Diorite			480.00	481.00	1.00
467.74	487.34	19.60	4d	Quartz Diorite – Fine to medium grained (sub mm up to mm scale) quartz diorite varying slightly in color but overall lighter brown-green. Occasionally, relict sedimentary textures observable in xenoliths, but more commonly partial assimilation and baking have destroyed original sedimentary fabric. Mica and amphibole rich, commonly exhibiting a strong mineral fabric.			Quartz Diorite – Veritextured Quartz Gabbro Contact	33	487.34	487.34	0.00

<u>From Meters</u>	<u>To Meters</u>	<u>Distance Meters</u>	<u>Lith Code</u>	<u>Discription Major Interval</u>	<u>Code</u>	<u>Description Minor Internal Interval</u>	<u>Measured Feature</u>	<u>Alignment TCA</u>	<u>From Meters</u>	<u>To Meters</u>	<u>Distance Meters</u>
				Quartz Diorite Continued - Quartzite xenoliths are common and range in size from 150mm to over 3000mm, commonly over 800mm. Strong mineral lineation / fabric is commonly observed, especially around xenoliths			Quartz Diorite – Veritextured Quartz Gabbro Contact	33	487.34	487.34	0.00
487.34	495.16	7.82	4d/4c	Veritextured Quartz Gabbro – coarse grained, with up to 15% quartz but more commonly 5-7% coarse grained, interconnected blue quartz 4mm x 1mm to 28mm x 4mm. 40-60% mafic minerals, most of which are green amphiboles from 2mm x 2mm to 30mm x 4mm, which commonly interlock / interconnect.. Bladed ilmenite common, blades up to 5mm x less than 1mm. Feldspars commonly interlocked with quartz crystals, trying to form granophyre. Trace chalcopyrite (up to 2 % over 100 mm) blebs and trace pyrrhotite blebs found throughout interval.		Fine grained intermediate zone with lots of dark clays and some mica minerals. Fine grained, cream to occasionally light sulfide colored mineral, commonly exhibiting fine blade texture (leucoxene?).			487.34	487.95	0.61

<u>From</u> <u>Meters</u>	<u>To</u> <u>Meters</u>	<u>Distance</u> <u>Meters</u>	<u>Lith</u> <u>Code</u>	<u>Discription</u> <u>Major Interval</u>	<u>Code</u>	<u>Description</u> <u>Minor Internal Interval</u>	<u>Measured</u> <u>Feature</u>	<u>Alignment</u> <u>TCA</u>	<u>From</u> <u>Meters</u>	<u>To</u> <u>Meters</u>	<u>Distance</u> <u>Meters</u>
				Veritextured Quartz Gabbro - Continued		Multiple generations (3 for sure, possibly 4) of jointing and filling, with structures cross cutting previous ones.	3% pyrrhotite and trace-.5% chalcopyrite roughly following mineral lineation, occasional larger bleb	32	487.95	488.35	0.40
							Joint	23	489.40	489.40	0.00
							fracture filling – mostly micacious material but one carbonate vein.	14	490.82	490.82	0.00
							Joint	60	494.91	494.91	0.00

<u>From</u> <u>Meters</u>	<u>To</u> <u>Meters</u>	<u>Distance</u> <u>Meters</u>	<u>Lith</u> <u>Code</u>	<u>Discription</u> <u>Major Interval</u>	<u>Description</u> <u>Code</u> <u>Minor</u> <u>Internal</u> <u>Interval</u>	<u>Measured</u> <u>Feature</u>	<u>Alignment</u> <u>TCA</u>	<u>From</u> <u>Meters</u>	<u>To</u> <u>Meters</u>	<u>Distance</u> <u>Meters</u>
495.16	521.90	26.74	4c	Quartz Gabbro – fine to medium grained with overall 5% quartz (less towards lower contact) and a “salt and pepper” texture. Very homogenous and consistent in regards to textural features and mineralogy. Rock fragments can be seen near the base of this unit and rarely throughout. Mafic minerals are predominantly amphibole (actinolite?) and mica (biotite?)		Veritextured Quartz Gabbro – Quartz Gabbro contact	40	495.16	495.16	0.00
521.90	566.88	44.98	4b	Melagabbro – Dark green, medium grained melagabbro with approximately 20% plagioclase, minor (1% or less) quartz, and approximately 75-80% amphiboles and chloritized mafic minerals. Pyroxenes have undergone a high degree of replacement. In areas, the melagabbro looks “washed out” and crystal boundaries seem mushy.		Contact between Quartz Gabbro and Melagabbro zone	36	519.70	519.70	0.00

<u>From</u> <u>Meters</u>	<u>To</u> <u>Meters</u>	<u>Distance</u> <u>Meters</u>	<u>Lith</u> <u>Code</u>	<u>Discription</u> <u>Major Interval</u>	<u>Code</u>	<u>Description</u> <u>Minor Internal Interval</u>	<u>Measured</u> <u>Feature</u>	<u>Alignment</u> <u>TCA</u>	<u>From</u> <u>Meters</u>	<u>To</u> <u>Meters</u>	<u>Distance</u> <u>Meters</u>
				Melagabbro Continued - Mineralization textures begin with blebby pyrrhotite and lesser chalcopyrite, followed by weakly interconnected pyrrhotite and lesser chalcopyrite, followed by disseminated pyrrhotite and chalcopyrite with rare blebs.		Intermediate between melagabbro and quartz gabbro. Small areas of higher quartz, but overall less than 3% quartz, less plagioclase, and more mafics. Salt and pepper texture comes and goes until finally in melagabbro (and mineralization) at 521.9			519.70	521.90	2.20
						Melagabbro Rock Fragment Phase – partially resorbed xenolithic fragments from 1mm x 1mm up to 50mm x 50mm, varying from rounded to angular/sub angular are commonly observed. Occasionally, fragments contain high (<70% sulfides, almost entirely chalcopyrite).			521.90	553.76	31.86
						15-20% interconnected sulfides. Appears as if blebs (or large disseminated grains) are present and connected by thinner, wispy sulfide. Approximately 14.5-19.5% pyrrhotite, .5% chalcopyrite.			521.90	522.16	0.26

<u>From</u> <u>Meters</u>	<u>To</u> <u>Meters</u>	<u>Distance</u> <u>Meters</u>	<u>Lith</u> <u>Code</u>	<u>Discription</u> <u>Major Interval</u>	<u>Code</u>	<u>Description</u> <u>Minor Interval</u>	<u>Measured</u> <u>Feature</u>	<u>Alignment</u> <u>TCA</u>	<u>From</u> <u>Meters</u>	<u>To</u> <u>Meters</u>	<u>Distance</u> <u>Meters</u>
				Melagabbro continued		9.5% pyrrhotite as blebby (to very weakly interconnected in areas) with .5% chalcopyrite. Blebs are ocassionally weakly interconnected			522.16	524.78	2.62
						Overall 4% pyrrhotite and .5% chalcopyrite as scattered, well formed blebs. Chalcopyrite forms along periphery of grains. Small areas (10 cm) with significantly less (2%) and significantly more (7%) sulfides are common.			524.78	530.91	6.13
						Overall 3% sulfides, 1.5% pyrrhotite, 1.5% chalcopyrite. Small areas are more sulfide rich due to fracture fillings and mineralized rock fragments (up to 7% over 10 cm)			530.91	532.91	2.00

<u>From</u> <u>Meters</u>	<u>To</u> <u>Meters</u>	<u>Distance</u> <u>Meters</u>	<u>Lith</u> <u>Code</u>	<u>Discription</u> <u>Major Interval</u>	<u>Code</u>	<u>Description</u> <u>Minor Internal Interval</u>	<u>Measured</u> <u>Feature</u>	<u>Alignment</u> <u>TCA</u>	<u>From</u> <u>Meters</u>	<u>To</u> <u>Meters</u>	<u>Distance</u> <u>Meters</u>
				Melagabbro continued		Overall 5% pyrrhotite and .5% chalcopyrite with one large (8 cm) fracture filling with ~60% pyrrhotite and ~5% chalcopyrite as moderately well formed blebs. Bits of amphibole, ect are common within the blebs and as a result are occasionally interstitial.	Thin cross cutting fracture fillings (one is pyrrhotite rich, one is chalcopyrite rich. Chalcopyrite rich cuts pyrrhotite rich)	40	532.91	535.15	2.24
						Quartz vein / fracture filling jacked with pyrrhotite becomes chalcopyrite rich near large (50 x 50 mm) rock fragment. Chalcopyrite seems to bleed into the rock fragment, maybe rock fragments act as a sponge?			533.00	533.10	0.10

<u>From</u> <u>Meters</u>	<u>To</u> <u>Meters</u>	<u>Distance</u> <u>Meters</u>	<u>Lith</u> <u>Code</u>	<u>Discription</u> <u>Major Interval</u>	<u>Code</u>	<u>Description</u> <u>Minor Interval</u>	<u>Measured</u> <u>Feature</u>	<u>Alignment</u> <u>TCA</u>	<u>From</u> <u>Meters</u>	<u>To</u> <u>Meters</u>	<u>Distance</u> <u>Meters</u>
				Melagabbro continued		5.5-6% pyrrhotite, 1 – 1.5% chalcopyrite as blebs and medium to coarse, poorly disseminated grains. Where chalcopyrite and pyrrhotite are found together, the chalcopyrite forms along the periphery. However, chalcopyrite only blebs are common. Pyrrhotite only grains are uncommon, and usually contain atleast a hint of chalcopyrite.			535.15	536.15	1.00
						Overall, 4.5-6% pyrrhotite and .5 to 1% chalcopyrite, as blebs with minor silicates entrained within. Occasional to rare disseminations.			536.15	540.45	4.30
						5.5% pyrrhotite, 1.5% chalcopyrite as blebs with minor disseminations			540.45	541.79	1.34
						6% pyrrhotite, 1% chalcopyrite, silicates entrained in blebs, occasional disseminations			541.79	544.82	3.03

<u>From</u> <u>Meters</u>	<u>To</u> <u>Meters</u>	<u>Distance</u> <u>Meters</u>	<u>Lith</u> <u>Code</u>	<u>Discription</u> <u>Major Interval</u>	<u>Code</u>	<u>Description</u> <u>Minor Internal Interval</u>	<u>Measured</u> <u>Feature</u>	<u>Alignment</u> <u>TCA</u>	<u>From</u> <u>Meters</u>	<u>To</u> <u>Meters</u>	<u>Distance</u> <u>Meters</u>
				Melagabbro continued		8% pyrrhotite and 2% chalcopyrite, mostly fine blebs with silicate entrained, but occasional disseminations			544.82	546.00	1.18
						6.5 – 8% pyrrhotite and .5 to 1.5% chalcopyrite as weak disseminations and attempted / poorly formed blebs			546.00	548.20	2.20
						5.5% pyrrhotite, 1.5% chalcopyrite as disseminations, occasionally rare blebs			548.20	549.40	1.20
						4-5.5% pyrrhotite and 1 – 1.5% chalcopyrite as disseminated grains and rare to absent blebs			549.40	561.39	11.99
				Melagabbro- Equigranular Phase		Melagabbro Equigranular Phase - Melagabbro Equigranular phase – Rock fragments rare to absent, texturally equigranular pyroxenes (replaced), amphiboles, and plagioclase present. Semi-blocky grains common			553.76	566.88	13.12
						2.5 – 4% pyrrhotite and .5- 1% cpy, as disseminated grains			561.39	563.16	1.77

<u>From</u> <u>Meters</u>	<u>To</u> <u>Meters</u>	<u>Distance</u> <u>Meters</u>	<u>Lith</u> <u>Code</u>	<u>Discription</u> <u>Major Interval</u>	<u>Code</u>	<u>Description</u> <u>Minor Interval</u>	<u>Measured</u> <u>Feature</u>	<u>Alignment</u> <u>TCA</u>	<u>From</u> <u>Meters</u>	<u>To</u> <u>Meters</u>	<u>Distance</u> <u>Meters</u>
				Melagabbro continued		1.5 – 1.75% pyrrhotite and .25-.5% chalcopyrite as patchy disseminated grains.			563.16	564.29	1.13
						2.5 – 4% pyrrhotite and .5-1% cpy, as disseminated grains			564.29	565.52	1.23
						7% pyrrhotite and 1% chalcopyrite as disseminated grains			565.52	565.67	0.15
						4-4.5% pyrrhotite and .5-1% chalcopyrite as patchy disseminated grains			565.67	566.88	1.21
566.88	606.00	39.12	3a/3b	Nipissing Quartz Gabbro – Fine to medium grained quartz gabbro with amphibole (actinolite?) replacing pyroxene. Biotite common.							
				Trace pyrrhotite and trace chalcopyrite as rare disseminated grains (1mm x							
						Blue quartz vein with a ribbon of carbonate and fine amphibole (actinolite?) / chlorite along edges. Chalcopyrite and pyrrhotite up to 20% in actinolite/chlorite, overall 3-5% in vein			566.88	567.98	1.10

<u>From Meters</u>	<u>To Meters</u>	<u>Distance Meters</u>	<u>Lith Code</u>	<u>Discription Major Interval</u>	<u>Code</u>	<u>Description Minor Internal Interval</u>	<u>Measured Feature</u>	<u>Alignment TCA</u>	<u>From Meters</u>	<u>To Meters</u>	<u>Distance Meters</u>
				Nipissing quartz gabbro continued			Quartz Vein with zoned carbonate and chalcopyrite/ pyrrhotite	18	580.85	581.20	0.35
							Carbonate vein with chalcopyrite and pyrrhotite	64	586.92	586.94	0.02
							Joint	30	590.40	590.40	0.00
							Joint	19	597.35	597.35	0.00
						Chalcopyrite and pyrrhotite associated with mafic chlorite / amphibole along edges of quartz vein.	Joint / Broken zone	5	604.84	604.84	0.00
606.00	624.00	18.00	3a/3b	Nipissing Gabbro - Medium grained Nipissing Gabbro with very flashy green amphiboles. Very similar to above nipissing gabbro, but much less quartz (very rare / absent) and biotite.			Quartz Vein with chalcopyrite and pyrrhotite	12	610.49	610.79	0.30
624.00	624.00	0.00	EOH	End of U-03-118 - Logged by Ian Dasti							

Appendix 2b - Core logs for diamond drill hole U-03-119

URSA Diamond Drill Hole Number: **U-03-119**

Azimuth of Diamond Drill Hole: **147 Degrees Az.**

Inclination of the Diamond Drill Hole: **-65.9 degrees head set with Flexit bore hole orientation device**

Diamond Drill Core Logging Carried Out By: **Harold J. Tracanelli, Getn, P.Geo., and Ian Dasti**

Total Depth of Diamond Drill Hole: **531 Meters**

<u>From</u> <u>Meters</u>	<u>To</u> <u>Meters</u>	<u>Distance</u> <u>Meters</u>	<u>Litho</u> <u>Code</u>	<u>Discription</u> <u>Major Interval</u>	<u>Description</u> <u>Minor Internal Interval</u>	<u>Measured</u> <u>Feature</u>	<u>Alignmen</u> <u>TCA</u>	<u>From</u> <u>Meters</u>	<u>To</u> <u>Meters</u>	<u>Distance</u> <u>Meters</u>
0.00	3.00	3.00	OB	Casing						0.00

<u>From</u> <u>Meters</u>	<u>To</u> <u>Meters</u>	<u>Distance</u> <u>Meters</u>	<u>Litho</u> <u>Code</u>	<u>Description</u> <u>Major Interval</u>	<u>Description</u> <u>Minor Internal Interval</u>	<u>Measured</u> <u>Feature</u>	<u>Alignmen</u> <u>TCA</u>	<u>From</u> <u>Meters</u>	<u>To</u> <u>Meters</u>	<u>Distance</u> <u>Meters</u>
3.00	268.73	265.73	1a	Quartzite, light white – grey blue, overall fine to medium grained with common rhythmic coarsening followed by fining of grainsize.. Commonly bedded in 900 to 1080 mm to over 3000mm intervals (commonly 2000 - 2500mm). Individual beds are marked by a fine grained, laminated siltstone that sometimes exhibits evidence of ductile deformation (stretching, lineation or minerals). The siltstone varies from 2-15mm to over 600mm, but is usually 50-100mm in thickness. Siltstone intervals increase in width down hole. Quartzite beds vary in purity, with occasional clean beds and more common beds with silt / mica impurities. Commonly dark, fine silt/mica bands cross bedding.		Quartz Vein				0.39
							16	13.32	13.71	
						Joint / Hematite Staining	24	14.00	14.00	0.00
						joint	50	19.00	19.00	0.00
						Fault	51	29.70	29.72	0.02
						Gouge				
						Fault	51	32.68	32.70	0.02
						Gouge				
						Bedding / joint	35	56.30	56.30	0.00
						joint	8	60.20	60.20	0.00

<u>From</u> <u>Meters</u>	<u>To</u> <u>Meters</u>	<u>Distance</u> <u>Meters</u>	<u>Litho</u> <u>Code</u>	<u>Description</u> <u>Major Interval</u>	<u>Code</u>	<u>Description</u> <u>Minor Internal Interval</u>	<u>Measured</u> <u>Feature</u>	<u>Alignmen</u> <u>TCA</u>	<u>From</u> <u>Meters</u>	<u>To</u> <u>Meters</u>	<u>Distance</u> <u>Meters</u>
				Quartzite continued					73.90	88.72	14.82
							joint	27	79.65	79.65	0.00
							joint	68	82.39	82.39	0.00
							joint	51	82.88	82.88	0.00
							joint	8	85.50	85.50	0.00
							Joint /				0.00
							Bedding	62	95.81	95.81	
							Cross	22	118.40	118.40	0.00
							Bedding				
							Joint /	29	136.28	136.28	0.00
							limonite				
							Pyrrhotite	42	154.02	154.14	0.12
							bearing				
							Quartz Vein				
							with mica /				
							amphibole				
							Fault	54	140.14	140.15	0.01
							Gouge				
							Quartz Vein	41	164.48	164.75	0.27
							joint	7	166.50	166.50	0.00

<u>From</u> <u>Meters</u>	<u>To</u> <u>Meters</u>	<u>Distance</u> <u>Meters</u>	<u>Litho</u> <u>Code</u>	<u>Discription</u> <u>Major Interval</u>	<u>Description</u> <u>Minor Internal Interval</u>	<u>Measured</u> <u>Feature</u>	<u>Alignmen</u> <u>TCA</u>	<u>From</u> <u>Meters</u>	<u>To</u> <u>Meters</u>	<u>Distance</u> <u>Meters</u>
				Quartzite continued		Quartz / K- Spar / Amphibole – Mica Vein	60	200.55	200.62	0.07
					Effects of Quartz Diorite obvious. Hornfels common and primary sedimentary features are becoming distorted. Quartz Diorite materials (foliated mica and amphiboles) become more common with increasing depth			219.14	268.73	49.59
						Annealed Fault Gouge				0.06
						Fault Gouge	52 62	219.14 219.72	219.2 219.74	0.02
						Quartz / K spar vein (shear?)	52	227.88	228.10	0.22

<u>From</u> <u>Meters</u>	<u>To</u> <u>Meters</u>	<u>Distance</u> <u>Meters</u>	<u>Litho</u> <u>Code</u>	<u>Description</u> <u>Major Interval</u>	<u>Code</u>	<u>Description</u> <u>Minor Interval</u>	<u>Measured</u> <u>Feature</u>	<u>Alignmen</u> <u>TCA</u>	<u>From</u> <u>Meters</u>	<u>To</u> <u>Meters</u>	<u>Distance</u> <u>Meters</u>
				Quartzite continued		Effects of Quartz Diorite obvious. Hornfels becoming more common and primary sedimentary features are becoming distorted. Quartz Diorite materials (foliated mica and amphiboles) become more common with increasing depth. Shots of quartz diorite material within quartzite unit are from 100 mm to over 1000mm, commonly 200mm – they commonly display mineral fabric and have a cream – green color when dry	Fault Gouge	58	241.86	242.07	0.21
							Mineral Fabric	50	252.00	252.00	0.00
							Fault Gouge	52	243.00	243.06	0.06
							joint	54	261.12	261.12	0.00
							joint	36	261.22	261.22	0.00
268.73	324.00	55.27	4d	Shakespeare quartz diorite roof zone, massive fine to locally visibly coarser grained, materials have incorporated several smaller scale 20 mm to 360 mm to 1,470 mm to 6,000 mm, average about 1,000 mm's, blue grey hornfels altered and visibly cooked quartzite							

<u>From</u> <u>Meters</u>	<u>To</u> <u>Meters</u>	<u>Distance</u> <u>Meters</u>	<u>Litho</u> <u>Code</u>	<u>Discription</u> <u>Major Interval</u>	<u>Code</u>	<u>Description</u> <u>Minor Internal Interval</u>	<u>Measured</u> <u>Feature</u>	<u>Alignmen</u> <u>TCA</u>	<u>From</u> <u>Meters</u>	<u>To</u> <u>Meters</u>	<u>Distance</u> <u>Meters</u>
324.00	344.54	20.54	4c	Shakespeare quartz gabbro		Appearance of the first small 2 mm somewhat ragged bleb of po			324.85	324.85	0.00
						Collection of small scattered 3 mm x 3 mm to 2 mm x 6mm to rare larger scale 4 mm x 30 mm blebs of po with some minor cpy, blebs associated with some local small diss'd grains of po and lesser cpy.			324.85	344.54	19.69
344.54	403.99	59.45	4b	Shakespeare melagabbro		Rock fragment bearing phase of the Shakespeare melagbbro.			344.54	367.08	22.54
				Shakespeare melabbro well mineralized with blebs and disseminated grains po po with lesser cpy down to 383.55 meters.		Estimated 15 to 20 % locally 25 % of sections of narrow less than 500 mm interconnected po with lesser cpy			344.54	346.63	2.09

<u>From</u> <u>Meters</u>	<u>To</u> <u>Meters</u>	<u>Distance</u> <u>Meters</u>	<u>Litho</u> <u>Code</u>	<u>Discription</u> <u>Major Interval</u>	<u>Code</u>	<u>Description</u> <u>Minor Internal Interval</u>	<u>Measured</u> <u>Feature</u>	<u>Alignmen</u> <u>TCA</u>	<u>From</u> <u>Meters</u>	<u>To</u> <u>Meters</u>	<u>Distance</u> <u>Meters</u>
				Melagabbro continued - From 383.55 meters down to 403.99 relatively barren looking melagabbro.		Estimated 10% to 12% possibly up to 15% of a combination of scattered average of 6 mm x 15 mm up 2 mm's x 29 mm's, rare 10 mm x 20 mm blebs of po with some cpy, associated with diss'd small 1 mm to 3 mm grains of po and cpy. There are a few local 1mm up to 140 mm quartz - epidote, cpy - po bearing fracture filling veins.			346.63	367.63	21.00
						Massive, equigranular Shakespeare melagabbro with abundant 10 % - 15 %, locally 15 5 to 17% well developed diss'd 1 mm to 3 mm grains of po with will developed cpy.			367.63	383.55	15.92
						Barren looking melagabbro with little or no visible sulphide minerals, rare traces of po and or cpy.			383.55	403.99	20.44
						A large scale blue grey quartz vein, sharp contacts with visible white to butter yellow calc carb - fe carb	qtz - carb vein	13	387.30	387.87	0.57

<u>From</u> <u>Meters</u>	<u>To</u> <u>Meters</u>	<u>Distance</u> <u>Meters</u>	<u>Litho</u> <u>Code</u>	<u>Description</u> <u>Major Interval</u>	<u>Code</u>	<u>Description</u> <u>Minor Interval</u>	<u>Measured</u> <u>Feature</u>	<u>Alignmen</u> <u>TCA</u>	<u>From</u> <u>Meters</u>	<u>To</u> <u>Meters</u>	<u>Distance</u> <u>Meters</u>
				Melagabbro continued		narrow, 10 mm to 15 mm chloritic fault gouge	Fault Gouge	17	392.20	392.30	0.10
						Weak to moderate visible alignment fabric developed in this lower part of the melagabbro unit. The large scale quartz carbonate vein is included within this deformed interval.	Foliation - Alignment Fabric	16	386.49	388.87	2.38
403.99	531.00	59.45	3b	Nipissing gabbro The Nipissing gabbro rocks typically contain several quartz - carbonate cpy and lesser po bearing fracture filling veins. There are a number of areas which contain locally disseminated cpy in the gabbro.							
						Coarse (veritextured) amphiboles and coarse carbonate inside quartz vein. Zoned (calcite at upper contact, followed by quartz and tourmaline?, followed by quartz)	zoned quartz/ coarse tourmaline? (30mm)/ Coarse Calcite (30mm)		399.16	399.30	0.14

<u>From</u> <u>Meters</u>	<u>To</u> <u>Meters</u>	<u>Distance</u> <u>Meters</u>	<u>Litho</u> <u>Code</u>	<u>Discription</u> <u>Major Interval</u>	<u>Code</u>	<u>Description</u> <u>Minor Internal Interval</u>	<u>Measured</u> <u>Feature</u>	<u>Alignmen</u> <u>TCA</u>	<u>From</u> <u>Meters</u>	<u>To</u> <u>Meters</u>	<u>Distance</u> <u>Meters</u>
				Nipissing gabbro continued		Large scale Quartz veins resulting from granophyric materials assimilating / baking into nipissing (or shakespeare) materials. Interlocking quartz / feldspar intervals minor, up to 400mm. Quartz veins over 1000mm common with amphiboles and micas (usually appearing as long string like ribbons within the quartz). Feldspars are uncommon in the quartz veins, but where present are associated with amphibole or near the edges of the veins.			434.72	451.02	16.30
							Quartz Vein	26	439.06	439.36	0.30
						Granophyre / Nipissing – More intact granophyre exhibiting classic Quartz-feldspar interlocking and visible K-Spar. Patchy granophyre intervals surrounded by nipissing material.			457.40	460.35	2.95

<u>From</u> <u>Meters</u>	<u>To</u> <u>Meters</u>	<u>Distance</u> <u>Meters</u>	<u>Litho</u> <u>Code</u>	<u>Description</u> <u>Major Interval</u>	<u>Description</u> <u>Minor Interval</u>	<u>Measured</u> <u>Feature</u>	<u>Alignmen</u> <u>TCA</u>	<u>From</u> <u>Meters</u>	<u>To</u> <u>Meters</u>	<u>Distance</u> <u>Meters</u>
				Nipissing gabbro continued		Shear?	5	460.30	461.78	1.48
						Mineral foliation and joint				
						Broken Zone and with mineral foliation	22	486.00	487.50	1.50
						joint	22	505.68	505.68	0.00
					Minor blotchy (100mm) granophyre materials with K-spar, quartz, and plagioclase within nipissing gabbro.			516.00	519.00	3.00
						joint	58	527.09	527.09	0.00
						joint	22	527.75	527.75	0.00
531.00	531.00	0.00		EOH End of Diamond Drill Hole U-03-119 - Core logging carried out by Harold Tracanelli, Getn, P.Geo and Ian Dasti						

Appendix 2c: Core logs for diamond drill hole U-03-122

URSA Diamond Drill Hole Number: **U-03-122**

Azimuth of Diamond Drill Hole: **147 Degrees Az.**

Inclination of the Diamond Drill Hole: **-75 degrees head set with Flexit bore hole orientation device**

Diamond Drill Core Logging Carried Out By: **Harold J. Tracanelli, Getn, P.Geo and Ian Dasti**

Total Depth of Diamond Drill Hole: **546 Meters**

<u>From</u> <u>Meters</u>	<u>To</u> <u>Meters</u>	<u>Distance</u> <u>Meters</u>	<u>Litho</u> <u>Code</u>	<u>Discription</u> <u>Major Interval</u>	<u>Description</u> <u>Minor Internal Interval</u>	<u>Measured</u> <u>Feature</u>	<u>Alignment</u> <u>TCA</u>	<u>From</u> <u>Meters</u>	<u>To</u> <u>Meters</u>	<u>Distance</u> <u>Meters</u>
0.00	3.00	3.00	OB	Casing				0.00	0.00	0.00
0.00	345.54	345.54	1a	Quartzite		joint / hematite	50	24.09	24.09	0.00
					Very broken zone, Very poor RQD			33.00	44.00	11.00
					Quartz Vein with huge 50x60mm blebs of massive marcassite, with minor pyrite. Dull lime green clays (not malachite). Likely a large structure	Quartz Vein , highly broken		39.6	40.6	1.00
						Joint joint / hematite	3	89.2	53 89.2	53.00
							61			

<u>From</u> <u>Meters</u>	<u>To</u> <u>Meters</u>	<u>Distance</u> <u>Meters</u>	<u>Litho</u> <u>Code</u>	<u>Discription</u> <u>Major Interval</u>	<u>Description</u> <u>Minor Internal Interval</u>	<u>Measured</u> <u>Feature</u>	<u>Alignment</u> <u>TCA</u>	<u>From</u> <u>Meters</u>	<u>To</u> <u>Meters</u>	<u>Distance</u> <u>Meters</u>
				Quartzite continued		Fault gouge / crumble joint / waxy surface		103.53		0.03
							48	103.5		
							24	150.24	150.24	0.00
					Silt interbed	bedding joint	50	190.69	191.01	0.32
						cross bedding	3	216.00	216.00	0.00
						foliation/ bedding	50	246.50	246.50	0.00
						fault gouge	58	253.83	254.25	0.42
							58	286.37	286.40	0.03
					Shear shear			286.34	286.98	0.64
								307.96	308.69	0.73
						Fault Gouge	59	308.42	308.44	0.02
					Pink Carbonate and quartz in silt interbed			339.85	339.89	0.04
					Melted / streched out quartzite			340.43	342.67	2.24
					Massive looking (lacking foliation) quartz diorite			345.54	346.76	1.22
					Shear with quartz veining and disrupted silt interbedding			361.72	362.28	0.56
						Fault Gouge	38	361.74	361.75	0.01

<u>From</u> <u>Meters</u>	<u>To</u> <u>Meters</u>	<u>Distance</u> <u>Meters</u>	<u>Litho</u> <u>Code</u>	<u>Discription</u> <u>Major Interval</u>	<u>Description</u> <u>Minor Internal Interval</u>	<u>Measured</u> <u>Feature</u>	<u>Alignment</u> <u>TCA</u>	<u>From</u> <u>Meters</u>	<u>To</u> <u>Meters</u>	<u>Distance</u> <u>Meters</u>
				Quartzite continued	Snow white colored quartzites, feels like sand paper (very likely altered / "blitzed" by some sort of hydrothermal fluid)			382.80	383.82	1.02
					disk jointing	jointing	90	383.65	383.80	0.15
					Heavy foliation and quartz vein			385.92	386.11	0.19
					shear with quartz veining. Within quartz veining, blebby chalcopyrite (trace) and pyrrhotite (up to 3%) present			387.57	388.94	1.37
388.94	392.96	4.02	4d	Quartz Diorite – Fine to medium grained (sub mm up to mm scale) quartz diorite varying slightly in color but overall lighter brown-green. Occasionally, relict sedimentary textures observable in xenoliths, but more commonly partial assimilation and baking have destroyed original sedimentary fabric. Mica and amphibole rich. Massive looking (lacking foliation)						

<u>From Meters</u>	<u>To Meters</u>	<u>Distance Meters</u>	<u>Litho Code</u>	<u>Discription Major Interval</u>	<u>Description Minor Internal Interval</u>	<u>Measured Feature</u>	<u>Alignment TCA</u>	<u>From Meters</u>	<u>To Meters</u>	<u>Distance Meters</u>
				Quartz Diorite continued		Shear / Quartz Vein joint	44	393.37	393.60	0.23
							14	398.63	398.96	0.33
392.89	457.37	64.48	4c	Shakespeare Intrusive Suite - Shakespeare Quartz Gabbro						0.00
Box 95				Typically dark to light grey, often quite massive looking, medium grained.	Local isolated, 1 mm to 5 mm to > 1,000 mm, hairline fracturing and visible mile to moderate deformation of some of the mineral constituents within the rock					0.00
				From: 406.36 m's down to 457.37 m's., fine , medium to locally coarser grained quartz diorite materials. From; 452.70 m's to 457.37 m's., there seems to be an intermixing in some cases of salt and pepper quartz gabbro to visibly finer grained, green like Shakespeare melagabbro.	From: 393.36 m's to 394.40 m's., mild to visible moderate looking alignment - deformation, visible fine grained light green micaceous - chlorite alteration.	Foliation	50	393.36	394.40	1.04

<u>From</u> <u>Meters</u>	<u>To</u> <u>Meters</u>	<u>Distance</u> <u>Meters</u>	<u>Litho</u> <u>Code</u>	<u>Discription</u> <u>Major Interval</u>	<u>Description</u> <u>Minor Internal Interval</u>	<u>Measured</u> <u>Feature</u>	<u>Alignment</u> <u>TCA</u>	<u>From</u> <u>Meters</u>	<u>To</u> <u>Meters</u>	<u>Distance</u> <u>Meters</u>
				Quartz Gabbro Continued	From: 393.30 m's to 393.49 m's 1 mm to 12 mm carbonate and 50 mm grey sub vitreous quartz veins developed parallel to the foliation fabric.	Qtz - Carb Veins	50	393.30	393.49	0.19
					From: 398.65 m's to 398.96 m's., grey - whit sub vitreous quartz with irregular sharp contacts, thin 1 mm to 2 mm scale chlorite alteration along contacts.	Qtz Vein	63 and 18	398.65	398.96	0.31
					From: 397.23 m's to 397.39 m's., altered xenolith of quartzite caught up within the quartz gabbro.	Xenolith		397.23	397.39	0.16
					From: 406.91 m's to 406.97 m's., grey white, quartz - carbonate fracture filling vein	Qtz - Carb Veins	36	406.91	406.97	0.06

<u>From</u> <u>Meters</u>	<u>To</u> <u>Meters</u>	<u>Distance</u> <u>Meters</u>	<u>Litho</u> <u>Code</u>	<u>Discription</u> <u>Major Interval</u>	<u>Description</u> <u>Minor Internal Interval</u>	<u>Measured</u> <u>Feature</u>	<u>Alignment</u> <u>TCA</u>	<u>From</u> <u>Meters</u>	<u>To</u> <u>Meters</u>	<u>Distance</u> <u>Meters</u>
				Quartz Gabbro continued	From: 405.81 m's., to 427.91 m's., typcially traces to 1/2% to 1% and less commonly 2%, to possible rare 3% of small grains and small 3 mm to 10 mm ragged blebs of po with minor cpy in a salt and pepper textured quartz gabbro. Likely would be low grade materials.	Weakly Distributed Sulphides		405.81	427.91	22.10
					From: 427.91 m's to 437.65 m's., typically 5% to 7%, possibly locally up to 10% or 12%, rarely less than 1% to 2% of mainly small 3 mm up to 10 mm x 20 mm blebs and small scale grains of po with traces to 1/2% locally 1% of cpy associated at edges of blebs. Looks like would not likely make ore grade.	Sulphides, Increased Concentrat ions		427.91	437.65	9.74

<u>From</u> <u>Meters</u>	<u>To</u> <u>Meters</u>	<u>Distance</u> <u>Meters</u>	<u>Litho</u> <u>Code</u>	<u>Discription</u> <u>Major Interval</u>	<u>Description</u> <u>Minor Internal Interval</u>	<u>Measured</u> <u>Feature</u>	<u>Alignment</u> <u>TCA</u>	<u>From</u> <u>Meters</u>	<u>To</u> <u>Meters</u>	<u>Distance</u> <u>Meters</u>
				Quartz Gabbro Continued	From: 437.65 m's., to 452.50 m's., very well - strongly developed, 10% to 15% locally 20% of scattered to possibly interconnected 3 mm up to 20 mm and 30 mm ragged blebs of po associated with 1% possibly 2% of cpy. Alignment of sulphide minerals, although somewhat faint in places are visible. Grade to high grade sections.	Sulphides Well Developed		437.65	452.50	14.85
						Alignment of Sulphide Minerals	44	442.00	442.00	0.00

<u>From</u> <u>Meters</u>	<u>To</u> <u>Meters</u>	<u>Distance</u> <u>Meters</u>	<u>Litho</u> <u>Code</u>	<u>Discription</u> <u>Major Interval</u>	<u>Description</u> <u>Minor Internal Interval</u>	<u>Measured</u> <u>Feature</u>	<u>Alignment</u> <u>TCA</u>	<u>From</u> <u>Meters</u>	<u>To</u> <u>Meters</u>	<u>Distance</u> <u>Meters</u>
				Quartz Gabbro continued	@ 447.69 m's., to 448.37 m's and from: 450.42 m's to 451.00 m's., 7 mm to 25 mm., and 3 mm to 15 mm., somewhat irregular fracture filling vein materials of fine grained po with some cpy. Sulphides would seem to have developed within a previously developed, both then fractured - brecciated subvitreous grey blue quartz materials -----> early fracture filling vein with later remobilized sulphide materials.	Po Rich Fracture Filling Vein	05	447.69	448.37	0.68
						Po Rich Fracture Filling Vein	<05	450.42	451.00	0.58

<u>From</u> <u>Meters</u>	<u>To</u> <u>Meters</u>	<u>Distance</u> <u>Meters</u>	<u>Litho</u> <u>Code</u>	<u>Discription</u> <u>Major Interval</u>	<u>Description</u> <u>Minor Internal Interval</u>	<u>Measured</u> <u>Feature</u>	<u>Alignment</u> <u>TCA</u>	<u>From</u> <u>Meters</u>	<u>To</u> <u>Meters</u>	<u>Distance</u> <u>Meters</u>
				Quartz Gabbro Continued	From: 452.50 m's., to 457.05 m's., noticeably reduced sulphide content, fine grained, 3% to 5%, possibly slightly higher in places at 6% or 7%, of smaller fine grained stretched out blebs of po with 1/2% to 1% cpy. In places visible alignment of the sulphides. Possibly close to or at grade.	Sulphide Mineralizat ion - Reduced	57	450.50	457.05	6.55
					457.05 m's to 460.82 m's., somewhat simialr to that described from: 437.65 m's to 452.50 m's., with visible increase to 15 to 3% locally possible 4% of cpy as 3 mm to 10 mm x 15 mm ragged blebs and streaks, faint to distinct alignment fabric imposed upon the po and cpy mineralization.	Sulphides Well Developed	44	457.05	460.82	3.77
					From: 443.81 m's., to 444.17 m's., a rather large scale grey white quartz fracture filling vein which has veeb fractured and infilled in places with po and lesser cpy.	Sulphide Bearing Fracture Filling Vein		443.81	444.17	0.36

<u>From</u> <u>Meters</u>	<u>To</u> <u>Meters</u>	<u>Distance</u> <u>Meters</u>	<u>Litho</u> <u>Code</u>	<u>Discription</u> <u>Major Interval</u>	<u>Description</u> <u>Minor Internal Interval</u>	<u>Measured</u> <u>Feature</u>	<u>Alignment</u> <u>TCA</u>	<u>From</u> <u>Meters</u>	<u>To</u> <u>Meters</u>	<u>Distance</u> <u>Meters</u>
				Quartz Gabbro Continued	From: 431.82 m's., to 432.00 m's., large scale grey white quartz fracture filling with with some visible fine grained chl and some fine grained po and cpy	Sulphide Bearing Fracture Filling Vein	65	431.82	432.00	0.18
					Throughout the quartz gabbro interval there are a few scattered narrow 3 mm to 17 mm typically grey white quartz and lesser carbonate fracture filling veins with po and cpy.	Sulphide Bearing Fracture Filling Veins	68 less common 51			0.00
					From: 423.00 m's +/- to 429.00 m's., +/-, 10 mm to 70 mm fragments - chlorite altered fragement, mineral segragations within the quartz gabbro.					0.00
457.37	462.00	4.63	4b / 4f	Shakespeare Intrusive Suite - Shakespeare Melagabbro - Rock Fragment Phase:						0.00

<u>From Meters</u>	<u>To Meters</u>	<u>Distance Meters</u>	<u>Litho Code</u>	<u>Discription Major Interval</u>	<u>Description Minor Internal Interval</u>	<u>Measured Feature</u>	<u>Alignment TCA</u>	<u>From Meters</u>	<u>To Meters</u>	<u>Distance Meters</u>
				Melagabbro Continued - Typical looking, washed out green, fine grained melagabbro with scattered small typically small < 10 mm to 7 mm x 30 mm, to 45 mm x 15 mm, to 115 mm and 180 mm, rock fragments occuring within 1.0 meters of the unit lower contact. Some of the smaller - elongated rock fragments appear to consist of a fine grained mafic to ultramafic matrerials, while the larger scale fragments consist of a fine to medium grained lueco gabbro - diorite materials, look to have undergone some alteration - cooking.	@ 461.76 m's to 461.87 m's., the large scale lueco gabbro - diorite fragement contains up to 15 mm x 30 mm irregular clots to smaller scale < 3 mm streaks and wisps of fine grained po with some py and lesser cpy. The largest collection of bulbous like sulphide minerals seems to have collected - concentrated around the edges of what looks to be partially cooked remobilized - zoned, interior parts of the larger scale rock fragment.	Remobilized Sulphides		461.76	461.87	0.11
					@ 461.92 m's., 20 mm to 30 mm x > 50 mm blocky minerals - ultramafic rock fragment containing abundant net textured - interconnected po and cpy.					0.00

<u>From</u> <u>Meters</u>	<u>To</u> <u>Meters</u>	<u>Distance</u> <u>Meters</u>	<u>Litho</u> <u>Code</u>	<u>Discription</u> <u>Major Interval</u>	<u>Description</u> <u>Minor Internal Interval</u>	<u>Measured</u> <u>Feature</u>	<u>Alignment</u> <u>TCA</u>	<u>From</u> <u>Meters</u>	<u>To</u> <u>Meters</u>	<u>Distance</u> <u>Meters</u>
462.00	474.00	12.00	4f? / 3a / 3b	Shakespeare Intrusive Suite - Shakespeare Melagabbro - Equigranular Phase:						0.00
				the bulk of the interval consists of massive, medium to locally coarse grained - vari textured Nipiising like gabbro to quartz gabbro, with multiple visible narrow 800 mm to 850 mm up to 2,800 mm injections of fine grained, green Shakespeare like melagabbro materials. The somewhat larger scale intervals of the Nipissing gabbro - quartz gabbro may represent possible very large scale rock fragments within the intruding Shakespeare melagabbro.	Visible sulphide minerals of typically po with lesser cpy are commonly developed within the melagabbro.					0.00

<u>From Meters</u>	<u>To Meters</u>	<u>Distance Meters</u>	<u>Litho Code</u>	<u>Discription Major Interval</u>	<u>Description Minor Internal Interval</u>	<u>Measured Feature</u>	<u>Alignment TCA</u>	<u>From Meters</u>	<u>To Meters</u>	<u>Distance Meters</u>
				Melagabbro continued - within the injections a number of smaller scale 10 mm up to 30 mm x 50 mm felsic looking - altered rock fragments.	From: 464.14 m's., to 464.61 m's., localized 15% to 20% to 25%., interconnected like 3 mm to 10 mm blebs of po and cpy in a mix like of melagabbro and Nipissing quartz gabbro - shakespeare quartz gabbro. It wouls seem that some minor po and cpy may have somehow migrated out into some of the surrounding - adjacent gabbro materials - rock fragement?	Sulphides, Interconne cted		464.14	464.61	0.47
					From: 473.25 m's to 473.90 m's., partially intact to strongly broken core - fracture zone - structure, with some local, partially developed < 1mm chloritic fault gouge	Fault Gouge	63	473.45	473.45	0.00
					Alignment fabric of the broken zone	Foliation	17	473.80	473.80	0.00

<u>From</u> <u>Meters</u>	<u>To</u> <u>Meters</u>	<u>Distance</u> <u>Meters</u>	<u>Litho</u> <u>Code</u>	<u>Discription</u> <u>Major Interval</u>	<u>Description</u> <u>Minor Internal Interval</u>	<u>Measured</u> <u>Feature</u>	<u>Alignment</u> <u>TCA</u>	<u>From</u> <u>Meters</u>	<u>To</u> <u>Meters</u>	<u>Distance</u> <u>Meters</u>
474.00	546.00	72.00	3a / 3b	Nipissing Type gabbro	Gabbro to quartz From: 514.42 m's to 515.66 m's., isolated injection of possible fine grained Shakespeare melagabbro materials into the larger scale mass of Nipissing type gabbro. The mafic rock have been tractured in places, injected with several 1 mm to 8 mm to 10 mm carbonate lesser quartz fracture fillings - ribbon like veins	4b		514.42	515.66	1.24
					From: 505.22 m's to 507.73 m's., look as if a 1,500 mm grey white, subvitreous quartz carbonate - lesser chlorite vein appears to have been intruded into a sheared - possible fine grained melagabbro like rock. The fine grained mafic rocks are visibly deformed, somewhat stretched out associated with multiple thin < 1 mm to 10 mm to 15 mm or sharp to irregular ribbons - wisps of carbonate - less quartz infillings.	Foliation - Shearing	61	505.22	507.73	2.51

<u>From</u> <u>Meters</u>	<u>To</u> <u>Meters</u>	<u>Distance</u> <u>Meters</u>	<u>Litho</u> <u>Code</u>	<u>Discription</u> <u>Major Interval</u>	<u>Description</u> <u>Minor Internal Interval</u>	<u>Measured</u> <u>Feature</u>	<u>Alignment</u> <u>TCA</u>	<u>From</u> <u>Meters</u>	<u>To</u> <u>Meters</u>	<u>Distance</u> <u>Meters</u>
				Nipissing Gabbro continued	From: 443.00 m's to 445.56 m's., a series of 2 mm to 180 mm white grey quartz carbonate - chlorite veins developed in the gabbro, prevaisive saturation of fe carb alteration of the gabbro adjacent to the veins.	Quartz - Carbonate Chlorite - Fe Carb Veining and Alteration	73	443.00	445.56	2.56
546.00	546.00	0.00	EOH	End off diamond drill hole U-03-122. Core logging carried out by Harold Tracanelli, Getn, P.Geo and Ian Dasti						0.00

Appendix 3 - Laboratory results from ICP-MS analysis.

The last row contains average data values obtained from Lightfoot and Naldrett (1996).

Analyte Symbol	Li	Na	Mg	Al	K	Ca	Cd	V	Cr	Mn	Fe	Hf	Ni	Er	Be	Ho	Ag	Cs	Co	Eu	Bi
Unit Symbol	ppm	%	%	%	%	%	ppm	ppm	ppm	ppm	%	ppm	ppm	ppm	ppm	ppm	ppm	ppm	ppm	ppm	ppm
Detection Limit	0.5	0.01	0.01	0.01	0.01	0.01	0.1	1	0.5	1	0.01	0.1	0.5	0.1	0.1	0.1	0.05	0.05	0.1	0.05	0.02
Analysis Method	TD-MS	TD-MS	TD-MS	TD-MS	TD-MS	TD-MS	TD-MS	TD-MS	TD-MS	TD-MS	TD-MS	TD-MS	TD-MS	TD-MS	TD-MS	TD-MS	TD-MS	TD-MS	TD-MS	TD-MS	TD-MS
119-269.8	23.9	1.16	2.68	> 10.0	3.34	2.48	< 0.1	99	177	435	6.03	1.6	133	1.3	1.6	0.4	< 0.05	2.43	33.8	1.2	0.11
119-307.5	26.7	0.96	3.21	> 10.0	1.96	3.46	< 0.1	308	302	607	6.85	2.6	202	1.7	1.5	0.6	0.07	1.1	58.4	1.41	0.23
119-315	26.7	0.99	3.36	> 10.0	2.4	2.09	< 0.1	387	360	593	7.1	4.8	249	1.5	1.4	0.5	0.14	1.48	64.9	1.08	0.22
119-328	20.7	1.33	2.54	8.5	2.06	4.54	< 0.1	342	372	822	7.81	3.2	171	2.8	1.2	1	0.09	6.94	39.8	1.46	0.16
119-330	27	1.82	2.48	9.09	1.53	4.99	< 0.1	172	114	950	7.98	2.7	111	2.6	1.2	0.9	< 0.05	2.87	39.9	1.5	0.21
119-336	24.6	0.96	5.73	8.23	0.93	4.12	< 0.1	423	385	1380	11.8	2.3	173	1.9	0.7	0.6	0.14	2.32	71.1	1.05	0.18
119-340	19.2	1.75	3.74	9.33	1.35	4.73	< 0.1	333	372	1140	9.66	3	637	2.1	1	0.7	0.21	4.13	91.8	1.31	0.81
119-350	18.2	1.52	4.33	8.4	1.12	4.75	0.3	329	382	925	10	1.9	2580	1.4	0.9	0.5	1.22	2.77	158	0.98	7.64
119-366	16.9	1.84	5.34	8.43	0.72	5.35	0.6	369	473	1340	12.5	1.9	3300	1.9	0.9	0.6	2.08	2.04	218	1.07	13.5
119-378.6	15.1	1.47	3.81	7.76	1.08	5.7	0.9	215	106	1550	11.4	2.1	3090	2.1	0.8	0.8	2.69	3.22	157	0.94	11.9
119-385	16.6	1.68	4.48	8.9	0.97	5.92	< 0.1	215	246	1410	9.6	2	186	1.9	0.7	0.7	0.12	3.47	69.9	1	0.6
119-388	32	0.81	4.18	8.41	3.07	7.34	< 0.1	204	79.8	1220	8.89	1.7	166	1.5	0.4	0.6	< 0.05	12.3	58.1	0.91	0.71
119-396	13.1	2.05	4.26	8.58	0.82	5.78	< 0.1	237	100	1290	8.59	1.9	130	1.9	0.7	0.6	0.11	2.87	52.4	1.03	0.23
119-402	12	2.1	4.48	8.91	0.88	6.66	< 0.1	248	122	1400	9.47	2	144	1.9	0.8	0.7	0.14	2.82	59.1	1.03	0.22
119-427.5	11.3	2.05	4.37	8.31	0.64	8.02	< 0.1	266	115	1230	8.58	1.9	143	1.9	0.7	0.7	0.08	1.8	50.2	0.99	0.12
119-435	9.4	1.31	3.37	5.98	0.37	5.66	< 0.1	199	141	1010	6.97	0.4	189	2.2	0.5	0.8	< 0.05	1.16	31.8	1.15	0.14
119-459	16.1	> 3.00	2.08	> 10.0	0.95	4.65	< 0.1	91	194	490	4.12	3.6	162	2.1	1.6	0.8	0.07	4.74	33.8	1.88	0.2
122-388.7	23	0.93	1.71	9.46	3.38	0.52	< 0.1	133	193	279	4.34	3.9	93.1	1.7	1.6	0.6	0.08	3.89	26.2	0.94	0.19
122-393.2	24.2	1.98	2.44	8.6	2.87	1.91	< 0.1	167	225	513	7.08	4.4	160	2.6	1.8	1	0.11	7.71	44.3	1.55	0.29
122-397.7	22.5	2.37	2.24	8.26	1.8	1.83	< 0.1	179	345	486	5.33	2.4	145	1.2	1.6	0.4	< 0.05	3.16	33.7	0.85	0.21
122-408.2	26.2	1.73	2.25	9.53	2.53	4.12	0.1	109	125	1170	9	2.5	179	3.1	1.9	1.1	0.22	8.34	47.9	1.46	0.47
122-414.2	32.4	1.63	2.13	8.32	1.7	4.17	< 0.1	100	147	899	7.84	1.5	165	2.5	1.5	0.9	< 0.05	5.9	42.1	1.36	0.26

Analyte Symbol	Se	Zn	Ga	As	Rb	Y	Sr	Zr	Nb	Mo	In	Sn	Sb	Te	Ba	La	Pr	Nd	Sm	Gd	Tb
Unit Symbol	ppm																				
Detection Limit	0.1	0.2	0.1	0.1	0.2	0.1	0.2	1	0.1	0.1	0.1	1	0.1	0.1	1	0.1	0.1	0.1	0.1	0.1	0.1
Analysis Method	TD-MS																				
119-269.8	0.4	38.2	22.4	15.8	148	10.8	154	57	< 0.1	0.2	< 0.1	1	< 0.1	< 0.1	469	20.8	4.3	15.5	2.7	2.8	0.4
119-307.5	1.5	76.2	21.8	6.6	70.1	14.1	170	90	1.7	3.7	< 0.1	2	0.1	< 0.1	349	23.4	4.8	17.9	3.2	3.4	0.5
119-315	1.9	77.2	21.1	7.9	81.3	13	120	180	4.4	7	< 0.1	2	0.3	0.3	595	20.4	4.5	16.2	3	3.1	0.5
119-328	1.2	88.1	20.3	0.7	106	23.4	173	120	3.4	6.9	< 0.1	3	0.2	< 0.1	333	24.2	5.6	21.4	4.4	5	0.8
119-330	0.9	90.6	22.3	1.7	75.1	22	192	99	0.7	2.6	< 0.1	2	0.1	< 0.1	358	23.7	5.4	20.7	4.2	4.8	0.7
119-336	0.8	140	18.7	4.7	40	15.7	78.3	81	2.5	4.1	< 0.1	2	< 0.1	< 0.1	181	16.8	3.9	15	3.1	3.5	0.5
119-340	3.3	97.2	21	8.7	57	17.5	195	106	5.5	8.4	< 0.1	2	0.3	0.5	287	19.3	4.4	16.8	3.4	4	0.6
119-350	8.4	77.3	17.3	9.9	47.1	11.9	166	71	3.9	7.1	< 0.1	2	0.3	2	281	13.9	3.1	11.6	2.3	2.6	0.4
119-366	10.2	112	19.1	62.5	31.9	15.2	172	65	3.8	4.4	0.1	2	0.3	2.8	162	11.9	2.9	11.7	2.5	3.1	0.5
119-378.6	9.4	116	18.4	22.7	43.1	17	177	83	4.4	7	0.1	2	0.2	2.2	211	14.8	3.8	15.4	3.5	3.3	0.6
119-385	0.7	91.3	18.7	3.6	43.5	16.1	188	68	2.2	3.9	< 0.1	1	< 0.1	< 0.1	187	11.9	3	12.3	2.8	3.3	0.5
119-388	0.5	92	20.2	0.7	169	13.1	139	60	0.4	1.3	< 0.1	< 1	< 0.1	< 0.1	534	10.4	2.7	11	2.5	3	0.5
119-396	0.6	101	18.3	1.4	38.9	16.1	181	69	2.4	2.5	< 0.1	< 1	< 0.1	< 0.1	163	11.6	2.9	12	2.7	3.3	0.5
119-402	0.9	83.7	17.8	4.8	29.5	15.8	198	68	3.6	3	< 0.1	1	< 0.1	< 0.1	177	11.2	2.8	11.8	2.7	3.4	0.6
119-427.5	0.9	72.3	17.3	3.4	15.7	15.1	195	66	2.6	3.4	< 0.1	< 1	< 0.1	< 0.1	142	9.7	2.4	10.2	2.4	3.3	0.5
119-435	0.5	58.6	12.2	0.2	13.7	19.4	89.5	14	0.7	6.7	< 0.1	< 1	< 0.1	< 0.1	67	9.8	2.4	10.4	2.5	3.6	0.6
119-459	0.6	37.7	18.6	11.8	57.7	19.2	234	139	3.9	1.2	< 0.1	< 1	< 0.1	< 0.1	133	64	14	50.1	9.1	7.5	1
122-388.7	1.2	32.6	25.8	1.3	120	15.2	44.8	144	4.9	4.7	< 0.1	2	< 0.1	< 0.1	786	27.2	6.1	22.1	3.8	3.5	0.5
122-393.2	1.8	54.7	19.3	0.9	158	24	145	164	5.4	5.9	< 0.1	1	0.2	< 0.1	399	38.7	8.6	32.8	6.2	6.8	1
122-397.7	0.4	54.3	20.1	13.8	74.4	10.1	167	92	0.9	2.4	< 0.1	< 1	< 0.1	< 0.1	355	15	3.3	12.1	2.2	2.3	0.4
122-408.2	1.2	103	25.4	1.5	119	25.8	215	105	1.2	1.4	< 0.1	1	0.1	< 0.1	373	32	7.4	29.1	6	5.3	0.8
122-414.2	1.2	90.1	22.2	1.5	92.6	22.4	194	61	0.1	1.3	< 0.1	1	0.2	< 0.1	370	24.5	5.6	21.3	4.1	4.5	0.7

Analyte Symbol	Dy	Cu	Ge	Tm	Yb	Lu	Ta	W	Re	Tl	Pb	Th	U
Unit Symbol	ppm												
Detection Limit	0.1	0.2	0.1	0.1	0.1	0.1	0.1	0.1	0.001	0.05	0.5	0.1	0.1
Analysis Method	TD-MS												
119-269.8	2.2	6.4	0.2	0.2	1.3	0.2	< 0.1	< 0.1	0.004	0.8	7.2	8.3	2.6
119-307.5	3	128	0.5	0.2	1.5	0.2	< 0.1	< 0.1	0.004	0.37	8.2	7.7	3
119-315	2.8	167	0.3	0.2	1.4	0.2	0.5	1.3	0.005	0.38	7.5	7.8	3.2
119-328	4.9	77.5	0.5	0.4	2.4	0.4	0.2	0.2	0.002	0.84	8.4	8	2.6
119-330	4.5	72	0.5	0.4	2.4	0.4	< 0.1	< 0.1	0.003	0.49	9	8	2.5
119-336	3.2	131	0.6	0.3	1.7	0.3	0.2	0.4	0.001	0.3	5	6.1	2
119-340	3.8	347	0.3	0.3	1.9	0.3	0.5	0.8	0.021	0.51	9.5	6.9	2.2
119-350	2.5	1830	0.5	0.2	1.3	0.2	0.4	0.7	0.051	0.37	10.3	4.4	1.5
119-366	3.1	3280	0.5	0.3	1.7	0.3	0.3	0.3	0.07	0.29	14.6	3.3	1.1
119-378.6	3.7	4040	0.2	0.3	1.6	0.3	0.4	0.8	0.06	0.38	12.3	4.1	1.4
119-385	3.3	109	0.6	0.3	1.8	0.3	0.2	0.1	0.002	0.35	9.4	3.5	1.1
119-388	2.8	63.4	0.2	0.2	1.3	0.2	< 0.1	< 0.1	0.003	1.28	7.8	3.3	1
119-396	3.3	148	0.5	0.3	1.7	0.2	0.2	< 0.1	0.002	0.27	8.1	3.4	1
119-402	3.4	155	0.6	0.3	1.7	0.3	0.3	0.3	0.002	0.26	7.6	3.1	1
119-427.5	3.3	104	0.6	0.3	1.7	0.3	0.2	0.3	0.002	0.17	6.9	2.9	1
119-435	4	5.6	0.4	0.3	1.7	0.2	< 0.1	< 0.1	0.002	0.09	4.7	2.1	1.2
119-459	4.9	18.2	0.6	0.3	1.6	0.2	0.2	< 0.1	0.001	0.56	11.3	12.9	4.7
122-388.7	3.1	93.1	0.4	0.3	1.8	0.3	0.1	0.6	0.003	0.65	8.4	12.2	4.1
122-393.2	5.3	178	0.4	0.4	2.1	0.3	0.2	0.3	0.004	1.02	10.6	13.2	5.2
122-397.7	2.1	25	0.3	0.2	1.1	0.2	< 0.1	< 0.1	0.005	0.47	9.4	6.1	2.6
122-408.2	5.4	139	0.3	0.4	2.3	0.3	< 0.1	0.2	0.003	1.01	13.9	9.7	3.1
122-414.2	4.5	99.5	0.3	0.3	2.2	0.3	< 0.1	< 0.1	0.005	0.64	9.1	7.4	2.4

Analyte Symbol	Li	Na	Mg	Al	K	Ca	Cd	V	Cr	Mn	Fe	Hf	Ni	Er	Be	Ho	Ag	Cs	Co	Eu	Bi
Unit Symbol	ppm	%	%	%	%	%	ppm	ppm	ppm	ppm	%	ppm	ppm	ppm	ppm	ppm	ppm	ppm	ppm	ppm	ppm
Detection Limit	0.5	0.01	0.01	0.01	0.01	0.01	0.1	1	0.5	1	0.01	0.1	0.5	0.1	0.1	0.1	0.05	0.05	0.1	0.05	0.02
Analysis Method	TD-MS	TD-MS	TD-MS	TD-MS	TD-MS	TD-MS	TD-MS	TD-MS	TD-MS	TD-MS	TD-MS	TD-MS	TD-MS	TD-MS	TD-MS	TD-MS	TD-MS	TD-MS	TD-MS	TD-MS	TD-MS
122-422.2	18.6	1.37	2.47	8.63	1.25	4.07	< 0.1	176	256	812	7.33	1.7	122	2	1.3	0.7	0.1	3.72	43.6	1.28	0.31
122-423.7	23.9	1.47	2.78	9.6	2.07	4.02	< 0.1	127	134	931	8.45	1.5	126	2	1.2	0.7	< 0.05	6.75	45.5	1.18	0.35
122-425.2	22.8	1.47	2.96	9.42	1.47	4.21	< 0.1	83	138	959	7.85	1.5	134	1.8	1.2	0.6	0.08	4.11	44.3	1.18	0.33
122-426.7	22.3	1.4	3.57	9.88	1.22	5.26	0.1	269	233	1050	8.67	1.5	407	1.6	1.1	0.5	0.32	3.6	84.1	1.32	0.8
122-427.7	30.2	1.4	3.65	8.87	2.83	5.13	0.1	288	193	934	7.41	1.8	357	1.6	1.3	0.6	0.2	8.9	60.5	1.18	0.7
122-428.7	21.2	1.8	3.49	> 10.0	1.14	3.69	0.1	333	583	839	9.98	2.2	1750	2	1.4	0.7	0.41	2.86	177	1.37	1.97
122-429.7	20.2	1.48	3.21	9.17	0.9	3.5	< 0.1	316	418	765	8.34	2.5	1290	1.7	1.3	0.6	0.19	1.96	128	1.06	1
122-435.7	21	1.3	3.52	8.75	1.39	4.05	< 0.1	447	855	766	8.32	2.8	1110	1.9	1	0.7	0.28	3.45	112	1.13	0.92
122-440.7	11.3	0.92	2.02	5.34	0.37	1.87	< 0.1	179	263	460	7.11	1.5	2120	1.2	0.6	0.4	0.24	1.01	160	0.7	2.4
122-442.7	18.8	1.63	3.07	9.67	1.09	3.44	0.3	258	278	839	11.7	3.1	2900	2.4	1.2	0.9	0.59	3.25	309	1.31	8.59
122-444.7	18.2	1.57	3.12	9.93	1.16	4.25	0.3	297	285	890	10.2	2.8	1660	2.2	1.2	0.8	0.81	4.11	133	1.43	5.19
122-451.7	17.1	0.94	3.71	8.58	1.81	4.64	0.6	295	209	1100	13.5	2.1	3480	1.9	0.8	0.6	2.08	6.87	258	1.2	29.7
122-454.7	20.2	1.23	4.89	9.74	1.03	4.5	0.5	352	433	1190	11.7	2	2050	1.7	0.9	0.6	1.35	3.11	142	1.18	8.53
122-455.7	19.6	1.19	4.6	9.75	0.89	4.59	0.6	338	428	1140	12.2	2.1	2900	1.7	0.8	0.6	1.76	2.5	173	1.2	9.38
122-467.7	23.4	1.49	4.17	9.44	1.15	6.66	< 0.1	304	140	1170	8.9	1.2	104	1.5	0.6	0.5	0.14	2.39	58.6	1	0.31
1340109	20.1	1.71	2.08	8.97	1.84	4.8	< 0.1	118	86.5	939	8.42	2.3	93.7	3.4	1.5	1.2	< 0.05	4.39	45.4	1.61	0.16
1340116	19.3	1.74	2.05	7.95	2.04	3.55	< 0.1	177	234	899	8.48	2.3	153	3	1.6	1	0.06	5.57	52	1.28	0.68
1340139	23.8	1.52	4.21	9.12	1.27	4.22	0.2	288	308	1020	9.19	2.5	676	1.8	1	0.6	0.39	3.55	91	1.18	1.53
1340401	20.2	1.16	4	7.68	0.75	4.91	0.5	295	265	1040	12.1	2	3640	1.6	1.1	0.5	1.69	2.69	268	1.06	14.2
183597	18.1	0.76	3.56	6.17	0.49	3.82	0.8	263	251	897	15.7	1.5	> 5000	1.3	0.8	0.5	2.95	1.9	457	0.86	14.2
183566	20.4	1.11	3.72	6.88	0.62	4.26	0.3	287	247	1010	13.1	2.1	4190	1.6	1	0.5	2.4	2.59	318	0.97	20.7
183555	17.9	1.14	3.08	7.72	0.99	5.08	0.7	224	162	1030	10.8	0.9	2890	1.2	0.9	0.4	2.81	3.71	251	1.19	14.5

Analyte Symbol	Se	Zn	Ga	As	Rb	Y	Sr	Zr	Nb	Mo	In	Sn	Sb	Te	Ba	La	Pr	Nd	Sm	Gd	Tb
Unit Symbol	ppm																				
Detection Limit	0.1	0.2	0.1	0.1	0.2	0.1	0.2	1	0.1	0.1	0.1	1	0.1	0.1	1	0.1	0.1	0.1	0.1	0.1	0.1
Analysis Method	TD-MS																				
122-422.2	1.2	79.2	21.8	0.7	61.6	17.4	196	64	0.3	1.9	< 0.1	1	0.2	< 0.1	255	22.1	4.7	17.9	3.3	3.6	0.6
122-423.7	0.9	90.1	22.7	0.7	104	17.2	196	59	0.7	0.9	< 0.1	< 1	< 0.1	< 0.1	428	23.1	4.9	18.3	3.3	3.6	0.6
122-425.2	0.6	89.8	22	1.1	70.1	15.9	210	59	0.6	0.7	< 0.1	< 1	< 0.1	< 0.1	307	24.5	5.2	19.1	3.4	3.6	0.6
122-426.7	2.8	95.4	23.2	8.6	59.4	13.1	213	56	3.1	5	< 0.1	1	0.2	< 0.1	233	17.7	3.7	13.8	2.5	2.6	0.4
122-427.7	1	87.7	21.9	13	154	14	165	71	3.8	4.3	< 0.1	1	< 0.1	0.2	428	20.5	4.3	16.1	3	3.2	0.5
122-428.7	8.3	81.1	21.6	12.6	49.5	16.8	201	78	6.3	17.8	< 0.1	1	0.5	1.4	234	25.8	5.5	20.5	3.8	4.1	0.6
122-429.7	5.2	75	19.8	32.9	37.7	14.5	190	91	4.2	19.8	< 0.1	1	0.3	0.6	209	21.4	4.6	17	3	3.3	0.5
122-435.7	5.2	80.1	21.6	12.6	61.7	15.8	184	104	5.7	13.2	< 0.1	< 1	0.3	0.9	320	18.4	4.2	15.7	3	3.2	0.5
122-440.7	9.2	46.4	12.3	27.1	17.8	9.8	97.1	58	3.7	17.6	< 0.1	< 1	0.2	1.7	74	12.7	2.8	10.7	2	2.2	0.3
122-442.7	11.1	84.6	21.4	154	51	20.8	191	120	4.5	17.4	< 0.1	1	0.1	0.5	209	23.4	5.4	21.1	4.2	4.8	0.7
122-444.7	7.5	92	22.6	31	56.1	19.6	213	105	5.7	20	< 0.1	2	0.3	0.9	204	22.2	5	19.6	3.8	4.4	0.7
122-451.7	14.9	110	20.2	31	93.5	15.8	145	78	4.1	12.4	< 0.1	2	0.1	3.5	101	16.5	3.8	15	3	3.4	0.5
122-454.7	6.9	108	20	86.1	47.6	13.9	151	74	4	8.3	< 0.1	1	0.3	2.4	187	16.3	3.6	14	2.8	3.1	0.5
122-455.7	11.3	101	18.9	31.8	38.6	13.9	155	76	4.2	14.7	< 0.1	1	0.3	2.5	170	16.5	3.6	14	2.8	3.2	0.5
122-467.7	0.7	82.5	18.2	0.8	48.7	11.9	163	44	2.4	2.4	< 0.1	< 1	< 0.1	< 0.1	240	9.8	2.3	9.2	2	2.5	0.4
1340109	1.4	89.4	25.1	1.8	87.5	28.8	203	90	0.2	0.5	< 0.1	1	0.1	< 0.1	396	30	7	26.7	5.3	6.1	1
1340116	1.4	95.6	24.5	3.1	100	25.7	178	89	2.1	1.8	< 0.1	2	0.1	< 0.1	447	24.8	5.9	23	4.6	5	0.8
1340139	3.4	83.5	19.6	6.9	55.1	15.3	180	91	4.7	4.6	< 0.1	1	< 0.1	0.2	278	19.5	4.2	16	3.1	3.5	0.5
1340401	14.8	102	23.7	79.9	40.6	13.9	157	79	4.7	21.5	< 0.1	1	0.7	4.8	177	13.1	3.2	11.9	2.3	3	0.4
183597	29.9	120	18.5	43.6	26.3	11.4	117	64	4	43.5	< 0.1	< 1	0.4	7.8	119	12.1	2.8	10.3	2	2.6	0.4
183566	18.8	84.3	21.2	118	33.2	14.1	129	82	4.4	22.6	< 0.1	1	0.4	6.5	153	12.9	3.2	11.8	2.4	3.1	0.5
183555	9.4	113	25.8	99.9	54.3	10.2	168	34	1.5	2.9	< 0.1	< 1	< 0.1	0.8	274	10.2	2.4	8.8	1.8	2.3	0.3

Analyte Symbol	Dy	Cu	Ge	Tm	Yb	Lu	Ta	W	Re	Tl	Pb	Th	U
Unit Symbol	ppm												
Detection Limit	0.1	0.2	0.1	0.1	0.1	0.1	0.1	0.1	0.001	0.05	0.5	0.1	0.1
Analysis Method	TD-MS												
122-422.2	3.5	220	0.5	0.3	1.8	0.3	< 0.1	< 0.1	0.002	0.44	8.3	6.6	2.2
122-423.7	3.5	110	0.3	0.3	1.8	0.3	< 0.1	< 0.1	0.002	0.75	8.9	7.4	2.6
122-425.2	3.3	40.8	0.2	0.3	1.6	0.2	< 0.1	< 0.1	0.003	0.48	10.1	7.3	2.4
122-426.7	2.5	340	0.6	0.2	1.5	0.2	0.2	< 0.1	0.014	0.45	11.9	5.2	1.8
122-427.7	2.8	320	0.4	0.2	1.6	0.3	0.2	< 0.1	0.008	1.11	7.3	5.7	2
122-428.7	3.7	1140	0.6	0.3	1.7	0.3	0.6	0.5	0.049	0.4	10.8	8.2	2.6
122-429.7	3	451	0.6	0.2	1.5	0.2	0.3	0.4	0.04	0.27	13.3	6.8	2.2
122-435.7	3.2	570	0.2	0.3	1.7	0.2	0.5	0.4	0.037	0.5	9.9	6.4	2.2
122-440.7	2	650	0.3	0.2	1	0.2	0.3	0.4	0.048	0.14	7.9	4.2	1.3
122-442.7	4.4	1590	0.6	0.3	2.1	0.3	0.2	0.1	0.096	0.37	13.6	7.7	2.6
122-444.7	4.2	1700	0.6	0.3	2	0.3	0.5	0.7	0.059	0.4	10.3	7.2	2.3
122-451.7	3.2	3980	0.7	0.3	1.7	0.3	0.3	0.2	0.085	0.74	8.5	5.7	1.9
122-454.7	2.9	2110	0.4	0.2	1.5	0.2	0.4	0.3	0.052	0.43	19.9	5.1	1.7
122-455.7	3	2600	0.5	0.2	1.5	0.2	0.4	0.5	0.088	0.37	8.5	5.1	1.7
122-467.7	2.6	165	0.5	0.2	1.3	0.2	0.2	0.2	0.001	0.29	6.3	3.3	0.9
1340109	6	130	0.3	0.5	2.8	0.4	< 0.1	< 0.1	0.001	0.64	9	10	3.3
1340116	5	181	0.3	0.4	2.6	0.4	< 0.1	< 0.1	0.004	0.72	8.1	8	2.6
1340139	3.3	498	0.6	0.3	1.6	0.2	0.4	0.9	0.018	0.43	8.9	6	2
1340401	2.6	3040	0.8	0.2	1.4	0.2	0.3	1	0.112	0.54	11.1	5.7	1.6
183597	2.2	4570	0.7	0.2	1.1	0.2	0.3	2	0.256	0.43	9.5	4.2	1.3
183566	2.7	2400	1	0.2	1.3	0.2	0.4	0.9	0.138	0.49	11.4	5.6	1.8
183555	2	4250	0.4	0.2	1.1	0.2	< 0.1	0.3	0.073	0.62	10.4	3.5	1.1

Analyte Symbol	Li	Na	Mg	Al	K	Ca	Cd	V	Cr	Mn	Fe	Hf	Ni	Er	Be	Ho	Ag	Cs	Co	Eu	Bi
Unit Symbol	ppm	%	%	%	%	%	ppm	ppm	ppm	ppm	%	ppm	ppm	ppm	ppm	ppm	ppm	ppm	ppm	ppm	ppm
Detection Limit	0.5	0.01	0.01	0.01	0.01	0.01	0.1	1	0.5	1	0.01	0.1	0.5	0.1	0.1	0.1	0.05	0.05	0.1	0.05	0.02
Analysis Method	TD-MS	TD-MS	TD-MS	TD-MS	TD-MS	TD-MS	TD-MS	TD-MS	TD-MS	TD-MS	TD-MS	TD-MS	TD-MS	TD-MS	TD-MS	TD-MS	TD-MS	TD-MS	TD-MS	TD-MS	TD-MS
183558	7.1	0.55	0.86	2.92	0.61	1.92	0.2	81	107	313	27.8	0.9	> 5000	0.9	0.7	0.3	2.03	2.39	> 500	0.62	13.7
183561	21.8	1.07	3.73	7.16	0.74	4.84	0.5	280	336	1020	11.9	2.3	3490	1.7	1.1	0.6	3.14	2.69	265	1.11	14.4
183578	24	0.73	3	6.98	1.19	4.51	0.4	217	247	936	11.8	2.4	2950	2	1.2	0.7	2.49	7.97	228	1.07	14.6
183433	20.9	1.17	4.78	6.96	0.63	5.16	0.9	283	336	1240	12.5	1.9	4290	1.8	1.1	0.6	3.93	1.93	275	0.99	21.3
183463	17.2	1.22	4.21	6.39	0.57	5.21	0.7	230	199	1170	10.5	1.6	2640	1.4	1	0.5	2.9	1.83	199	0.78	12.5
183600	29.5	1.24	2.89	7.84	1.2	3.72	3	251	346	746	9.45	3	1860	2.1	1.4	0.7	2.77	3.23	202	1.2	2.03
Average	20.538	1.3922	3.3722	8.278	1.3836	4.3734	0.5522	243.62	260.93	944.88	9.6868	2.206	1247.7	1.896	1.106	0.662	1.04	3.8098	123.72	1.1558	5.0716
Nipissing Gabbro		2.12	8.10	14.47	0.87	10.02					11.43										
Average	n.p	Na2O	MgO	Al2O3	K2O	CaO	n.p	224	248	n.p	Fe2O3	1.21	138	1.66	n.p	0.69	n.p	0.68	48	0.65	n.p
LREE																					
HREE																					
n.p: not published																					

Analyte Symbol	Se	Zn	Ga	As	Rb	Y	Sr	Zr	Nb	Mo	In	Sn	Sb	Te	Ba	La	Pr	Nd	Sm	Gd	Tb	
Unit Symbol	ppm	ppm	ppm	ppm	ppm	ppm	ppm	ppm	ppm	ppm	ppm	ppm	ppm	ppm	ppm	ppm	ppm	ppm	ppm	ppm	ppm	ppm
Detection Limit	0.1	0.2	0.1	0.1	0.2	0.1	0.2	1	0.1	0.1	0.1	1	0.1	0.1	1	0.1	0.1	0.1	0.1	0.1	0.1	0.1
Analysis Method	TD-MS	TD-MS	TD-MS	TD-MS	TD-MS	TD-MS	TD-MS	TD-MS	TD-MS	TD-MS	TD-MS	TD-MS	TD-MS	TD-MS	TD-MS	TD-MS	TD-MS	TD-MS	TD-MS	TD-MS	TD-MS	TD-MS
183558	73.4	38.5	11.5	8.8	41.3	7.3	77.8	35	2.4	27.9	< 0.1	< 1	0.2	5.6	151	7.9	1.9	6.9	1.4	1.8	0.3	
183561	14	108	22.5	78.2	38.6	13.5	153	88	4.5	20.7	< 0.1	72	0.4	5.2	179	13.1	3.2	11.9	2.5	3.1	0.5	
183578	12.4	110	27.9	12.2	90.2	16.7	141	88	6.1	19.8	< 0.1	2	0.4	4.5	324	16.4	3.8	14.6	3	3.9	0.6	
183433	16.1	113	22.1	78.6	30.4	14.5	138	71	4.4	12.2	0.1	2	0.3	4.3	197	12.6	3.1	11.6	2.5	3.2	0.5	
183463	9.2	99.7	19.7	74.4	29.4	11.8	142	61	3.3	5.9	0.1	2	0.5	2.9	163	9.6	2.3	9	2	2.6	0.4	
183600	11.3	427	27.8	61.8	60.2	16.7	177	115	6	33.2	< 0.1	< 1	0.4	2	322	20.5	4.9	17.8	3.4	4.2	0.6	
Average	7.016	93.42	20.728	25.946	65.4	16.064	164.37	82.52	3.2694	9.252	0.1	3.5143	0.2727	2.5769	273.82	18.976	4.308	16.394	3.23	3.612	0.556	
Nipissing Gabbro																						
Average	n.p	80	16	n.p	32	16	169	66	5.12	n.p	n.p	n.p	n.p	n.p	290	6.29	1.75	7.37	2.08	2.5	0.39	
LREE																						
HREE																						
n.p: not published																						

Analyte Symbol	Dy	Cu	Ge	Tm	Yb	Lu	Ta	W	Re	Tl	Pb	Th	U
Unit Symbol	ppm	ppm	ppm	ppm	ppm	ppm	ppm	ppm	ppm	ppm	ppm	ppm	ppm
Detection Limit	0.1	0.2	0.1	0.1	0.1	0.1	0.1	0.1	0.001	0.05	0.5	0.1	0.1
Analysis Method	TD-MS	TD-MS	TD-MS	TD-MS	TD-MS	TD-MS	TD-MS	TD-MS	TD-MS	TD-MS	TD-MS	TD-MS	TD-MS
183558	1.5	1240	0.8	0.1	0.8	0.1	0.2	0.8	0.2	0.44	6.5	2.9	1
183561	2.8	2910	0.3	0.3	1.4	0.2	0.4	0.8	0.128	0.56	11.4	5.6	1.7
183578	3.4	1150	0.3	0.3	1.8	0.3	0.5	0.8	0.126	1.02	10.5	6.7	3.1
183433	3	4500	0.9	0.3	1.5	0.2	0.3	0.9	0.116	0.35	13.6	4.5	1.5
183463	2.4	3110	0.2	0.2	1.1	0.2	0.2	0.6	0.074	0.3	10.5	4.4	0.9
183600	3.5	1430	0.5	0.3	1.8	0.3	0.5	0.9	0.084	0.57	739	9.1	2.6
Average Nipissing Gabbro	3.346	1132.3	0.468	0.274	1.656	0.254	0.3194	0.5853	0.0434	0.515	24.292	6.25	2.108
Average	2.26	130 n.p	0.44 n.p	0.22	0.18 n.p	n.p	n.p	n.p	n.p	n.p	1.69	0.52	
LREE													
HREE													

n.p: not published

Appendix 4: Laboratory results from the ICP-AES analysis

Sample ID	As	Ba	Bi	Co	Cr	Cu	Li	Mn	Ni	P	Pb	Ti	Zn	Zr
DL	ppm	ppm	ppm	ppm	ppm	ppm	ppm							
119-257.8	<2	168	9	8	52	61	3	<100	92	125	5	808	<1	<1
119-260.8	18	457	26	34	236	35	30	436	272	251	11	3586	28	81
119-262.3	<2	392	26	26	207	24	16	448	209	275	6	3462	27	<1
119-263.8	<2	362	16	39	263	34	26	488	262	236	10	3771	39	27
119-265.8	6	342	24	36	265	42	20	461	239	312	7	3789	32	<1
119-266.8	13	415	16	34	285	24	28	369	182	<100	5	3406	27	<1
119-268.2	<2	366	15	21	138	26	25	304	145	241	10	3372	15	72
119-269.8	29	409	29	34	280	31	33	453	253	201	9	4431	33	131
119-272.8	69	332	38	49	303	23	25	459	198	274	12	3871	29	25
119-274.3	13	314	22	33	285	41	24	434	240	280	15	3509	28	31
119-275.8	<2	202	4	6	57	62	4	<100	186	122	4	794	<1	<1
119-277.3	<2	239	<1	5	49	37	7	<100	132	125	11	936	6	<1
119-278.8	<2	133	<1	1	44	11	13	<100	94	<100	9	573	<1	8
119-279.3	<2	577	8	29	185	60	27	403	135	250	19	3855	77	<1
119-279.3	<2	545	12	27	176	53	22	385	121	235	20	3649	75	<1
119-280.8	<2	204	<1	8	49	69	10	<100	129	111	4	697	<1	20
119-280.8	<2	196	<1	9	48	68	8	<100	129	<100	2	631	<1	2
119-283.3	9	424	17	46	307	151	27	509	202	257	11	3881	36	47
119-284.8	13	369	29	42	287	71	27	515	329	223	14	3441	37	54
119-286.4	21	268	28	50	339	129	24	567	235	265	8	4011	44	49
119-287.8	31	225	21	57	342	173	20	551	222	239	8	3782	41	6
119-289.4	38	284	24	48	320	65	24	539	316	225	3	3693	42	26
119-291	9	273	23	44	357	148	23	588	196	251	11	3972	46	10
119-292.5	4	277	26	50	365	131	22	588	206	239	12	3881	44	<1
119-294	3	319	38	45	353	112	30	512	193	207	19	2719	47	22
119-295.5	<2	436	16	15	137	54	13	168	190	231	10	1744	14	6

Sample ID	As	Ba	Bi	Co	Cr	Cu	Li	Mn	Ni	P	Pb	Ti	Zn	Zr
DL	ppm	ppm	ppm	ppm	ppm	ppm	ppm							
119-298.5	<2	476	7	27	189	57	22	323	121	117	12	2532	35	3
119-300	2	237	2	50	384	131	20	603	229	198	10	3585	60	<1
119-301.5	5	212	15	57	355	169	19	565	250	200	9	3187	54	<1
119-303	2	255	10	45	332	132	22	532	223	215	91	2922	112	<1
119-306	5	372	42	40	358	87	28	583	323	223	8	3777	58	64
119-307.5	5	284	23	51	335	141	28	605	210	260	9	3257	59	4
119-309	<2	256	26	52	361	171	21	611	207	227	8	3563	59	<1
119-310.5	4	299	10	51	362	134	16	595	287	224	9	3151	60	<1
119-312	<2	312	15	10	72	89	7	107	166	129	6	1010	4	<1
119-313.5	4	320	21	52	339	149	25	567	229	250	16	3168	55	41
119-315	4	406	26	53	395	167	18	566	296	240	9	2376	57	<1
119-318	<2	356	24	64	425	217	19	650	394	265	10	3048	70	<1
119-319.5	<2	367	19	64	419	254	29	579	430	223	10	2350	60	45
119-321	<2	211	8	4	62	45	2	<100	146	<100	4	512	2	<1
119-322.5	<2	261	19	53	331	152	19	673	293	221	12	3575	69	<1
119-325	<2	329	28	44	151	145	24	780	147	555	14	5704	64	48
119-326	<2	276	28	45	252	71	18	866	225	241	13	5390	124	<1
119-327	<2	292	15	50	213	153	19	911	275	441	12	3985	81	<1
119-328	<2	302	15	42	378	97	21	888	248	399	12	3888	73	16
119-329	<2	265	33	45	136	109	21	930	149	443	13	4868	73	24
119-329	<2	258	15	44	133	100	20	945	142	408	16	5277	72	31
119-330	<2	304	27	43	117	84	30	921	154	462	16	5758	73	37
119-332	<2	287	23	46	98	167	15	835	194	554	10	5564	73	<1
119-333	<2	296	27	52	108	185	25	935	218	397	15	5703	86	34
119-334	<2	253	<1	52	209	225	16	984	261	398	10	5367	81	<1
119-335	<2	180	17	33	105	155	10	594	115	236	11	3348	50	<1

Sample ID	As	Ba	Bi	Co	Cr	Cu	Li	Mn	Ni	P	Pb	Ti	Zn	Zr
DL	ppm	ppm	ppm	ppm	ppm	ppm	ppm	ppm	ppm	ppm	ppm	ppm	ppm	ppm
119-336	<2	145	15	58	267	139	26	1201	178	256	7	3573	107	<1
119-337	2	228	16	117	238	1054	30	1028	1060	331	17	3892	88	<1
119-337	<2	221	44	129	259	1177	16	1109	1186	333	16	3535	100	<1
119-338	<2	276	44	65	268	270	24	1095	521	330	13	4139	90	16
119-338	<2	272	31	68	268	273	25	1121	535	331	10	4274	87	33
119-339	<2	238	31	96	277	533	23	1079	589	346	12	4053	83	28
119-340	8	252	21	83	282	394	21	1044	582	343	13	3859	88	<1
119-341	8	224	29	118	287	874	24	1107	1128	359	15	3660	89	27
119-342	<2	198	17	54	454	190	18	1083	241	223	15	3421	78	28
119-343	<2	223	40	74	303	325	23	1259	403	323	15	3873	91	15
119-344	<2	225	32	68	266	181	25	1270	366	280	14	3672	88	41
119-345	43	152	58	318	322	612	24	1159	4205	205	25	2515	89	25
119-347	23	193	58	146	280	5537	27	1104	2521	318	21	3223	109	43
119-348	45	217	29	139	288	2580	25	1073	2055	258	20	3471	78	22
119-349	6	238	34	111	309	1894	17	1013	1508	250	15	3217	72	<1
119-350	9	243	25	129	340	1819	20	922	2007	244	15	2866	66	<1
119-351	<2	255	26	60	380	358	23	1046	536	332	14	4036	60	11
119-352	5	239	37	85	373	1684	22	947	947	287	14	3385	73	14
119-353	17	243	35	111	420	1389	17	982	1405	290	11	3605	65	<1
119-354	118	200	51	216	444	3888	25	1056	3047	323	22	3394	96	32
119-355	99	185	57	234	447	6130	22	1087	3777	302	25	3255	112	15
119-355	94	184	38	230	443	6153	22	1085	3788	312	26	3301	112	9
119-358	37	185	40	156	519	2672	24	1219	2262	301	21	3422	95	18
119-358	35	170	52	154	510	2591	20	1205	2222	290	16	3290	91	<1
119-359	73	135	27	226	344	4291	19	1095	3646	264	20	3710	90	<1
119-359.3	5	538	19	29	219	81	20	387	214	273	11	2777	95	<1
119-361	78	158	43	210	323	4509	21	1163	3308	306	20	3689	97	<1
119-362	90	157	55	223	321	4672	22	1236	3604	384	15	4459	102	2

Sample ID	As	Ba	Bi	Co	Cr	Cu	Li	Mn	Ni	P	Pb	Ti	Zn	Zr
DL	ppm	ppm	ppm	ppm	ppm	ppm	ppm	ppm	ppm	ppm	ppm	ppm	ppm	ppm
119-363	107	157	53	201	431	3849	20	1262	2992	383	10	3789	100	<1
119-364	73	154	37	155	470	13709	25	1085	2262	356	20	3374	139	54
119-365	104	99	36	141	401	2482	23	1291	1647	359	<1	4140	98	14
119-366	56	117	42	166	386	2722	13	1165	2398	282	18	3064	85	<1
119-367	64	143	41	164	312	2458	19	1302	2273	310	19	3724	94	<1
119-368	80	131	43	193	385	3741	15	1219	2893	295	19	3126	89	<1
119-369	34	172	41	184	312	4335	17	1107	2823	292	16	3069	85	<1
119-370	71	137	38	184	213	3504	17	1281	2836	261	23	2937	96	<1
119-371	63	162	52	247	183	6159	20	1242	4359	282	19	3431	113	<1
119-372	53	134	40	201	160	4686	15	1187	3373	273	21	3350	93	<1
119-373	5	117	49	226	118	1116	20	1126	4572	258	23	3512	63	19
119-374	56	161	44	186	267	4558	16	1177	3487	445	20	3047	86	<1
119-375	23	147	43	180	311	6043	13	1212	3874	374	22	3353	102	<1
119-377	37	170	44	202	122	5984	21	1251	3818	343	22	4065	111	15
119-378.6	17	163	38	124	89	3748	15	1195	2281	362	11	4305	88	<1
119-379	61	119	46	192	170	2004	11	1119	3080	287	20	3098	81	<1
119-380	37	181	52	185	102	6419	17	1263	3147	366	21	3904	117	<1
119-381	6	179	27	60	229	481	19	1249	270	369	12	4435	72	<1
119-382	90	149	52	176	241	6901	18	1227	2758	368	19	3521	117	<1
119-383	24	159	39	193	109	2506	22	1273	3220	332	18	4134	90	28
119-384	<2	161	45	59	106	143	22	1251	198	328	18	4344	71	17
119-385	<2	165	43	66	104	174	22	1335	261	335	15	4469	74	12
119-386	<2	196	29	56	97	194	28	1215	168	312	7	4011	69	<1
119-387	<2	170	14	56	244	340	29	1194	195	297	11	3671	70	<1
119-388	<2	482	21	59	104	87	39	1385	228	345	15	4763	80	<1
119-389	<2	141	32	53	226	410	14	1073	257	274	17	3632	65	<1
119-390	<2	169	33	54	263	271	21	1259	205	356	16	3968	76	6
119-391.5	<2	120	25	53	75	254	15	1285	150	293	9	4230	67	<1

Sample ID	As	Ba	Bi	Co	Cr	Cu	Li	Mn	Ni	P	Pb	Ti	Zn	Zr
DL	ppm	ppm	ppm	ppm	ppm	ppm	ppm							
119-393	<2	141	23	55	72	87	27	1304	150	348	12	4491	77	12
119-394.5	<2	174	41	53	70	157	21	1243	136	326	15	4087	71	<1
119-396	<2	138	26	51	66	145	16	1176	130	333	13	4138	60	<1
119-397.5	<2	141	12	52	73	105	18	1239	163	305	9	4214	65	4
119-400.5	<2	124	25	55	64	249	15	1212	206	288	8	3866	68	<1
119-402	4	139	26	51	55	155	16	1187	141	305	11	4403	56	<1
119-402	<2	133	27	50	54	153	13	1173	143	297	11	4270	60	<1
119-403.5	<2	132	19	50	60	251	16	1145	208	345	14	4466	59	<1
119-405	10	87	17	62	85	228	14	1182	341	219	14	4977	62	<1
119-406.5	7	139	19	53	68	209	12	1185	248	368	12	4505	64	<1
119-406.5	<2	150	29	51	68	183	17	1220	218	379	13	4771	64	<1
119-408	<2	132	27	51	60	207	19	1208	138	496	12	4835	69	<1
119-409.5	<2	126	29	51	68	135	16	1248	172	333	14	4166	69	<1
119-411	<2	145	9	54	66	150	21	1266	148	388	7	5047	68	25
119-412.5	<2	102	24	53	60	391	28	1210	161	336	10	4648	73	<1
119-412.5	<2	117	19	60	68	452	34	1347	180	375	17	5265	86	2
119-414	<2	112	16	46	61	417	15	1155	180	353	10	4964	58	<1
119-415.5	<2	153	24	48	52	178	14	1160	139	299	5	4147	61	<1
119-417	4	92	25	57	67	198	19	1350	212	303	7	4137	72	<1
119-418.5	<2	135	34	51	55	190	17	1220	217	340	11	4115	68	4
119-420	<2	137	24	47	69	102	25	1182	142	355	13	4688	71	13
119-421.5	<2	108	24	43	45	19	21	1195	142	290	3	4181	70	<1
119-423	5	84	20	60	127	107	14	1088	528	457	5	5214	48	25
119-423	<2	83	15	58	130	95	12	1103	476	465	13	5198	50	6
119-426	<2	115	11	42	54	110	10	1055	138	282	14	3972	50	<1
119-426	2	119	23	45	56	116	10	1099	147	294	11	4134	54	<1
119-427.5	<2	119	21	46	61	113	19	1110	141	306	6	4322	55	21
119-429	2	47	30	47	81	195	10	1057	240	352	12	4139	47	<1

Sample ID	As	Ba	Bi	Co	Cr	Cu	Li	Mn	Ni	P	Pb	Ti	Zn	Zr
DL	ppm	ppm	ppm	ppm	ppm	ppm	ppm							
119-430.5	<2	34	21	44	67	69	18	1252	170	209	13	3358	55	6
119-432	5	111	20	53	70	193	19	1255	155	131	9	4144	65	<1
119-433.5	<2	113	22	47	59	121	15	1094	135	283	14	3998	49	<1
119-435	<2	56	31	31	93	8	12	1057	193	175	8	3243	46	<1
119-436.5	<2	130	23	47	100	524	29	953	175	285	14	5004	67	28
119-438	<2	92	18	47	90	272	13	1172	159	289	11	3707	53	<1
119-441	9	19	<1	5	769	13	9	112	44	<100	10	400	1	12
119-442.5	<2	11	<1	3	907	17	4	111	55	<100	2	450	<1	<1
119-444.5	5	68	14	23	71	239	18	377	156	184	10	2623	16	24
119-448.5	<2	118	21	19	308	23	14	389	73	243	8	3594	12	20
119-448.5	2	117	4	18	308	19	14	384	73	234	10	3561	20	24
119-450	<2	34	25	28	69	11	13	979	140	<100	8	1849	43	<1
119-451.5	<2	116	15	38	98	178	11	1052	157	262	7	3483	44	<1
119-453	<2	91	39	47	106	82	15	1135	159	265	13	3875	48	<1
119-453.3	28	444	33	38	240	55	30	422	327	295	24	3046	38	55
119-454.5	<2	92	24	49	110	105	14	1121	181	266	12	3330	53	<1
119-454.8	33	345	13	42	277	40	22	455	227	323	8	3724	32	<1
119-456	<2	86	17	45	107	99	12	1122	147	252	11	3692	51	<1
119-459	15	121	32	39	194	35	19	539	208	265	6	5469	24	<1
119-462	<2	146	38	43	154	38	21	1175	179	323	12	4202	56	<1
119-463.5	<2	91	32	44	169	79	17	1065	161	263	9	3688	44	1
119-465	<2	65	9	41	177	219	12	1123	159	216	12	3289	36	<1
119-466.5	2	93	33	46	210	82	15	1113	178	242	12	3522	45	<1
119-468	<2	41	13	39	216	40	8	1093	173	227	11	3305	38	<1
122 426.7	2	190	15	78	202	377	21	992	465	196	13	6554	72	<1
122-388.7	<2	734	18	29	147	121	22	328	216	324	10	2801	25	<1
122-390.2	<2	426	21	40	239	131	23	596	287	519	13	4294	56	<1
122-391.7	<2	358	27	53	246	176	25	636	318	477	6	4325	63	1

Sample ID	As	Ba	Bi	Co	Cr	Cu	Li	Mn	Ni	P	Pb	Ti	Zn	Zr
DL	ppm	ppm	ppm	ppm	ppm	ppm	ppm	ppm	ppm	ppm	ppm	ppm	ppm	ppm
122-393.2	<2	361	19	49	214	210	27	553	275	580	13	4352	50	22
122-394.7	7	258	10	39	291	41	32	840	249	359	11	3107	83	15
122-397.7	12	243	21	33	166	70	11	434	189	188	7	2772	37	<1
122-399.2	<2	381	27	53	113	66	36	870	368	773	25	7596	110	36
122-400.7	<2	282	29	44	91	86	24	937	202	553	10	6717	78	40
122-402.2	<2	268	16	50	96	197	25	930	321	544	13	5896	74	51
122-405.2	<2	276	39	44	110	146	25	854	230	554	12	6161	75	35
122-406.7	<2	111	17	45	312	220	15	847	262	527	17	5617	56	22
122-408.2	<2	299	18	48	120	145	24	948	266	498	10	6409	80	19
122-409.7	<2	293	27	53	116	201	21	884	302	539	6	5949	77	21
122-411.2	2	364	17	55	281	317	23	892	307	504	9	6081	93	28
122-412.7	<2	292	23	49	137	119	25	1054	301	565	19	6633	83	91
122-414.2	<2	311	16	46	127	126	18	953	272	662	15	6003	85	<1
122-415.7	<2	315	37	55	136	223	18	955	343	474	16	6397	75	9
122-419.2	<2	295	22	66	254	306	22	943	389	249	18	6460	75	<1
122-420.7	<2	170	28	71	250	449	25	1118	348	274	20	6083	86	34
122-422.2	<2	242	21	47	177	269	24	931	264	314	11	5161	73	24
122-423.7	<2	369	40	47	173	147	25	925	268	302	11	5967	86	2
122-425.2	<2	267	28	62	160	79	24	935	471	288	22	6447	73	<1
122-427.7	<2	373	20	61	258	371	26	939	454	237	13	4074	78	<1
122-428.7	9	199	19	144	578	1253	23	792	1565	259	13	3522	75	<1
122-429.7	37	174	21	105	411	498	18	759	1079	209	15	3403	67	<1
122-429.7	34	180	19	106	408	494	19	758	1056	206	14	3398	67	<1
122-430.7	164	202	34	263	425	1418	22	742	2609	291	17	3298	69	<1
122-431.7	11	233	32	53	391	252	24	744	549	308	15	3741	61	<1
122-432.7	64	239	7	118	617	688	22	718	1260	292	19	3492	61	<1
122-433.7	127	267	17	195	615	1005	25	767	2098	289	16	3312	66	41
122-434.7	53	233	27	182	463	1228	19	751	2140	324	16	3618	73	<1

Sample ID	As	Ba	Bi	Co	Cr	Cu	Li	Mn	Ni	P	Pb	Ti	Zn	Zr
DL	ppm	ppm	ppm	ppm	ppm	ppm	ppm	ppm	ppm	ppm	ppm	ppm	ppm	ppm
122-435.7	21	297	41	110	696	676	25	842	1161	364	16	3555	75	2
122-436.7	61	273	30	188	441	1632	27	789	2003	335	681	4036	427	2
122-438.7	31	163	34	265	531	1044	23	780	3562	278	18	3517	67	<1
122-439.7	14	210	31	205	545	4799	22	742	2927	354	16	3563	91	12
122-440.7	45	116	20	229	391	1191	19	811	2976	285	7	4311	71	<1
122-440.7	45	113	15	227	387	1162	22	814	2938	288	19	4423	70	<1
122-441.7	63	224	47	324	353	2758	26	765	4416	326	23	4544	84	44
122-441.7	67	228	34	328	358	2851	26	759	4513	335	20	4340	82	28
122-442.7	184	144	18	205	245	1270	12	676	1983	435	11	3918	62	<1
122-443.7	167	147	33	310	287	3590	13	664	4302	417	18	3130	83	<1
122-444.7	36	182	36	121	297	1718	23	860	1520	447	14	4201	81	24
122-445.7	53	179	30	234	309	1106	21	875	3291	367	17	4386	75	10
122-446.7	23	197	48	289	307	10358	21	876	4477	395	22	4427	157	46
122-446.7	27	197	64	283	311	11114	22	867	4389	390	20	4426	189	58
122-447.7	<2	76	63	897	131	1297	13	461	18740	117	35	1816	58	21
122-448.7	7	284	43	199	260	1317	22	957	3008	332	14	4402	77	<1
122-451.7	24	238	61	199	188	3885	19	1016	2855	338	13	4226	95	<1
122-452.7	<2	240	24	165	275	928	17	974	2511	180	19	2940	72	<1
122-452.7	<2	250	33	164	274	931	19	963	2484	180	15	2898	69	<1
122-453.7	529	140	59	360	263	2900	22	1063	4234	237	11	2973	121	<1
122-454.7	63	130	28	97	236	1687	15	924	1389	224	28	2511	81	<1
122-455.7	24	142	32	132	273	2422	20	1011	2256	287	18	3030	85	<1
122-456.7	56	130	38	226	332	2909	18	962	3297	247	20	2993	83	<1
122-457.7	41	98	41	440	386	4876	18	984	8280	247	24	2813	105	<1
122-458.7	42	146	42	234	326	5994	19	1013	3455	335	18	3335	94	<1
122-459.7	117	122	59	276	333	2281	22	983	3815	248	23	3335	73	32
122-460.7	167	229	53	253	238	4583	19	1017	3116	238	14	6875	92	<1
122-463.2	5	196	28	73	146	798	27	1425	412	546	8	14519	103	27

Sample ID	As	Ba	Bi	Co	Cr	Cu	Li	Mn	Ni	P	Pb	Ti	Zn	Zr
DL	ppm	ppm	ppm	ppm	ppm	ppm	ppm	ppm	ppm	ppm	ppm	ppm	ppm	ppm
122-466.7	66	169	51	140	179	2907	27	1300	2324	304	22	3742	143	31
122-467.7	<2	187	16	48	147	169	24	1053	158	227	12	3252	64	<1
122-469.2	<2	112	18	67	138	224	13	1178	243	214	18	3685	75	<1
1340104	21	752	22	34	190	<1	22	443	125	275	<1	4051	<1	<1
1340105	4	506	28	65	205	221	38	926	338	389	9	6321	31	<1
1340106	4	252	38	36	90	316	20	910	93	432	5	4837	12	<1
1340107	37	176	23	54	72	73	17	800	96	520	<1	4698	21	<1
1340108	4	229	40	27	70	38	16	746	95	613	<1	4869	<1	<1
1340109	<2	367	29	43	83	110	23	890	100	586	<1	5995	23	<1
1340110	6	368	38	37	82	64	15	923	70	589	<1	5520	20	<1
1340110	3	358	19	37	78	63	14	889	73	569	7	5201	17	<1
1340111	10	358	45	36	78	70	19	906	70	564	<1	5583	16	<1
1340112	<2	372	29	37	79	91	18	848	74	569	<1	5674	19	<1
1340113	4	352	48	37	86	88	19	971	82	581	6	6183	23	<1
1340114	<2	406	49	45	70	123	30	997	80	619	<1	7278	34	<1
1340115	4	351	57	35	66	38	13	924	69	531	<1	5340	18	<1
1340116	10	466	36	57	120	179	20	973	180	544	<1	5790	29	<1
1340117	2	402	40	38	89	90	20	955	88	596	1	6173	18	<1
1340118	4	381	29	36	80	68	19	944	73	579	1	5852	20	<1
1340119	8	351	39	39	75	61	17	931	69	592	<1	5875	14	<1
1340120	11	377	14	40	75	32	20	1061	70	575	<1	6224	27	<1
1340120	12	387	32	41	77	33	21	1093	75	590	3	6363	24	<1
1340121	14	372	36	38	76	39	19	971	73	497	<1	6053	13	<1
1340122	9	267	20	38	78	73	19	862	76	564	4	6308	9	<1
1340123	7	122	53	35	60	56	20	1191	67	444	4	4553	36	<1
1340124	10	351	46	35	76	71	24	927	77	596	3	5914	20	<1
1340125	4	427	27	37	74	68	21	948	70	589	<1	5880	19	<1
1340126	7	411	45	41	99	83	19	1033	96	645	<1	6663	36	<1

Sample ID	As	Ba	Bi	Co	Cr	Cu	Li	Mn	Ni	P	Pb	Ti	Zn	Zr
DL	ppm	ppm	ppm	ppm	ppm	ppm	ppm	ppm	ppm	ppm	ppm	ppm	ppm	ppm
1340127	6	410	44	36	80	70	17	945	78	579	1	6038	34	<1
1340128	6	415	27	39	86	90	17	980	79	601	2	6097	23	<1
1340129	5	395	31	40	85	67	18	997	82	619	3	6276	20	<1
1340130	<2	407	35	38	86	70	14	915	78	574	1	5340	19	<1
1340130	5	404	35	38	81	68	16	908	75	570	3	5741	14	<1
1340131	10	345	37	38	81	61	18	974	75	594	<1	5746	9	<1
1340132	2	371	47	36	102	13	20	896	106	517	<1	5804	15	<1
1340133	10	296	34	51	166	51	19	1121	251	339	<1	3752	26	<1
1340135	48	160	40	206	231	1883	17	1185	2285	312	3	2755	44	<1
1340136	16	195	57	210	204	1736	18	1176	2886	282	8	2965	58	<1
1340137	<2	198	51	59	249	1168	15	1066	429	352	5	3442	28	<1
1340138	32	260	29	77	272	1053	29	1070	583	383	2	4249	18	<1
1340139	8	247	23	70	246	466	29	913	532	302	2	3660	8	<1
1340140	7	361	16	51	279	244	30	1015	275	321	1	3699	<1	<1
1340140	2	358	12	48	279	239	28	1015	271	327	4	3625	<1	<1
1340142	27	183	51	92	315	1889	28	991	769	370	2	3857	19	<1
1340143	16	201	15	66	341	729	29	984	565	358	6	4119	16	<1
1340145	10	232	41	70	393	419	24	979	611	324	5	3680	7	<1
1340146	18	219	42	65	418	784	25	1025	485	336	2	3941	9	<1
1340149	21	216	42	102	441	1336	21	1061	1221	288	<1	3591	20	<1
1340150	14	195	24	101	452	1742	23	1111	1102	262	<1	3420	22	<1
1340150	19	184	53	104	473	1813	17	1133	1145	266	<1	3072	28	<1
1340151	18	183	35	95	397	1408	20	1010	1035	259	3	2826	8	<1
1340152	28	193	53	156	428	2862	25	1167	1973	280	<1	3132	33	<1
1340154	48	184	36	160	418	2963	25	1153	2033	266	7	3080	30	<1
1340155	38	165	60	175	438	3314	27	1191	2294	262	<1	3053	38	<1
1340156	52	159	45	163	411	3422	27	1165	2355	255	3	3111	34	<1
1340157	44	184	52	164	415	3316	22	1168	2363	295	2	3358	35	<1

Sample ID	As	Ba	Bi	Co	Cr	Cu	Li	Mn	Ni	P	Pb	Ti	Zn	Zr
DL	ppm	ppm	ppm	ppm	ppm	ppm	ppm	ppm	ppm	ppm	ppm	ppm	ppm	ppm
1340158	72	154	40	216	365	4473	21	1123	3266	253	2	2902	31	<1
1340159	38	179	43	170	309	3535	22	1162	2513	254	<1	2947	32	<1
1340160	44	137	47	181	289	3277	19	1161	2771	225	1	2882	29	<1
1340160	49	134	54	181	287	3267	18	1161	2754	227	<1	2898	24	<1
1340161	58	122	42	228	260	4906	17	1183	3489	244	8	2744	35	<1
1340162	62	130	49	228	257	6424	18	1181	3801	252	4	2740	32	<1
1340163	35	131	44	171	267	3961	18	1202	2682	246	<1	2789	28	<1
1340164	72	112	29	224	276	6206	18	1222	3730	283	<1	3045	37	<1
1340165	37	141	52	147	290	3058	19	1226	2197	258	<1	3204	26	<1
1340166	26	119	45	142	266	3087	22	1240	2176	247	16	3130	580	<1
1340167	783	109	27	361	248	1613	17	1233	2327	217	3	3092	23	<1
1340168	45	128	49	109	227	2019	17	1229	1367	240	<1	3225	40	<1
1340169	53	122	63	172	222	4152	21	1218	2711	242	1	3115	50	<1
1340171	73	161	44	162	230	4061	19	1220	2584	258	8	3136	40	<1
1340172	49	123	43	114	244	2048	16	1205	1557	234	2	3157	223	<1
1340173	16	116	49	84	248	1723	18	1234	954	254	3	3287	36	<1
1340174	16	144	30	71	119	771	18	1221	533	150	3	3624	21	<1
1340176	22	93	53	67	87	1098	12	1128	667	154	<1	2799	<1	<1
1340177	6	132	13	65	61	1072	14	1163	512	186	6	2092	9	<1
1340178	10	146	32	46	47	155	13	1129	145	210	4	3250	<1	<1
1340179	3	138	26	47	49	122	15	1215	131	252	<1	3974	5	<1
1340180	6	160	27	50	54	175	13	1251	173	268	<1	4360	15	<1
1340180	2	150	42	47	51	119	10	1207	130	254	3	4103	11	<1

Appendix 5: Laboratory results from FA/AAS analysis

Sample ID	Au ppb	Pt ppb	Pd ppb	Rh ppb
DL	5 ppb	15 ppb	10 ppb	5 ppb
119-257.8	<5	<15	<10	<5
119-260.8	<5	<15	13	<5
119-262.3	<5	<15	<10	<5
119-263.8	30	<15	19	<5
119-265.8	<5	18	<10	<5
119-266.8	10	<15	<10	<5
119-268.2	<5	17	<10	<5
119-269.8	<5	16	<10	<5
119-272.8	12	19	<10	<5
119-274.3	7	<15	<10	<5
119-275.8	<5	23	<10	<5
119-277.3	<5	22	<10	<5
119-278.8	7	<15	<10	<5
119-279.3	8	<15	<10	<5
119-279.3	6	<15	<10	<5
119-280.8	11	<15	<10	<5
119-280.8	9	<15	<10	<5
119-283.3	<5	<15	<10	<5
119-284.8	7	<15	16	<5
119-286.4	6	25	18	<5
119-287.8	<5	16	<10	<5
119-289.4	7	<15	<10	<5
119-291	12	<15	<10	<5
119-292.5	8	<15	<10	<5
119-294	6	<15	<10	<5
119-295.5	<5	<15	10	<5
119-298.5	<5	<15	<10	<5
119-300	11	<15	<10	<5
119-301.5	9	18	12	<5
119-303	11	<15	<10	<5
119-306	6	<15	<10	<5
119-307.5	10	<15	<10	<5
119-309	<5	18	<10	<5
119-310.5	<5	31	<10	<5
119-312	<5	<15	<10	<5
119-313.5	<5	<15	17	<5
119-315	<5	26	<10	<5
119-316.5	ample Received			
119-316.5	fficient Sample			

Sample ID	As	Ba	Bi	Co	Cr	Cu	Li	Mn	Ni	P	Pb
DL	ppm										
119-318	18	5	18	<10	<5						
119-319.5		11	39	21	<5						
119-321		<5	<15	<10	<5						
119-322.5		6	<15	<10	<5						

Sample ID	Au ppb	Pt ppb	Pd ppb	Rh ppb
DL	5 ppb	15 ppb	10 ppb	5 ppb
119-325	14	<15	<10	<5
119-326	6	<15	<10	<5
119-327	<5	27	<10	<5
119-328	<5	24	<10	<5
119-329	<5	<15	<10	<5
119-329	<5	<15	<10	<5
119-330	13	<15	<10	<5
119-332	<5	<15	<10	<5
119-333	13	<15	<10	<5
119-334	14	<15	<10	<5
119-335	<5	<15	<10	<5
119-336	11	<15	<10	<5
119-337	16	111	107	7
119-337	20	106	104	7
119-338	8	18	32	<5
119-338	16	<15	<10	<5
119-339	15	47	32	<5
119-340	21	38	42	<5
119-341	45	111	89	<5
119-342	31	60	18	<5
119-343	13	<15	22	<5
119-344	11	75	16	<5
119-345	177	140	236	22
119-347	274	588	476	14
119-348	183	291	294	10
119-349	72	163	134	5
119-350	110	159	210	10
119-351	35	93	65	<5
119-352	45	90	76	<5
119-353	90	140	95	8
119-354	250	303	495	17
119-355	220	386	468	19
119-355	219	404	455	22
119-358	124	279	252	11
119-358	124	271	250	10
119-359	252	460	527	24
119-359.3	5	<15	<10	<5
119-361	244	397	449	20
119-362	260	590	546	23
119-363	213	490	425	18
119-364	308	455	397	24
119-365	146	283	269	12
119-366	196	428	356	15
119-367	150	335	323	14
119-368	254	540	529	24

Sample ID	Au ppb	Pt ppb	Pd ppb	Rh ppb
DL	5 ppb	15 ppb	10 ppb	5 ppb
119-369	210	414	457	23
119-370	184	346	377	21
119-371	337	616	705	27
119-372	245	416	511	20
119-373	292	559	577	28
119-374	274	684	521	25
119-375	261	555	537	26
119-377	308	502	609	20
119-378.6	184	390	396	21
119-379	311	571	645	26
119-380	248	435	442	21
119-381	24	58	49	9
119-382	294	506	537	24
119-383	325	477	559	28
119-384	19	34	39	5
119-385	10	29	42	6
119-386	24	28	42	9
119-387	41	72	50	10
119-388	38	45	29	<5
119-389	28	120	32	<5
119-390	22	103	56	<5
119-391.5	<5	<15	<10	8
119-393	<5	<15	39	9
119-394.5	<5	28	37	<5
119-396	6	25	37	7
119-397.5	12	19	43	5
119-400.5	<5	28	46	10
119-402	<5	<15	<10	6
119-402	<5	<15	<10	7
119-403.5	13	<15	32	<5
119-405	22	<15	41	<5
119-406.5	29	20	59	<5
119-406.5	30	22	60	<5
119-408	9	<15	47	8
119-409.5	7	28	21	<5
119-411	<5	31	25	9
119-412.5	11	<15	39	10
119-412.5	14	38	44	9
119-414	13	17	27	7
119-415.5	6	<15	12	7
119-417	8	21	48	9
119-418.5	11	<15	13	<5
119-420	6	38	21	9
119-421.5	10	<15	19	8
119-423	31	27	72	8

Sample ID	Au ppb	Pt ppb	Pd ppb	Rh ppb
DL	5 ppb	15 ppb	10 ppb	5 ppb
119-423	40	65	71	9
119-426	10	46	<10	10
119-426	6	<15	22	8
119-427.5	<5	<15	<10	6
119-429	18	<15	23	<5
119-430.5	<5	<15	<10	6
119-432	12	32	<10	8
119-433.5	6	<15	<10	8
119-435	8	<15	<10	7
119-436.5	13	16	<10	10
119-438	10	<15	24	7
119-441	24	<15	<10	7
119-442.5	29	<15	<10	6
119-444.5	10	18	<10	<5
119-447	Efficient Sample			
119-448.5	19	<15	17	<5
119-448.5	<5	25	24	<5
119-450	7	<15	<10	9
119-451.5	15	27	68	8
119-453	<5	<15	<10	9
119-453.3	<5	TBA	TBA	<5
119-454.5	<5	<15	<10	<5
119-454.8	<5	<15	<10	<5
119-456	6	38	<10	9
119-459	<5	<15	11	<5
119-462	6	30	18	7
119-463.5	<5	<15	<10	8
119-465	7	<15	<10	8
119-466.5	<5	<15	<10	8
119-468	8	19	14	6
122-426.7	41	82	47	<5
122-388.7	19	41	12	<5
122-390.2	21	44	17	<5
122-391.7	24	37	15	<5
122-393.2	14	73	24	<5
122-394.7	16	26	16	<5
122-397.7	22	<15	<10	<5
122-399.2	9	16	20	<5
122-400.7	13	62	19	<5
122-402.2	14	42	<10	<5
122-405.2	11	<15	<10	<5
122-406.7	35	179	27	<5
122-408.2	17	63	19	<5
122-409.7	19	<15	<10	<5
122-411.2	22	140	62	<5

Sample ID	Au ppb	Pt ppb	Pd ppb	Rh ppb
DL	5 ppb	15 ppb	10 ppb	5 ppb
122-412.7	13	<15	<10	<5
122-414.2	16	55	45	<5
122-415.7	21	52	15	<5
122-419.2	38	30	13	<5
122-420.7	35	<15	22	<5
122-422.2	17	<15	<10	<5
122-423.7	14	40	15	5
122-425.2	9	<15	<10	<5
122-427.7	37	16	19	<5
122-428.7	62	182	120	20
122-429.7	44	37	84	<5
122-429.7	34	106	132	<5
122-430.7	46	297	219	13
122-431.7	16	<15	28	<5
122-432.7	60	137	104	9
122-433.7	59	184	164	12
122-434.7	45	125	172	5
122-435.7	41	112	87	5
122-436.7	62	62	148	11
122-438.7	57	221	189	16
122-439.7	48	346	204	12
122-440.7	70	202	180	12
122-440.7	62	299	211	12
122-441.7	82	256	248	15
122-441.7	80	271	243	18
122-442.7	291	231	259	14
122-443.7	685	472	486	24
122-444.7	90	134	96	7
122-445.7	206	270	265	21
122-446.7	567	604	506	23
122-446.7	554	480	507	24
122-447.7	51	29	98	<5
122-448.7	320	319	334	<5
122-451.7	688	816	656	24
122-452.7	292	245	203	10
122-452.7	312	267	203	14
122-453.7	1129	660	691	22
122-454.7	168	190	212	11
122-455.7	116	126	150	11
122-456.7	351	473	417	19
122-457.7	134	481	262	39
122-458.7	283	488	418	24
122-459.7	375	582	579	21
122-460.7	256	224	439	20
122-463.2	14	54	11	<5

Sample ID	Au ppb	Pt ppb	Pd ppb	Rh ppb
DL	5 ppb	15 ppb	10 ppb	5 ppb
122-466.7	262	371	322	9
122-467.7	11	15	24	<5
122-469.2	15	<15	<10	<5
1340104	10	20	<10	8
1340105	32	132	60	10
1340106	13	21	<10	5
1340107	17	43	14	6
1340108	8	35	<10	<5
1340109	7	20	<10	<5
1340110	11	26	<10	7
1340110	7	21	<10	<5
1340111	11	18	<10	<5
1340112	11	22	<10	5
1340113	11	17	<10	6
1340114	13	<15	<10	<5
1340115	8	22	<10	5
1340116	39	26	<10	6
1340117	11	22	<10	6
1340118	6	37	13	5
1340119	<5	17	11	7
1340120	<5	21	<10	<5
1340120	<5	36	<10	<5
1340121	<5	28	11	5
1340122	5	16	<10	7
1340123	<5	<15	<10	5
1340124	<5	<15	13	<5
1340125	<5	32	<10	6
1340126	<5	31	<10	6
1340127	9	<15	<10	6
1340128	10	<15	<10	<5
1340129	8	<15	<10	<5
1340130	11	<15	<10	<5
1340130	6	19	<10	<5
1340131	13	<15	<10	6
1340132	14	<15	<10	7
1340133	15	<15	<10	<5
1340135	58	160	160	15
1340136	141	226	216	18
1340137	32	31	23	5
1340138	39	69	63	8
1340139	30	56	56	8
1340140	29	<15	25	8
1340140	29	<15	23	<5
1340142	40	49	56	8
1340143	29	36	28	6

Sample ID	Au ppb	Pt ppb	Pd ppb	Rh ppb
DL	5 ppb	15 ppb	10 ppb	5 ppb
1340145	44	69	65	7
1340146	35	65	41	5
1340149	80	138	138	9
1340150	81	82	150	9
1340150	81	124	143	6
1340151	249	270	180	11
1340152	122	176	222	14
1340154	130	212	261	16
1340155	156	221	305	16
1340156	135	233	289	19
1340157	219	392	455	23
1340158	189	324	400	24
1340159	156	315	346	19
1340160	190	345	401	20
1340160	196	362	414	21
1340161	229	435	501	26
1340162	247	479	535	26
1340163	168	267	120	20
1340164	225	427	501	26
1340165	136	290	285	17
1340166	145	251	293	18
1340167	121	319	404	22
1340168	88	197	193	16
1340169	207	322	401	21
1340171	197	316	377	22
1340172	136	182	265	17
1340173	136	142	191	15
1340174	71	87	114	12
1340176	66	112	131	11
1340177	61	95	118	12
1340178	17	44	35	10
1340179	12	23	<10	7
1340180	13	15	43	8
1340180	10	<15	44	8

Appendix 6: Laboratory results from the LECO total carbon - total sulfur analysis

Sample ID	Total Sulfur	Total Carbon
	ALTS1	ALTC1
	%	%
119-450	< 0.01	0.14
119-408	0.02	0.05
119-453	0.01	0.05
119-411	0.01	0.00
119-463.5	0.02	0.10
119-432	0.03	0.05
119-436.5	0.09	0.00
119-393	0.02	0.04
119-456	0.01	0.05
119-412.5	0.07	0.00
119-465	0.01	0.22
119-430.5	0.01	0.14
119-441	< 0.01	< 0.01
119-420	0.01	0.10
119-427.5	0.31	0.24
119-466.5	0.24	0.55
119-417	0.24	0.20
119-421.5	0.18	0.28
119-433.5	0.17	0.19
119-402	0.36	0.20
119-391.5	0.22	0.20
119-415.5	0.91	0.10
119-442.5	< 0.01	< 0.01
119-468	0.22	0.68
119-435	0.05	0.20
119-414	< 0.01	0.15
119-378.6	1.35	0.23
119-387	1.90	0.19
119-386	< 0.01	0.91
119-426	0.10	0.19
119-369	1.61	< 0.01
119-400.5	< 0.01	0.05
119-451.5	0.08	0.15
119-381	0.07	0.20
119-438	0.30	0.25
119-377	2.49	0.25
119-447	0.03	0.60
119-384	0.12	0.34
119-373	3.72	0.29
119-423	0.16	0.31
119-397.5	< 0.01	< 0.01
119-396	0.39	0.13

Sample ID	Au ppb	Pt ppb	Pd ppb	Rh ppb
Sample ID	5 ppb	15 ppb	10 ppb	5 ppb
		Total Sulfur		Total Carbon
		ALTS1		ALTC1
		%		%
119-365		0.96		0.23
119-368		0.49		0.34
119-383		2.20		0.22
119-385		0.03		0.20
119-462		< 0.01		0.25
119-394.5		0.30		0.21
119-444.5		< 0.01		0.25
119-448.5		< 0.01		< 0.01
119-359		2.52		0.03
119-403.5		0.02		0.08
119-372		2.25		0.07
119-342		0.65		0.09
119-353		0.86		0.07
119-380		2.28		0.13
119-344		0.24		0.09
119-367		1.35		0.03
119-364		2.47		< 0.01
119-358		< 0.01		< 0.01
119-390		< 0.01		< 0.01
119-409.5		< 0.01		< 0.01
119-459		< 0.01		< 0.01
119-454.5		< 0.01		< 0.01
119-366		1.27		< 0.01
119-382		1.94		< 0.01
119-389		< 0.01		0.43
119-379		2.23		< 0.01
119-352		0.13		< 0.01
119-355		2.45		0.05
119-343		< 0.01		0.05
119-351		< 0.01		0.04
119-363		1.69		< 0.01
119-371		2.78		0.05
119-429		< 0.01		< 0.01
119-374		2.42		< 0.01
119-418.5		< 0.01		< 0.01
119-375		2.33		< 0.01
119-370		1.38		< 0.01
119-406.5		< 0.01		< 0.01
119-388		< 0.01		1.75
119-362		2.13		< 0.01
119-405		< 0.01		< 0.01
119-348		0.85		< 0.01
119-361		1.94		0.05
119-345		5.01		0.09

Sample ID	Total Sulfur ALTS1 %	Total Carbon ALTC1 %
119-333	0.10	0.05
119-330	0.07	0.15
119-325	0.24	0.09
119-280.8	0.13	< 0.01
119-266.8	0.03	0.05
119-286.4	0.29	< 0.01
119-292.5	0.30	0.05
119-278.8	0.08	0.05
119-347	2.42	0.10
119-291	0.17	0.03
119-294	0.22	0.05
119-336	0.01	0.00
119-307.5	0.28	0.05
119-279.3	0.14	0.05
119-300	0.30	0.05
119-303	0.28	< 0.01
119-272.8	0.03	0.04
119-257.8	0.17	< 0.01
119-298.5	0.12	< 0.01
119-341	1.27	0.09
119-340	0.53	0.05
119-339	0.71	0.10
119-329	0.14	0.05
119-301.5	0.45	< 0.01
119-287.8	0.33	< 0.01
119-335	0.16	0.09
119-283.3	0.18	0.05
119-309	0.34	< 0.01
119-350	1.44	0.09
119-354	2.14	0.10
119-359.3	< 0.01	0.05
119-326	0.05	0.04
119-316.5	0.27	0.05
119-454.8	0.04	0.09
119-332	0.14	< 0.01
119-277.3	0.03	< 0.01
119-262.3	< 0.01	0.30
119-334	0.27	0.05
119-327	0.20	0.05
119-322.5	0.24	0.10
119-310.5	0.21	< 0.01
119-269.8	0.01	< 0.01
119-337	1.54	0.10
119-265.8	0.03	0.01

Sample ID	Au ppb	Pt ppb	Pd ppb	Rh ppb
Sample ID	5 ppb	15 ppb	10 ppb	5 ppb
		Total Sulfur		Total Carbon
		ALTS1		ALTC1
		%		%
119-318		0.38		0.06
119-268.2		0.02		0.06
119-349		0.85		0.10
119-275.8		0.02		0.01
119-312		0.11		0.01
119-328		0.09		0.06
119-315		0.30		0.01
119-295.5		0.06		0.06
119-338		0.22		0.15
119-453.3		0.02		0.06
119-284.8		0.06		0.10
119-306		0.13		0.05
119-260.8		< 0.01		0.06
119-289.4		0.10		0.35
119-263.8		0.01		0.06
119-319.5		0.61		0.05
119-274.3		0.02		0.06
119-321		0.03		0.01
122-427.7		0.08		0.83
122-422.2		0.12		0.16
122-453.7		3.37		0.06
122-435.7		0.88		0.10
122-420.7		0.49		0.01
122-458.7		3.23		0.14
122-430.7		2.95		0.06
122-432.7		1.20		0.10
122-431.7		0.28		0.10
122-469.2		0.16		0.16
122-452.7		2.06		0.13
122-443.7		4.62		0.07
122-438.7		3.78		0.08
122-460.7		2.42		0.12
122-444.7		1.32		0.08
122-405.2		0.09		0.08
122-447.7		17.70		0.11
122-425.2		0.03		0.17
122-455.7		1.77		0.13
122-456.7		2.71		0.08
122-429.7		0.15		0.07
122-434.7		2.12		0.12
122-419.2		0.56		0.27
122-459.7		3.31		0.12
122-433.7		2.06		0.17
122-412.7		0.16		0.40

Sample ID	Total Sulfur ALTS1 %	Total Carbon ALTC1 %
122-467.7	0.07	0.71
122-399.2	0.05	0.12
122-466.7	1.13	0.08
122-463.2	4.70	0.05
122-446.7	0.07	0.05
122-411.2	1.78	0.10
122-439.7	3.23	0.14
122-428.7	0.27	0.05
122-448.7	2.85	0.29
122-423.7	0.06	0.10
122-414.2	0.13	0.05
122-391.7	0.37	0.05
122-406.7	1.99	0.05
122-408.2	0.13	0.21
122-441.7	4.38	0.10
122-402.2	0.15	0.05
122-400.7	0.06	< 0.01
122-394.7	0.02	0.05
122-393.2	0.46	0.05
122-390.2	0.21	0.04
122-415.7	0.28	0.10
122-451.7	2.92	< 0.01
122 426.7	0.36	0.10
122-388.7	0.26	0.09
122-440.7	3.01	0.09
122-457.7	5.93	0.05
122-409.7	0.18	< 0.01
122-445.7	3.24	< 0.01
122-436.7	2.20	0.14
122-454.7	1.05	0.05
122-442.7	2.37	0.00
122-397.7	< 0.01	0.00

Sample ID	Au ppb	Pt ppb	Pd ppb	Rh ppb
DL	5 ppb	15 ppb	10 ppb	5 ppb

Appendix 7: Laboratory results from the fused disk XRF analysis. All values are normalized so that totals equal 100%. Fe₂O₃ represents total iron.

Sample ID	SiO ₂	TiO ₂	Al ₂ O ₃	Fe ₂ O ₃	MnO	MgO	CaO	Na ₂ O	K ₂ O	P ₂ O ₅	V ₂ O ₅	Cr ₂ O ₃	LOI
	%	%	%	%	%	%	%	%	%	%	%	%	%
119-257.8	81.64	0.08	4.96	1.31	0.01	0.36	0.36	1.55	1.33	0.04	0.08	0.09	8.19
119-260.8	58.32	0.78	18.33	7.08	0.07	4.02	2.42	1.01	3.81	0.05	0.12	0.14	3.85
119-262.3	58.45	0.70	16.17	6.25	0.07	3.50	3.09	1.23	3.20	0.08	0.11	0.12	7.03
119-263.8	55.64	0.91	18.83	8.19	0.07	4.51	3.18	1.55	2.99	0.05	0.12	0.16	3.80
119-265.8	57.93	0.87	17.83	7.64	0.07	4.06	3.88	1.18	2.88	0.09	0.12	0.15	3.30
119-266.8	60.25	0.85	16.89	7.36	0.06	4.05	2.61	0.99	3.29	0.03	0.13	0.15	3.34
119-268.2	69.21	0.60	13.88	5.03	0.05	2.47	2.30	1.13	3.00	0.05	0.11	0.12	2.05
119-269.8	55.18	0.77	17.02	7.59	0.07	4.00	2.94	1.25	3.27	0.04	0.12	0.13	7.62
119-272.8	53.82	0.77	16.78	7.32	0.06	4.06	3.85	1.65	2.68	0.06	0.12	0.14	8.69
119-274.3	58.78	0.74	17.31	7.66	0.07	4.23	3.62	1.13	2.84	0.06	0.13	0.14	3.29
119-275.8	90.07	0.10	5.09	1.18	0.02	0.36	0.45	0.53	1.34	0.02	0.09	0.10	0.65
119-277.3	81.05	0.12	5.89	1.21	0.02	0.43	0.81	0.73	1.46	0.02	0.09	0.10	8.07
119-278.8	89.73	0.06	5.11	0.89	0.02	0.35	1.09	0.91	0.83	0.05	0.10	0.11	0.75
119-279.3	57.66	0.78	15.31	6.61	0.06	3.20	1.71	1.20	4.37	0.06	0.11	0.13	8.80
119-279.3	57.51	0.78	15.17	6.59	0.06	3.23	1.72	1.16	4.30	0.06	0.11	0.11	9.20
119-280.8	92.54	0.06	3.26	1.34	0.02	0.33	0.38	0.24	0.83	0.01	0.09	0.10	0.80
119-280.8	92.09	0.06	3.37	1.37	0.02	0.41	0.40	0.63	0.83	0.08	0.09	0.10	0.55
119-283.3	54.73	0.73	16.79	8.07	0.07	4.09	3.26	0.94	3.08	0.06	0.12	0.14	7.92
119-284.8	60.54	0.63	15.88	7.79	0.08	4.09	3.62	1.31	2.45	0.04	0.13	0.14	3.30
119-286.4	56.77	0.77	17.03	9.26	0.08	4.54	4.71	1.29	1.98	0.09	0.13	0.15	3.20
119-287.8	54.46	0.77	16.29	8.70	0.08	4.24	4.77	1.21	1.67	0.06	0.13	0.14	7.48
119-289.4	56.73	0.78	16.94	8.14	0.08	4.42	5.16	1.22	2.50	0.04	0.13	0.16	3.70
119-291	57.01	0.76	17.08	8.76	0.09	4.71	4.81	1.14	1.97	0.07	0.14	0.15	3.31
119-292.5	56.31	0.81	17.36	8.99	0.09	4.78	4.78	1.08	2.04	0.07	0.14	0.16	3.39
119-294	57.93	0.65	17.28	8.27	0.08	4.71	3.51	1.12	2.36	0.04	0.14	0.16	3.75

Sample ID	SiO ₂	TiO ₂	Al ₂ O ₃	Fe ₂ O ₃	MnO	MgO	CaO	Na ₂ O	K ₂ O	P ₂ O ₅	V ₂ O ₅	Cr ₂ O ₃	LOI
119-295.5	77.66	0.33	10.96	3.23	0.03	1.45	0.34	0.31	3.62	0.05	0.10	0.12	1.80
119-298.5	61.67	0.35	10.23	3.87	0.04	2.05	0.88	9.77	2.63	0.02	0.08	0.09	8.32
119-300	54.35	0.68	15.46	8.87	0.08	4.57	4.25	1.39	1.81	0.06	0.13	0.16	8.19
119-301.5	52.70	0.69	15.93	8.81	0.08	4.58	4.38	1.08	1.83	0.05	0.13	0.15	9.59
119-303	54.30	0.65	16.08	7.97	0.08	4.55	3.95	1.61	2.07	0.06	0.12	0.14	8.42
119-306	59.53	0.73	16.23	8.07	0.09	4.69	3.38	1.04	2.51	0.04	0.13	0.16	3.40
119-307.5	52.84	0.70	16.14	8.43	0.08	4.78	4.02	1.13	1.83	0.05	0.13	0.14	9.73
119-309	52.41	0.77	16.93	8.94	0.09	4.90	4.65	1.04	1.71	0.05	0.13	0.15	8.23
119-310.5	53.28	0.66	17.01	8.43	0.09	4.93	4.31	1.44	1.98	0.06	0.13	0.31	7.37
119-312	86.06	0.15	6.97	1.86	0.02	0.78	0.47	0.41	1.98	0.03	0.09	0.13	1.05
119-313.5	53.67	0.63	16.55	8.31	0.08	4.58	4.14	1.34	1.92	0.06	0.12	0.14	8.46
119-315	59.65	0.52	16.06	8.94	0.09	5.01	2.52	1.03	2.36	0.06	0.14	0.16	3.46
119-318	55.59	0.67	17.38	9.02	0.09	5.30	4.28	1.18	2.06	0.08	0.14	0.17	4.04
119-319.5	58.47	0.45	15.99	9.20	0.08	5.32	3.27	1.21	2.11	0.04	0.14	0.17	3.55
119-321	92.89	0.06	3.74	0.69	0.01	0.18	0.22	0.85	0.82	0.00	0.09	0.10	0.35
119-322.5	53.87	0.66	15.56	8.23	0.09	4.70	4.16	1.82	1.23	0.05	0.12	0.14	9.37
119-325	57.55	1.22	14.70	10.88	0.12	3.74	5.87	1.37	2.62	0.14	0.12	0.12	1.55
119-326	52.98	0.96	14.45	10.22	0.12	4.21	5.19	1.47	1.91	0.06	0.12	0.13	8.18
119-327	52.49	0.66	13.31	10.77	0.12	4.32	5.27	1.29	2.14	0.12	0.12	0.12	9.27
119-328	57.62	0.75	14.38	10.92	0.13	4.29	6.07	1.51	2.27	0.12	0.13	0.16	1.65
119-329	51.30	1.05	14.10	10.98	0.14	3.56	6.01	1.66	1.81	0.10	0.11	0.11	9.07
119-329	51.34	1.05	13.78	10.77	0.14	3.48	6.00	1.57	1.78	0.12	0.11	0.11	9.75
119-330	55.42	1.23	14.75	11.17	0.14	3.86	6.74	1.89	1.76	0.11	0.12	0.12	2.69
119-332	51.70	1.27	14.17	10.85	0.13	3.06	5.51	1.97	1.76	0.12	0.11	0.10	9.25
119-333	54.44	1.52	15.20	12.50	0.16	4.11	6.22	1.78	1.93	0.10	0.13	0.12	1.79
119-334	52.31	0.94	13.54	11.07	0.13	3.79	5.61	1.72	1.55	0.09	0.11	0.12	9.02
119-335	63.44	0.68	9.19	7.61	0.09	2.55	3.37	1.22	1.12	0.05	0.10	0.11	10.47
119-336	53.63	0.67	12.09	14.63	0.18	8.02	5.22	1.37	0.95	0.06	0.14	0.14	2.90
119-337	48.85	0.69	13.76	14.17	0.14	5.57	5.52	1.75	1.17	0.11	0.12	0.12	8.03

Sample ID	SiO ₂	TiO ₂	Al ₂ O ₃	Fe ₂ O ₃	MnO	MgO	CaO	Na ₂ O	K ₂ O	P ₂ O ₅	V ₂ O ₅	Cr ₂ O ₃	LOI
119-338	54.17	0.79	14.84	12.24	0.15	5.65	3.23	1.95	1.39	0.07	0.13	0.14	2.25
119-338	54.07	0.79	14.82	12.23	0.16	5.72	6.26	1.93	1.39	0.11	0.13	0.14	2.25
119-339	49.87	0.79	13.76	12.51	0.15	5.58	5.96	1.92	1.18	0.09	0.12	0.13	7.94
119-340	50.61	0.79	14.02	11.97	0.14	5.51	5.78	1.82	1.31	0.07	0.12	0.13	7.73
119-341	49.14	0.69	13.36	14.19	0.16	5.68	5.69	1.53	1.19	0.08	0.12	0.15	8.02
119-342	51.89	0.82	13.74	13.14	0.17	7.11	7.39	3.16	0.77	0.08	0.13	0.15	1.45
119-343	53.18	0.70	14.91	13.06	0.17	5.87	6.83	1.72	1.22	0.07	0.13	0.14	2.00
119-344	49.97	0.79	12.91	17.41	0.18	6.24	7.39	1.89	1.06	0.08	0.12	0.11	1.85
119-345	45.80	0.50	13.06	21.32	0.16	6.89	5.87	1.25	0.74	0.04	0.13	0.15	4.09
119-347	50.19	0.63	13.54	16.51	0.17	7.31	5.68	1.18	0.98	0.07	0.14	0.15	3.45
119-348	49.59	0.77	12.69	17.00	0.17	7.76	6.42	1.21	0.89	0.07	0.13	0.15	3.15
119-349	51.86	0.64	14.36	13.41	0.15	7.20	6.10	1.59	1.25	0.06	0.13	0.15	3.10
119-350	48.21	0.57	13.41	13.43	0.14	7.02	5.97	1.61	1.18	0.06	0.12	0.15	8.13
119-351	53.03	0.72	14.62	11.59	0.15	7.47	6.12	2.32	1.17	0.07	0.13	0.16	2.45
119-352	53.40	0.68	14.29	12.22	0.14	7.38	5.28	2.10	1.10	0.07	0.13	0.16	3.05
119-353	51.25	0.72	14.23	12.99	0.15	7.32	6.17	2.81	1.18	0.07	0.14	0.17	2.80
119-354	46.75	0.63	12.60	14.94	0.15	7.06	5.70	1.31	0.86	0.06	0.13	0.16	9.65
119-355	49.60	0.65	13.22	16.71	0.16	7.60	6.16	1.16	0.92	0.06	0.14	0.17	3.45
119-355	49.48	0.64	13.28	16.73	0.16	7.59	6.14	1.19	0.92	0.06	0.14	0.17	3.50
119-358	54.30	0.75	10.56	16.03	0.16	6.85	5.69	2.82	0.86	0.07	0.13	0.18	1.60
119-358	53.13	0.86	13.62	11.76	0.18	6.41	8.35	2.83	0.95	0.08	0.12	0.11	1.60
119-359	48.43	0.69	12.36	17.54	0.17	7.89	6.39	1.83	0.75	0.06	0.14	0.16	3.59
119-359.3	55.75	0.72	17.97	6.91	0.06	3.86	1.75	1.07	3.87	0.07	0.11	0.13	7.73
119-361	34.17	1.84	57.79	1.94	0.04	0.23	0.14	0.21	0.19	0.10	0.15	0.15	3.05
119-362	49.36	0.88	12.22	17.54	0.18	7.67	6.44	1.05	0.97	0.10	0.14	0.15	3.30
119-363	50.09	0.78	12.05	17.24	0.18	7.84	6.47	1.11	0.96	0.09	0.14	0.17	2.88
119-364	47.72	0.71	12.31	16.79	0.18	7.88	6.81	2.45	0.85	0.07	0.13	0.15	3.95
119-365	48.81	0.94	12.34	17.81	0.21	9.42	5.69	1.21	0.64	0.09	0.13	0.17	2.54
119-366	49.78	0.73	12.83	16.46	0.18	7.63	6.70	1.48	0.77	0.06	0.13	0.16	3.09

Sample ID	SiO ₂	TiO ₂	Al ₂ O ₃	Fe ₂ O ₃	MnO	MgO	CaO	Na ₂ O	K ₂ O	P ₂ O ₅	V ₂ O ₅	Cr ₂ O ₃	LOI
119-367	52.87	0.67	14.17	13.41	0.18	5.97	6.79	2.01	1.25	0.06	0.13	0.14	2.35
119-368	49.39	0.72	11.97	18.30	0.19	8.05	7.46	1.00	0.90	0.07	0.13	0.17	1.65
119-369	48.56	0.69	12.37	17.03	0.18	7.35	6.93	2.79	1.13	0.08	0.13	0.16	2.60
119-370	49.49	0.56	12.92	16.81	0.18	7.75	7.21	1.37	0.74	0.06	0.13	0.13	2.65
119-371	47.67	0.66	12.90	18.98	0.18	7.10	6.76	1.29	0.90	0.06	0.12	0.13	3.25
119-372	47.22	0.61	12.13	17.12	0.18	6.87	6.76	5.05	0.86	0.07	0.12	0.12	2.89
119-373	48.46	0.73	11.99	20.85	0.17	6.27	7.08	1.85	0.69	0.07	0.12	0.12	1.60
119-374	49.49	0.75	12.82	17.65	0.18	5.69	7.42	2.14	0.94	0.11	0.12	0.14	2.55
119-375	48.81	0.86	12.52	18.55	0.20	6.59	6.91	1.66	0.88	0.08	0.12	0.13	2.69
119-377	50.73	0.78	12.65	17.84	0.18	6.03	7.23	1.38	0.97	0.07	0.12	0.12	1.90
119-378.6	49.27	0.70	12.45	17.39	0.18	7.55	6.90	1.89	1.02	0.06	0.13	0.16	2.30
119-379	48.81	0.86	12.57	18.50	0.20	6.55	6.91	1.63	0.89	0.08	0.12	0.13	2.75
119-380	52.01	0.73	13.80	12.88	0.15	7.31	6.25	2.61	1.18	0.08	0.14	0.17	2.69
119-381	52.17	0.91	13.88	13.06	0.19	6.11	8.61	2.05	1.17	0.09	0.12	0.14	1.50
119-382	50.33	0.83	12.99	16.74	0.19	6.07	7.56	1.25	0.91	0.07	0.12	0.14	2.80
119-383	49.28	0.79	13.33	17.65	0.19	6.45	7.27	1.56	0.92	0.07	0.12	0.12	2.25
119-384	53.70	0.79	13.99	12.71	0.19	6.48	7.84	2.08	1.00	0.08	0.12	0.12	0.90
119-385	52.32	0.80	13.72	12.62	0.19	6.63	8.08	1.81	1.07	0.08	0.12	0.11	2.45
119-386	51.13	0.75	13.06	10.55	0.16	6.27	10.16	2.22	0.69	0.07	0.13	0.11	4.70
119-387	51.73	0.73	13.55	12.40	0.19	6.62	7.33	2.64	1.60	0.07	0.12	0.12	2.90
119-388	38.72	0.82	14.47	13.42	0.19	6.97	11.51	0.98	3.81	0.09	0.13	0.11	8.78
119-389	56.24	0.67	17.74	8.80	0.09	4.89	4.38	1.35	2.04	0.06	0.14	0.16	3.44
119-390	52.24	0.84	13.86	11.77	0.18	6.43	8.17	3.57	0.96	0.09	0.12	0.11	1.66
119-391.5	51.67	0.76	13.77	11.25	0.17	6.30	9.01	3.94	1.03	0.08	0.12	0.10	1.80
119-393	51.80	0.80	14.39	12.64	0.19	6.97	7.40	2.22	0.88	0.08	0.12	0.11	2.40
119-394.5	53.04	0.79	13.98	11.99	0.18	6.59	8.36	2.26	1.10	0.08	0.12	0.11	1.40
119-396	53.16	0.86	13.75	11.84	0.18	6.47	8.35	2.32	0.94	0.10	0.12	0.11	1.80
119-397.5	53.77	0.77	14.11	12.05	0.18	6.54	8.67	2.44	0.91	0.08	0.12	0.11	0.25
119-400.5	54.16	0.78	13.85	12.29	0.19	6.73	8.89	1.92	0.84	0.07	0.12	0.11	0.05

Sample ID	SiO ₂	TiO ₂	Al ₂ O ₃	Fe ₂ O ₃	MnO	MgO	CaO	Na ₂ O	K ₂ O	P ₂ O ₅	V ₂ O ₅	Cr ₂ O ₃	LOI
119-402	53.15	0.83	13.74	11.44	0.18	6.37	5.58	3.07	0.93	0.08	0.12	0.11	1.40
119-402	52.09	0.80	13.41	11.22	0.17	6.25	8.42	4.74	0.93	0.09	0.12	0.11	1.65
119-403.5	51.42	0.81	15.07	11.52	0.18	6.24	8.49	2.40	0.91	0.09	0.12	0.11	2.64
119-405	52.88	0.91	14.63	11.06	0.17	6.15	9.41	2.32	0.63	0.06	0.12	0.11	1.55
119-406.5	52.37	0.93	14.44	12.25	0.18	6.17	8.52	2.19	0.96	0.11	0.12	0.11	1.65
119-406.5	52.12	0.93	14.64	12.30	0.18	6.18	8.52	2.19	0.95	0.10	0.13	0.11	1.65
119-408	53.15	0.85	13.82	12.03	0.18	6.11	8.77	1.82	0.88	0.11	0.12	0.11	2.05
119-409.5	52.97	0.80	13.76	11.80	0.18	6.16	9.40	2.53	0.88	0.08	0.12	0.12	1.20
119-411	53.27	0.90	13.93	12.00	0.18	6.21	9.30	1.83	0.91	0.09	0.12	0.11	1.15
119-412.5	52.16	0.88	13.67	12.25	0.19	7.13	8.08	1.91	0.92	0.08	0.12	0.11	2.50
119-412.5	52.11	0.87	13.61	12.06	0.18	7.12	8.27	1.94	0.89	0.08	0.12	0.11	2.64
119-414	51.58	0.83	13.34	15.83	0.18	6.05	7.50	1.35	1.04	0.07	0.12	0.11	2.00
119-415.5	95.96	0.02	0.27	0.98	0.02	0.04	0.16	0.70	0.03	0.00	0.09	0.23	1.50
119-417	52.13	0.71	13.10	12.66	0.20	7.33	9.00	1.54	0.58	0.07	0.12	0.11	2.45
119-418.5	52.65	0.78	14.20	11.27	0.17	6.37	9.69	2.23	0.78	0.08	0.12	0.11	1.55
119-420	53.80	0.84	13.20	11.31	0.18	6.71	7.90	2.21	1.33	0.08	0.12	0.12	2.20
119-421.5	50.10	0.82	14.26	12.19	0.18	7.51	8.34	3.45	0.61	0.07	0.12	0.11	2.24
119-423	52.44	0.70	13.60	10.80	0.18	7.44	10.63	2.37	0.63	0.07	0.13	0.11	0.90
119-423	52.38	0.68	13.68	10.74	0.17	7.53	10.67	2.35	0.64	0.08	0.12	0.11	0.85
119-426	52.63	0.77	13.34	10.97	0.17	6.47	10.54	2.48	0.72	0.07	0.13	0.11	1.60
119-426	52.30	0.80	13.89	12.39	0.19	6.74	8.22	2.93	0.87	0.09	0.12	0.11	1.35
119-427.5	52.91	0.74	13.87	10.66	0.16	6.52	10.20	2.27	0.66	0.07	0.13	0.11	1.70
119-429	51.45	0.73	14.46	10.31	0.15	6.15	11.26	3.21	0.33	0.11	0.13	0.11	1.60
119-430.5	49.70	0.54	14.54	11.17	0.18	7.18	11.99	2.08	0.19	0.04	0.13	0.11	2.15
119-432	51.59	0.68	13.37	11.50	0.17	7.47	10.86	1.80	0.60	0.02	0.13	0.11	1.70
119-433.5	52.26	0.78	13.28	10.71	0.17	7.03	9.94	2.85	0.82	0.07	0.13	0.11	1.85
119-435	53.33	0.90	13.89	10.84	0.17	5.88	9.45	3.21	0.62	0.08	0.12	0.11	1.40
119-436.5	56.27	0.86	14.54	9.87	0.14	5.72	6.57	2.33	0.65	0.07	0.12	0.16	2.70
119-438	52.04	0.67	13.17	10.43	0.18	7.59	10.74	2.46	0.63	0.07	0.12	0.11	1.79

Sample ID	SiO ₂	TiO ₂	Al ₂ O ₃	Fe ₂ O ₃	MnO	MgO	CaO	Na ₂ O	K ₂ O	P ₂ O ₅	V ₂ O ₅	Cr ₂ O ₃	LOI
119-441	97.68	0.01	0.49	1.07	0.02	0.10	0.24	0.06	0.03	0.00	0.09	0.21	0.00
119-442.5	52.23	0.62	13.43	9.43	0.16	8.03	12.15	3.22	0.42	0.06	0.12	0.13	0.00
119-444.5	79.17	0.41	7.95	3.67	0.05	1.86	3.09	2.42	0.44	0.03	0.10	0.11	0.70
119-448.5	56.59	0.76	14.76	9.26	0.14	5.71	6.77	4.08	0.83	0.06	0.11	0.13	0.80
119-448.5	54.49	0.78	14.98	10.14	0.15	6.10	7.01	4.09	0.79	0.08	0.12	0.12	1.15
119-450	64.88	0.30	8.97	8.46	0.15	5.73	7.57	1.37	0.29	0.01	0.11	0.11	2.05
119-451.5	54.52	0.66	13.58	9.27	0.16	7.68	10.25	2.37	0.86	0.06	0.13	0.11	0.35
119-453	52.92	0.65	13.32	10.11	0.16	7.46	10.52	1.95	0.52	0.06	0.12	0.11	2.10
119-453.3	61.12	0.73	16.86	6.60	0.06	3.70	2.38	1.14	3.79	0.06	0.12	0.14	3.30
119-454.5	52.94	0.64	13.16	11.02	0.16	7.56	10.51	1.95	0.52	0.06	0.12	0.11	1.25
119-454.8	54.37	0.78	16.75	7.20	0.06	3.88	3.52	1.10	3.08	0.07	0.12	0.13	8.94
119-456	52.73	0.66	13.38	10.33	0.17	7.82	10.39	2.27	0.53	0.06	0.12	0.11	1.43
119-459	54.74	1.15	19.45	6.20	0.08	3.63	6.38	6.69	1.13	0.06	0.11	0.13	0.25
119-462	48.43	0.79	15.57	11.62	0.18	8.98	10.49	1.76	0.72	0.11	0.13	0.12	1.10
119-463.5	51.42	0.64	14.10	9.70	0.16	7.53	11.35	2.15	0.53	0.06	0.13	0.13	2.10
119-465	51.38	0.61	13.23	9.12	0.17	7.65	13.12	2.05	0.28	0.04	0.12	0.13	2.10
119-466.5	50.93	0.63	13.47	10.13	0.17	8.10	10.82	1.80	0.52	0.05	0.13	0.16	3.09
119-468	60.44	0.55	9.73	9.29	0.15	5.52	7.52	2.57	0.41	0.04	0.12	0.11	3.55
122-426.7	50.96	1.39	16.74	12.04	0.16	5.61	6.79	1.56	1.30	0.04	0.13	0.13	3.15
122-388.7	63.32	0.72	16.65	6.64	0.05	2.82	0.87	1.03	4.96	0.07	0.11	0.12	2.64
122-390.2	60.26	0.78	15.63	8.62	0.09	3.30	4.14	1.94	2.81	0.12	0.12	0.14	2.05
122-391.7	58.83	0.79	15.38	9.93	0.09	3.68	4.23	1.85	2.74	0.11	0.12	0.15	2.10
122-393.2	59.82	0.82	14.64	9.93	0.08	3.92	2.91	2.31	3.50	0.13	0.11	0.13	1.70
122-394.7	54.27	0.64	15.46	9.35	0.11	4.51	3.58	2.03	1.52	0.07	0.12	0.13	8.21
122-397.7	62.13	0.63	15.58	7.69	0.08	3.89	2.61	2.99	2.10	0.04	0.12	0.24	1.90
122-399.2	46.87	1.64	20.44	11.79	0.14	4.70	6.01	3.25	3.14	0.18	0.12	0.12	1.60
122-400.7	58.41	1.32	14.59	11.22	0.14	3.17	5.43	1.67	2.35	0.12	0.12	0.11	1.35
122-402.2	57.93	1.24	14.73	11.32	0.14	3.17	5.78	1.79	2.20	0.12	0.12	0.11	1.35
122-405.2	57.89	1.26	14.66	11.25	0.13	3.40	5.58	1.67	2.27	0.13	0.12	0.14	1.50

Sample ID	SiO ₂	TiO ₂	Al ₂ O ₃	Fe ₂ O ₃	MnO	MgO	CaO	Na ₂ O	K ₂ O	P ₂ O ₅	V ₂ O ₅	Cr ₂ O ₃	LOI
122-406.7	51.78	0.65	14.52	15.52	0.15	6.57	5.92	1.64	0.98	0.06	0.13	0.15	1.93
122-408.2	56.98	1.19	14.78	11.53	0.14	3.35	5.16	1.97	2.55	0.11	0.12	0.12	2.00
122-409.7	57.90	1.19	14.50	11.63	0.13	3.44	5.61	1.72	2.22	0.12	0.12	0.12	1.30
122-411.2	56.04	1.30	15.31	12.05	0.13	3.65	5.64	1.94	2.32	0.11	0.12	0.14	1.25
122-412.7	57.45	1.25	14.64	11.84	0.15	3.54	6.01	1.81	1.79	0.13	0.12	0.12	1.15
122-414.2	54.87	1.23	14.57	11.06	0.13	3.46	5.59	1.86	1.90	0.14	0.12	0.12	4.95
122-415.7	57.16	1.21	14.75	11.87	0.14	3.54	5.60	1.78	2.00	0.11	0.12	0.12	1.60
122-419.2	53.11	1.21	16.19	12.40	0.14	4.36	5.65	1.97	2.10	0.05	0.13	0.14	2.55
122-420.7	55.06	1.18	15.15	12.86	0.16	4.91	4.91	1.54	1.00	0.06	0.13	0.14	2.90
122-422.2	55.82	0.96	15.83	11.04	0.14	4.37	5.84	1.64	1.49	0.07	0.12	0.13	2.55
122-423.7	55.24	1.19	16.14	11.42	0.14	4.51	5.14	1.68	2.24	0.06	0.12	0.12	2.00
122-425.2	53.94	1.46	16.39	11.05	0.15	4.90	5.62	1.81	1.61	0.08	0.12	0.13	2.74
122-427.7	48.04	1.00	15.58	10.86	0.14	5.81	7.43	1.58	3.40	0.06	0.12	0.13	5.85
122-428.7	52.14	0.73	17.00	13.59	0.12	5.41	5.09	1.89	1.24	0.06	0.13	0.19	2.41
122-429.7	52.31	1.11	18.47	10.61	0.11	4.97	4.46	2.17	2.74	0.13	0.13	0.14	2.65
122-429.7	52.23	1.06	18.12	10.99	0.12	5.14	4.58	2.06	2.57	0.13	0.13	0.17	2.70
122-430.7	51.15	0.73	15.65	15.49	0.11	4.99	4.71	1.88	1.07	0.07	0.13	0.17	3.85
122-431.7	55.24	0.78	16.87	10.07	0.12	5.08	5.18	2.01	1.24	0.07	0.13	0.17	3.04
122-432.7	54.22	0.78	16.19	12.02	0.11	5.09	5.01	1.73	1.25	0.06	0.13	0.21	3.20
122-433.7	52.87	0.70	16.19	13.36	0.11	5.07	5.03	1.84	1.44	0.06	0.13	0.20	3.00
122-434.7	50.81	0.69	16.18	14.46	0.12	5.53	5.18	1.55	1.28	0.09	0.14	0.17	3.80
122-435.7	54.27	0.68	15.52	11.89	0.12	5.59	5.45	1.45	1.60	0.08	0.14	0.21	3.00
122-436.7	52.73	0.78	15.30	14.24	0.11	5.04	4.93	1.60	1.49	0.07	0.13	0.17	3.41
122-438.7	49.90	0.72	14.75	18.00	0.11	5.04	4.28	1.80	1.05	0.06	0.13	0.21	3.95
122-439.7	51.09	0.78	15.03	16.91	0.12	4.77	4.86	1.23	1.32	0.07	0.13	0.19	3.50
122-440.7	50.53	0.83	14.85	17.17	0.12	5.24	4.52	1.58	0.76	0.06	0.13	0.16	4.05
122-440.7	50.37	0.84	14.95	17.25	0.12	5.27	4.51	1.59	0.75	0.06	0.13	0.16	4.00
122-441.7	49.95	0.88	14.25	18.90	0.11	4.42	4.76	1.51	1.37	0.07	0.13	0.16	3.49
122-441.7	49.67	0.87	13.98	18.58	0.11	4.37	4.75	1.48	1.35	0.07	0.13	0.14	4.50

Sample ID	SiO ₂	TiO ₂	Al ₂ O ₃	Fe ₂ O ₃	MnO	MgO	CaO	Na ₂ O	K ₂ O	P ₂ O ₅	V ₂ O ₅	Cr ₂ O ₃	LOI
122-442.7	53.35	0.98	14.61	15.28	0.12	4.50	4.77	1.70	1.14	0.12	0.13	0.15	3.15
122-443.7	52.40	0.81	13.40	18.23	0.10	3.87	4.55	1.55	1.03	0.09	0.13	0.15	3.69
122-444.7	54.19	0.83	15.18	13.55	0.13	4.45	5.75	1.72	1.23	0.11	0.12	0.14	2.60
122-445.7	51.02	0.88	13.80	17.85	0.13	4.55	5.44	1.47	1.22	0.08	0.13	0.15	3.28
122-446.7	50.65	0.94	13.04	18.93	0.13	4.10	6.20	1.14	1.38	0.06	0.13	0.15	3.15
122-446.7	50.22	0.94	13.16	19.12	0.13	4.09	6.15	1.18	1.38	0.06	0.13	0.15	3.29
122-447.7	37.37	0.32	5.88	43.52	0.05	1.66	2.69	0.73	0.83	0.01	0.11	0.12	6.71
122-448.7	49.35	0.87	13.75	17.84	0.14	5.31	6.23	0.90	2.34	0.07	0.12	0.14	2.94
122-451.7	49.97	0.90	13.47	18.05	0.16	5.36	6.36	0.60	1.96	0.06	0.13	0.13	2.85
122-452.7	50.41	0.52	14.15	15.86	0.14	6.04	6.34	1.36	2.13	0.03	0.13	0.14	2.75
122-452.7	50.90	0.54	13.79	15.59	0.14	5.98	6.42	1.37	2.10	0.04	0.13	0.15	2.85
122-453.7	49.41	0.58	13.37	18.80	0.15	6.06	5.45	0.87	1.00	0.05	0.13	0.18	3.95
122-454.7	51.54	0.59	14.39	14.70	0.16	6.91	5.97	1.16	1.06	0.05	0.13	0.14	3.20
122-455.7	50.96	0.64	14.24	15.65	0.16	6.67	5.93	1.22	0.92	0.08	0.13	0.15	3.25
122-456.7	48.79	0.61	14.13	17.23	0.15	6.61	6.35	1.27	0.93	0.07	0.14	0.16	3.56
122-457.7	44.35	0.54	12.50	24.22	0.13	6.49	5.28	0.72	0.64	0.04	0.13	0.16	4.80
122-458.7	47.90	0.63	13.33	19.28	0.15	6.65	5.93	0.73	1.09	0.06	0.14	0.16	3.95
122-459.7	49.41	0.61	13.14	19.10	0.15	6.35	5.34	1.30	0.77	0.04	0.14	0.16	3.49
122-460.7	48.57	1.59	14.80	16.83	0.16	5.53	6.82	1.21	1.27	0.03	0.15	0.14	2.90
122-463.2	54.30	2.85	14.95	11.76	0.18	4.37	6.16	2.19	0.81	0.09	0.15	0.13	2.06
122-466.7	51.49	0.56	14.61	14.41	0.16	5.93	8.26	1.26	0.73	0.04	0.13	0.12	2.30
122-467.7	51.56	0.64	14.88	11.63	0.17	6.21	8.32	1.70	1.18	0.05	0.13	0.13	3.40
122-469.2	51.04	0.68	13.94	13.37	0.17	7.09	8.34	1.27	0.70	0.05	0.13	0.12	3.10
1340104	62.44	0.78	15.69	6.81	0.07	3.23	1.85	2.78	3.99	0.07	0.11	0.13	2.05
1340105	51.90	1.31	14.70	14.12	0.13	5.56	3.10	2.30	4.03	0.09	0.13	0.13	2.50
1340106	55.82	1.12	14.74	10.30	0.14	4.33	5.92	2.03	2.16	0.11	0.12	0.11	3.10
1340107	58.73	1.03	14.85	8.78	0.13	3.78	6.16	2.30	1.14	0.13	0.11	0.11	2.75
1340108	59.19	1.05	15.28	8.77	0.12	2.83	5.78	3.20	1.32	0.14	0.11	0.11	2.10
1340109	57.67	1.20	14.31	11.02	0.13	3.04	5.74	2.99	1.87	0.15	0.12	0.11	1.65

Sample ID	SiO ₂	TiO ₂	Al ₂ O ₃	Fe ₂ O ₃	MnO	MgO	CaO	Na ₂ O	K ₂ O	P ₂ O ₅	V ₂ O ₅	Cr ₂ O ₃	LOI
1340110	58.27	1.23	14.38	11.09	0.14	3.01	5.72	2.53	1.90	0.15	0.12	0.11	1.35
1340110	57.91	1.22	14.35	11.04	0.14	3.01	5.72	2.97	9.90	0.16	0.12	0.11	1.35
1340111	57.76	1.21	14.31	11.47	0.14	3.04	5.66	2.60	1.99	0.14	0.12	0.11	1.45
1340112	58.06	1.22	14.33	11.17	0.13	2.97	5.48	2.79	1.98	0.14	0.12	0.11	1.50
1340113	58.03	1.21	14.25	11.51	0.14	2.98	5.77	2.95	1.83	0.15	0.12	0.11	0.95
1340114	53.01	1.46	14.64	12.49	0.15	3.39	5.21	5.24	2.07	0.16	0.12	0.11	1.95
1340115	55.05	1.40	14.80	12.21	0.16	3.17	6.21	2.90	1.92	0.15	0.12	0.11	1.80
1340116	56.10	1.17	14.02	12.91	0.14	3.19	5.03	2.89	2.48	0.13	0.12	0.12	1.70
1340117	58.15	1.21	14.06	11.13	0.14	3.02	5.62	2.74	1.98	0.17	0.12	0.11	1.55
1340118	58.37	1.19	14.06	11.04	0.14	2.89	5.63	2.84	1.93	0.14	0.11	0.11	1.55
1340119	58.65	1.18	14.05	11.24	0.14	2.97	5.96	2.29	1.80	0.14	0.12	0.11	1.35
1340120	56.20	1.31	14.74	12.51	0.16	3.24	6.27	2.28	1.97	0.14	0.12	0.11	0.95
1340120	56.31	1.32	14.60	12.46	0.16	3.20	6.32	2.28	1.98	0.14	0.12	0.11	1.00
1340121	57.46	1.26	14.58	11.85	0.15	3.12	6.00	2.26	2.01	0.13	0.12	0.11	0.95
1340122	54.26	0.90	15.11	13.49	0.18	3.82	7.50	2.06	0.67	0.13	0.12	0.11	1.65
1340123	56.84	1.19	13.62	10.91	0.13	2.94	5.44	2.27	1.70	0.13	0.12	0.12	4.59
1340124	58.70	1.22	14.19	11.08	0.14	3.02	5.54	2.31	1.74	0.14	0.11	0.11	1.70
1340125	58.74	1.23	14.32	11.14	0.14	2.91	5.69	2.16	2.05	0.14	0.12	0.11	1.25
1340126	58.78	1.24	14.16	11.19	0.14	2.85	5.74	2.25	1.98	0.14	0.12	0.11	1.30
1340127	58.85	1.22	14.27	11.28	0.14	2.90	5.58	2.18	2.06	0.14	0.12	0.11	1.15
1340128	57.90	1.21	13.87	11.20	0.14	2.93	5.57	3.06	1.99	0.15	0.12	0.11	1.75
1340129	57.79	1.29	14.26	11.62	0.15	2.96	5.99	2.33	2.04	0.14	0.12	0.11	1.20
1340130	58.50	1.23	14.22	11.23	0.14	2.90	5.76	2.36	2.09	0.14	0.12	0.11	1.20
1340130	58.13	1.23	14.06	11.15	0.14	2.89	5.72	2.89	2.07	0.15	0.11	0.11	1.35
1340131	57.45	1.26	14.04	11.42	0.15	2.99	6.35	2.75	1.76	0.15	0.12	0.11	1.45
1340132	55.93	1.17	14.78	10.95	0.13	3.37	5.25	4.33	1.95	0.12	0.11	0.11	1.80
1340133	53.58	0.73	14.41	12.68	0.17	5.30	6.23	2.88	1.65	0.08	0.12	0.12	2.05
1340135	49.68	0.69	12.87	17.84	0.18	6.37	5.58	1.95	0.91	0.06	0.13	0.14	3.60
1340136	47.25	0.62	12.15	18.83	0.16	6.68	5.10	2.42	1.05	0.06	0.11	0.12	5.45

Sample ID	SiO ₂	TiO ₂	Al ₂ O ₃	Fe ₂ O ₃	MnO	MgO	CaO	Na ₂ O	K ₂ O	P ₂ O ₅	V ₂ O ₅	Cr ₂ O ₃	LOI
1340137	52.76	0.77	14.83	11.90	0.16	6.23	6.02	2.10	1.07	0.08	0.13	0.15	3.80
1340138	47.74	0.82	16.24	12.68	0.15	6.79	6.63	2.63	1.27	0.09	0.13	0.13	4.70
1340139	51.42	0.72	13.88	11.57	0.13	6.03	5.29	2.55	1.29	0.08	0.12	0.13	6.79
1340140	51.51	0.66	14.03	10.92	0.14	6.44	6.14	2.05	1.87	0.09	0.12	0.13	5.90
1340140	51.57	0.65	14.16	10.92	0.14	6.49	6.15	2.59	1.90	0.09	0.12	0.13	5.09
1340142	52.45	0.75	14.16	12.52	0.14	6.96	5.02	2.32	0.87	0.08	0.13	0.15	4.45
1340143	52.82	0.78	14.23	11.55	0.15	6.82	5.24	2.98	0.96	0.09	0.13	0.15	4.10
1340145	51.27	0.72	14.55	11.33	0.15	6.79	6.25	3.30	1.08	0.08	0.13	0.15	4.20
1340146	50.67	0.73	14.06	11.25	0.15	7.15	6.22	3.45	1.00	0.08	0.13	0.16	4.95
1340149	50.64	0.67	13.63	13.52	0.16	7.74	6.37	1.77	1.09	0.06	0.14	0.16	4.05
1340150	49.50	0.61	12.66	13.27	0.16	7.99	6.26	3.04	0.95	0.07	0.13	0.16	5.20
1340150	49.09	0.61	13.05	13.52	0.16	8.03	6.20	3.79	0.97	0.07	0.14	0.17	4.20
1340151	50.13	0.62	13.54	13.78	0.16	7.99	6.25	1.74	0.93	0.06	0.14	0.16	4.50
1340152	48.13	0.59	12.41	15.14	0.16	8.12	5.95	2.72	0.88	0.07	0.13	0.15	5.55
1340154	49.05	0.59	12.33	14.92	0.16	8.12	6.04	2.51	0.90	0.07	0.12	0.15	5.04
1340155	47.85	0.54	12.14	15.37	0.16	8.54	6.02	2.40	0.73	0.07	0.13	0.15	5.90
1340156	48.40	0.57	12.13	15.58	0.16	8.97	5.80	2.05	0.70	0.06	0.13	0.15	5.30
1340157	48.17	0.61	12.01	16.34	0.16	8.12	6.29	1.35	0.98	0.06	0.12	0.15	5.64
1340158	48.05	0.58	11.66	17.50	0.17	8.33	5.94	1.22	0.83	0.06	0.12	0.15	5.39
1340159	48.21	0.57	12.49	15.86	0.17	8.24	6.35	1.20	0.93	0.07	0.12	0.14	5.65
1340160	48.38	0.58	12.60	16.79	0.17	8.34	6.39	1.02	0.77	0.04	0.13	0.14	4.65
1340160	48.30	0.57	12.43	16.53	0.17	8.22	6.33	1.22	0.77	0.05	0.12	0.14	5.15
1340161	47.35	0.56	12.05	17.66	0.17	8.28	6.39	0.80	0.70	0.05	0.12	0.13	5.74
1340162	47.08	0.55	12.13	17.70	0.17	8.08	6.30	2.08	0.72	0.06	0.12	0.16	4.85
1340163	48.21	0.57	12.26	16.14	0.17	8.22	6.58	2.40	0.75	0.06	0.13	0.21	4.30
1340164	47.16	0.59	12.24	17.66	0.17	7.98	6.51	1.07	0.63	0.06	0.12	0.16	5.65
1340165	49.02	0.60	12.87	15.57	0.17	8.30	6.63	1.39	0.82	0.06	0.13	0.14	4.30
1340166	47.86	0.58	12.20	15.19	0.18	8.40	6.87	1.80	0.72	0.06	0.12	0.27	5.75
1340167	48.86	0.57	12.54	14.91	0.19	8.58	7.29	2.68	0.65	0.05	0.13	0.15	3.40

Sample ID	SiO ₂	TiO ₂	Al ₂ O ₃	Fe ₂ O ₃	MnO	MgO	CaO	Na ₂ O	K ₂ O	P ₂ O ₅	V ₂ O ₅	Cr ₂ O ₃	LOI
1340168	49.14	0.58	12.45	14.41	0.18	8.66	6.85	3.14	0.82	0.07	0.12	0.13	3.45
1340169	46.62	0.53	11.77	15.79	0.17	8.07	6.57	5.60	0.70	0.07	0.12	0.13	11.8
1340171	47.14	0.52	12.53	15.00	0.17	8.11	6.92	4.65	0.80	0.06	0.12	0.13	6
1340172	49.77	0.60	13.22	14.61	0.18	8.68	7.07	1.27	0.63	0.05	0.13	0.14	3.85
1340173	51.77	0.62	13.03	13.63	0.18	8.91	7.08	1.48	0.57	0.06	0.13	0.14	2.40
1340174	52.97	0.68	13.66	12.14	0.18	7.31	8.10	1.74	0.84	0.04	0.12	0.12	2.10
1340176	53.14	0.54	14.56	11.46	0.17	7.06	8.78	2.18	0.60	0.04	0.12	0.11	1.24
1340177	51.00	0.36	13.85	12.00	0.17	6.90	8.67	4.50	0.82	0.07	0.11	0.10	1.45
1340178	52.66	0.61	14.83	10.80	0.17	5.96	9.28	4.06	0.80	0.06	0.12	0.10	0.55
1340179	52.71	0.74	13.76	11.34	0.18	6.08	9.13	4.03	0.78	0.08	0.12	0.10	0.95
1340180	52.40	0.80	13.76	12.14	0.18	6.08	9.20	3.55	0.89	0.08	0.12	0.10	0.70
1340180	53.14	0.82	13.87	12.35	0.18	6.11	9.33	2.45	0.89	0.07	0.13	0.11	0.55